

Composite Action in Prestressed NU I-Girder
Bridge Deck Systems Constructed with
Bond Breakers to Facilitate Deck Removal

By

Chaohui Li

Submitted to the graduate degree program in Civil, Environmental, and Architectural
Engineering and the Graduate Faculty of the University of Kansas in partial fulfillment of the
requirements for the degree of Doctor of Philosophy.

Chair: Dr. Rémy Lequesne

Dr. Alfred Ho

Dr. Andrés Lepage

Dr. Adolfo Matamoros

Dr. Matt O'Reilly

Date Defended: 25 August 2017

The dissertation committee for Chaohui Li certifies that this is the approved version of the following dissertation:

**Composite Action in Prestressed NU I-Girder
Bridge Deck System Constructed with
Bond Breakers to Facilitate Deck Removal**

Chair: Dr. Rémy Lequesne

Date Approved: 30 August 2017

Table of Contents

Acknowledgments	v
List of Figures.....	vi
List of Tables.....	x
Abstract.....	xii
Chapter 1: Introduction.....	1
1.1 Background.....	1
1.2 Problem Statement	2
1.3 Objectives	2
1.4 Approach.....	3
Chapter 2: Literature Review.....	4
2.1 Shear Transfer across Concrete-to-Concrete Interfaces.....	4
2.1.1 Findings from Previous Tests of Push-off Specimens	5
2.1.2 Current Provisions for Horizontal Shear Transfer	13
2.1.3 Summary and Insights	16
2.2 Composite Behavior of Large-Scale Girders	17
2.2.1 Findings from Previous Large-Scale Girder Tests	18
2.2.2 Provisions for Horizontal Shear Transfer in Composite Concrete Flexural Members.....	24
2.2.3 Summary and Insights	25
2.3 Concrete Deck Removal	25
2.3.1 Kansas and Nebraska State Requirements	25
2.3.2 Previous Studies.....	26
2.3.3 Summary and Insights	29
Chapter 3: Push-off Tests	30
3.1 Experimental Program	30
3.1.1 Push-off Specimens.....	30
3.1.2 Materials	32
3.1.3 Specimen Fabrication	35
3.1.4 Test Setup and Instrumentation.....	36
3.1.5 Testing Process	39

3.2 Behavior of Push-off Specimens	40
3.2.1 Force versus Slip Relationship	40
3.2.2 Interface Slip and Crack Width	43
3.2.3 Influence of Rotation	50
3.2.4 Observation of Specimens after Failure.....	53
3.3 Interpretation and Comparison of Test Results	55
3.3.1 Interpretation of Typical Force-Slip Curves.....	55
3.3.2 Interface Shear Stress	60
3.3.2.1 Influence of Surface Preparation and Bond Breakers.....	61
3.3.2.2 Influence of Reinforcement Parameters	63
3.3.2.3 Influence of Interface Area.....	66
3.4 Conclusions from Push-off Tests	68
Chapter 4: NU I-Girder Testing	70
4.1 NU I-Girder Specimens.....	70
4.1.1 Girder Reinforcement	71
4.1.2 Top Flange Detailing for Composite Action	74
4.1.3 Bridge Deck Reinforcement	75
4.1.4 Materials	76
4.2 Bridge Deck Construction	78
4.3 Concrete Deck Removal	80
4.3.1 Deck Removal Procedures	81
4.3.1.1 Saw-cutting.....	81
4.3.1.2 Removal of Saw-cut Deck Sections.....	82
4.3.2 Evaluation of Connection Details	86
4.3.2.1 Effort Required for Deck Demolition	86
4.3.2.2 Damage to Bridge Girders Due to Bridge Deck Demolition	87
4.3.2.3 Condition of Girder Top Flange Surfaces after Bridge Deck Demolition	89
4.3.3 Conclusions from Deck Removal	91
4.4 Fatigue Tests	93
4.4.1 Construction of Replacement Bridge Deck	93
4.4.2 Description of Experimental Program	94

4.4.2.1 Test Setup and Instrumentation	94
4.4.2.2 Loading Protocol	97
4.4.3 Fatigue Test Results	99
4.4.3.1 Force-Displacement Relationship	99
4.4.3.2 Relative Slip across Interface	102
4.4.3.3 Strain Gauge Results	104
4.4.4 Conclusions from Fatigue Tests	108
4.5 Tests of Girders to Failure	110
4.5.1 Experimental Program	110
4.5.1.1 Test Setup	110
4.5.1.2 Instrumentation	112
4.5.1.3 Testing Procedure	113
4.5.2 Test Results	113
4.5.2.1 Observations during Testing	113
4.5.2.2 Force versus Displacement	118
4.5.2.4 Relative Slip across Interface	120
4.5.2.5 Relative Rotation Along Girder Span	128
4.5.3 Interface Shear Stress	129
4.5.4 Conclusions from Ultimate Strength Tests	130
Chapter 5: Modeling of Composite Action	131
5.1 Description of Models	131
5.2 Model Verification with Experimental Test Results	133
5.2.1 Force versus Deflection and Girder Stiffness	134
5.2.2 Distribution of Link Forces and Interface Cracking	136
5.3 Effect of Aspect Ratio	137
5.4 Effect of Load Position	140
5.5 Conclusions from Modelling of Composite Action	143
Chapter 6: Conclusions and Recommendations	145
6.1 Conclusions	145
6.1.1 Conclusions from Push-off Tests	145
6.1.2 Conclusions from Deck Removal	146

6.1.3 Conclusions from Composite Girder Tests	147
6.1.4 Conclusions from Modeling of Composite Action.....	148
6.2 Recommendations for Deck Removal.....	149
6.2.1 Procedure A: For girders with a roughened and or troweled top flange	149
6.2.2 Procedure B: For girders with roofing felt placed over the top flange except for directly over the web.....	149
6.2.3 Potential modification to either Procedure A or B for use of larger jackhammers	150
References.....	152
Appendix A.....	156
Appendix B.....	158
Appendix C.....	164
Appendix D.....	169
Appendix E	186
Appendix F	189

Acknowledgments

The Kansas Department of Transportation is gratefully acknowledged for funding the research described herein. Coreslab Structures is acknowledged for their donation of girders. The University of Kansas Department of Civil, Environmental, and Architectural Engineering, The University of Kansas School of Engineering, and The University of Kansas Office of Graduate Studies are acknowledged for providing testing facilities and space and for partially funding my studies.

In addition to the funding agencies, I would like to acknowledge those who offered their help, support, and friendship to me throughout my time in graduate school. Numerous people helped me in the laboratory to complete the experimental work reported herein. The specimens could not be built and tested without the hard work and expertise of Kent Dye, David Woody, and Matthew Maksimowicz. Furthermore, numerous fellow Ph.D. students volunteered their time to help me in the laboratory. Included among these students are Alexander Weber-Kamin, Abdalkader Al-Sabawy, Krishna Ghimire, Eduardo Suillen Sucre, and Mohammad (Sajed) Huq.

I want to thank my dissertation committee for their time and input. In particular, I want to thank Prof. O'Reilly for the time he spent helping me solve experimental problems, answering questions, and reviewing my dissertation. I especially owe a great debt of gratitude to my advisor, Prof. Lequesne, for his immeasurable contribution to the dissertation and to my own career development. In addition as an excellent advisor, he is a terrific engineer, teacher, co-worker, and friend. I greatly appreciate his trust in me and patience in supervising my research work throughout the past three years. His extremely thorough attitude and passion in research will keep influencing me in my future endeavors as an engineer.

Finally, I owe the greatest thanks to my family. I want to thank my parents for having been unconditionally supportive of my endeavors since I was born. Their trust and expectations drove me to keep me working hard and pursue a doctoral degree. I want to thank my wife, Qingqing for being such a wonderful addition to my life. Being with her has made the last two and a half years of my Ph.D. the most enjoyable part of the process. I also want to thank my unborn daughter who will be an amazing addition to my future life.

List of Figures

Figure 1.1: Example AASHTO I-Girder and NU I-Girder.....	1
Figure 2.1: Typical Push-off Specimen.....	5
Figure 2.2: Saw-Tooth Model (adapted from Birkeland and Birkeland,1966).....	7
Figure 2.3: Connection Detail.....	27
Figure 3.1: Push-off Specimen Detail.....	30
Figure 3.2: Stress-strain Curves for No. 5 bars Used as Interface Shear Reinforcement....	34
Figure 3.3: Fabrication of Push-off Specimens.....	37
Figure 3.4: Elevation View of the Test Setup.....	38
Figure 3.5: Test Setup and Instrumentation.....	39
Figure 3.6: Force versus Time for RM-12-F-12-NR and T-12-E-12-NR.....	40
Figure 3.7: Force versus Slip (Specimens Affected by Rotation are Omitted).....	41
Figure 3.8: Force versus Slip up to a Slip of 0.06 in.....	43
Figure 3.9 Force versus Relative Horizontal Displacement for Selected Specimens.....	44
Figure 3.10 Force versus Crack Width.....	45
Figure 3.11: Crack Width versus Slip for Rough Middle Specimens.....	47
Figure 3.12: Crack Width versus Slip for Roughened Specimens.....	48
Figure 3.13: Crack Width versus Slip for Troweled Specimens without Bond Breakers....	49
Figure 3.14: Crack Width versus Slip for Bonded Troweled Specimens.....	49
Figure 3.15: Coordinate System of the 3-Dimensional Position Tracking System.....	51
Figure 3.16: Force versus Rotation for Specimens Influenced by Rotation.....	52
Figure 3.17: Force versus Slip Curve for Specimens affected by Rotation.....	52
Figure 3.18: Interface of T-24-F-12-NR after Testing.....	54
Figure 3.19: Interface of R-24-NB-12-NR after Testing.....	54
Figure 3.20: Schematic of Force versus Slip for Bonded and Unbonded Specimens.....	56
Figure 3.21: Average Shear Stress versus Slip Curves for Bonded Specimens.....	62
Figure 3.22: Average Shear Stress versus Slip Curves for Troweled Specimens.....	62
Figure 3.23: Average Shear Stress versus Slip for Fully Troweled Surface.....	64

Figure 3.24: Average Shear Stress versus Slip for Partially Roughened Surface with Felt	64
Figure 3.25: Average Shear Stress versus Slip for 24 in. Wide Specimens.....	65
Figure 3.26: Average Shear Stress versus Slip for Troweled Specimens with Felt.....	67
Figure 3.27: Average Shear Stress versus Slip for Roughened Specimens.....	67
Figure 4.1: Elevation View of Composite NU35 Girder.....	70
Figure 4.2: Elevation and Cross Section View of NU35 Girder Specimens.....	71
Figure 4.3: Connection Details for NU35 Girders.....	75
Figure 4.4: Concrete Bridge Deck Reinforcement.....	76
Figure 4.5: Stress versus Strain for No. 5 Bars Used as Deck Reinforcement.....	78
Figure 4.6: Deck Casting Procedures.....	79
Figure 4.7: Primary Tools Used for Deck Removal.....	80
Figure 4.8: Saw-Cutting Procedures.....	82
Figure 4.9: Removal of Bridge Deck Concrete over Girder Edges.....	84
Figure 4.10: Removal of Deck Concrete over Girder Webs.....	85
Figure 4.11: Girder Damage Types Due to Deck Removal.....	89
Figure 4.12: Girder #3 Surface after Deck Removal (Originally Fully Roughened).....	90
Figure 4.13: Girder #2 Surface after Deck Removal (Originally Partially Roughened with Roofing Felt over the Flange Tips).....	90
Figure 4.14: Girder #1 Surface after Deck Removal (Originally Fully Troweled).....	91
Figure 4.15: Surface Preparation and Deck Reinforcement before Casting.....	93
Figure 4.16: Fatigue Test Setup and Instrumentation.....	94
Figure 4.17: Details of Test Setup and Instrumentation.....	95
Figure 4.18: Photo of Fatigue Test Setup.....	96
Figure 4.19: Ramp Function used for Data Collection.....	97
Figure 4.20: Sinusoidal Function used for Application of Cycles of Force.....	98
Figure 4.21: Force versus Deflection for Girder #1 Prior to Fatigue Loading.....	100
Figure 4.22: Ratio of Girder Stiffness to Initial Girder Stiffness.....	102
Figure 4.23: Relative Slip at 80 kips throughout Fatigue Tests.....	103

Figure 4.24: Ratio of Deck Slip at 80 kips to the Initial Deck Slip at 80 kips.....	103
Figure 4.25: Strain Gauge Locations and Naming Convention.....	104
Figure 4.26: Strain Distribution along Girder Depth at Midspan in Girder #1.....	105
Figure 4.27: Strain Distribution along Girder Depth at Midspan in Girder #2.....	105
Figure 4.28: Strain Distribution along Girder Depth at Midspan in Girder #3.....	106
Figure 4.29: Strain Ratio for Girder #1.....	107
Figure 4.30: Strain Ratio for Girder #2.....	108
Figure 4.31: Test Setup and Instrumentation.....	110
Figure 4.32: Test Setup and Instrumentation Details.....	111
Figure 4.33: Test Setup.....	112
Figure 4.34: Photos of Girder #1 During and After Testing.....	114
Figure 4.35: Photos of Girder #2 During and After Testing.....	116
Figure 4.36: Photos of Girder #3 During and After Testing.....	117
Figure 4.37: Force versus Deflection.....	118
Figure 4.38: Force versus Deflection (different scale).....	119
Figure 4.39: Elevation View of Girder with Stations for Relative Slip Calculation.....	121
Figure 4.40: Slip versus Force for the First Test of Girder #1.....	122
Figure 4.41: Slip versus Force for the Final Test of Girder #1.....	123
Figure 4.42: Distribution of Slip over Girder Length (Girder #1).....	123
Figure 4.43: Slip versus Force (Girder #2).....	125
Figure 4.44: Distribution of Slip over Girder Length (Girder #2).....	125
Figure 4.45: Slip versus Force (Girder #3).....	126
Figure 4.46: Slip versus Force for 6-W (Girder #3).....	127
Figure 4.47: Distribution of Slip over Girder Length (Girder #3).....	127
Figure 4.48: Relative Rotation along Girder Span (Girder #2).....	128
Figure 4.49: Relative Rotation along Girder Span (Girder #3).....	128
Figure 5.1: Force versus Slip of Link Element.....	133
Figure 5.2: Composite Girder Model.....	134
Figure 5.3: Plot of Force versus Midspan Deflection.....	135

Figure 5.4: Link Force versus Link Location for Model #4 at Varied Imposed Forces.....	137
Figure 5.5: Models of Girders with Different Aspect Ratios.....	138
Figure 5.6: Link Shear Force versus Position along Half Span at 200 kips.....	140
Figure 5.7: Link Shear Force Distribution for a 200 kip Point Load Located at $L/8$ and $3L/8$	141
Figure 5.8: Maximum Link Shear Force for Load Positions between $L/12$ and $L/2$ (Maximum Link Force is plotted at the Load Position, Not the Position of Maximum Link Force).....	142

List of Tables

Table 2.1: Upper Limit for Eq. 2-8.....	13
Table 2.2: Coefficient of Friction for Eq. 2-8.....	14
Table 2.3: Cohesion and Friction Factors for Eq. 2-9.....	14
Table 2.4: Coefficients for Eq. 2-10.....	16
Table 2.5: Nominal Horizontal Shear Strength.....	24
Table 3.1: Summary of Push-off Specimens.....	31
Table 3.2: Mixture Proportions per yd^3 (SSD).....	33
Table 3.3: Measured Concrete Strengths.....	33
Table 3.4: Measured Reinforcement Properties.....	34
Table 3.5: Specimen Strength, Slip, and Stiffness.....	42
Table 3.6: Force and Crack Width at Critical Points.....	46
Table 3.7: Cause for Termination of Tests.....	53
Table 3.8: Summary of Force and Slip Values.....	57
Table 3.9: Comparison of Experimental and Calculated Nominal Strengths.....	59
Table 3.10: Relationship between Post-peak Strength and Reinforcement Parameters.....	60
Table 3.11: Summary of Interface Shear Stresses.....	61
Table 4.1: Concrete Mixture Proportions per yd^3 for NU35 Girder and Bridge Deck (SSD)	77
Table 4.2: Measured Reinforcement Properties for Bridge Deck.....	77
Table 4.3: Person-Hours Required for Bridge Deck Demolition.....	86
Table 4.4: Interface Shear Stress at 72 kip Load Increment.....	99
Table 4.5: Stiffness Summary.....	101
Table 4.6 Summary of Results.....	120
Table 4.7 Slip Measured with LVDT and 3D Position Tracking Systems at Peak Force...	121
Table 4.8 Estimate of Cracking and Maximum Interface Shear Stresses.....	130
Table 5.1: Assigned Material Properties.....	131
Table 5.2: Link Element Properties.....	133

Table 5.3: Models of Girder Test Results.....	134
Table 5.4: Stiffness Summary.....	135
Table 5.5: Cracking Force.....	137
Table 5.6: Model Details.....	138
Table 5.7: Location of Maximum Force/Slip.....	140
Table 5.8: Summary of Maximum Link Forces and Location.....	142

Abstract

Results are reported from tests of small scale push-off and large-scale composite NU I-girder specimens conducted to establish an interface connection detail that 1) Facilitates in-situ removal of the bridge deck without damaging prestressed girders and 2) Maintains composite action between the prestressed girder and reinforced concrete deck throughout the service-life of the structure. Results are also reported from simple 3D models developed to simulate horizontal shear transfer in composite girders.

Sixteen small scale push-off tests were conducted to investigate the influence of surface preparation, bond breakers (epoxy and roofing felt), and interface reinforcement properties (yield strength, reinforcement amount, and means of anchorage) on horizontal shear transfer between precast and cast-in-place concrete surfaces. Based on the push-off test results, a connection detail was proposed that consists of roughening the top flange of the girder directly over the girder web and debonding the remainder of the interface using No. 30 ASTM D4869/D4869M-16a Type I organic roofing felt. Three full-scale composite NU35 girders, designed and fabricated using the proposed connection detail and two control connection details, were then subjected to a series of tests. First, decks were cast and then removed to quantify the extent to which the proposed connection detail reduced the effort to remove the deck and to document the types and extent of damage caused to the girders by the process. After replacing the decks, the composite girders were subjected to 2×10^6 cycles of simulated traffic load and then loaded monotonically to failure. A series of 3D composite girder models were created in SAP2000 to better understand factors affecting the distribution of slip along the horizontal interface. The girder and deck were simulated using elastic frame and shell elements, respectively, and interface shear was simulated using a series of multilinear link elements. These models were used to simulate the experimental girder tests under service-level loads and to investigate the effects of beam aspect ratio and load position on the distribution of interface shear.

The proposed connection (partially roughened/partially debonded with a roofing felt bond breaker) is a viable option for use in practice; its use led to a 2/3 reduction in the effort required to remove the deck over the girder and protected the girder from all non-saw-related damage while

also effectively sustaining composite action through 2×10^6 cycles of simulated traffic load after deck replacement. The proposed connection can be conservatively designed by neglecting the debonded area when calculating interface shear strength. Other test results showed that surface preparation has a large influence on the stiffness, strength at cracking, and peak strength of a horizontal shear connection; each was greatest for specimens with a fully roughened surface followed by the partially roughened surface, troweled surface, and debonded surface. Increasing the amount of interface shear reinforcement increases the initial stiffness, shear strength at cracking, peak and post-peak strength, and does so more effectively than a similar increase in reinforcement yield strength. Casting and removal of bridge decks without bond breakers does alter the top surface of bridge girders, but the surface can be returned to a qualitatively roughened surface with reasonable effort and care. Despite the changes to the top girder surface caused by deck removal, composite action was developed across the interface and remained stable through 2×10^6 cycles of loading. Finally, the analytical study indicated that models of composite action that consider flexibility of the horizontal shear interface allow for a better estimation of the composite member stiffness and allow for a more accurate assessment of the distribution of slip along the interface than models based on a rigid connection. The interface shear force demand was, however, conservatively estimated for all cases considered with AASHTO provisions.

Chapter 1: Introduction

1.1 Background

NU I-Girders are a series of standardized prestressed concrete girder cross-sections developed by the Center for Infrastructure Research at the University of Nebraska in the 1990s. Figure 1.1 shows the cross-section of an NU35 girder (the shallowest NU I-Girder available) alongside the cross-section of a 36-in. deep Type II AASHTO I-Beam. As shown in Figure 1.1, NU I-Girders have relatively wide and thick bottom flanges (which allows placement of a large number of strands and greater stability during transport), wide and thin top flanges (which provides a large platform for workers during construction), and curved fillets (which are aesthetically pleasing and make concrete placement easier). Regardless of depth, NU I-Girders all have the same flange dimensions. This significantly reduces the formwork necessary for construction of NU I-Girders. Owing to their structural efficiency, economy, and aesthetic appeal, NU I-Girders have been extensively used in Nebraska and several other US states and Canadian provinces (Beacham & Derrick, 1999).

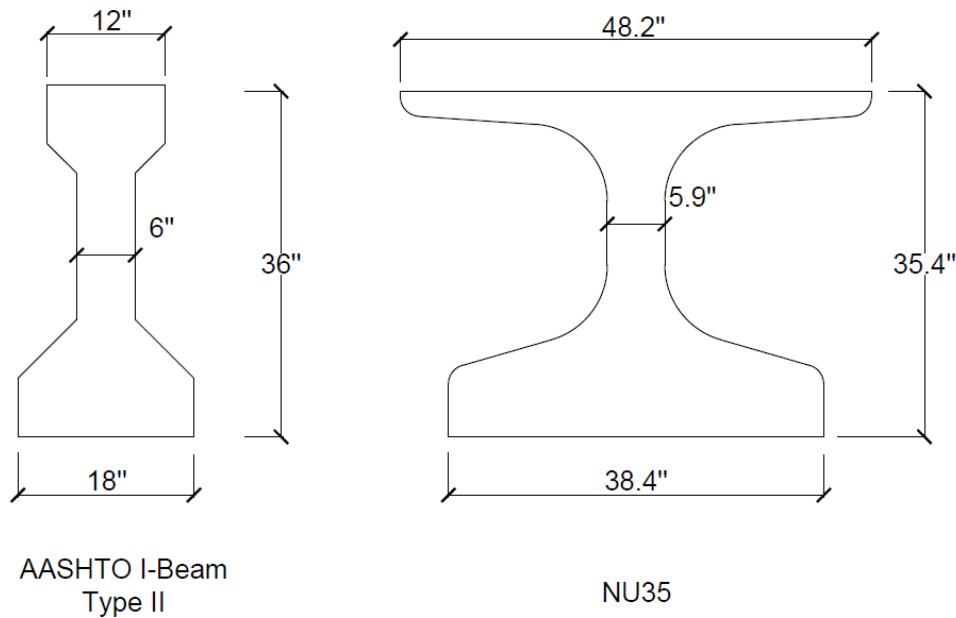


Figure 1.1: Example AASHTO I-Girder and NU I-Girder

1.2 Problem Statement

Despite their advantages, use of NU I-Girders is limited in Kansas. One reason is the concern that future deck removal will irreparably damage the thin top flanges of the girders and thereby compromise the longevity of the system. Deck removal is a destructive process during which saws and hammers are used to cut and chip deck concrete away from the supporting precast girders. Contact interfaces between the girder and deck concrete as well as dowel reinforcement protruding into the deck are prone to being damaged by this process. It is reasonable to expect that girders with wide and thin top flanges, like the NU I-Girders, are especially prone to damage during deck removal.

To maximize the return on its investment in new bridge construction, the State of Kansas has therefore recognized the need for a proven construction method for NU I-Girder bridge deck systems to facilitate in-situ removal of the deck without damaging beam components or compromising composite action between the prestressed girder and reinforced concrete deck throughout its service life. This composite action, which relies on horizontal shear transfer across the girder-to-deck interface, is important for ensuring both bridge strength and stiffness.

1.3 Objectives

This study is motivated by the need for a simple top flange connection detail that facilitates deck removal and protects prestressed components while also ensuring composite action between the girder and deck. To accomplish this aim, the following objectives have been identified:

- a) Evaluate alternative connection details in terms of strength, stiffness, and constructability,
- b) Select a preferred connection detail and evaluate the constructability, fatigue life, and strength of the connection relative to a control in full-scale tests,
- c) Provide guidance for selection of deck removal procedures to limit damage to girders,
- d) Develop methods for calculating horizontal shear strength that are validated against current and previous test results, and
- e) Develop recommendations for interface design.

1.4 Approach

The research approach was comprised of experimental and analytical components and extensive review of previously reported test results.

Literature Review: An extensive literature review, summarized in Chapter 2, was conducted that was focused on shear transfer between concrete-to-concrete interfaces, composite concrete girder testing, and concrete deck removal techniques.

Small-Scale Experimental Tests: Sixteen small-scale “push-off”-type specimens were tested to address Objective (a). The tests were designed to investigate the strength and stiffness of shear transfer across an interface. Variables included use of bond breakers; combinations of roughened and smooth surfaces (within a given specimen); amount, yield strength (60 and 120 ksi), and anchorage type (hooked and headed) of reinforcement crossing the interface; and contact area of the shear plane. Results informed the selection of a preferred connection detail.

Large-Scale Experimental Testing: Three large-scale NU35 girders were tested to address Objectives (b), (c) and (d). The precast girders were constructed with either a fully roughened, partially roughened, or smooth top surface. At the laboratory, a deck was cast into place, removed, and then replaced to evaluate the effectiveness of the detail as a means of facilitating deck removal and to quantify damage to the girders. Fatigue and ultimate strength tests were then performed to study the long-term composite performance of different connection systems.

Analytical Study: Finite element models were developed to study interface shear in large-scale specimens. The models allowed for deformation-based study of composite action, a problem that is typically treated as solely force-based.

Design Recommendations: Outcomes from the preceding work form the basis for design recommendations for interface shear design, thereby addressing Objective (e).

Chapter 2: Literature Review

The literature review is composed of three parts. Section 2.1 addresses shear transfer between concrete-to-concrete interfaces. Results of previous push-off tests and major conclusions are summarized. Section 2.2 summarizes previous large-scale composite girder tests with results that inform the design for horizontal shear transfer between precast concrete girders and cast-in-place concrete decks. Both fatigue and ultimate strength tests are included. Section 2.3 describes concrete bridge deck removal techniques and procedures as well as research that has been done on methods for facilitating rapid deck replacement.

2.1 Shear Transfer across Concrete-to-Concrete Interfaces

Composite action between precast and cast-in-place concrete relies on shear transfer across the interface. According to Zilch and Reinecke (2002), horizontal shear transfer between concrete surfaces consists of three components: adhesion, shear friction, and dowel action. Adhesion refers to the bond between concrete surfaces at an uncracked cold joint, which contributes significantly to the initial horizontal shear strength. The contribution of adhesion diminishes quickly when cracking occurs. As relative (sliding) displacement increases, mechanical interlock will develop and reinforcement crossing the interface will be tensioned. As a result, a compression force will be applied at the interface that tends to enhance mechanical interlock. Shear stress that is transferred in this manner is often referred to as shear friction. As slippage increases further, reinforcement crossing the interface will be subjected to shear and will contribute directly to resisting sliding through a mechanism called dowel action.

This mechanism of horizontal shear transfer has been studied extensively through push-off tests of specimens similar to that shown in Figure 2.1. Since the 1960s, a significant amount of work has been done in this area. The following summarizes key contributions in chronological order.



Figure 2.1: Typical Push-off Specimen

2.1.1 Findings from Previous Tests of Push-off Specimens

Hanson (1960) reported results from 62 push-off tests designed to study the shear transfer mechanism between precast concrete girders and cast-on-site concrete decks. Concrete used to represent the slab and girder had specified compressive strengths of 3 and 5 ksi, respectively. The interface was a constant 8 in. wide with a varied contact length (6 in., 12 in. and 24 in.). Most specimens had U-shaped stirrups (Grade 50 steel conforming to ASTM A305) serving as dowel reinforcement extending 4 in. into the concrete deck from the girder section. The reinforcement ratio, calculated as the area of reinforcement perpendicular to the interface divided by the total interface area was varied from 0 to 0.0083. Some specimens had 5 in. by 5 in. shear keys extending 2 ½ in. into the top surface of the beam. The influence of adhesive bond (between concrete layers at the cold joint), surface roughness (rough and smooth), shear keys, and reinforcement ratio on shear transfer behavior were studied. Debonded interfaces were prepared by painting the interface with a silicone compound that prevented bond formation between old and new concrete. For testing, shear load was applied monotonically and relative slip at the interface was recorded at several load increments. Shear stress (calculated using shear load divided by interface area) versus slip curves

were developed for each specimen. According to the stress versus slip curves, bonded connections can develop high shear stresses at low slip (mostly less than 0.003 in.) while considerable slip is required for an unbonded interface to develop high shearing stresses. It was found that shear keys do not increase the strength of a joint with a rough bonded interface. Joint shear strength due to dowel reinforcement was independent of that due to interface characteristics. Hanson concluded that dowel reinforcement (No. 4 bars) contribute approximately 175 psi for each percent reinforcement crossing the interface, and the maximum shearing stress for rough and smooth bonded interfaces are 500 psi and 300 psi, respectively.

Anderson (1960) tested 18 push-off specimens to study shear transfer across a cold joint. Each specimen was composed of two antisymmetric L-shaped parts (similar to the one shown in Figure 2.1). The interface of the precast part was roughened with undulations having a depth of approximately ¼ in. Concrete used to represent the precast portion had a specified compressive strength of 7.5 ksi while that for the cast-in-place part had a specified compressive strength of either 3 or 7.5 ksi. Reinforcement crossing the interface consisted of No. 2 and No. 5 bars with reinforcement ratios between 0.2 and 2.48 percent. The specimens were loaded monotonically in shear along the interface. The specimens behaved like monolithic concrete up to 75 to 85 percent of ultimate load before differential slip was recorded across the interface. According to the test results, the ultimate shear strength was linearly proportional to reinforcement ratio for a given concrete compressive strength. For a given reinforcement ratio, the ultimate shear stress increased as the compressive strength of the cast-in-place concrete increased from 3 to 7.5 ksi.

Birkeland and Birkeland (1966) were the first to propose the “shear friction” theory wherein reinforcement crossing a shear plane is assumed to provide a clamping force that induces friction across the interface. A saw-tooth model (Figure 2.2) was proposed to describe the behavior across a cracked interface. Equation 2-1 was proposed to calculate shear transfer strength.

$$v_u = \rho f_y \tan \phi \leq 800 \text{ psi} \quad \text{Eq. 2-1}$$

Where: ρ is the reinforcing steel ratio calculated as the cross-sectional area of reinforcement oriented perpendicular to the interface divided by the total interface area, f_y is yield strength of the

reinforcing bars and must not exceed 60 ksi, and $\tan\phi$ is a friction coefficient varies from 0.8 to 1.7 for different surface conditions. Equation 2-1 works for monolithic concrete, cold joints with both rough and smooth surfaces, and joints between concrete and steel surfaces. Based on this equation, the ultimate shear transfer strength is reached when the reinforcement crossing the interface yields. To use the equation, concrete compressive strength f'_c should be larger than 4 ksi, the interface must be sound and free from laitance, concrete must be well confined with hoops, and reinforcement must be well anchored to develop yielding.

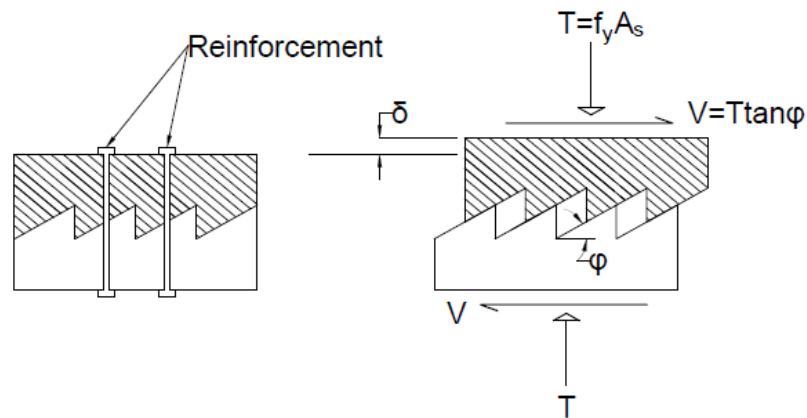


Figure 2.2: Saw-Tooth Model (adapted from Birkeland and Birkeland,1966)

Hofbeck, Ibrahim, and Mattock (1969) tested 38 monolithically cast push-off specimens. The influence on shear transfer strength of the following variables was investigated: pre-existing cracking at the shear plane; dowel action of reinforcement crossing the shear plane; yield strength (from 48.0 to 66.1 ksi), size (from No. 1 to No. 5 bars) and arrangement of reinforcement perpendicular to the shear plane; and concrete compressive strength (2.4 to 4.5 ksi). To investigate the effect of dowel action, soft rubber sleeves (2 in. long and 1/8 in. thick) were used for some specimens along legs of bars crossing the shear plane to reduce bearing between the reinforcement and surrounding concrete. According to the results, pre-existing cracks along the interface reduce the shear transfer strength and increase slip at all load levels. Dowel action of reinforcement across the interface is substantial in specimens with pre-existing cracking at the interface and insignificant at small levels of slip in initially uncracked concrete. For specimens with initially cracked concrete, the shear transfer strength v_u was shown to be affected by reinforcement crossing the shear plane

as a function of ρf_y (the product of reinforcement ratio and yield stress). For specimens with initially cracked concrete, v_u and ρf_y were found to be proportional up to a limit equal to the lesser of $0.15f'_c$ and 600 psi. Above this limit, changes in ρf_y have limited effects on v_u .

Mattock (1976) performed 52 push-off tests to study shear transfer between concretes cast at different times. The push-off specimens were composed of eight precracked monolithic specimens and 44 composite specimens with interfaces that were either precracked or uncracked. The main variables included surface roughness (either rough or smooth), bond, and cracking conditions. A bond breaker (made of soft soap and talc) was applied over the surface of certain specimens to create a debonded interface. Concrete with specified compressive strengths of 3 and 5 ksi was used together with dowel bars made from deformed reinforcement (with a nominal yield stress of 50 ksi and conforming to ASTM A615-72). According to the tests, the mechanism of shear transfer across a cold joint that was intentionally roughened is similar to that of comparable monolithically cast concrete with an initially cracked interface. The shear transfer strength of cold joints with a smooth interface, which is mainly attributable to dowel action of the reinforcement, is much less than that of a rough interface, which is attributable to a combination of frictional resistance, mechanical interlocking (shear friction) and dowel action. For specimens with a roughened cold joint surface, Eq. 2-2 was proposed for calculating the shear transfer strength.

$$v_u = 0.8\rho_v f_y + 400 \text{ psi} \leq 0.2f'_c (\text{psi}) \quad \text{Eq. 2-2}$$

Where: ρ_v is the reinforcement ratio, f_y is the yield stress of the reinforcement, and f'_c is the concrete compressive strength.

Mattock and Chow (1975) tested six series of push-off specimens to investigate the effects of moment and forces normal to the shear interface on the shear transfer strength across a plane in monolithically cast concrete. A combination of moment and shear was applied to four series of corbel-type push-off specimens, consisting of a total of 12 specimens, by applying the transverse load at varied eccentricities to the interface. The remaining nine specimens were similar to push-off-type specimens (shown in Fig. 2.1), but with forces applied normal to the interface in addition to shearing forces. This was done using high-strength post-tensioned steel bolts passing through

sleeves oriented perpendicular to the interface. All the specimens were constructed with concrete that had a target compressive strength of 4 ksi and varied amounts of shear transfer reinforcement (closed No. 3 stirrups with a yield stress of 53 ksi) crossing the interface. According to the test results, moments less than or equal to the ultimate flexural strength of the specimen do not reduce the shear transfer strength. Tension forces applied perpendicular to the shear plane reduce the shear transfer strength in the same way as reducing the amount of reinforcement perpendicular to the shear plane.

Mattock, Li and Wang (1976) investigated shear transfer strength between lightweight reinforced concrete surfaces through tests of sixty-six monolithic push-off specimens. The specimens were constructed from either all-lightweight concrete (using either coated rounded lightweight aggregate or crushed angular lightweight aggregate), sand-lightweight concrete (by replacing fine lightweight aggregate with natural sand), and normal-weight concrete (using gravel and natural sand). Those specimens were either precracked or uncracked along the interface. The compressive strength of the concrete varied from 2.5 to 6 ksi and different amounts of reinforcement (No. 3 stirrups with a yield stress of 50 ksi) were used across the interface. Ultimate measured shear strength was presented in terms of slip and as a function of ρf_y (the product of reinforcement ratio and reinforcement yield stress). For sand-lightweight and all-lightweight concrete, existence of a crack along the shear plane reduces the shear transfer strength by an almost constant amount for a given ρf_y value. For normal-weight concrete, however, the reduction of shear strength due to existence of a crack decreases continually as ρf_y increases. For precracked specimens with similar concrete compressive strengths and ρf_y , the shear transfer strength of specimens made with normal-weight concrete is around 20% larger than that of specimens with sand-lightweight concrete. The shear strength of specimens with sand-lightweight concrete is larger than that of specimens with all-lightweight concrete by a varied amount. The shear strength of lightweight concrete specimens, however, is not significantly influenced by the type of lightweight aggregate. Expressions for calculating the ultimate shear transfer strength were proposed for interfaces in all-lightweight and sand-lightweight concrete.

In their review of the literature, Santos and Júlio (2012) credit Loov (1978) as being the first to propose an equation to calculate shear strength between concrete interfaces that included concrete compressive strength as a variable. The equation credited to Loov is given as Eq. 2-3.

$$v_u = k \sqrt{(\rho f_y + \sigma_n) f'_c} \quad \text{Eq. 2-3}$$

Where: v_u is the ultimate shear stress, ρ is the reinforcement ratio, f_y is the yield stress of the transverse reinforcement, σ_n is the external normal stress applied at the interface, and k is a constant (0.5 for uncracked interfaces).

Walraven, Frenay and Pruijsser (1987) tested 88 push-off specimens in three different series. The first two series were aimed at investigating the influence of concrete compressive strength on the shear transfer strength, and the third series aimed to study effects of load history. All the specimens were precracked. The amount of reinforcement crossing the interface, in the form of closed hoops with a yield stress of either 66 or 79 ksi, was varied. Concrete compressive strength (3 to 11 ksi) and the product of reinforcement ratio and reinforcement yield stress were the main variables. For the first two series of tests, specimens were loaded pseudo-statically to failure. Eq. 2-4 was proposed based on test results and existing data. Like Eq. 2-3 proposed by Loov, Eq. 2-4 includes concrete compressive strength as a basic parameter.

$$v_{u,th} = C_3 (0.007 \rho_v f_y)^{C_4} (psi)$$

$$C_3 = 15.686 f'_{cc}{}^{0.406} \quad \text{Eq. 2-4}$$

$$C_4 = 0.0353 f'_{cc}{}^{0.30}$$

Where: $v_{u,th}$ is the shear transfer strength, ρ_v is the reinforcement ratio, f_y is the reinforcement yield stress, and f'_{cc} is the concrete compressive strength measured from 5.9 in. cubes ($f'_c \approx 0.85 f'_{cc}$).

For the third series of tests reported by Walraven, Frenay and Pruijsser (1987), both repeated loading and sustained loading tests were performed to study the influence of load history. Repeated loading consisted of a sinusoidal wave of 60 cycles per minute with an amplitude

alternating between zero and a maximum load, which varied between 46 and 66 percent of the static ultimate strength for each specimen. The number of load cycles varied between 193,725 and 769,400. After the repeated loading, the specimens were loaded monotonically to failure. For the sustained loading tests, each specimen was subjected to a load between 40 and 82 percent of the static ultimate strength for a period of time varying from 76 to 273 days. After that, each specimen was loaded monotonically to failure at an age that varied between 160 to 407 days. Load history was found to have an insignificant effect on the ultimate recorded shear transfer strength.

Hsu, Mau, and Chen (1987) proposed a theory to predict shear transfer strength between uncracked concrete interfaces. The model consists of a truss comprised of a series of inclined struts crossing the interface, where each strut is assigned constitutive properties appropriate for concrete in compression. It is assumed that a critical zone exists in the vicinity of the shear plane where shear stresses are distributed approximately uniformly when cracks form. In the critical zone, strains for the given stress condition can be obtained according to governing equations derived from the theory. This allows for a complete shear force-slip curve to be calculated, where the peak force represents the ultimate shear transfer strength of the connection. According to the theory, reinforcement located parallel to the interface can have a significant effect on the ultimate shear transfer strength; an effect that is neglected by design codes and standards.

Kahn and Mitchell (2002) tested 50 push-off specimens to study shear transfer between high-strength concrete (with concrete compressive strengths between 6.8 and 17.9 ksi). Two-leg stirrups made from Grade 60 No. 3 bars were used as shear reinforcement oriented perpendicular to the interface. The reinforcement ratio varied from 0.37 to 1.47 percent. Interfaces were either pre-cracked monolithic concrete, uncracked monolithic concrete, or uncracked cold joints. Equation 2-5 was proposed to calculate the shear strength of cold joints and uncracked interfaces.

$$v_u = 0.05f'_c + 1.4\rho_v f_y \leq 0.2f'_c \text{ (psi)} \quad \text{Eq. 2-5}$$

Where: ρ_v represents the shear reinforcement ratio, f_y ($\leq 60 \text{ ksi}$) is the yield stress of the reinforcement, and f'_c is the concrete compressive strength. The equation is based on results from tests of specimens with f'_c between 4 and 17.9 ksi. After peak, the test results showed that the

residual shear strength of the interfaces was similar among specimens with similar reinforcement configurations, regardless of interface type.

Mansur, Vinayagam, and Tan (2008) also investigated shear transfer behavior across a crack in reinforced high-strength concrete. Nineteen precracked push-off specimens with concrete compressive strengths varying between 5.8 and 15.4 ksi were tested monotonically. Clamping stress, provided by reinforcement and calculated as $\rho_v f_y$, was varied from 0.19 to 2.05 ksi. The test results showed that increases in either concrete strength or clamping stress increased the stiffness of the initial linear portion of the stress versus slip curve, ultimate strength, and deflection at peak strength. Equation 2-6 was proposed to calculate the ultimate shear transfer strength across a crack.

$$v_u = 0.566(\rho_v f_y f'_c)^{0.5} \quad \text{Eq. 2-6}$$

Where: ρ_v is the reinforcement ratio crossing the interface (area of steel divided by total interface area), f_y is the yield stress of reinforcement, and f'_c is the concrete compressive strength.

Zeno (2009) investigated the influence of high-strength steel on shear transfer between concrete surfaces. The study consisted of eight push-off specimens with cold joint interfaces that were roughened to an amplitude of at least $\frac{1}{4}$ in. The specified compressive strength of concrete used for both sides of the joint was 5 ksi. All specimens had three double-legged ties (either No. 3 or No. 4) crossing the interface. Two types of reinforcement were used across the interface: ASTM A615 (with a nominal yield stress of 60 ksi) and ASTM A1035 (with a nominal yield stress of 100 ksi). Strain gauges were attached to the reinforcement about 3 in. from the concrete interface. Applied load, interface slip, reinforcement strain, and crack width perpendicular to the interface were measured during testing. The results showed that shear friction capacity is mainly attributable to the concrete component, and steel strains develop only after significant cracking occurs. Recorded strains indicated that steel reinforcement crossing the interface never reached the specified yield stress, and thus use of high-strength reinforcement did not affect the shear strength. Based on the experimental data, Eq. 2-7 was proposed to calculate shear friction strength of reinforced concrete members.

Cold joint: $V_{ni} = 0.060A_{cv}f'_c + 0.0014A_{vf}E_s \leq 0.20A_{cv}f'_c$ Eq. 2-7a

Monolithic (uncracked): $V_{ni} = 0.075A_{cv}f'_c + 0.0014A_{vf}E_s \leq 0.20A_{cv}f'_c$ Eq. 2-7b

Monolithic (pre-cracked): $V_{ni} = 0.0014A_{vf}E_s \leq 0.20A_{cv}f'_c$ Eq. 2-7c

Where: V_{ni} is the shear friction strength, A_{cv} is the interface area, f'_c is the concrete compressive strength, A_{vf} is the cross-section area of reinforcement crossing the interface perpendicularly, and E_s is the elastic modulus of reinforcement.

2.1.2 Current Provisions for Horizontal Shear Transfer

Both ACI 318-14 (2014) and the 6th edition of the AASHTO LRFD Bridge Design Specification (2012) include equations to calculate the shear transfer strength between concrete interfaces when interface reinforcement crosses the shear plane. The provisions in ACI 318-14 for horizontal shear strength (shear friction) are summarized in Eq. 2-8, Table 2.1, and Table 2.2. These provisions apply to any reinforced concrete structures, except that special provisions, described later in Section 2.2.2, apply to composite action in flexural members.

$$V_n = \mu A_{vf} f_y \leq \text{upper limit (Table 2.1)} \quad \text{Eq. 2-8}$$

Where: V_n is the nominal shear strength, μ is a coefficient of friction representing the surface preparation at the interface (Table 2.2), A_{vf} is the area of reinforcement crossing perpendicular to the shear plane, A_c is area of the contact interface, and f_y is the reinforcement yield stress.

Table 2.1: Upper Limit for Eq. 2-8

Upper Limit	Surface Preparations
Least of $0.2f'_c A_c$, $480 (psi) + 0.08f'_c$, $1600(psi)A_c$	Monolithic and Cold joint with Rough Interface
Lesser of $0.2f'_c A_c$ and $800(psi)A_c$	Other Cases

Table 2.2: Coefficient of Friction for Eq. 2-8

Contact Surface Condition	Coefficient of friction, μ
Concrete placed monolithically	1.4
Concrete placed against hardened concrete that is clean, free of laitance, and intentionally roughened to a full amplitude of approximately 1/4 in.	1
Concrete placed against hardened concrete that is clean, free of laitance, and not intentionally roughened	0.6

The AASHTO Specification equation is given in Eq. 2-9. Values for μ , c , K_1 , and K_2 are given in Table 2.3.

$$V_{ni} = cA_{cv} + \mu(A_{vf}f_y + P_c) \leq \text{lesser of } K_1f'_cA_{cv} \text{ \& } K_2A_{cv} \quad \text{Eq. 2-9}$$

Where: V_{ni} (kip) is the nominal interface shear resistance, c is a cohesion factor, A_{cv} (in.²) is the area of concrete engaged in interface shear transfer, A_{vf} (in.²) is the area of shear reinforcement crossing perpendicular to the shear plane within A_{cv} , P_c is the permanent net compressive force normal to the shear plane (if any), K_1 is the fraction of concrete strength available to resist interface shear, and K_2 is the limiting interface shear resistance.

Table 2.3: Cohesion and Friction Factors for Eq. 2-9

Surface Preparation	Friction Factor, μ	Cohesion, c (ksi)	K_1 (ksi)	K_2 (ksi)
Cast-in-place concrete slab on clean concrete girder surfaces, free of laitance with surface roughened to an amplitude of 1/4 in.	1.0	0.28	0.23	1.8
Normal-weight concrete placed monolithically	1.4	0.40	0.25	1.5
Normal-weight concrete placed against a clean concrete surface, free of laitance, with surface intentionally roughened to an amplitude of 1/4 in.	1.0	0.24	0.25	1.5
Concrete placed against a clean concrete surface, free of laitance, but not intentionally roughened	0.6	0.075	0.50	0.80

Equation 2-8 is the same form as early horizontal shear strength equations, such as that given in Eq. 2-1. Equations of this form attribute all horizontal shear strength to the reinforcement crossing the shear plane. The AASHTO Specification equation, Eq. 2-9, includes terms representing contributions to strength from adhesion (or cohesion) and reinforcement crossing the interface. The form of Eq. 2-9 is consistent with equations proposed by Mattock (1976), Kahn and Mitchell (2002) and Zeno (2009), among others, for calculating the first-peak shear strength of an interface. Although neither Eqs. 2-8 nor 2-9 include f'_c as a variable, both have upper limits that are a function of f'_c , consistent with findings from Hofbeck, Ibrahim, and Mattock (1969).

The fib Model Code for Concrete Structures (2010) also provides equations to estimate interface shear strength between concrete cast at different times (Eq. 2-10).

$$\tau_{Rdl} = c_a f_{ctd} + \mu \sigma_n \leq 0.5 \nu f_{cd} \quad \text{Eq. 2-10a}$$

$$\tau_{Rdl} = c_r f_{ck}^{1/3} + \mu \sigma_n + \kappa_1 \rho f_{yd} (\mu \sin \alpha + \cos \alpha) + \kappa_2 \rho \sqrt{f_{yd} f_{cd}} \leq \beta_c \nu f_{cd} \quad \text{Eq. 2-10b}$$

Where: τ_{Rdl} is the interface shear strength, c_a is a coefficient for adhesive bond (Table 2.4), f_{ctd} is the design value for concrete tensile strength, μ is a friction coefficient (Table 2.4), σ_n is the lowest expected compressive stress resulting from an eventual normal force acting on the interface, ν is an effectiveness factor for the concrete which equals $0.55(30/f_{ck})^{1/3}$, f_{cd} is the specified cylinder compressive strength of concrete, c_r is a coefficient for aggregate interlock effects at rough interfaces (Table 2.4), f_{ck} is the characteristic value of cylinder compressive strength of concrete, κ_1 is an interaction coefficient for tensile force activated in the reinforcement or dowels (Table 2.4), ρ is the reinforcement ratio of the reinforcing steel crossing the interface, f_{yd} is the specified yield stress of non-prestressing reinforcement crossing the interface, α is the inclination of reinforcement crossing the interface, κ_2 is an interaction coefficient for flexural resistance (Table 2.4), and β_c is a coefficient for the strength of the compression strut (Table 2.4).

Eq. 2-10a is used for interfaces without reinforcement and Eq. 2-10b is used for interfaces intersected by dowels and reinforcement. Eq. 2-10b includes the contribution of dowel action (the last term), which is not included in ACI or AASHTO.

Table 2.4: Coefficients for Eq. 2-10

Surface Roughness	c_a	c_r	κ_1	κ_2	β_c	μ	
						$f_{ck} \geq 20$	$f_{ck} \geq 35$
Very rough $R_t \geq 3.0$ mm ^a	0.5	0.2	0.5	0.9	0.5	0.8	1
Rough $R_t \geq 1.5$ mm	0.4	0.1	0.5	0.9	0.5	0.7	
Smooth	0.2	0	0.5	1.1	0.4	0.6	
Very Smooth	0.025	0	0	1.5	0.3	0.5	

^a R_t is the surface roughness derived from the sand patch method

2.1.3 Summary and Insights

In previous studies, the influence on interfacial shear strength of crack conditions (cracked versus uncracked), surface roughness, reinforcement ratio, and concrete compressive strength have been most extensively investigated. Through these studies, multiple approaches have been proposed for calculation of the maximum shear strength. Several researchers have also aimed to identify a critical slip value associated with a composite interface shear failure.

However, the following parameters have not been extensively studied:

- **Interface Stiffness:** Very limited work has been done to characterize interface shear transfer in terms of the initial stiffness of the shear stress-slip relationship. The stiffness of this stress-slip relationship may be an important factor governing the distribution of slip along the length of a girder-to-concrete deck interface.
- **Alternative Interface Surface Preparations:** Although surface roughness and bond conditions have been shown to be key factors governing the horizontal shear strength of an interface, most studies have considered only either fully roughened or smooth surface conditions. The combination of partially roughened and partially smooth surfaces has not been tested. Likewise, the behavior of cold joint interfaces pre-treated with bond breakers has been seldom studied.

- **High-Strength Interface Reinforcement:** The yield stress is limited in design to 60 ksi due largely to lack of data, because most push-off tests have been conducted using normal strength steel (f_y less or equal to 60 ksi) as dowel reinforcement. One study (Zeno 2009) showed that use of higher strength reinforcement is not effective at increasing interface shear strength, but the findings have not been repeated.
- **Headed Dowel Reinforcing Bars:** No research has evaluated whether reinforcement crossing the interface can be effectively anchored using headed reinforcing bars; a detail that may simplify future deck removal as it eliminates interference from the tail of the hook.
- **Cold Joints with Different Concrete Strengths:** Prestressed concrete girders are often constructed using concrete with a much higher concrete compressive strength than the cast-in-place concrete decks (8,000 psi versus 4,000 psi is common, per Terry Fleck of Coreslab Structures, personal communication, 2015). Most cold joint push-off tests, however, have been conducted on specimens constructed of two layers of the same concrete mixture.

2.2 Composite Behavior of Large-Scale Girders

Large-scale girder tests have also been performed to investigate shear transfer behavior at concrete-to-concrete interfaces. Most specimens have consisted of a precast concrete girder with a cast-in-place concrete deck. The connection surfaces have typically been either roughened or smooth, and most specimens have had reinforcing bars protruding into the deck. The specimens have typically been simply supported with a monotonically applied load at midspan. Interface shear stress is typically approximated using Eq. 2-11.

$$v = \frac{VQ}{Ib} \quad \text{Eq. 2-11}$$

Where: v is the shear stress, V is the internal shear force, Q is the first moment of the area above the interface, taken about the centroid of the section, I is the moment of inertia of the transformed composite section, and b is the beam width. Findings from key studies are presented below.

2.2.1 Findings from Previous Large-Scale Girder Tests

In addition to push-off tests, Hanson (1960) reported results from tests of ten T-shaped composite girders designed to study the effectiveness of different details at transferring horizontal shear across the interface between precast and cast-in-place concrete. Primary variables were adhesive bond, surface roughness (either smooth or rough), and amount of reinforcement crossing the interface (ratio of reinforcement varied from 0 to 0.46 percent). Specimens with a debonded interface were prepared by applying a silicone compound over the top surface of the precast girder to prevent formation of bond with the cast-in-place deck. Concrete used for the slab and girder had specified compressive strengths of 3 and 5 ksi, respectively. The ASTM A305-compliant No. 3 stirrups that crossed the interface had a yield stress of 50 ksi. The specimens were designed so that composite shear failure would occur before flexural failure. Dimensions and tensile reinforcement in the precast girders were held constant, except that specimens in the second series had a smaller contact area between the precast and cast-in-place concrete (achieved by creating a 4 in. by ½ in. void between the deck and top of the girders). The girders were tested under monotonically increasing point loads (two-point loads for series one and three-point loads for series two) located near midspan until failure, which was characterized by debonding along the beam-slab interface by design. Midspan deflection and slip between the girder and deck at several locations were recorded throughout the tests. These measurements were used to characterize composite action throughout the tests. Interface shear stress was calculated using Eq. 2-11. During testing, the initial and maximum slip both occurred near the quarter-point of the girder span. The results showed that a slip of approximately 0.005 in. was a critical value beyond which bond between the interfaces quickly deteriorated. Shear stress versus slip curves derived from the girder test results were similar to those from push-off tests.

Seamann and Washa (1964) tested 42 composite beams to investigate the effects of several parameters on the horizontal shear strength between precast concrete girders and cast-in-place concrete slabs. Girders with three different span lengths (8, 11 and 20 ft) were tested. The same strength of concrete was used for both girder and slab parts of each specimen. The primary variables were roughness of the contact interface (smooth, intermediate, and rough), reinforcement ratio of bars crossing the interface (varied from 0.0 to 1.07 percent), shear span length (3, 4.5 and

9 ft), shear keys, position of the joint with respect to the neutral axis, and concrete compressive strength (3, 4.5, and 5.5 ksi). The intermediate finish (1/8 in. depression) was prepared by brushing out the mortar between pieces of coarse aggregate and the rough finish (3/8 in. depression) was prepared by removing particles of coarse aggregate with a board having protruding nails. For testing, two point loads (12 in. on either side of midspan) were applied monotonically until failure. Midspan deflection, slip between the beam and slab, and concrete strain along the member depth at midspan were measured. Three failure types were observed: flexural tension, interface shear, and a combination of the two. Test results indicated that shear strength increased as the contact surface roughness increased from smooth to intermediate, and specimens with intermediate roughness had a similar shear strength as beams with keys. Ultimate shear strength increased as the ratio of shear span to effective depth decreased. Equation 2-12 was proposed for calculating horizontal shear strength.

$$Y = \frac{2700}{X+5} + 300P\left(\frac{33-X}{X^2+6X+5}\right) \quad \text{Eq. 2-12}$$

Where: Y is the ultimate shear strength, X is the ratio of shear span to effective depth, and P is the reinforcement ratio for steel crossing the joint.

Following the quasi-static composite beam tests by Seamann and Washa (1964), Badoux and Hulsbos (1967) performed tests of 29 composite beams to investigate the effect of repeated loading on horizontal shear strength. The test series included 26 small-sized beams and three full-sized box girders. The primary variables were the amount of joint reinforcement (0.0 to 0.52 percent except for full sized beams which had 0.05 percent), ratio of shear span to effective beam depth (2.6 to 7.7), and joint roughness. Intermediate and rough interface preparations were considered; these were prepared the same way as in Seamann and Washa (1964). Testing was conducted under simply supported conditions with two point loads applied near midspan (located symmetrically either 12 or 30 in. on either side of midspan). Before doing the fatigue test, the specimens were loaded statically to the maximum load to be used for fatigue test. The same static test was performed ten times at regular intervals during the fatigue loading. For the fatigue testing,

a sinusoidal cyclic load was applied at a rate of 250 cycles per minute until either failure occurred or two million cycles was reached, whichever came first. The amplitudes of the sinusoidal loads varied among the specimens based on results from monotonic strength tests, with a maximum fatigue load of approximately 70 percent of the static strength for each specimen and minimum fatigue load of approximately 20 percent of maximum fatigue load (or about 15% of the static strength). Midspan deflection, strain distributions along beam depth at midspan, and slip between the slab and beam were measured. Joint failure, as identified based on relative slip along the interface, joint cracking, and beam deflection, occurred in 19 specimens. The 10 specimens subjected to two million cycles without exhibiting joint failure were subsequently loaded quasi-statically until failure. Joint fatigue strength was conservatively assumed to be the maximum horizontal shear imposed on specimens that did not fail at the joint during the fatigue loading. Roughening the interface was beneficial to fatigue strength, as rough joints were much stronger than intermediate joints. Joint fatigue strength was found to be related to the amount of joint reinforcement and slightly influenced by shear span to effective depth ratio. Eq. 2-13 was proposed to calculate a conservative estimate of allowable stress for horizontal shear in composite members under fatigue loadings.

$$\text{Intermediate:} \quad v = \frac{2000}{11 + \frac{a}{d}} + 200\rho \quad \text{Eq. 2-13a}$$

$$\text{Rough:} \quad v = \frac{3500}{11 + \frac{a}{d}} + 200\rho \quad \text{Eq. 2-13b}$$

Where: v is the allowable shear stress under fatigue load, ρ is the reinforcement ratio across the interface, and a/d is the ratio of shear span-to-effective depth. During testing, joint cracking with a resulting loss of composite action initiated at about two-thirds of the shear span measured from the support due to diagonal tension cracking of the precast beam that progressed towards the load points. It appears that the loss of composite action was initiated by a shear failure.

Chung and Chung (1976) tested 18 prestressed concrete composite T-beams in four series to investigate the effect of repeated loading on the horizontal shear performance between precast

concrete girders and cast-in-place concrete decks. The amount of reinforcement crossing the interface (reinforcement ratio varied from 0 to 0.3 percent) and intensity of the repeated load were the main variables. The compressive strength of the concrete in the girder and deck were 6.0 and 4.4 ksi respectively. The joint interface was roughened such that the coarse aggregate was exposed. An aluminum strip (1½ in. wide) was placed in the middle of the interface to reduce the contact area. Specimens were simply supported and loaded near midspan with two point loads (applied 12 in. on either side of midspan). For each series of specimens, one specimen was first loaded quasi-statically to failure to determine the strength of the interface before the rest were loaded under repeated cycles. Specimens tested under repeated load were subjected to one million cycles at a rate of 240 cycles per minute. The maximum amplitude of the load cycles load varied from 45 to 70 percent of static ultimate strength, while the minimum amplitude of the load cycles was kept constant at 10 percent of ultimate strength. Slip between the girder and the deck was measured during testing along with midspan deflection. For specimens that did not fail during the fatigue loading, a quasi-static flexural test was performed to failure. Test results showed the fatigue strength of rough bonded interfaces is greater than 55 percent of the static strength and 0.001 in. is a critical slip value beyond which composite action deteriorates quickly. Specimens subjected to 1 million cycles of repeated load to an amplitude less than that required to cause a fatigue failure exhibited no reduction in horizontal shear strength when loaded quasi-statically to failure.

Loov and Patnaik (1994) reported results from tests of 16 composite concrete T-beams designed to study the effects on horizontal shear strength of reinforcement crossing the shear plane ($\rho_v f_y$ varied from 59 to 1,120 psi) and concrete compressive strength (varied from 5 to 7 ksi). The same strength of concrete was used for both deck and beam parts. Interface shear reinforcement consisted of No. 3 bars with a yield stress of 60 ksi. The interface preparation was left as-cast with coarse aggregate protruding from the surface, instead of a rough surface with an amplitude of 0.25 in. For testing, a point load was applied monotonically at midspan until failure occurred. Slip between deck and girder as well as strain of transverse reinforcement at the level of the interface were recorded at regular load intervals. Horizontal shear stresses were calculated using Eq. 2-11. Based on the results, Eq. 2-14 was proposed for calculating the horizontal shear strength of an interface.

$$v_n = k\lambda\sqrt{(0.1 + \rho_v f_y)} \leq 0.25f'_c \text{ (psi)} \quad \text{Eq. 2-14}$$

Where: k is a constant for different surface conditions, λ is a constant used to account for the effect of concrete density, ρ_v is the transverse reinforcement ratio, f_y is the yield stress of the reinforcing bars, and f'_c is the concrete compressive strength. According to the tests, the “left-as-cast” interface has a shear strength similar to that of a roughened surface. The results also showed that slip and transverse reinforcement stresses were insignificant until horizontal shear stresses of approximately 220 to 290 psi were imposed. Stirrups were most effective when located further from midspan, except for the region near the support.

Patnaik (2001) tested 24 composite beams with smooth interfaces to study the effects of concrete compressive strength (2.5 to 5 ksi), effective depth-to-tie spacing ratio (0.7 to 2.8), and clamping stress (44 to 522 psi). Both rectangular-shaped and T-shaped specimens were tested. The yield stress for shear reinforcement was varied from 50 to 100 ksi. For a given specimen, all concrete had the same compressive strength. A monotonically increased concentrated load was applied at midspan for testing of the specimens. Slip between beam and deck (measured at deck end) as well as deflection (at midspan and quarter-span) were recorded. The test results showed that concrete strength and ratio of effective depth-to-tie spacing ratio do not have an effect on the horizontal shear strength across a smooth interface. As expected, large slip at the flange ends was observed when composite action was lost. Based on current and previous test results, Eq. 2-15 was proposed for calculating the horizontal shear strength of composite beams with a smooth interface.

$$v_u = 0.6 + \rho_{vf} f_{yf} \leq 0.2f'_c \text{ and } 800 \text{ psi} \quad \text{Eq. 2-15a}$$

$$v_u = 0 \quad \text{for } \rho_{vf} f_{yf} < 51 \text{ psi} \quad \text{Eq. 2-15b}$$

Where: f_{yf} is the yield stress of the reinforcement, ρ_{vf} is the reinforcement ratio, and f'_c is the concrete compressive strength.

Kahn and Slapkus (2004) tested six composite T-beams to study the interface shear strength of joints in high-strength concrete (7 to 12 ksi) and to evaluate whether provisions for horizontal shear strength in the AASHTO Specification and ACI 318 are applicable to such members. The T-

beams were similar to those tested by Loov and Patnaik (1994), which were constructed with normal-strength concrete (5 to 7 ksi). The precast beams were cast using concrete with a compressive strength of 12 ksi, and the flanges were cast with concrete having a compressive strength of either 7 or 11 ksi (three specimens each). Different amounts of No. 3 stirrups (Grade 60 and conforming to ASTM A617/A617M, which was withdrawn in 1999) were placed across the interface. The top surface of the precast beam was left as-cast, like in the Loov and Patnaik (1994) tests, and the transverse reinforcement ratio across the joint was varied (from 0.19 to 0.37 percent). Two monotonically increased point loads were applied symmetrically about midspan (4.5 in. from midspan) until the specimens failed either in interface shear or flexural failure (concrete crushing). Interface shear stresses were calculated using the global force equilibrium equation (total force in longitudinal reinforcement divided by the interface area). Test results were compared with values calculated using existing equations in codes and standards. According to the analysis, equations in the AASHTO Specification and ACI 318 can be applied to concrete with a compressive strength up to 11 ksi. The results showed that interface shear strength depends not only on clamping stress but also on concrete compressive strength.

Kovach and Naito (2008) performed tests of 41 girders to investigate the horizontal shear strength of composite concrete beams without horizontal shear reinforcement. Interface roughness and the compressive strength of the cast-in-place deck were the main variables. Concrete compressive strengths used for the cast-in-place deck were either 3 or 6 ksi while that for the precast girder was 8 ksi. Five surface preparation methods were used: smooth, as-placed roughness, rough broom finish, ¼ in. rake finish, and sheepsfoot void. For testing, point loads were applied monotonically near midspan to failure. Midspan deflection, slip along the interface, and strain along flange depth were recorded. It was found that interface roughness has a pronounced effect on the horizontal shear capacity of composite sections without reinforcement crossing the shear plane. The influence on shear strength of deck concrete compressive strength was found to be inconclusive. The peak horizontal shear stress imposed in the tests ranged from 475 to 1000 psi; much higher than the ACI Code limit of 80 psi for composite sections without interface reinforcement. It was also found that a decrease of composite action may occur due to differential

shrinkage if the time period between placement of the concrete deck and the precast web is relatively large.

2.2.2 Provisions for Horizontal Shear Transfer in Composite Concrete Flexural Members

ACI 318-14 (2014) includes separate provisions regarding horizontal shear transfer strength calculation for composite concrete flexural members.

When factored shear horizontal force $V_u \leq \Phi(500b_v d)$, nominal horizontal shear strength V_{nh} should be calculated according to Table 2.5. When $V_u \geq \Phi(500b_v d)$, V_{nh} should be calculated according to provisions for shear friction in ACI 318-14 (Eq. 2-8, Table 2.1, and Table 2.2).

Table 2.5: Nominal Horizontal Shear Strength

Shear Transfer Reinforcement	Contact Surface Preparation	V_{nh} , lb	
$A_v \geq A_{v,min}$	Concrete placed against hardened concrete intentionally roughened to a full amplitude of approximately 1/4 in.	Lesser of :	$\lambda(260 + 0.6 \frac{A_v f_{yt}}{b_v s})b_v d$ $500b_v d$
	Concrete placed against hardened concrete not intentionally roughened		$80b_v d$
Other cases	Concrete placed against hardened concrete intentionally roughened		$80b_v d$

Where: Φ is a strength reduction factor of 0.75, A_v is the area of shear reinforcement within spacing s , $A_{v,min}$ is the minimum area of shear reinforcement within spacing s (the larger of $0.75\sqrt{f'_c} b_w s / f_y$ and $50 b_w s / f_y$), b_v is the width of the contact surface, b_w is girder web width, d is the distance from the extreme compression fiber for the entire composite section to the centroid of prestressed and nonprestressed longitudinal reinforcement, f_{yt} is the specified yield strength of the transverse reinforcement, and λ is a modification factor to reflect the reduced mechanical properties of lightweight concrete relative to normalweight concrete of the same compressive strength.

2.2.3 Summary and Insights

Most previous tests of composite bridge girders that were designed to study horizontal shear strength have been simply supported beams loaded monotonically near midspan to failure. However, actual bridges are subjected to daily traffic loads that are better represented by fatigue testing. Furthermore, the author is aware of no tests of composite girders conducted on specimens after the deck has been removed and then re-cast, a condition that frequently exists in practice. Finally, the influence of a partially debonded interface on horizontal shear transfer has not been investigated thoroughly, even though a few composite bridge girder specimens have included a partially debonded interface. There is a need to study whether such a detail compromises the fatigue life of the composite system.

2.3 Concrete Deck Removal

The procedures required for bridge deck removal differ depending on whether the portion of the deck being considered is located between girders or over a girder. Removal of deck parts between girders is mainly done by first saw-cutting longitudinally through the thickness of the deck alongside the tips of the girder flanges, and then lifting the saw-cut concrete to the ground. This process is relatively fast. Removal of deck concrete over girders is more time-consuming and tedious due to the connection between the deck and girders and the desire to protect the girders for reuse. Although different equipment and techniques are available for deck removal over girders, the presence of wide and thin top girder flanges (characteristic of NU I-Girders, see Figure 1.1) introduces challenges. Not only is the contact area between the girder and deck significantly larger than for other girder types, many deck removal methods are not suitable for use over wide and thin top girder flanges if damage is to be minimized.

2.3.1 Kansas and Nebraska State Requirements

The Standard Specifications for State of Road & Bridge Construction of the Kansas Department of Transportation (2015) has special requirements limiting the means and methods employed for bridge deck removal. The depth of saw cutting is to be limited to a maximum depth

of three inches directly above any girder and within three inches of the edge of a girder top flange. Use of drop-type pavement breakers is forbidden. Hoe rams are not to be used directly above any girder or within one foot of either edge of a girder top flange. For removing concrete near and above the top flange of a girder, only jackhammers no heavier than 15 pounds are allowed. The Bridge Office Policies and Procedure Manual of the Nebraska Department of Roads (2004) has similar requirements regarding use of jackhammers for deck removal over girders. When used along the edge of a girder flange and oriented no more than 45 degrees from horizontal, jackhammers are limited to 15 lb. For use in other areas of the bridge, jackhammers up to 30 lb are permitted. When I-girders with wide top flanges are used, bridge owners often require an 8 in. wide strip of smooth-sealed surface along the edges of top flanges to prevent possible damage of the thin flange tips.

2.3.2 Previous Studies

Vorster et al. (1992) investigated partial removal of concrete from the deck and other parts of bridge structures. Their recommendations indicate that methods of concrete removal will be determined by three main factors: area of concrete to be removed, location of concrete to be removed, and depth of concrete removal required. In terms of removal depth, the methods can be classified as: 1) For surface removal of less than ½ in, scabbling, planning, sand blasting, and shot blasting are preferred, 2) For removing cover concrete to a depth less than the clear cover to the steel, the recommended method is concrete milling, 3) For removing concrete to a depth greater than the depth of reinforcement without damaging reinforcing steel, methods include pneumatic breakers and hydro-demolition, and 4) For removal of core concrete, recommended methods include sawing and lancing.

Use of pneumatic breakers is described in detail in the Vorster et al. (1992) report. Due to their light weight and excellent maneuverability, hand-held pneumatic breakers are widely used and are well established tools for removing contaminated and deteriorated concrete from small, isolated areas and from vertical and overhead surfaces on bridges. Hand-held breakers can be powered by several energy sources including pneumatic pressure, hydraulic pressure, a gasoline

engine, and an electric motor. Use of pneumatic breakers powered by pneumatic pressure is more effective and economical than use of breakers powered by other energy sources when used to remove deteriorated or contaminated concrete. Breakers are classified by the weight (ranging from under 20 lb to under 100 lb). Pneumatic breakers are easily transportable and can be operated in limited space where large equipment cannot be used. For concrete removal around reinforcement of bridge components, use of breakers is the primary method. However, this method is labor-intensive and sensitive to cost and availability of labor.

Kamel (1996) proposed a concrete girder-to-deck connection system to facilitate deck replacement and provide sufficient strength for full composite action. The proposed connection detail consisted of an unbonded interface with formed shear keys protruding from the top surface of the girder as illustrated in Figure 2.3. U-shaped epoxy-coated shear connector bars, separate from girder vertical shear reinforcement, extended 6 in. into the concrete deck from the girder. In the study, both push-off tests and full-scale girder tests were performed. Different surface preparations (smooth, rough, and shear key), steel connectors (using 100 ksi high-strength threaded bars or Grade 60 normal-strength reinforcing bars), and bond condition were the main variables.

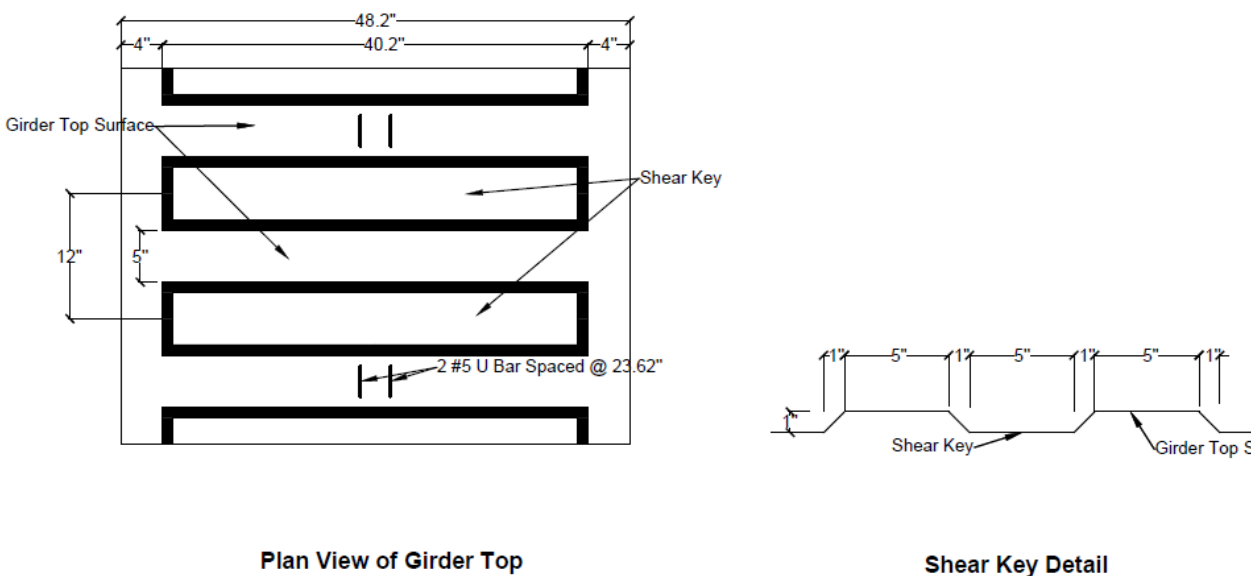


Figure 2.3: Connection Detail

To ensure an unbonded interface, a debonding sealant was applied to the top flange prior to casting of the deck concrete. In addition, deck removal was performed using a 60 pound pneumatic jackhammer on one series of push-off specimens to evaluate the effectiveness of the various surface preparation methods at facilitating deck removal. It was reported that debonding the interface facilitated deck removal and that the main difficulty was in clearing the concrete from around the reinforcement that crossed the interface. Damage to shear keys was observed as a result of the deck removal process. Test results showed that beams designed with the proposed unbonded shear key interface perform similar in terms of flexural and shear behavior to beams with a conventional bonded rough interface.

Tadros and Baishya (1998) conducted an extensive review of existing rapid bridge-deck replacement methods and explored new superstructure designs aimed at facilitating future rapid deck replacement. The study focused on three main areas: 1. Procedures and equipment used for demolition; 2. Details and design of alternative deck systems; and 3. Details for connecting concrete decks to the underlying concrete or steel girders. According to nationwide surveys and interviews, the most common equipment used for removing concrete included boom-mounted breakers, saws, and hand-held hammers. Damage-types that commonly resulted from deck removal include: saw-cuts and microcracks on the top surface of concrete girders, saw-cuts into the top flanges of steel girders, and spalling/buckling of top flanges of concrete and steel girders due to impact from rig-mounted breakers. The researchers investigated the use of modular deck systems, deck surface protection methods, alternative shear connector types, and pretensioning or post-tensioning in decks. Although the study was wide in scope, only one connection detail was considered for joining cast-in-place reinforced concrete decks and precast concrete girders: the same debonded shear key system proposed by Kamel (1996).

Two deck removal methods were reported by Tadros and Baishya (1998) to have been performed on a steel girder using the combination of saw-cutting, jack-hammering and crane-removal. The same transverse cut was used for both methods. The first method had only one longitudinal cut along one side of the stud line. Electric jackhammers (60 lb) were used to break concrete around studs before the large pieces were removed by crane. The second method had additional longitudinal cuts along the other side of the stud line; a 10 lb sledgehammer was used

to break the concrete strip between the studs. The remaining concrete was removed by crane after being broken free of the studs. The second method took considerably less effort than the first.

Assad and Morcouc (2014) investigated the efficacy and impact on structural performance of different deck removal methods performed on precast prestressed girders with wide and thin top flanges. The trials were conducted on two NU I-girders that were to be removed from service and demolished by the Nebraska Department of Transportation. Both saw-cutting and jackhammering were performed on concrete decks between girders and on top of girders. To study the performance of the girder deck system after deck removal, reinforced concrete decks were again cast onto the two NU I-Girders after deck removal was completed, and the composite beams were then tested in flexure. According to the investigation, saw-cutting, jackhammering and hydro-demolition are the most common methods of deck removal for re-decking. From the investigation, debonding of the outermost 8 in. of the top flange is effective for aiding the removal of decks between girders without damaging the top flanges. The width is suggested to be extended to at least 12 in. for NU I-girders to minimize time for jackhammering. For deck removal above the girder, saw-cutting outside the line of shear connectors and then jackhammering the remaining concrete is suggested for existing bridges. A 60 lb jackhammer is recommended for use down to the level of the shear connectors, followed by a 30 lb jackhammer for the concrete below the shear connectors.

2.3.3 Summary and Insights

Prior work has indicated that a combination of jackhammering and saw-cutting is suitable for removal of concrete decks over girders, especially when minimal damage of the supporting beams is required. This technique has been tested on NU I-Girders and has gained acceptance in practice. As for connection details, there is currently only one system (debonded shear keys) that has been proven to facilitate future deck removal for NU I-Girders. However, the special forms required to produce the shear key system will increase the total fabrication cost and will lead to even thinner top flanges. In addition, the preparation process is complicated. A simple connection detail that facilitates future concrete deck removal and ensures good composite action is still required.

Chapter 3: Push-off Tests

Small scale tests, referred to as push-off tests, were conducted to investigate the influence of several variables on horizontal shear transfer between precast and cast-in-place concrete surfaces.

3.1 Experimental Program

3.1.1 Push-off Specimens

Push-off specimen dimensions and reinforcement layouts are shown in Figure 3.1. Each specimen was composed of two antisymmetric L-shaped parts connected across a 12 in. long interface that was either 12 or 24 in. wide, depending on the specimen. The bottommost L-section, which was cast first using 7 ksi concrete, was meant to represent the top flange of a precast concrete bridge girder. The topmost L-section represented the cast-in-place concrete deck. This section was cast several days after the first using 4 ksi concrete. A pair of 1.5 in. wide gaps were formed between the two concrete parts above and below the 12 in. long interface.

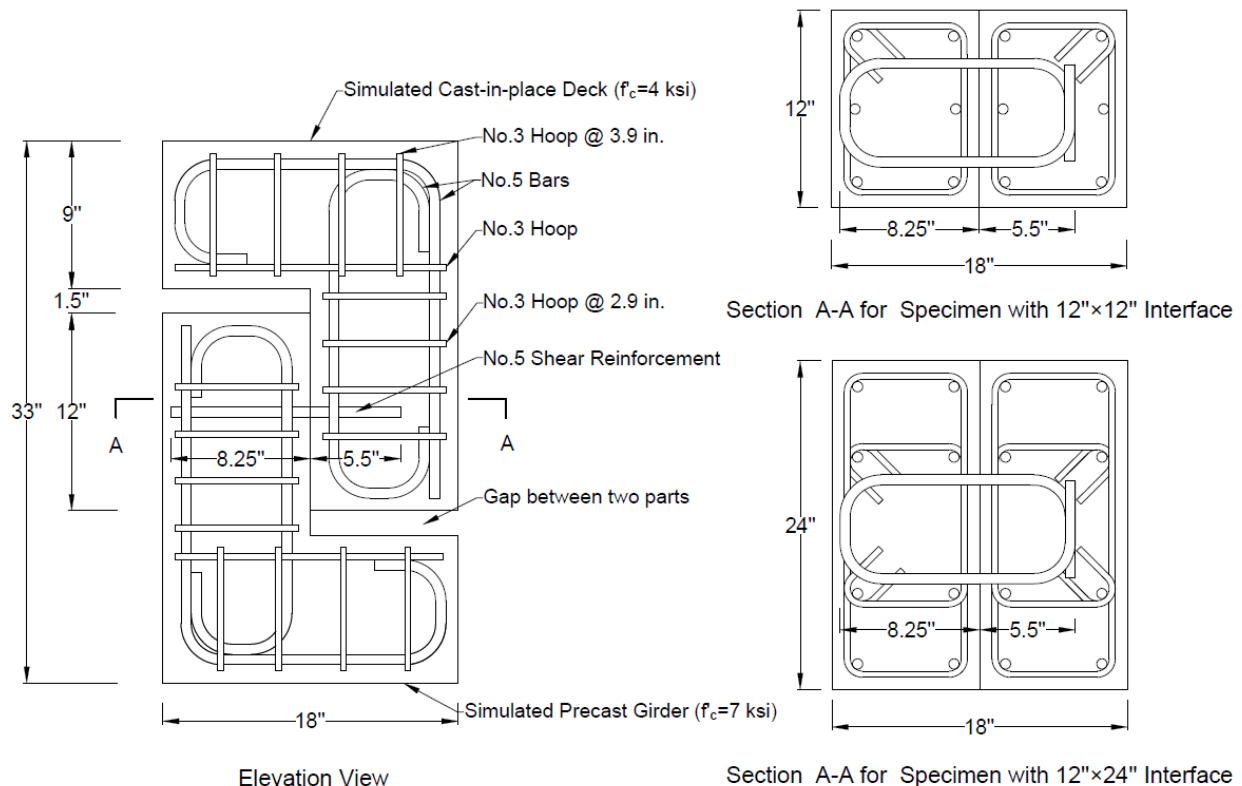


Figure 3.1: Push-off Specimen Detail

The specimens were reinforced as shown in Figure 3.1. The reinforcement layout used in both L-shaped sections was designed to prevent failure of the L-shaped sections prior to slip along the 12 in. long interface. For each specimen, either one or two pairs of No. 5 bars were placed across the interface to act as horizontal shear reinforcement. This interface shear reinforcement, which consisted of either hooked or headed bars, was placed perpendicular to the interface near its centroid. For specimens with two pairs of No. 5 bars, a spacing between pairs of 6 in. was used.

Table 3.1: Summary of Push-off Specimens

Specimen ID ^a	Surface Preparation	Bond Breaker	Interface Area (in. ²)	Shear Reinforcement Area (in. ²)	Shear Reinforcement Ratio ^b	Deck Concrete Mixture ^c
R-12-NB-12-NR	Rough ^d	NA	144	0.62	0.0043	4 ksi-2
R-12-NB-6-NR	Rough	NA	144	1.24	0.0086	4 ksi-2
R-12-NB-12-HR	Rough	NA	144	0.62	0.0043	4 ksi-2
R-24-NB-12-NR	Rough	NA	288	0.62	0.0022	4 ksi-1
R-24-NB-12-HB	Rough	NA	288	0.62	0.0022	4 ksi-2
T-12-NB-12-NR	Troweled	NA	144	0.62	0.0043	4 ksi-1
T-12-F-12-NR	Troweled	Felt	144	0.62	0.0043	4 ksi-1
T-12-E-12-NR	Troweled	Epoxy	144	0.62	0.0043	4 ksi-1
T-12-NB-6-NR	Troweled	NA	144	1.24	0.0086	4 ksi-2
T-12-NB-12-HR	Troweled	NA	144	0.62	0.0043	4 ksi-2
T-24-F-12-NR	Troweled	Felt	288	0.62	0.0022	4 ksi-1
T-24-NB-12-HB	Troweled	NA	288	0.62	0.0022	4 ksi-2
RM-12-F-12-NR	Rough Middle ^e	Felt	144	0.62	0.0043	4 ksi-1
RM-12-E-12-NR	Rough Middle ^e	Epoxy	144	0.62	0.0043	4 ksi-1
RM-12-F-6-NR	Rough Middle ^e	Felt	144	1.24	0.0086	4 ksi-2
RM-24-F-12-NR	Rough Middle ^f	Felt	288	0.62	0.0022	4 ksi-2

^a Specimen ID consists of five terms: first term = surface preparation (R is rough, T is troweled, RM is rough middle); second term = specimen width (12 or 24 in.); third term = bond breaker (NB is no bond breaker, F is roofing felt, E is epoxy); fourth term = shear reinforcement spacing (12 in. spacing represents one pair of No. 5 bars and 6 in. represents two pairs of No. 5 bars); and fifth term = reinforcement parameters (NR is normal-strength hooked reinforcement, HR is high-strength hooked reinforcement, HB is high-strength headed reinforcement)

^b Area of reinforcement perpendicular to the interface divided by the interface area

^c Two concrete mixtures were used for deck casting. More details in Section 3.1.2

^d Orthogonal dents with an amplitude of approximately ¼ in. were made over the whole interface at regular intervals

^e The middle 6 in. of the interface was roughened while the remainder of the interface was troweled smooth. Bond breakers were applied to the troweled portion of the interface

^f The middle 8 in. of the interface was roughened while the remainder of the interface was troweled smooth. Bond breakers were applied to the troweled portion of the interface

The sixteen push-off specimens included in this study are summarized in Table 3.1. The specimen names include references to the major variables considered in this study, following the convention described in the first footnote to Table 3.1. For the push-off specimens, the primary variables included surface preparation of the base (7 ksi) concrete, use of debonding agents at the interface, and horizontal shear reinforcement properties. Three surface preparation methods were considered: rough, troweled (smooth), and rough middle, wherein the middle 6 in. or 12 in. of the interface was roughened and the remainder of the interface was troweled smooth. Two debonding agents were considered: epoxy, which was applied to the base concrete after initial set and again prior to placement of the second layer, and roofing felt (detailed information about the bond breakers is provided in Section 3.1.2). The debonding agents were always applied over concrete that had been troweled smooth (for rough middle specimens with a debonding agent, the debonding agent was only applied to the troweled portion). Other variables included horizontal shear reinforcement anchorage type (hooked or headed), yield strength (Grade 60 or Grade 120), and area.

3.1.2 Materials

Concrete mixture proportions used for the push-off specimens are listed in Table 3.2 (details regarding mixture constituents are in the Table 3.2 footnotes). In each specimen, the concrete used to cast one L-shaped portion had a specified compressive strength of 7 ksi to simulate a precast concrete bridge girder. The other portion was cast using concrete with a specified compressive strength of 4 ksi to simulate a bridge deck. Push-off tests were conducted in two series with different mixture proportions for the 4 ksi concrete used in each series (referred to as 4 ksi-1 and 4 ksi-2). The change in mixture proportions was not expected to affect specimen behavior.

For each concrete placement, 4 by 8 in. concrete cylinders and 6 by 6 by 20 in. concrete prisms were cast to allow for measurement of the concrete compressive strength and modulus of rupture. These cylinders and prisms were stored beside, and cured in the same way as, the push-off specimens. The mean concrete strengths measured 28 days after casting and on the day of testing are summarized in Table 3.3. The cylinders were tested in accordance with ASTM

C39/C39M – 12a and the prisms were tested under four-point bending in accordance with ASTM C78/C78M – 16. Detailed results are provided in Appendix A.

Table 3.2: Mixture Proportions per yd³ (SSD)

Content	4 ksi-1	4 ksi-2	7 ksi (for both series)
Water (lb)	237	274	300
Cement ^a (lb)	538	583	650
Fly Ash ^b (lb)	0	0	150
Fine Aggregate ^c (lb)	1270	1880	1160
Coarse Aggregate #1 ^d (lb)	562	0	501
Coarse Aggregate #2 ^e (lb)	1420	0	1180
Coarse Aggregate #3 ^f (lb)	0	1230	0
High Range Water Reducing Admixture ^g (oz)	0	17.0	0
Measured Density (pcf)	148	145	NA

^a Type I Portland Cement

^b Class C

^c Kansas River sand

^d Pea gravel, maximum aggregate size of 3/8 in.

^e Crushed granite, maximum aggregate size of 3/4 in.

^f Crushed limestone, maximum aggregate size of 3/4 in.

^g ADVA 195 (compliant with ASTM C494/C494M-16)

Table 3.3: Measured Concrete Strengths

Material Properties		First Series		Second Series	
		Girder Part	Deck Part	Girder Part	Deck Part
f_{cm} (ksi)	28-day	7.5	5.0	6.6	5.6
	Testing Day	7.5	5.1	6.6	5.6
Modulus of Rupture (psi)		548	417	572	434

For each reinforcing bar grade used to fabricate the specimens, at least two samples were tested under direct tension. The average steel properties determined from tests are listed in Table 3.4 and sample plots of stress versus strain are shown in Figure 3.2 (plots of stress versus strain are provided for all steel in Appendix B). The interface shear reinforcement consisted of normal-strength (ASTM A615/A615M-16 Grade 60) or high-strength (ASTM A1035/A1035M-16 Grade 120) reinforcing bars. Grade 60 ASTM A615 steel was used for all of the ancillary reinforcement.

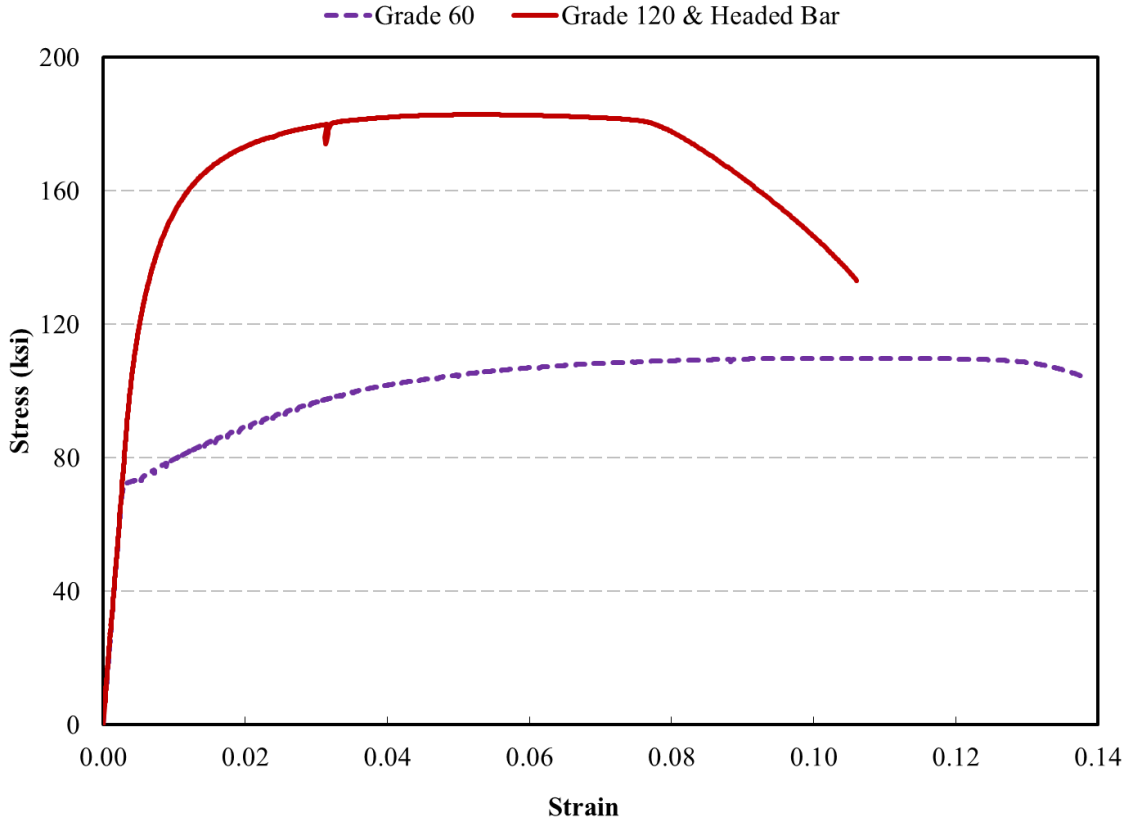


Figure 3.2: Stress-strain Curves for No. 5 bars Used as Interface Shear Reinforcement

Table 3.4: Measured Reinforcement Properties

Material Property	Grade 60 No. 5	Grade 120 No. 5
f_y^a (ksi)	72	140
ϵ_y^b	0.0025	0.0069
f_u^c (ksi)	109	184
ϵ_u^d	0.099	0.050

^a Yield stress, calculated using the 0.2% strain offset method

^b Strain at yield stress, calculated as either f_y divided by modulus if there is a yield plateau or as the strain at which the 0.2% offset method intersects the stress versus strain plot if there is no yield plateau

^c Maximum stress

^d Strain at maximum stress

The interface shear reinforcement was anchored in the simulated deck concrete (the L-shaped section with lower strength concrete) with either a standard 90 degree hook or a headed

mechanical anchor. The headed mechanical anchors were HRC Type 110-4A_b rectangular heads, which have a bearing area of approximately four times the cross-sectional area of the bar. Use of headed bars was a small component of this study, as there are no provisions for use of headed bars in the 6th edition of the AASHTO LRFD Bridge Design Specifications.

The two bond breakers used in this study are referred to throughout as roofing felt and epoxy. The roofing felt was a No. 30 ASTM D4869/D4869M-16a Type I organic felt (saturated with asphalt); a product that is commonly used as an underlayment for asphalt shingles in the roofing process. For specimen preparation, the roofing felt was first cut to the necessary dimension and placed (not bonded to) the surface of the simulated girder concrete prior to placement of the simulated deck concrete. The epoxy used in this study was a water-based liquid-membrane-forming resin curing compound. This type of epoxy is often used as a curing compound for freshly finished concrete to slow drying and increase cement hydration. For specimen preparation, the epoxy was spread over the surface of the simulated girder concrete with a brush immediately after water disappeared from the concrete surface. In practice, this product could also be applied as a spray. A second coat was then applied prior to placement of the simulated deck concrete to increase the thickness of the membrane and thereby reduce the bond between concrete layers. These two products were selected from among several possible bond breakers based on input from Kansas Department of Transportation (KDOT) engineers and precast girder fabricators. Of the two, it was expected that roofing felt would be simplest to install and least likely to lead to problems on site.

3.1.3 Specimen Fabrication

Figure 3.3 shows photos taken during fabrication of the push-off specimens. Figure 3.3(a) and 3.3(b) show the formwork and reinforcement cages prior to casting of the concrete. Before the reinforcement was placed inside the formwork, the inner surfaces of the formwork were brushed with polyurethane and allowed to dry. The reinforcement for the bottom L-shaped section (the one representing the girder) was then placed inside the formwork. The concrete for the bottom section of the specimens was then delivered from a local ready-mix facility, placed directly into the formwork from the chute of the truck, and consolidated using an electric concrete vibrator (Figure 3.3(c)). The surface of the concrete that would later connect with the top L-shaped section was

first troweled smooth and then roughened, where appropriate. Roughened surfaces were prepared using a ¼ in. thick wood shim to make orthogonal dents with an amplitude of about ¼ in. at regular intervals over the designated roughened surface as shown in Figure 3.3(d). For specimens with an epoxy bond breaker, the epoxy was brushed onto the troweled portions of the specimens at this time. Figure 3.3(e) shows that after casting, specimens were cured under damp burlap and plastic sheets. The first L-shaped section was allowed to cure for four days before the specimens were prepared for casting of the second section.

Casting of the second portion of the specimen began with placement of 1½ in. thick foam insulation to form gaps between the L-shaped sections (shown in Figure 3.1). The roofing felt was placed (not bonded) on the troweled portions of the appropriate specimens and epoxy, wherever used, was reapplied and allowed to dry. The reinforcement cages were then assembled and installed. As with the first L-shaped section, the concrete for the top section of the specimens was delivered from a local ready-mix facility, placed directly into the formwork from the chute of the truck, and consolidated using an electric concrete vibrator. Five days after casting of the second section, the formwork was removed (Figure 3.3(f)).

3.1.4 Test Setup and Instrumentation

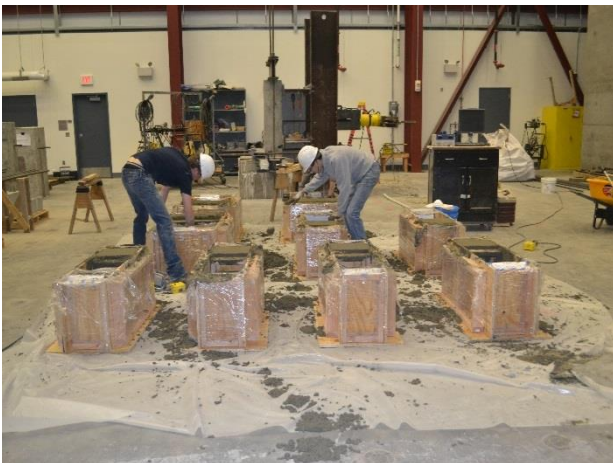
An elevation view of the test setup and instrumentation is shown in Figure 3.4. A photo of the test setup before testing is also shown in Figure 3.5. The setup consisted of a self-reacting frame composed of two steel bearing surfaces linked together with four 3 in. diameter 100 ksi steel rods. Each steel bearing surface was constructed from two WT10.5x66 sections welded together along the flange tip and stiffened with several 5/8 in. steel plates oriented perpendicular to the T-section webs. The result was a stiff bearing surface reinforced bi-directionally for bending. The push-off specimens were placed concentric with the vertical axis of the test frame on a bed of gypsum cement. Either one or two hand-operated hydraulic 100-ton jacks were installed between the specimen and the top bearing surface (two jacks were used for specimens with a 12 × 24 in. interface). A ½-in. thick steel plate was placed between the hydraulic jack and specimen. To measure forces imposed on the specimen, a pass-through-type load-cell was placed on each steel rod between the top surface of the top plate and a nut twisted onto the rod.



(a) Formwork



(b) Reinforcement Cages



(c) Casting Concrete



(d) Finished Rough Middle Surface



(e) Concrete Curing



(f) Push-off Specimens after Demolding

Figure 3.3: Fabrication of Push-off Specimens

A non-contact infrared-based 3D position tracking system was used to collect data on the location of 12 high-speed markers (placed as shown in Figure 3.4) throughout the tests. These data were then used to calculate deformations of the specimen under load, including crack width, rotation, and relative slip at the interface.

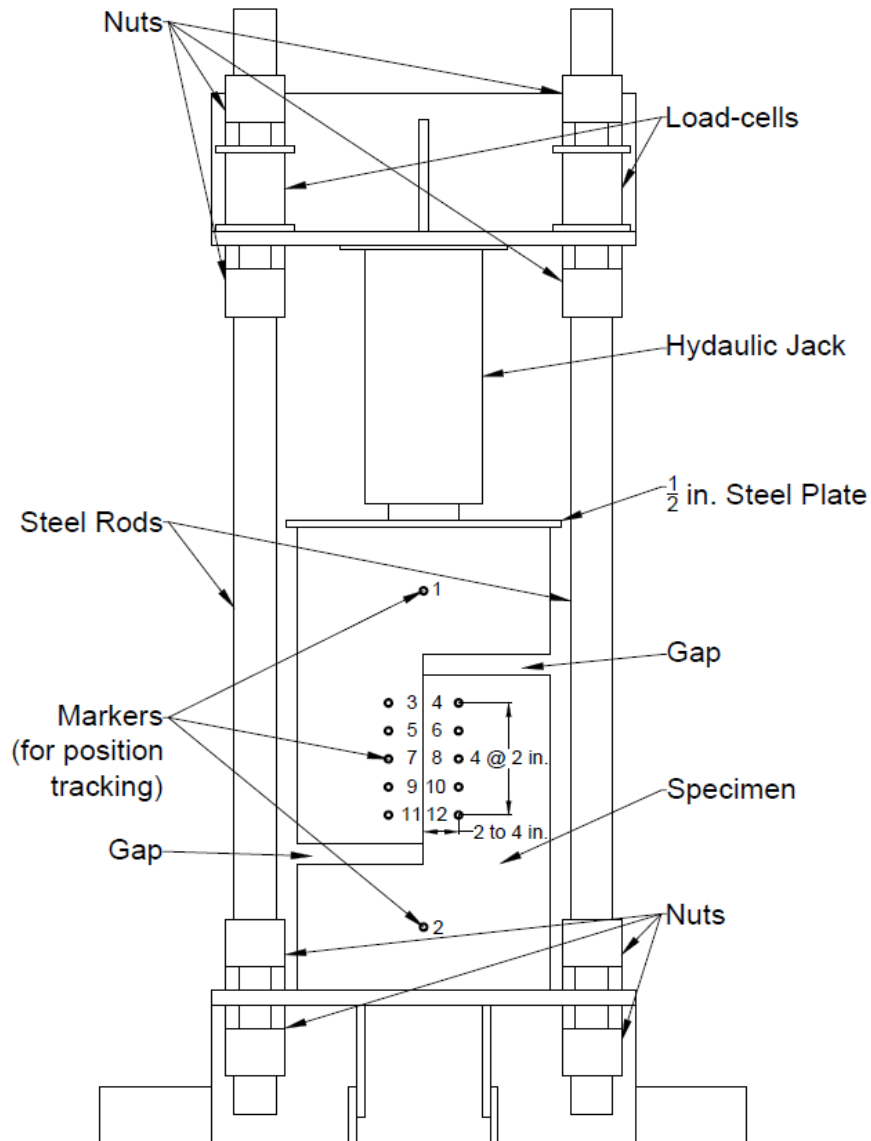


Figure 3.4: Elevation View of the Test Setup

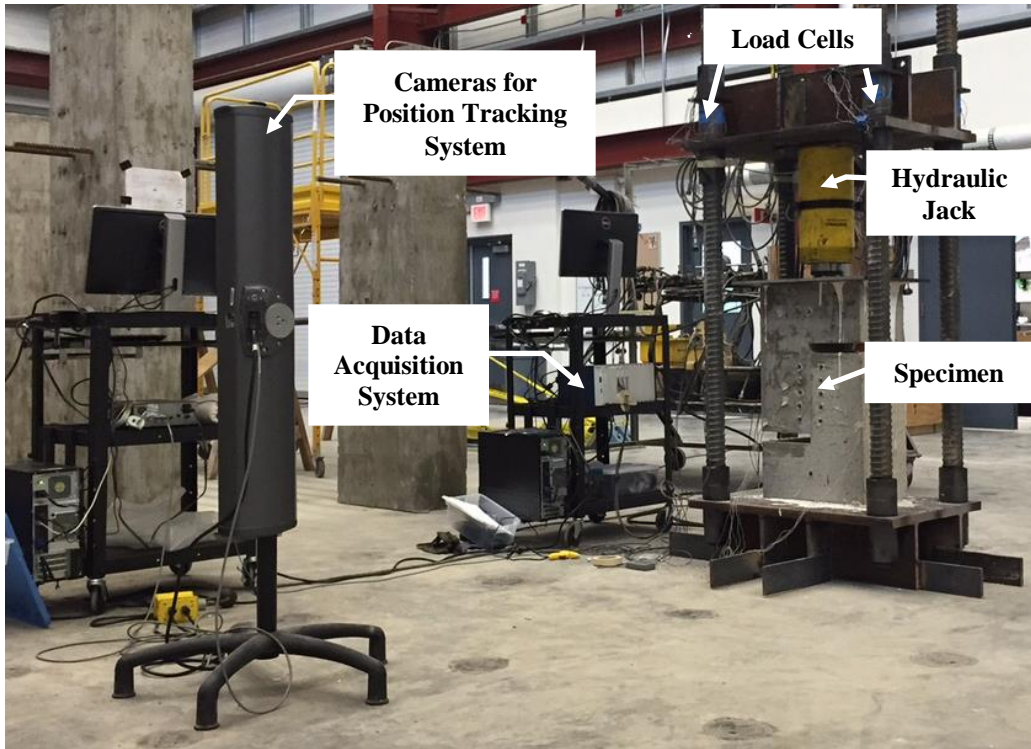


Figure 3.5: Test Setup and Instrumentation

3.1.5 Testing Process

For testing, force was monotonically applied to the top of the specimens using the hand-pumped hydraulic jack shown in Figure 3.5. A plot of force versus time is shown for two specimens (RM-12-F-12-NR and T-12-E-12-NR) in Figure 3.6, where force is the sum of forces recorded by the four load cells. Load was applied pseudostatically in increments of 10 to 20 kip and paused to observe and document specimen behavior (the loading rate during the loading phases did not exceed 2.5 kips/sec). After peak, loading was paused periodically to document observations. With two exceptions, the tests were terminated due to either fracture of the interface shear reinforcement or closing of the gap between the two parts of the specimen (indicating a total relative slip of approximately 1.5 in.). For the two exceptions (T-24-NB-12-HB and RM-24-F-12-NR), the test was terminated at a slip of approximately $\frac{1}{4}$ in.

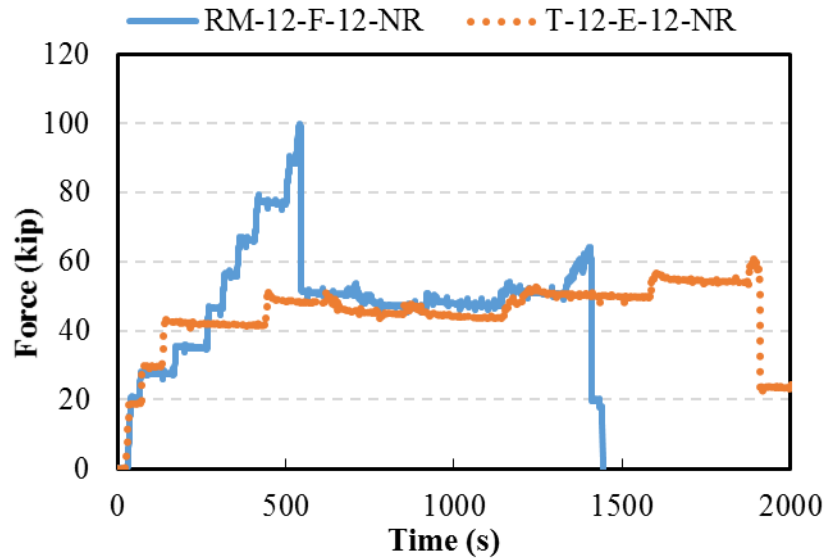


Figure 3.6: Force versus Time for RM-12-F-12-NR and T-12-E-12-NR

3.2 Behavior of Push-off Specimens

3.2.1 Force versus Slip Relationship

Force is plotted versus slip for 13 of the 16 specimens in Figure 3.7. Results from R-12-NB-12-HR, R-12-NB-6-NR, and RM-24-F-12-NR are discussed separately in Section 3.2.3 because they were influenced by unintended rotation during testing. Similar plots of smaller groups of specimens are provided in Appendix C. The peak force, slip at peak force, and stiffness are listed in Table 3.5. The reported force is the sum of forces recorded by the four load cells. Slip represents the relative vertical displacement across the interface between the two parts of the specimen, and is calculated as the change in vertical distance between markers 1 and 2 (Figure 3.4).

The specimens exhibited an approximately linear relationship between force and slip early in the tests followed by a nearly horizontal relationship, where the imposed force was maintained (or slightly increased) as slip increased. The peak force was strongly influenced by interface area and surface preparation, where fully roughened specimens exhibited the greatest strength followed by the rough middle specimens and then the troweled and debonded specimens. For specimens with a completely debonded interface (either roofing felt or epoxy), and for two of the four troweled specimens without bond breakers (T-12-NB-12-NR and T-12-NB-12-HR), the linear loading branch transitioned at slip values between approximately 0.01 and 0.03 in. to a nearly

horizontal line, where the imposed force was maintained (or slightly increased) as slip increased. For these specimens, the peak force was reached at large values of slip (Table 3.5). For the rest of the specimens, the linear ascending branch continued until the peak force (or initial peak force) was reached at slip values between 0.01 and 0.05 in. (Table 3.5). Upon reaching peak strength, a sudden drop in force was observed in conjunction with a sudden increase in slip. After the sudden drop in force, the specimens continued to support a nearly constant force as the slip was increased similar to the behavior observed in the fully debonded specimens. In all specimens, the force resisted by the specimen at large slips (greater than approximately 0.1 in.) was strongly influenced by reinforcement area and grade and not by interface preparation, suggesting that dowel action dominated at this stage of testing.

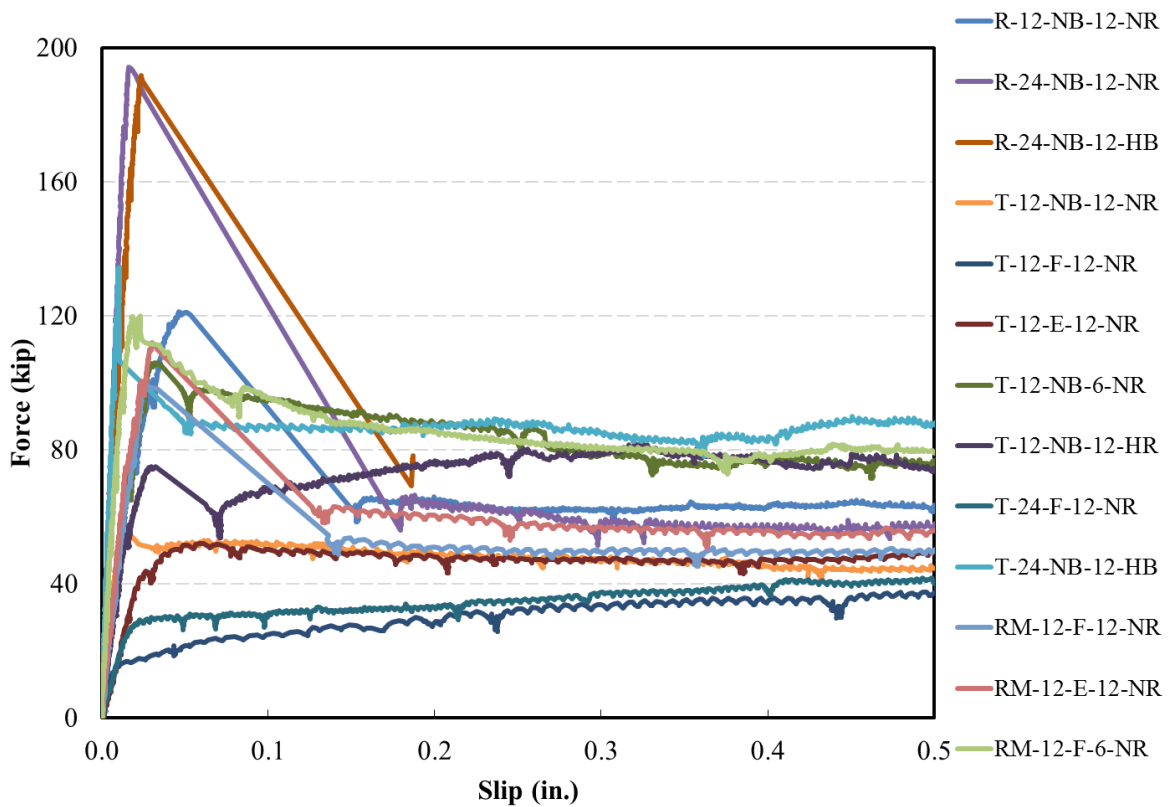


Figure 3.7: Force versus Slip (Specimens Affected by Rotation are Omitted)

Table 3.5: Specimen Strength, Slip, and Stiffness

Specimen ID	Peak Strength (kip)	Slip at Peak Strength (in.)	Stiffness #1 ^a (kip/in.)	Stiffness #2 ^a (kip/in.)	Ratio of Stiffness #2/ #1
R-12-NB-12-NR	121	0.047	3460	1920	0.55
R-12-NB-6-NR	– ^b	– ^b	5750	– ^b	– ^b
R-12-NB-12-HR	– ^b	– ^b	2906	– ^b	– ^b
R-24-NB-12-NR	194	0.017	13300	11500	0.86
R-24-NB-12-HB	192	0.024	– ^c	– ^c	– ^c
T-12-NB-12-NR ^d	58.3 (57.9)	1.0 (0.012)	5630	4770	0.77
T-12-F-12-NR ^d	50.3 (15.4)	1.0 (0.0094)	1690	– ^e	– ^e
T-12-E-12-NR ^d	61.1 (39.7)	0.86 (0.022)	1980	– ^e	– ^e
T-12-NB-6-NR	106	0.032	6720	2230	0.48
T-12-NB-12-HR ^d	82.1 (75.8)	0.32 (0.032)	4280	1720	0.40
T-24-F-12-NR ^d	44.4 (24.3)	0.53 (0.015)	1590	– ^e	– ^e
T-24-NB-12-HB	134	0.010	11700	– ^e	– ^e
RM-12-F-12-NR	99.9	0.026	4660	3850	0.83
RM-12-E-12-NR	112	0.030	5120	2330	0.46
RM-12-F-6-NR	119.9	0.035	8410	5360	0.64
RM-24-F-12-NR	– ^b	– ^b	10100	– ^b	– ^b

^a For bonded specimens, stiffness #1 and #2 were calculated before and after first cracking (Section 3.2.2)

^b Results were influenced by unintentional rotation near peak force

^c Omitted because specimen was cracked prior to testing

^d The peak strength occurred when slip was large. The force and slip at the end of the linear ascending branch is reported in parentheses

^e For fully debonded specimens and T-24-NB-12-HB, there was only one linear portion of the loading

Two stiffness values are given in Table 3.5 because most specimens exhibited an approximately bi-linear force-slip relationship prior to peak. An example of this is shown in Figure 3.8, a plot of force versus slip for R-12-NB-12-NR, RM-12-E-12-NR, and RM-12-F-12-NR up to a slip of 0.06 in. In Figure 3.8, the circles show the transition points between the first and second linear portions of loading. Table 3.5 lists the calculated slope of the initial (Stiffness #1) and secondary (Stiffness #2) loading branches for each specimen, which represent the stiffness before and after cracking at the interface (as discussed in Section 3.2.2). For specimens with a fully debonded interface, no slope is given for the secondary loading branch because these specimens were effectively “cracked” from the beginning of the test and no change in loading branch slope was observed. The slopes of the initial and secondary loading branches varied significantly as a function of interface preparation. The ratio in Table 3.5 shows that the change in stiffness between first and second branch is smallest for fully troweled specimens and largest for fully roughened

specimens. It appears that reduction of stiffness is related to surface roughness after cracking. Also, the initial stiffness is related to the area of interface shear reinforcement. As the area of reinforcement doubled, the initial stiffness increased for all bonded specimens.

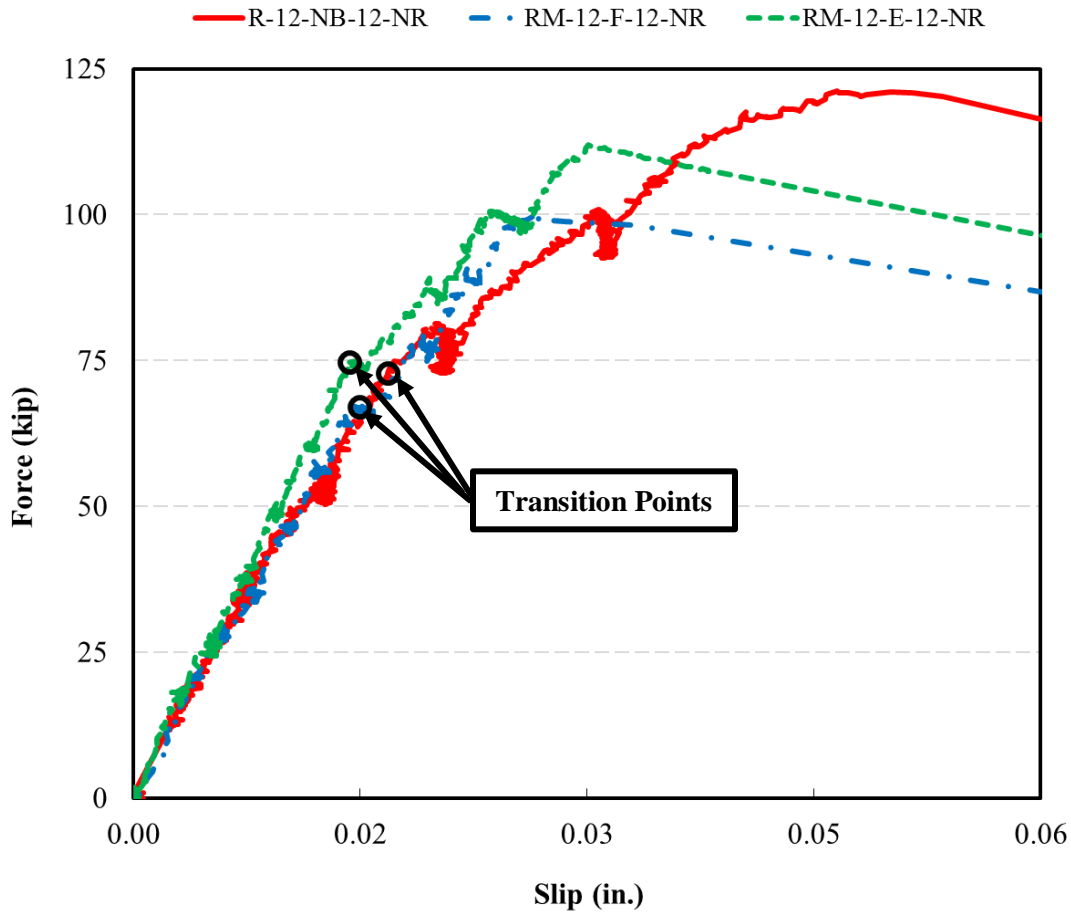


Figure 3.8: Force versus Slip up to a Slip of 0.06 in.

3.2.2 Interface Slip and Crack Width

The width of interface cracks throughout the tests was calculated to allow study of the relationships between surface preparation, crack width, and behavior. To calculate crack width, the relative displacement (separation) across the interface was first calculated as the average change in horizontal distance between two pairs of markers placed on opposite sides of the interface (Figure 3.4). Preference was given to the top-most and bottom-most pairs of markers, but intermediate pairs were selected when necessary when localized effects, such as cracking,

compromised the data collected for a given marker. Figure 3.9 shows force plotted versus relative displacement for a subset of specimens. For the two unbonded specimens (T-12-E-12-NR and T-12-F-12-NR), the plotted results start with an approximately linear initial portion followed by a transition to an approximately horizontal segment. This behavior is very similar to the force versus slip relationships in Figure 3.7. For the specimens with some or all of the interface intentionally roughened (R-12-NB-12-NR, RM-12-E-12-NR, RM-12-F-12-NR), the relationship prior to peak strength is clearly composed of two segments with markedly different slopes. The transition point between the initial and secondary loading segments is the same as for the force versus slip relationships and coincides with cracking at the interface. After this transition point (cracking), relative displacements increased with load at a much greater rate than before. Although not visible in Figure 3.9, the initial ascending branch for T-12-NB-12-NR was also approximately bi-linear.

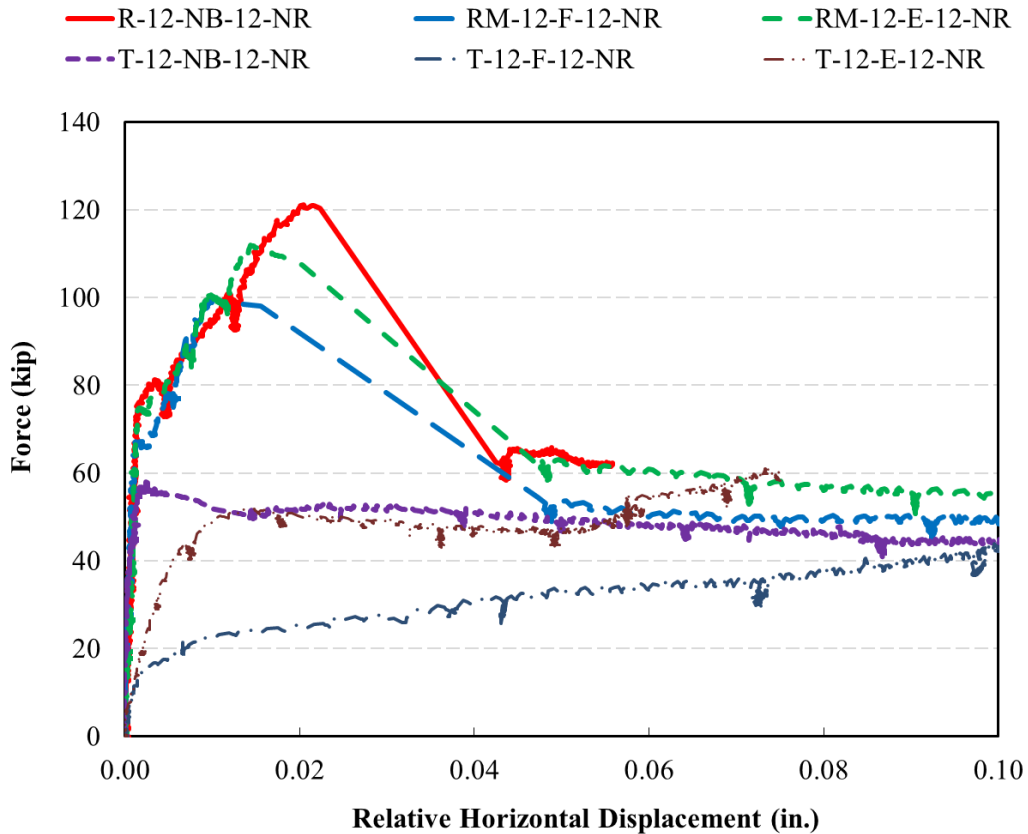


Figure 3.9 Force versus Relative Horizontal Displacement for Selected Specimens

For troweled specimens without a bond breaker, the length of the second linear portion was shorter than for roughened specimens, indicating that peak force occurred at or shortly after cracking in these specimens.

To estimate crack width in specimens with some portion of the interface that was initially bonded, it was assumed that crack width was zero until first cracking and that crack width after cracking was equal to the calculated relative horizontal displacement between markers minus the relative horizontal displacement at first cracking. This method does not account for any rebound of strains that might occur within the concrete between the markers and the interface after cracking, but it is believed that inaccuracies due to this omission are minor. For specimens with a fully debonded interface, it was assumed that calculated relative horizontal displacements were entirely attributable to separation of the surfaces (a “crack”). For these specimens, crack width was set equal to relative horizontal displacement. Force is plotted versus crack width in Figure 3.10 for the same specimens shown in Figure 3.9.

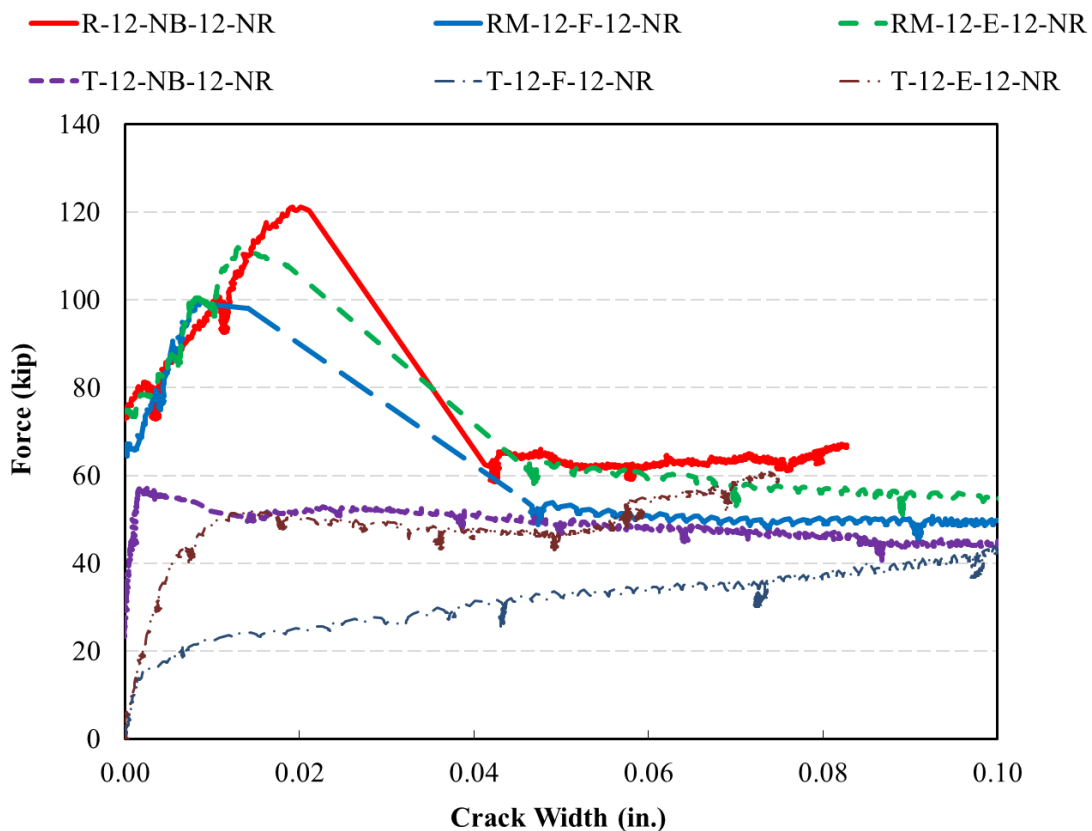


Figure 3.10 Force versus Crack Width

The force at first cracking, crack width at peak strength, and slip at peak strength are listed in Table 3.6. The force at first cracking was strongly affected by surface preparation, with fully roughened specimens having the greatest cracking force followed by rough middle specimens and then troweled specimens. Among fully roughened and troweled specimens, the force at cracking was also correlated with reinforcement area. This was not the case among the rough middle specimens.

Table 3.6 also shows that crack width at peak force tended to increase as surface roughness increased. Among specimens with the same surface preparation, slip and crack width at peak strength were somewhat correlated (i.e. slip at peak force was greatest in specimens with the greatest crack width at peak force).

Table 3.6: Force and Crack Width at Critical Points

Specimen ID	Force at First Cracking (kip)	Crack Width at Peak Strength (in.)	Slip at Peak Strength (in.)
R-12-NB-12-NR	72.9	0.019	0.047
R-12-NB-6-NR	107	– ^a	– ^a
R-12-NB-12-HR	50.6	– ^a	– ^a
R-24-NB-12-NR	118	0.0064	0.017
R-24-NB-12-HB	– ^b	0.013	0.024
T-12-NB-12-NR	23.3	0.0023 ^c	0.012 ^c
T-12-F-12-NR	– ^d	0.11	1.02
T-12-E-12-NR	– ^d	0.073	0.86
T-12-NB-6-NR	62.2	0.0080	0.032
T-12-NB-12-HR	31.4	0.011 ^c	0.032 ^c
T-24-F-12-NR	– ^d	0.080	0.53
T-24-NB-12-HB	134	0.0 ^e	0.010
RM-12-F-12-NR	66.9	0.0085	0.026
RM-12-E-12-NR	74.6	0.013	0.030
RM-12-F-6-NR	78.5	0.013	0.035
RM-24-F-12-NR	64.5	– ^a	– ^a

^a Results were influenced by unintentional rotation near peak force

^b Omitted because specimen was cracked prior to testing

^c Corresponds to first peak (limit of proportionality) not absolute peak

^d Unbonded specimens are effectively cracked prior to testing

^e First cracking occurred at peak strength

Crack width is plotted versus slip for most specimens in Figures 3.11 through 3.14 (individual plots are provided in Appendix D). Results for rough middle (RM-12-F-12-NR, RM-12-E-12-NR, and RM-12-F-6-NR) and rough specimens (R-12-NB-12-NR, R-24-NB-12-NR, and R-24-NB-12-HB) are shown in Figures 3.11 and 3.12. Both figures show that the specimens typically exhibited some slip (up to approximately 0.015 in.) prior to cracking. After cracking, crack width and slip increased somewhat proportionally, although the slope varied among the specimens. This post-cracking but pre-peak region of behavior is what most researchers refer to as shear friction – where slip requires a proportional increase in crack width and, therefore, strain in the reinforcement crossing the interface. For most specimens included in Figures 3.11 and 3.12, the proportional region of behavior clearly transitioned to one with a reduced slope, where increasing slip was associated with a smaller change in crack width. This transition coincided with the peak strength shown in Figure 3.7. Therefore, after the specimens reached peak strength, slip increased rapidly while crack width increased slowly.

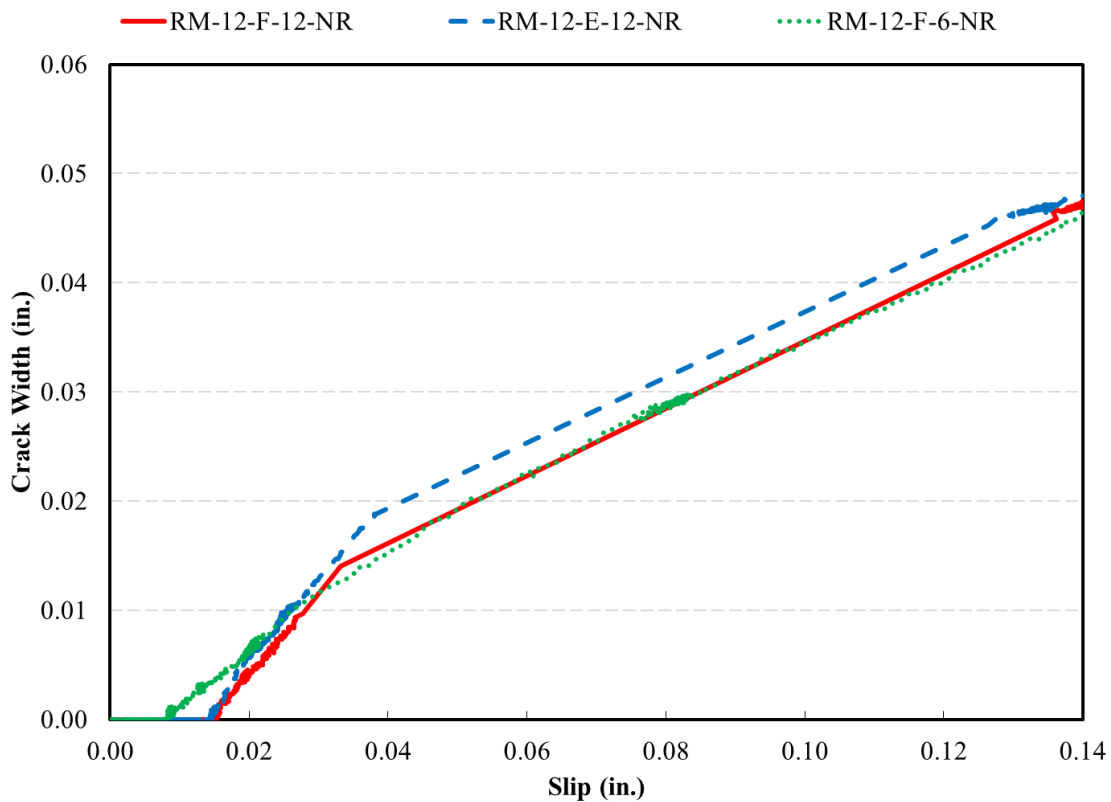


Figure 3.11: Crack Width versus Slip for Rough Middle Specimens

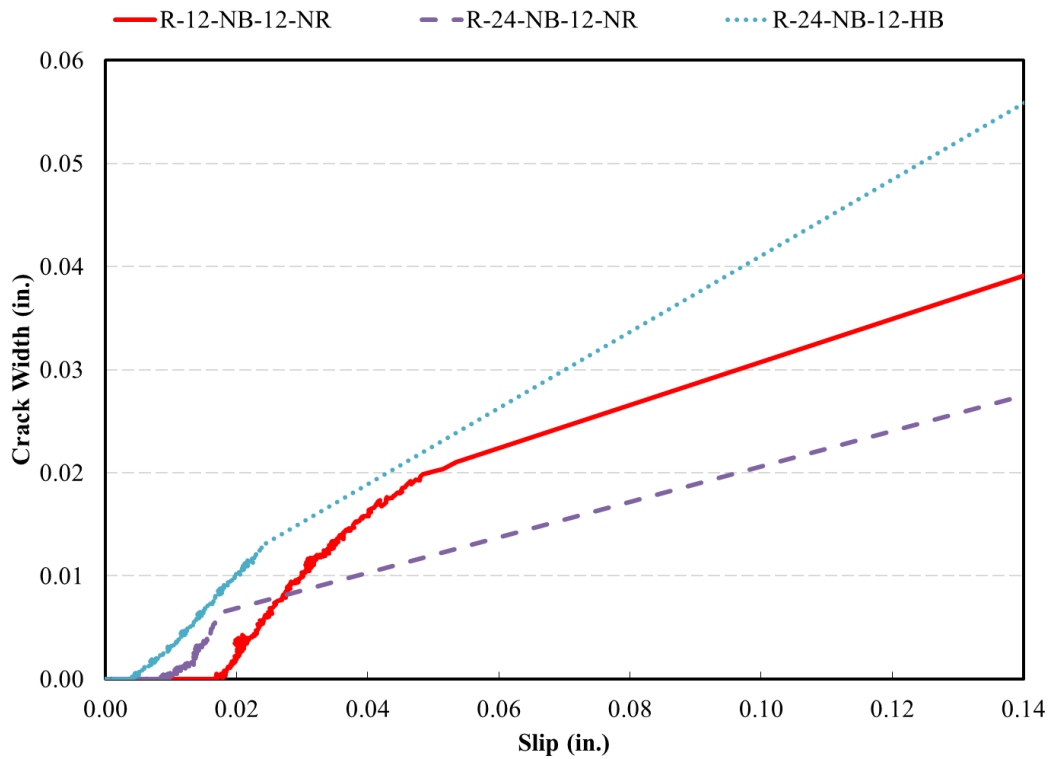


Figure 3.12: Crack Width versus Slip for Roughened Specimens

Crack width is plotted versus slip in Figure 3.13 for bonded troweled specimens (T-12-NB-12-NR, T-12-NB-6-NR, T-12-NB-12-NR and T-24-NB-12-NR) and in Figure 3.14 for debonded troweled specimens (T-12-F-12-NR, T-12-E-12-NR, T-24-F-12-NR). All of the bonded troweled specimens exhibited slip (of approximately 0.01 in.) prior to cracking. After cracking, three of the four bonded troweled specimens (T-12-NB-12-NR, T-12-NB-6-NR, T-12-NB-12-NR) exhibited the approximately bi-linear post-cracking response typical of roughened specimens. However, the slope of the post-cracking region for the three specimens was much less than that of typical roughened specimens and the transition between peak and post-peak is not very obvious in these figures. Only T-24-NB-12-NR did not exhibit the bi-linear post-cracking response typical of roughened specimens; instead it exhibited a sudden transition after reaching first cracking (the peak strength of the specimen coincided with first cracking of the section). The difference in observed behavior among the bonded troweled specimens could be due to minor (and unintended) differences in the surface condition prior to casting. The surface condition of the three specimens

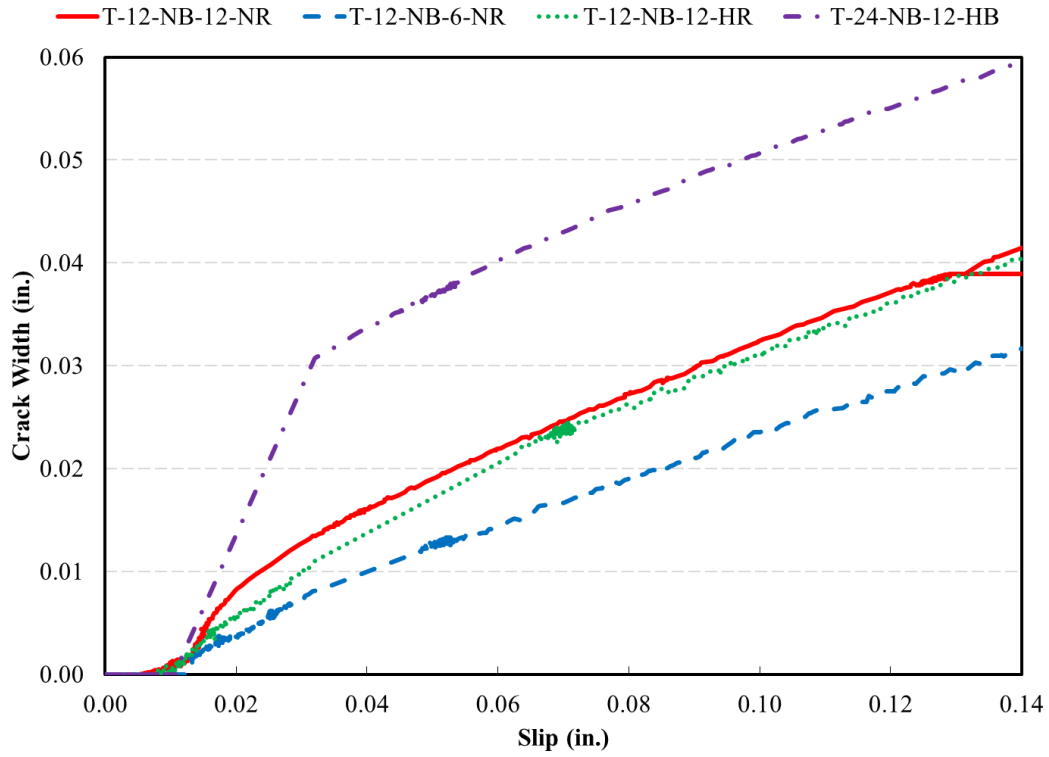


Figure 3.13: Crack Width versus Slip for Troweled Specimens without Bond Breakers

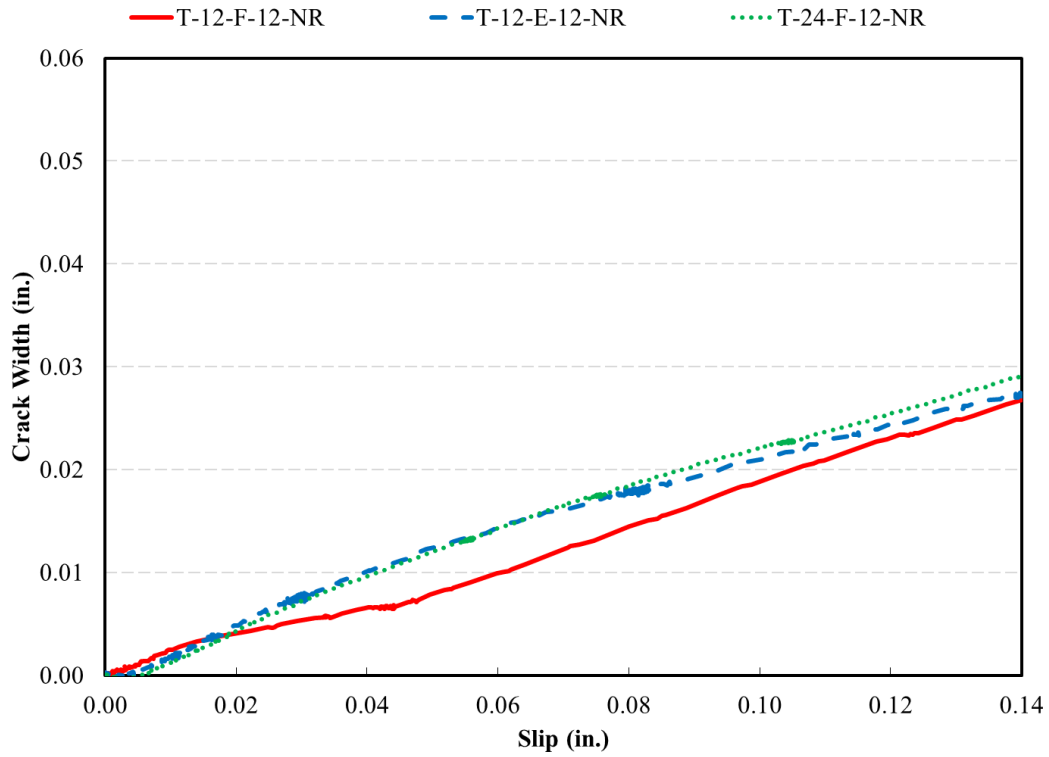


Figure 3.14: Crack Width versus Slip for Debonded Troweled Specimens

that showed a bi-linear post-cracking response may not have been as smooth as intended. For a “perfectly troweled” surface, the crack width versus slip relationship would be expected to be similar to that of T-24-NB-12-HB (i.e. cracking and peak coincide). Among the bonded troweled specimens, the specimen with the shallowest post-cracking slope had the largest area of interface reinforcement. This is logical, given that interface reinforcement resists opening of a crack at the interface; however, the same trend was not observed among the roughened and rough middle specimens. For the debonded troweled specimens, crack width increased with slip, although with a very shallow slope, from the beginning of the test. The interface was effectively “cracked” prior to testing, as expected.

3.2.3 Influence of Rotation

The markers fixed to the surface of the specimen were also used to calculate the relative rotations between the antisymmetric L-shaped portions of the specimens throughout each test. The location of each marker was recorded based on the coordinate system illustrated in Figure 3.15, where the X- and Y-axes coincide with the surface of the specimen and the Z-axis is perpendicular to the surface. Although relative rotation about the Y-axis was negligible in all tests, relative rotations about either the X- or Z-axes were occasionally important. Relative rotation was calculated as the angle change between two imaginary marker lines (one connecting markers 3 and 11, and the second connecting markers 4 and 12) located on opposite sides of the interface. Relative rotations between the two marker lines about the X- and Z-axes were calculated using Eq. 3-1.

$$\theta_x = \tan^{-1} \left\{ \frac{(3_z - 4_z) - (11_z - 12_z)}{0.5((11_y - 3_y) + (12_y - 4_y))} \right\} \quad \text{Eq. 3-1-a}$$

$$\theta_z = \tan^{-1} \left\{ \frac{(3_x - 4_x) - (11_x - 12_x)}{0.5((11_y - 3_y) + (12_y - 4_y))} \right\} \quad \text{Eq. 3-1-b}$$

Where θ_x and θ_z are the relative rotation between opposite faces of the interface about the X- and Z-axes, and the number with the subscript represents the X-, Y-, or Z-axes coordinate of the given marker number in 3-dimensional space.

Force is plotted versus rotation (θ_x and θ_z) up to peak force in Figure 3.16 for specimens that had non-negligible rotation about either the X- or Z-axes (R-12-NB-6-NR, R-12-NB-12-HR and RM-24-F-12-NR). For these specimens, either θ_x or θ_z started to increase shortly after cracking and continued to increase to values greater than 0.003 radians when the specimen reached its peak strength. Both θ_x and θ_z were negligible (less than 0.001 radians) for other specimens.

In Figure 3.17, force is plotted versus slip for R-12-NB-6-NR, R-12-NB-12-HR and RM-24-F-12-NR; the specimens influenced by rotation. All three specimens exhibited a truncated peak that was not exhibited by other specimens (Figure 3.7). The truncated peak is attributable to the large θ_x and θ_z values. This unintended relative rotation is not representative of bridge structures in practice and is believed to have influenced the force, slip, and crack width near peak strength. Throughout this report, results from these tests are reported when they are not impacted by this rotation (e.g. initial stiffness, force at cracking). Any result that may have been influenced by rotation is not reported.

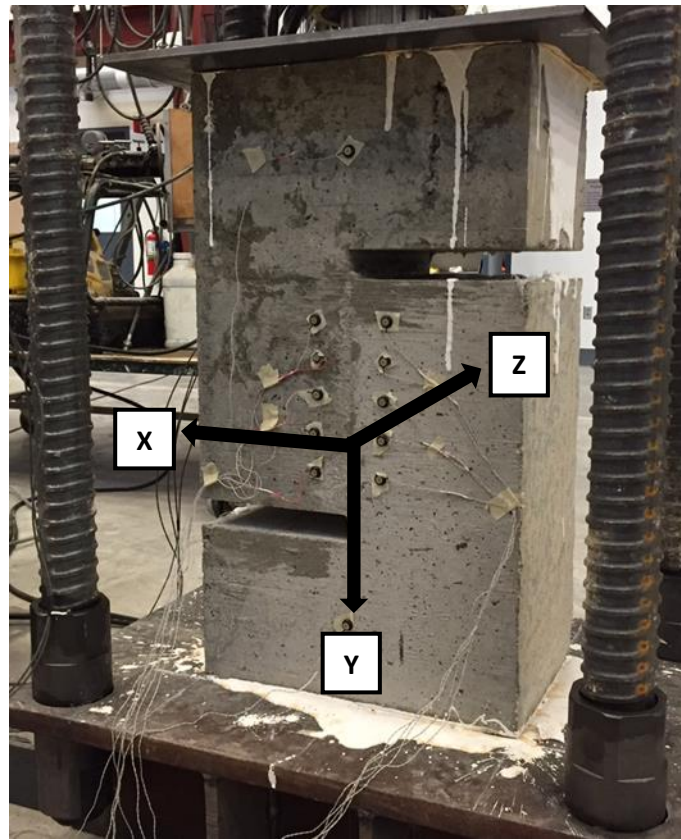


Figure 3.15: Coordinate System of the 3-Dimensional Position Tracking System

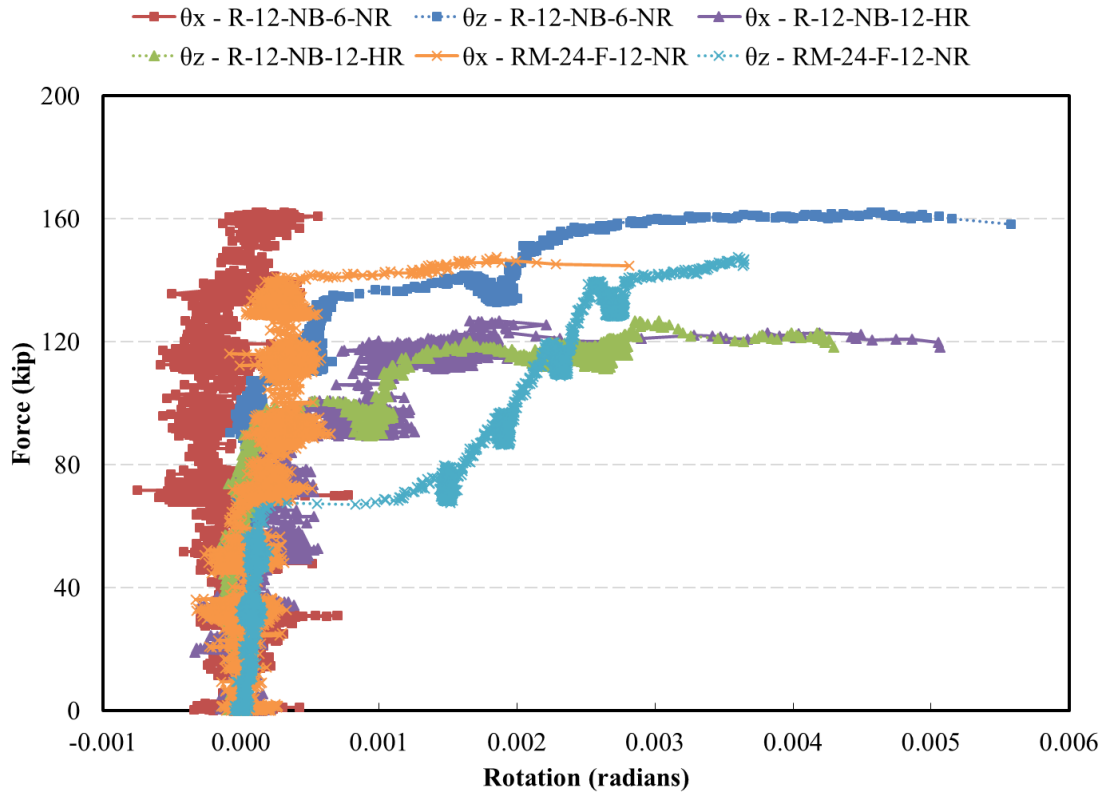


Figure 3.16: Force versus Rotation for Specimens Influenced by Rotation

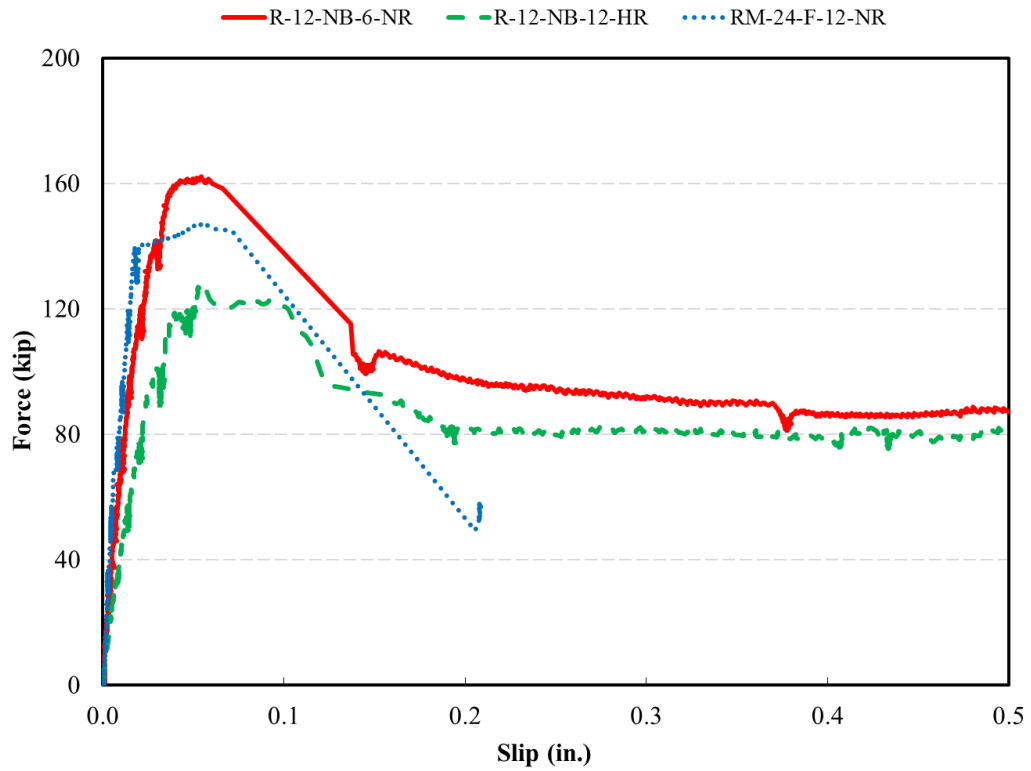


Figure 3.17: Force versus Slip for Specimens Affected by Rotation

3.2.4 Observation of Specimens after Failure

During the tests, little was observed aside from sliding of one L-shaped section of the specimen past the other. All observable deformations and cracking occurred at the interface. The reason for termination of each test, shown in Table 3.7, did differ among the specimens. Specimens with Grade 60 interface shear reinforcement exhibited fracture of at least one of the interface shear reinforcing bars, resulting in a significant loss of strength and forcing termination of the test. These bar fractures occurred at large values of slip, between 0.56 and 1.1 in. Two of the 24 in. wide Grade 60 specimens (T-24-F-12-NR and R-24-NB-12-NR) failed by simultaneous fracture of both interface shear reinforcing bars, resulting in a complete separation of the L-shaped segments of the specimens. Specimens with either hooked or headed Grade 120 interface shear reinforcing bars did not exhibit bar fracture; instead, the tests of these specimens (with the exception of R-24-NB-12-HB) were terminated when the 1.5 in. gap between the two parts of the specimen (shown in Figure 3.1) closed.

Table 3.7: Cause for Termination of Tests

Specimen ID	Cause for Termination
R-12-NB-12-NR	Bar Fracture
R-12-NB-6-NR	Bar Fracture
R-12-NB-12-HR	Closing of the Gap
R-24-NB-12-NR	Bars Fracture (All bars)
R-24-NB-12-HB	N/A ^a
T-12-NB-12-NR	Bar Fracture
T-12-F-12-NR	Bar Fracture
T-12-E-12-NR	Bar Fracture
T-12-NB-6-NR	Bar Fracture
T-12-NB-12-HR	Closing of the Gap
T-24-F-12-NR	Bars Fracture (All bars)
T-24-NB-12-HB	Closing of the Gap
RM-12-F-12-NR	Bar Fracture
RM-12-E-12-NR	Bar Fracture
RM-12-F-6-NR	Bar Fracture
RM-24-F-12-NR	N/A ^a

^a Testing was terminated shortly after reaching peak strength



4 ksi Section



7 ksi Section

Figure 3.18: Interface of T-24-F-12-NR after Testing



4 ksi Section



7 ksi Section

Figure 3.19: Interface of R-24-NB-12-NR after Testing

The condition of the interface after testing was documented for the two specimens that completely separated. Photos of the two interface surfaces are shown in Figures 3.18 and 3.19 for T-24-F-12-NR and R-24-NB-12-NR, respectively. For T-24-F-12-NR, which was fully debonded with roofing felt, both surfaces were unchanged from the as-cast condition except for concrete breakout damage visible in the narrow region between the two interface reinforcing bars. Although expected, this is further evidence that the roofing felt effectively diminished interaction between the layers of concrete and is likely to make deck removal significantly easier. For R-24-NB-12-

NR, which was fully roughened, it appears that the failure surface penetrated both the 4 and 7 ksi concrete elements. This is evidence of the strong bond developed across the roughened interface. It is therefore reasonable to expect that removal of deck concrete from a girder is likely to cause damage to the top flange of the girder cast with higher strength concrete. The majority of the failure surface, however, appears to have remained within the simulated deck element cast with lower strength concrete. This includes a portion (circled in Figure 3.19) where the roughened surface of the higher strength concrete is still visible after testing because the lower strength concrete sheared off directly above the roughened surface. It is therefore recommended that the lower concrete strength be used as the basis for calculation of horizontal shear strength when considering an interface between elements cast with different strength concretes. No observations are reported for other specimens because it was not possible to separate the other specimens for observation without damaging the interface.

3.3 Interpretation and Comparison of Test Results

3.3.1 Interpretation of Typical Force-Slip Curves

Figure 3.20 shows a schematic representation of typical force versus slip relationships for both bonded and unbonded specimens. These are based qualitatively on the test results summarized in Table 3.8. As shown in Figure 3.20, the responses of specimens with a bonded cold-joint interface were composed of four segments separated by three key points. The behavior was linear until reaching the limit of proportionality, which coincided with cracking along the interface (at a slip between 0.005 and 0.02). Up to cracking, adhesion is understood to contribute significantly to shear resistance (Zilch and Reinecke, 2012). After cracking, the slope of the force versus slip relationship reduced but the force continued to increase with slip for specimens with some portion of the interface that was roughened. It is understood that shear friction is important in this region of behavior because crack width increases with slip, which tends to strain the interface shear reinforcement causing increased compression across the interface. The second key point corresponds to the peak strength, where slip was generally less than 0.06 in. Based on the literature

review (Chapter 2), it is common for peak strength to be estimated using a combination of cohesion and shear friction terms (Eq. 3-2).

$$V_{peak} = c + C_1 A_s f_y \quad \text{Eq. 3-2}$$

Where V_{peak} is the peak strength, c is a cohesion term, C_1 is a constant, A_s is the projected cross-sectional area of interface reinforcement on the interface, and f_y is the reinforcement yield stress.

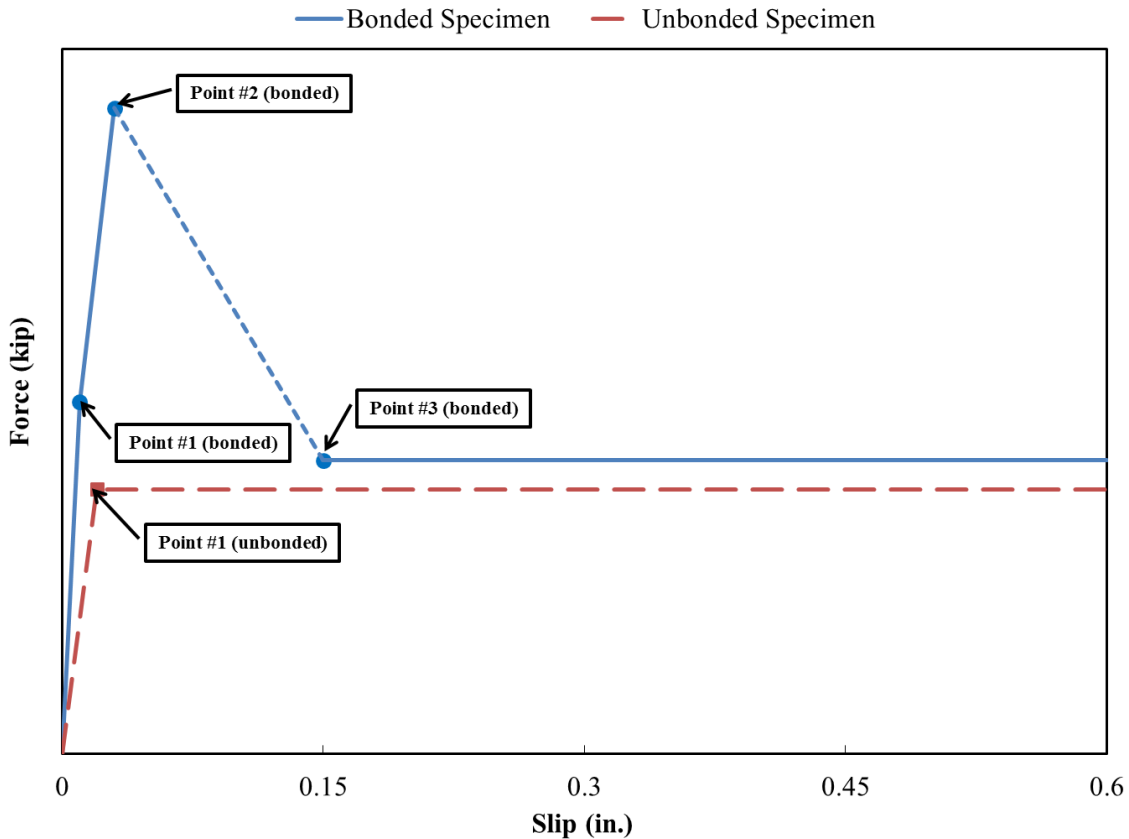


Figure 3.20: Schematic of Force versus Slip for Bonded and Unbonded Specimens

After peak strength there is a rapid reduction in strength associated with an increase in slip (shown as a dashed line in Figure 3.20). The slope of this descending branch is not reported because it is more strongly related to test setup stiffness than specimen characteristics. Beginning at point 3 in Figure 3.20, the shear strength stabilizes and remains approximately constant as slip increases.

Troweled bonded specimens exhibited behavior similar to that shown for roughened specimens in Figure 3.20 although Points #2 and #3 were relatively close (except for T-24-NB-12-NB, which had coincident peak and cracking strengths). After peak strength, it is understood that shear resistance is primarily due to dowel action of the interface shear reinforcement (Eq. 3-3).

$$V_{post-peak} = C_2 A_s f_y \quad \text{Eq. 3-3}$$

Where $V_{post-peak}$ is the post-peak strength and C_2 is an empirical constant.

Table 3.8: Summary of Force and Slip Values

Specimen ID	Force at Cracking (kip)	Slip at First Cracking (in.)	Peak Force (kip)	Slip at Peak Force (in.)	Post-Peak Strength ^a (kip)
R-12-NB-12-NR	72.9	0.017	121	0.047	62
R-12-NB-6-NR	107	0.018	– ^b	– ^b	94
R-12-NB-12-HR	50.6	0.012	– ^b	– ^b	80
R-24-NB-12-NR	118	0.0084	194	0.017	60
R-24-NB-12-HB	– ^c	– ^c	192	0.024	78
T-12-NB-12-NR	23.3	0.0043	57.9 ^d	0.012 ^d	48
T-12-F-12-NR	– ^e	– ^e	15.4 ^d	0.0094 ^d	32
T-12-E-12-NR	– ^e	– ^e	39.7 ^d	0.0022 ^d	47
T-12-NB-6-NR	62.2	0.012	106	0.032	82
T-12-NB-12-HR	31.4	0.0079	75.8 ^d	0.032 ^d	79
T-24-F-12-NR	– ^e	– ^e	24.3 ^d	0.015 ^d	35
T-24-NB-12-HB	134 ^f	0.010	134	0.010	87
RM-12-F-12-NR	66.9	0.015	100	0.026	49
RM-12-E-12-NR	74.6	0.014	112	0.030	57
RM-12-F-6-NR	67.2	0.0075	120	0.035	83
RM-24-F-12-NR	64.5	0.0059	– ^b	– ^b	57

^a Strength of specimens at slip of 0.25 in.

^b Results were influenced by unintentional rotation near peak force

^c Omitted because specimen was cracked prior to testing

^d Force at peak corresponds to the limit of proportionality

^e Force at cracking is not applicable to debonded troweled specimens

^f Force at cracking coincided with force at peak for T-24-NB-12-HB

The schematic representation in Figure 3.20 of debonded specimen behavior is composed of two segments separated by a key point, the limit of proportionality. The initial slope is much

less than for bonded specimens because it relies primarily on the dowel bars and not friction between concrete surfaces. Furthermore, because the surfaces are smooth, the interface reinforcement tensile strains required for shear friction to occur are negligible. After reaching a slip between 0.01 and 0.03 in. the response of debonded specimens became horizontal like the last portion of the bonded-specimen response.

Comparisons between the experimentally determined strength and the calculated strength determined with various provisions are shown in Table 3.9 for each specimen. The ratio of the calculated to experimental strengths is given in parentheses beside the nominal strength calculated for each specimen based on ACI 318-14, AASHTO Specification, and fib Model Code provisions. All of the calculated nominal strengths were less than the corresponding measured strengths, sometimes by large margins. Table 3.9 shows that the provisions of the AASHTO Specification resulted in the most accurate calculated strengths, with values that were 74, 66, and 71% of the measured value for rough, troweled and rough middle specimens. Provisions of ACI 318-14 and the fib Model Code were more conservative, with calculated nominal strengths that were 14 to 65% of the measured strength. The fib Model Code was the only one of the specifications considered that provides guidance for estimating the strength of fully debonded specimens (by calculating the dowel action of shear reinforcement). The calculated nominal strengths for the debonded specimens were, on average, 53% of the measured strength.

As summarized in Table 3.10, an attempt was made to extract the constants used in Eqs. 3-2 and 3-3 from the test results. The constant C_2 was estimated by dividing the post-peak strength at 0.25 in. of slip, when dowel action dominated the specimen response, by $A_s f_y$. This ratio is listed in column (5) of Table 3.10. The average value of C_2 was 1.1 for specimens with normal-strength reinforcement and 0.93 for specimens with high-strength reinforcement. The contribution of cohesion to peak force was then estimated by solving Eq. 3-2 for c and substituting C_2 for C_1 (either 1.1 or 0.93 were substituted into Eq. 3-2 depending on the specimen). This approach assumes that C_1 and C_2 are equal. Although approximate, this is believed to be appropriate given that the debonded specimens had entered into the horizontal region of behavior (dominated by dowel action) at slip values that were typically smaller than the slip at peak force in bonded specimens. The resulting estimate of cohesion at peak force is listed in column (6) of Table 3.10.

As expected, cohesion was significant in roughened specimens, smaller in specimens with a partially roughened interface, and near zero in troweled and debonded specimens.

Table 3.9: Comparison of Experimental and Calculated Nominal Strengths

Specimen ID	Measured Peak Force kip	Calculated Strength kip (% of experimental value)			
		ACI 318-14		AASHTO (2012)	fib Model Code (2010)
		Shear Friction	Composite Flexural ^a		
R-12-NB-12-NR	121	44.6 (37%) ^b	64.2 (53%)	85.0 (70%)	72.8 (60%)
R-12-NB-6-NR	– ^c	89.3 (– ^c)	72.0 (– ^c)	129.6 (– ^c)	96.3 (– ^c)
R-12-NB-12-HR	– ^c	86.8 (– ^c)	72.0 (– ^c)	127 (– ^c)	91.2 (– ^c)
R-24-NB-12-NR	194	44.6 (23%)	102 (52%)	125 (65%)	122 (63%)
R-24-NB-12-HB	192	86.8 (45%)	127 (66%)	167 (87%)	140 (73%)
T-12-NB-12-NR	58.3 (57.9) ^d	26.8 (46%)	11.5 (20%)	37.6 (65%)	21.7 (38%)
T-12-F-12-NR	50.3 (15.4) ^d	– ^e	– ^e	– ^e	12.0 (78%)
T-12-E-12-NR	61.1 (39.7) ^d	– ^e	– ^e	– ^e	12.0 (30%)
T-12-NB-6-NR	106	53.6 (51%)	11.5 (11%)	64.4 (61%)	43.5 (41%)
T-12-NB-12-HR	82.1 (75.8) ^d	52.1 (69%)	11.5 (15%)	62.9 (83%)	37.3 (49%)
T-24-F-12-NR	44.4 (24.3) ^d	– ^e	– ^e	– ^e	12.0 (49%)
T-24-NB-12-HB	134	52.1 (39%)	11.5 (9%)	73.7 (55%)	37.3 (28%)
RM-12-F-12-NR	100	44.6 (45%)	36.0 (36%)	64.8 (65%)	48.1 (48%)
RM-12-E-12-NR	112	44.6 (40%)	36.0 (32%)	64.8 (58%)	66.0 (59%)
RM-12-F-6-NR	120	89 (74%)	36.0 (30%)	108 (90%)	71.7 (60%)
RM-24-F-12-NR	– ^c	44.6 (– ^c)	64.2 (–^c)	85.0 (– ^c)	96.3 (– ^c)
	Mean of Rough:	35%	57%	74%	65%
	Mean of Troweled:	51%	14%	66%	39%
	Mean of Rough Middle:	53%	33%	71%	56%
	Mean of Fully Debonded:	–	–	–	53%

^a Method for calculating stress from composite action in flexural members can be used only if interface shear stress is no larger than 500 psi, otherwise the method of shear friction shall be used. The bolded value indicate an instance when the method would apply if this were a composite girder

^b The value in the parentheses is the ratio between calculated strength and measured strength

^c Results were influenced by unintentional rotation near peak force

^d The peak strength occurred when slip was large, the force at the end of the linear ascending branch is reported in parentheses and used to calculate the strength ratio

^e ACI and AASHTO do not provide equations to calculate the strength of fully debonded specimens

Table 3.10: Relationship between Post-peak Strength and Reinforcement Parameters

Specimen ID	Peak Force (kip)	Post-peak Strength (kip)	$A_s f_y$ ^a (kip)	(3)/(4)	Estimated Cohesion, c (kip) (2) – $C_1 \cdot (4)$ ^b
(1)	(2)	(3)	(4)	(5)	(6)
R-12-NB-12-NR	121	62.0	45	1.4	72
R-12-NB-6-NR	– ^c	94.2	89	1.1	– ^c
R-12-NB-12-HR	– ^c	79.9	87	0.9	– ^c
R-24-NB-12-NR	194	59.7	45	1.3	140
R-24-NB-12-HB	192	78.1	87	0.9	110
T-12-NB-12-NR	57.9 ^d	47.9	45	1.1	10
T-12-F-12-NR	15.4 ^d	31.7	45	0.7	-33
T-12-E-12-NR	39.7 ^d	47.2	45	1.1	-8.0
T-12-NB-6-NR	106	82.3	89	0.9	14
T-12-NB-12-HR	75.8 ^d	78.7	87	0.9	-5.0
T-24-F-12-NR	24.3 ^d	34.6	45	0.8	-24
T-24-NB-12-HB	134	87.2	87	1.0	49
RM-12-F-12-NR	100	49.4	45	1.1	52
RM-12-E-12-NR	112	57.1	45	1.3	62
RM-12-F-6-NR	120	82.6	89	0.9	24
RM-24-F-12-NR	– ^c	56.8	45	1.3	– ^c
Mean of NR specimens (C_2):				1.1	
Mean of HR and HB specimens (C_2):				0.93	

^a The product of total area and measured yield stress of interface shear reinforcement

^b C_1 is taken as 1.1 for specimens with normal-strength reinforcement and 0.93 for specimens with high-strength reinforcement

^c Results were influenced by unintentional rotation near peak force

^d Force at peak corresponds to the proportionality limit

3.3.2 Interface Shear Stress

Interface shear stresses at key points in the loading are summarized in Table 3.11 for all specimens. Average interface shear stress, $\tau_{avg.}$, was calculated using the peak shear force, V , divided by the interface area, A_c , which was taken as either the full interface area or only the area of the roughened portions for rough-middle specimens (Eq. 3-4).

$$\tau_{avg.} = \frac{V}{A_c} \quad \text{Eq. 3-4}$$

3.3.2.1 Influence of Surface Preparation and Bond Breakers

When stress is calculated based on total interface area, cracking and peak stress are both greatest for specimens with a fully roughened surface followed by the rough middle specimens, the troweled specimens, and the debonded specimens (Table 3.11). This is also shown in Figure 3.21; a plot of shear stress calculated over the total interface area versus slip for several bonded specimens with a 12 by 12 in. interface. In Figure 3.21 the fully roughened specimen had the highest shear strength (830 psi), rough middle specimens with epoxy and felt had slightly reduced strengths of 760 psi and 690 psi, and the troweled specimen had a strength of 400 psi.

Table 3.11: Summary of Interface Shear Stresses

Specimen ID	Area used for Calculation (in. ²)	Stress at Cracking (psi)	Peak Stress (psi)	Stress at 0.25 in. slip (psi)	Estimated Cohesion ^a (psi)
R-12-NB-12-NR	144	510	830	430	500
R-12-NB-6-NR	144	740	– ^b	650	– ^b
R-12-NB-12-HR	144	350	– ^b	560	– ^b
R-24-NB-12-NR	288	410	660	210	490
R-24-NB-12-HB	288	– ^c	660	270	380
T-12-NB-12-NR	144	160	400 ^d	330	70
T-12-F-12-NR	144	– ^e	100 ^d	220	-230
T-12-E-12-NR	144	– ^e	280 ^d	330	-56
T-12-NB-6-NR	144	430	760	570	97
T-12-NB-12-HR	144	220	530 ^d	550	-35
T-24-F-12-NR	288	– ^e	83 ^d	120	-83
T-24-NB-12-HB	288	470 ^f	470	300	170
RM-12-F-12-NR ^g	144 (72)	470 (930)	690 (1400)	340 (690)	360 (720)
RM-12-E-12-NR ^g	144 (72)	520 (1000)	760 (1500)	400 (790)	430 (860)
RM-12-F-6-NR ^g	144 (72)	550 (1100)	830 (1700)	570 (1100)	170 (330)
RM-24-F-12-NR ^g	288 (144)	220 (450)	– ^b	200 (400)	– ^b
Mean for Rough Specimens:		500	720	420	460
Mean for Rough-Middle Specimens:		440 (880)	760 (1530)	380 (760)	320 (640)
Mean for Bonded Troweled Specimens:		320	540	440	76
Mean for Debonded Specimens:		– ^e	160 ^d	220	-120

^a Column (6) in Table 3.10 divided by area

^b Results were influenced by unintentional rotation near peak force

^c Omitted because specimen was cracked prior to testing

^d Force at peak corresponds to the proportionality limit

^e Unbonded specimens are effectively cracked prior to testing

^f First cracking occurred at peak strength

^g For partially bonded specimens, stress outside the parentheses was calculated based on the full interface area while stress inside the parentheses was calculated using the roughened area

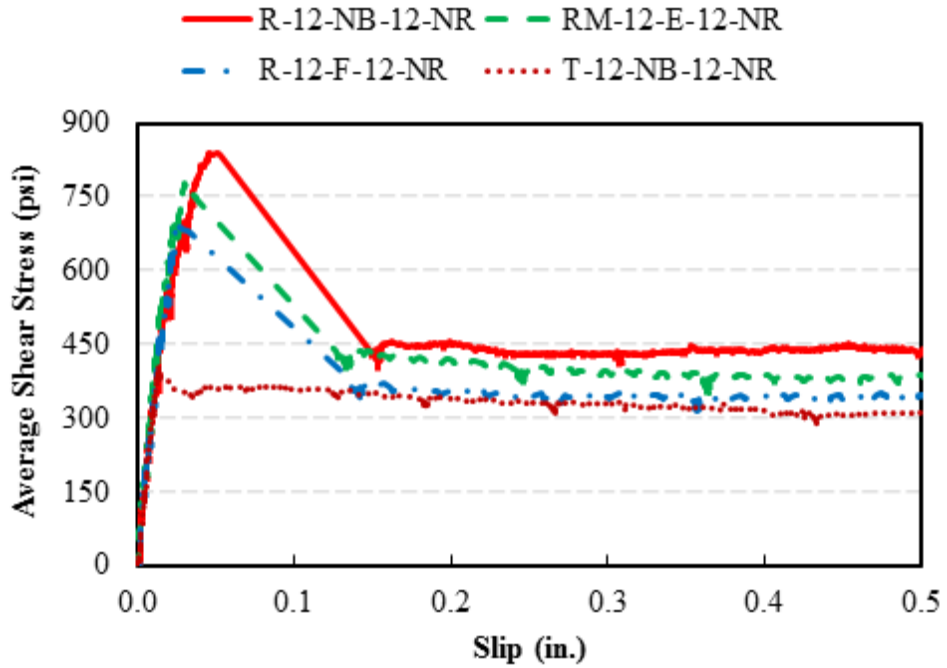


Figure 3.21: Average Shear Stress versus Slip Curves for Bonded Specimens

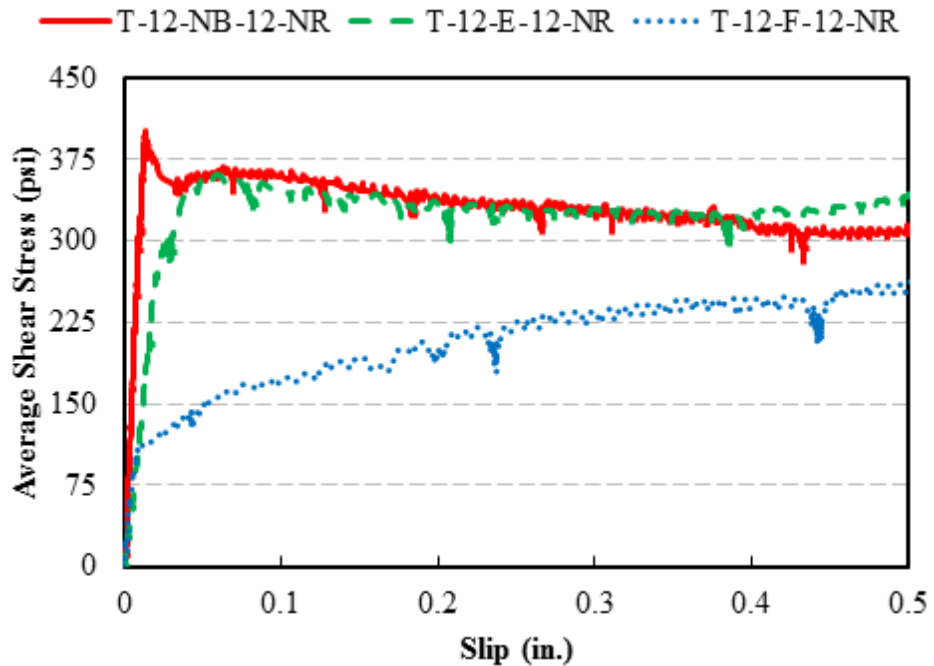


Figure 3.22: Average Shear Stress versus Slip Curves for Troweled Specimens

Among specimens with partially or completely debonded interfaces, use of roofing felt resulted in a more complete disruption of bond than epoxy. This is shown in Figure 3.22 where stress is plotted versus slip for troweled specimens with 12 by 12 in. interfaces. The specimen with

roofing felt deviated from the initial slope earlier than other specimens and ultimately had the lower strength. This is evidence that the contribution to horizontal shear strength of any portion of the girder-deck interface covered with roofing felt or other bond breakers should be neglected.

If the contribution to shear strength of debonded portions of an interface are to be neglected in design, then shear stresses for rough middle specimens should be calculated based only on the area of the roughened interface. Table 3.11 shows that when calculated based on the area of roughened concrete, specimens with a roughened middle surface and bond breakers (RM-12-F-12-NR and RM-12-E-12-NR) had much greater first cracking stresses and between 1.8 and 2.1 times greater peak stress than the fully roughened companion specimen (R-12-NB-12-NR). This strength of the rough middle specimens is still greater than for the fully roughened specimens if a correction is made for the increased reinforcement ratio ($460 \text{ psi} + 0.62 \text{ in.}^2 \times 72 \text{ ksi} / 72 \text{ in.}^2 = 977 \text{ psi}$, which is less than 1530 psi). It is therefore conservative to neglect the debonded portions of an interface in design.

3.3.2.2 Influence of Reinforcement Parameters

The series of push-off tests also included several secondary variables related to the interface shear reinforcement. These variables included reinforcement grade (Grade 60 and Grade 120), reinforcement amount (either 1 or 2 pairs of No. 5 bars for areas of 0.62 and 1.24 in.²), and shear reinforcement anchorage type (hooked and headed bars).

As shown in Table 3.11 and Figures 3.23 and 3.24, which show plots of average shear stress versus slip for fully troweled and rough middle specimens, increasing the amount of interface reinforcement tended to result in higher stress at first cracking, peak, and post-peak, although the effect was somewhat inconsistent. When the interface reinforcement area was doubled, stress at cracking increased by 46% for roughened specimens (R-12-NB-6-NR and R-12-NB-12-NR), 17% for rough middle specimens (RM-12-F-6-NR and RM-12-F-12-NR), and 170% for troweled specimens (T-12-NB-6-NR and T-12-NB-12-NR). For the same pairs of specimens, peak stress increased by 4.9% for roughened specimens, 20% for rough middle specimens, and 90% for troweled specimens when reinforcement area was doubled; post-peak stress increased by 52% for roughened specimens, 67% for rough middle specimens, and 72% for troweled specimens when

reinforcement area was doubled. For these same pairs of specimens, doubling the amount of interface reinforcement also increased the initial stiffness for rough specimens by 66%, for rough middle specimens by 80%, and for bonded troweled specimens by 19%. It is not clear why the effect of increased bar area varied so much between pairs of specimens with different surface preparations.

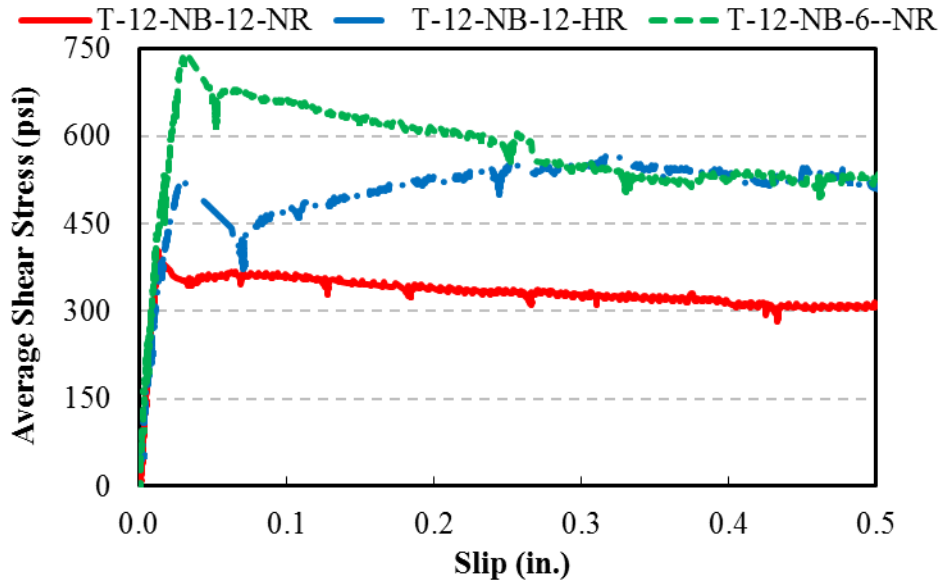


Figure 3.23: Average Shear Stress versus Slip for Fully Troweled Surface

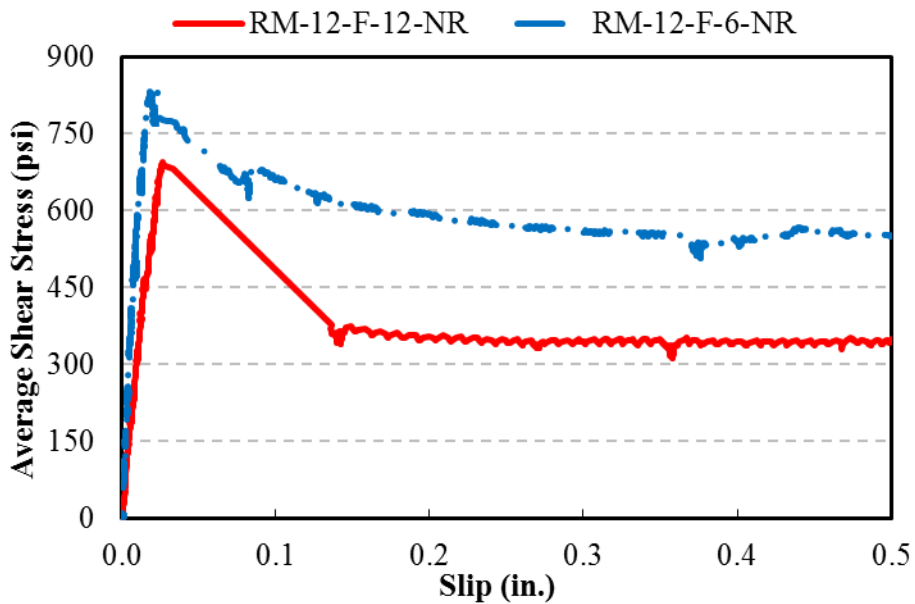


Figure 3.24: Average Shear Stress versus Slip for Partially Roughened Surface with Felt

Increasing the yield strength of the interface shear reinforcement by 100% had no clear effect on the cracking stress and increased peak strength by only approximately 30%. This is based on comparisons between two pairs of roughened specimens (R-12-NB-12-HR and R-12-NB-12-NR as well as R-24-NB-12-HB and R-24-NB-12-NR) and one pair of troweled specimens (T-12-NB-12-HR and T-12-NB-12-NR). Among roughened specimens, the specimen with a higher reinforcement grade had a 30% lower cracking strength (which is likely unrelated to use of high-strength steel) and approximately equal peak strength. Among the troweled specimens, cracking stress and peak stress increased by 38 and 31%, respectively. When specimens with high-strength steel were compared to specimens with an increased area of interface shear reinforcement (e.g. R-12-NB-12-HR and R-12-NB-6-NR, where either grade or reinforcement area were doubled relative to the control, R-12-NB-12-NR) increasing reinforcement area was a more effective means of increasing interface shear strength than increasing reinforcement grade. Although based on very limited data, this finding is consistent with findings from other research groups (Harries and Zeno, 2012). It is possible this is attributable to the short anchorage length provided that may not have allowed for the higher grade bars to fully develop their capacity. Additional investigation is necessary if high-strength steel is to be used in shear friction applications.

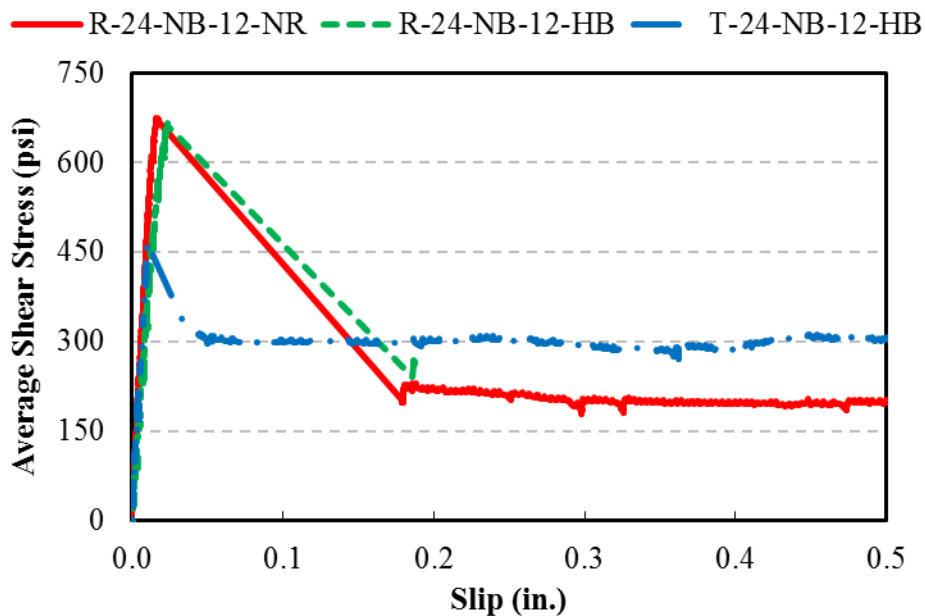


Figure 3.25: Average Shear Stress versus Slip for 24 in. Wide Specimens

Headed bars were only used in two specimens (R-24-NB-12-HB and T-24-NB-12-HB) both of which had a 12 by 24 in. interface. Average shear stress is plotted versus slip for these specimens in Figure 3.25 along with the result from the test of R-24-NB-12-NR. According to Table 3.11, stress at peak is the same for R-24-NB-12-HB and R-24-NB-12-NR, implying that the anchorage type (hooked or headed) did not affect behavior. Use of headed bars as interface shear reinforcement may therefore be a viable option. This is however a very small number of tests, so no firm conclusion can be drawn.

3.3.2.3 Influence of Interface Area

The influence of interface area was explored for two types of specimens with the same interface shear reinforcement: troweled specimens with roofing felt and fully roughened specimens with no bond breaker. Average shear stress is plotted versus slip in Figure 3.26 for troweled specimens with roofing felt (T-12-F-12-NR and T-24-F-12-NR). Stress at peak for T-24-F-12-NR is about 44% that of T-12-F-12-NR. This is understandable because the peak strength was mainly due to dowel action in troweled specimens, and both specimens had the same area of reinforcement. With regard to stiffness, T-12-F-12-NR and T-24-F-12-NR had approximately equal stiffness in terms of force per in. of deflection (Table 3.5) despite T-24-F-12-NR having an interface area twice that of T-12-F-12-NR. In terms of stress per in. of deflection, the specimen with the smaller interface exhibited the larger stiffness. These observations are consistent with initial stiffness of debonded troweled interfaces being a function of interface reinforcement area.

Average shear stress is plotted versus slip in Figure 3.27 for bonded specimens with a fully roughened interface (R-12-NB-12-NR and R-24-NB-12-NR). According to Table 3.11, stress at cracking and peak for R-24-NB-12-NR were both approximately 80% that of R-12-NB-12-NR. Table 3.11 shows both specimens had effectively the same estimated cohesion, indicating the whole interface was similarly engaged regardless of cross-section or reinforcement ratio. The difference in peak stress between R-12-NB-12-NR and R-24-NB-12-NR was therefore attributable to the difference in reinforcement ratio between the specimens (they had the same area of interface reinforcement but different interface areas). The larger interface area also resulted in an increase in stiffness of 280% (Table 3.5).

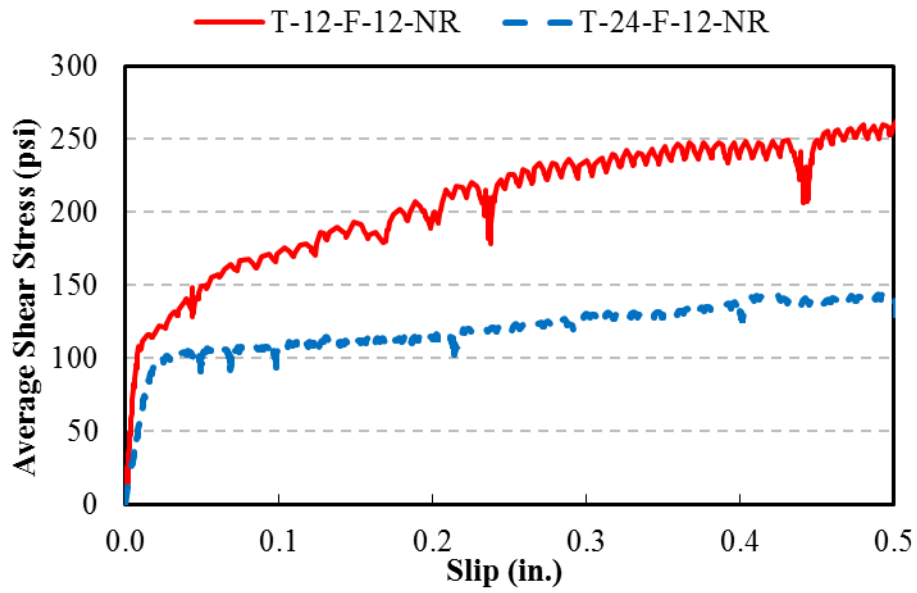


Figure 3.26: Average Shear Stress versus Slip for Troweled Specimens with Felt

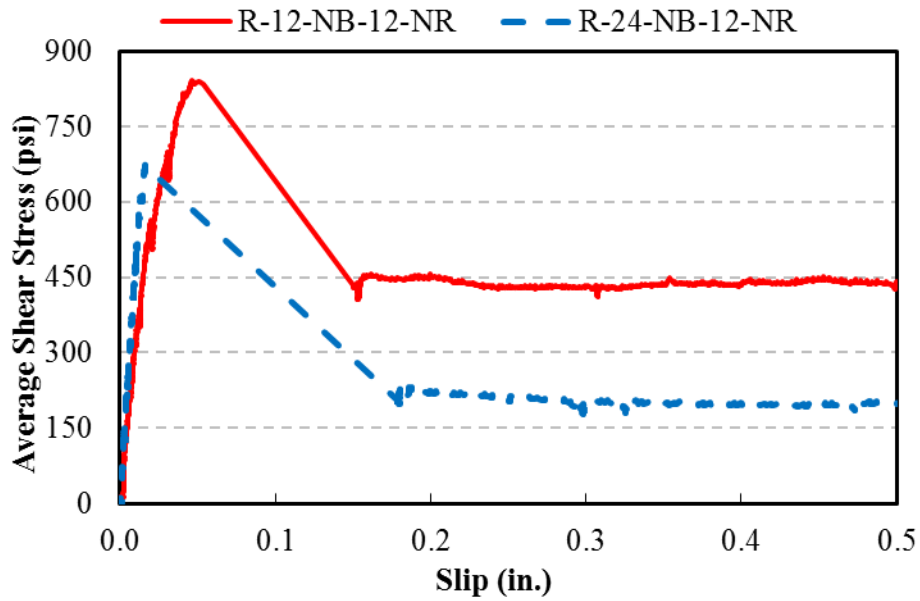


Figure 3.27: Average Shear Stress versus Slip for Roughened Specimens

3.4 Conclusions from Push-off Tests

The following conclusions are drawn from push-off test results:

1. Surface preparation has a large influence on shear transfer performance up to peak strength. Stiffness, stresses at cracking, and peak strength are greatest for specimens with a fully roughened surface followed by those with a rough middle surface, troweled specimens, and fully debonded specimens. After peak, surface preparation had little effect on specimen strength, as behavior was dominated by reinforcement dowel action.
2. Use of an interface that is partially roughened and partially troweled with a bond breaker is a viable connection detail for horizontal shear transfer. Compared to specimens with a fully roughened interface, specimens with a partially roughened interface resisted somewhat lower force at first cracking and at peak, as expected. However, when considered in terms of stress calculated based on the area of roughened concrete and corrected for reinforcement ratio, specimens with a partially roughened interface had greater first cracking and peak strength than comparable fully-roughened specimens.
3. The ascending branch of the force versus slip relationship for specimens with at least a partially roughened interface was composed of two distinct branches representing behavior before and after cracking of the interface. Interface cracking occurred, on average, at a stress of 500 psi in specimens with a fully roughened interface. In troweled bonded specimens, cracking (at an average stress of 320 psi) is approximately equal to the peak strength. As expected, troweled debonded specimens behaved as though cracked from the start of the test.
4. Assuming shear strength can be expressed as the sum of cohesion and reinforcement terms, the contributions of cohesion and reinforcement to peak strength were estimated from test results. Cohesion, which was sensitive to variability of testing results, was calculated to be, on average, 460, 320, 76, and -120 psi for roughened, rough-middle, troweled, and debonded specimens. These values are approximately double and equal to the values recommended in the AASHTO Specification for roughened and troweled interfaces (240 and 75 psi). The negative cohesion value for debonded specimens indicates that the reinforcement was not fully effective when the entire interface was debonded. The contribution of normal strength (Grade

- 60) reinforcement was, on average, $1.1A_s f_y$. The coefficient of 1.1 is larger than those recommended by AASHTO Specifications (1.0 and 0.6 for roughened and troweled interfaces).
5. It is recommended that areas treated with either epoxy or roofing felt debonding agents be neglected when calculating interface shear strength. Fully debonded specimens exhibited lower initial stiffness, lower strength at the proportionality limit, and very large slip (greater than 0.25 in.) at peak strength. When applied to specimens with partially debonded interfaces, this recommendation would result in conservative estimates of strength, as the peak stress resisted by rough middle specimens was greater than other specimens when the debonded portions of the interface were neglected.
 6. When an interface is between two elements cast with different concrete strengths, the lower concrete strength should be used to calculate horizontal shear strength (when concrete compressive strength is considered). This is based on observations after testing that the failure plane occurs primarily in the lower strength concrete.
 7. Increasing the amount of interface shear reinforcement increases the initial stiffness of the connection, interface shear strength at cracking, peak strength, and post-peak strength, though not in proportion to the increase in reinforcement area.
 8. Use of high-strength steel as interface shear reinforcement had no discernable effect on stiffness or cracking strength, and a less substantial effect on peak strength and post-peak strength than a comparable increase in reinforcement area (doubling reinforcement area and yield strength respectively led to increases in peak strength of 5 to 90% and 0 to 30%). Additional study is needed however, as the number of specimens was small.
 9. Use of headed bars as interface shear reinforcement appears viable, as pairs of specimens with either headed or hooked bars exhibited similar behavior. Additional study is needed however, as the number of specimens was small.

Chapter 4: NU I-Girder Testing

The second phase of the experimental program consisted of the construction and testing of three large-scale NU I-Girders designed to compare three different beam-to-deck connection details in terms of constructability, fatigue behavior, and ultimate strength. The girder specimens, which were designed in accordance with the 6th edition of the AASHTO LRFD Bridge Design Specifications, were fabricated at a local precast concrete facility and delivered to the University of Kansas laboratory. Once at the laboratory, simulated bridge decks were cast onto the top of the girders, removed after approximately 28 days in a manner designed to simulate deck removal in the field, and then recast. The composite girders were then placed on simple supports and subjected to 2×10^6 cycles of simulated traffic load at midspan. After all three girders were subjected to the 2×10^6 cycles of load, each was loaded monotonically at midspan until failure.

4.1 NU I-Girder Specimens

As shown schematically in Figure 4.1, the precast girders were 27 ft long, 35 in. deep, and had a 170 in. long 7 in. thick deck cast at midspan. As described further in Section 4.4, the girders were set on simple supports spaced 20 ft-3 in. apart and loaded at midspan. The deck was cast shorter than the beam span to make the horizontal shear connection between the deck and girder more critical and thereby allow for study of the connection.

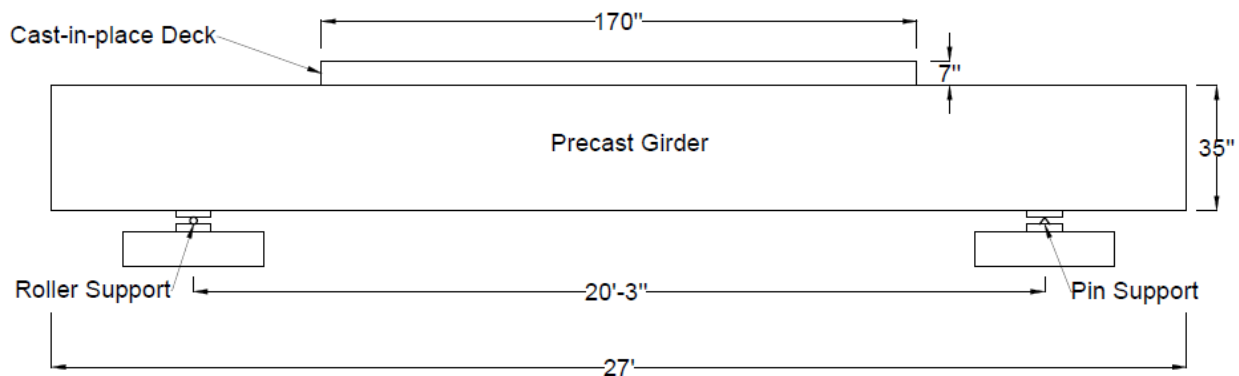


Figure 4.1: Elevation View of Composite NU35 Girder

4.1.1 Girder Reinforcement

Figure 4.2 shows elevation and cross-sectional views of the NU35 girders. Girders #1 and #2 were designed so that the flexural and transverse shear strengths of the composite girder were large enough to ensure that the horizontal shear strength of the girder-to-deck connection could be evaluated. Girder #3 was instead designed to fail in a flexural mode because it was not possible to design it to fail at the interface without first exceeding the maximum permitted web shear stress (i.e. the girder would likely exhibit a web compression failure).

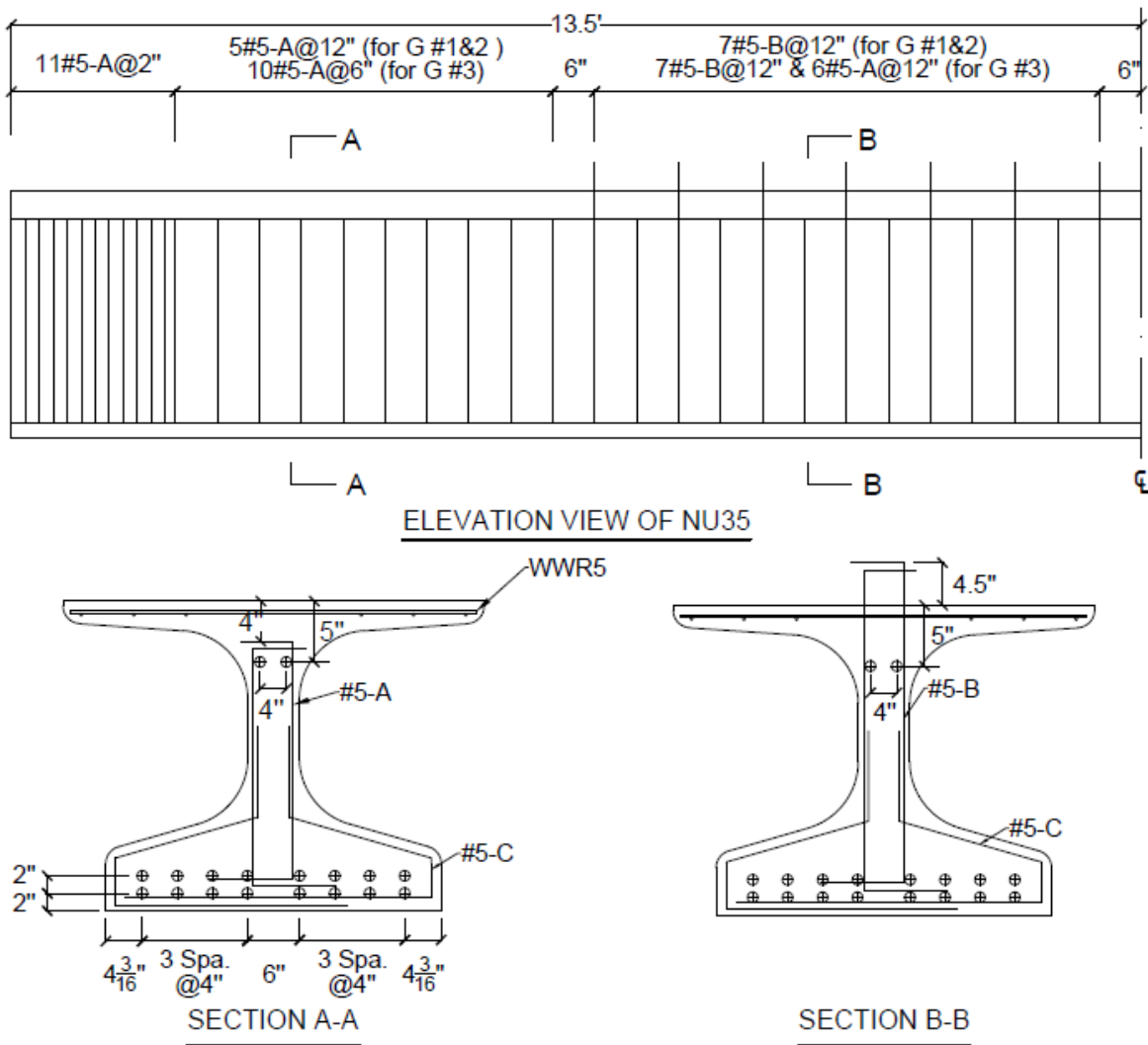


Figure 4.2: Elevation and Cross Sectional Views of NU35 Girder Specimens

Each specimen had 18 straight 0.6 in. diameter seven-wire low-relaxation strands (ASTM A416/A416M-16 Grade 270), with 16 strands distributed within the bottom flange and two strands placed 5 in. below the top of the girder (Figure 4.2). The strands placed near the top of the section were included to ensure that the tensile stress in the top flange at tendon release would remain below an allowable stress of 240 psi, or $3\sqrt{f'_{ci}}$ (psi) from ACI 318-14, where f'_{ci} is the compressive strength of concrete at the time of initial prestress. For design, the initial tendon stress was assumed to be 75% of the ultimate tendon strength, or 203 ksi. The nominal flexural strength of the girders, calculated to be 500 kip-ft, exceeded the moment required to exceed the horizontal shear strength of the girder-to-deck connections estimated based on the push-off test results in Girders #1 and #2.

Transverse reinforcement consisted of ASTM A615/A615M-16 Grade 60 No. 5 bars spaced at 12 in. for Girders #1 and #2 and at 6 in. for Girder #3. For the 170 in. long portion of the beam that had an interface with the concrete deck, stirrups spaced at 12 in. were extended 4.5 in. above the top flange as horizontal shear reinforcement. The stirrups extending into the deck terminated with a standard 90 degree hook turned towards the center axis of the girder. A longitudinally-oriented deck reinforcing bar was later placed under these standard hooks before the deck concrete was placed. This standard hook therefore satisfied the requirements of AASHTO Specification Section 15.11.2.6 for transverse reinforcement anchorage.

Design for vertical shear was done using the simplified AASHTO Specification shear design procedures with the aim of ensuring that a horizontal shear failure would occur along the girder-to-deck connection before the transverse shear strength of the specimens was exceeded. The contribution of concrete to member shear strength, V_c , was calculated as the lesser of V_{ci} , the concrete resistance to flexural-shear cracking (Eq. 4-1), and V_{cw} , the concrete resistance to web-shear cracking (Eq. 4-2). The contribution of transverse reinforcement to shear strength, V_s , was calculated with Eq. 4-3.

$$V_{ci} = 0.02\sqrt{f'_c}b_vd_v + V_D + \left(\frac{\Delta V_u \times \Delta M_{cr}}{\Delta M_u}\right) \geq 0.06\sqrt{f'_c}b_vd_v \quad \text{Eq. 4-1}$$

$$V_{cw} = (0.06\sqrt{f'_c} + 0.3f_{pc})b_vd_v + V_p \quad \text{Eq. 4-2}$$

$$V_s = \cot\theta \frac{A_v f_y d_v}{s} \quad \text{Eq. 4-3}$$

$$\cot\theta = 1 + 3 \frac{f_{pc}}{\sqrt{f'_c}} \leq 1.8 \text{ (for } V_{ci} > V_{cw}, \text{ otherwise } \cot\theta = 1) \quad \text{Eq. 4-4}$$

Where: f'_c is the concrete compressive strength (ksi), b_v is the effective web width, d_v is the effective shear depth, V_D is the shear force due to unfactored dead load at the section considered, ΔV_u is the factored shear force due to externally applied load at the section considered, ΔM_{cr} is the moment in excess of the dead load moment that causes flexural cracking in the precompressed tensile fiber at section considered, ΔM_u is the maximum factored bending moment due to externally applied load at the section considered, f_{pc} is the concrete compressive stress at the centroid of the cross-section when subjected to externally applied loads, V_p is the component of prestressing force in the direction of applied shear, s is the spacing of transverse reinforcement, A_v is the area of transverse reinforcing steel within a distance s , f_y is the yield strength of the transverse reinforcing steel, and θ is the angle of inclination of the diagonal compressive strut. Eq. 4-4 was used to calculate $\cot\theta$. The nominal shear strength was 260 kip for Girders #1 and #2 and 440 kip for Girder #3 assuming fully composite behavior.

As shown in Figure 4.2, the end zones of the specimens had No. 5 transverse reinforcing bars spaced at 2 in. The required area of transverse reinforcement in the end zones was calculated using Eq. 4-5 from the 16th edition of the AASHTO Standard Specification (1996), as cited by Naaman (2012).

$$A_v = 0.04 \frac{F_i}{\bar{f}_s} \quad \text{Eq. 4-5}$$

Where: A_v is the required area of stirrups in the end zones (to be uniformly distributed over a distance of 0.2 times the girder depth, h , from the end of the girder), F_i is the total initial prestressing force, and \bar{f}_s is the design allowable stress in the transverse bars (20 ksi per the AASHTO Specification). It was calculated that A_v was required to be 1.4 in.² within 7 in. of the end of the beam. The No. 5 U-shaped stirrups spaced at 2 in. provided 1.86 in.² within 7 in. of the end of the beam, or approximately 30% more than the minimum required. This close spacing of

stirrups was conservatively extended to approximately $0.75h$ of the ends of the specimens to eliminate the potential of bond-related failures. These additional stirrups were located beyond the location of the supports in both the fatigue and ultimate strength tests.

Mild steel welded wire fabric (WWR5) was provided in the top flanges of the girders. The topmost bars (“wires”) were oriented transverse to the axis of the girder, had a diameter of 0.504 in., and were spaced at 6 in. These were welded to six W8 wires oriented parallel to the axis of the girder. The six W8 wires, which had a nominal diameter of 0.319 in., were spaced at 6 in. beginning 2 in. from the flange tips, leaving a 20 in. gap between wires over the girder web.

4.1.2 Top Flange Detailing for Composite Action

The top flange of each girder was finished in accordance with one of the three details shown in Figure 4.3: Girder #1 had a fully troweled surface, Girder #2 was troweled except for an 8 in. wide strip over the web that was roughened, and Girder #3, which represents current practice, had a fully roughened surface except for 6 in. wide strips along the edges of both flange tips. These details were selected to allow an examination of the effect of these different surface preparations on the constructability and composite behavior of girder-deck systems relative to the mostly roughened top flange detail typical in practice.

Reinforcement consisting of No. 5 hooked bars spaced at 12 in. was placed across the girder-deck interface in all three specimens. This amount of interface shear reinforcement ($0.62 \text{ in}^2/\text{ft}$) exceeds the minimum area required ($0.48 \text{ in}^2/\text{ft}$) by the AASHTO Specification by 29%. The minimum area of interface shear reinforcement, A_{vf} , is calculated with Eq. 4-6.

$$A_{vf} = \frac{0.05A_{cv}}{f_y} \quad \text{Eq. 4-6}$$

Where: A_{cv} is the interface area (taken as the product of top flange width, 48.2 in., and horizontal shear reinforcement spacing, 12 in.) and f_y is the yield stress of the shear reinforcement (60 ksi).

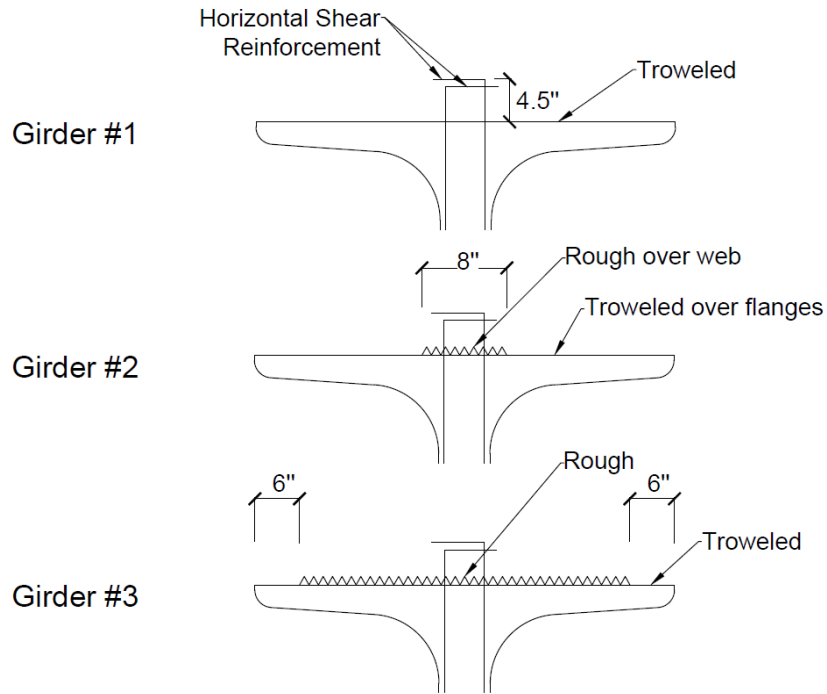


Figure 4.3: Connection Details for NU35 Girders

4.1.3 Bridge Deck Reinforcement

Two months after the precast girders were delivered to the laboratory, simulated reinforced concrete bridge decks were constructed on top of each specimen (Figure 4.4). The simulated bridge decks were 7 in. thick (the minimum depth of deck permitted by the AASHTO Specification), spanned the full width of the top girder flange (48.2 in.), and had a total length of 170 in. The selected deck thickness is representative of practice; typical bridge decks in Kansas without overlays reportedly have thicknesses between approximately 7 and 8.5 in. (Schwensen and Farlow, personal communication 2015). The bridge deck reinforcement was designed based on Section 9 of the AASHTO Specification with the topmost and bottommost layers of deck reinforcement oriented perpendicular to the girder axis (in the direction of deck spans). Four layers of isotropic reinforcement were provided using ASTM A615/A615M-16 Grade 60 No. 5 reinforcing bars. The top layers of reinforcement were spaced at 21 and 24 in., resulting in 0.17 and 0.16 in.²/ft of reinforcement perpendicular and parallel to the girder axis, respectively. The bottom layers of reinforcement, spaced at 14 and 16 in., had 0.27 in.²/ft and 0.23 in.²/ft of reinforcement

perpendicular and parallel to the girder axis, respectively. The deck reinforcement was therefore close to the minimum required per Section 9.7.2.5 of the AASHTO Specification: $0.18 \text{ in.}^2/\text{ft}$ for top reinforcement and $0.27 \text{ in.}^2/\text{ft}$ for bottom reinforcement. The 7 in. thick decks had 2 in. of clear cover over the top bars and 1 in. of clear cover below the bottom bars.

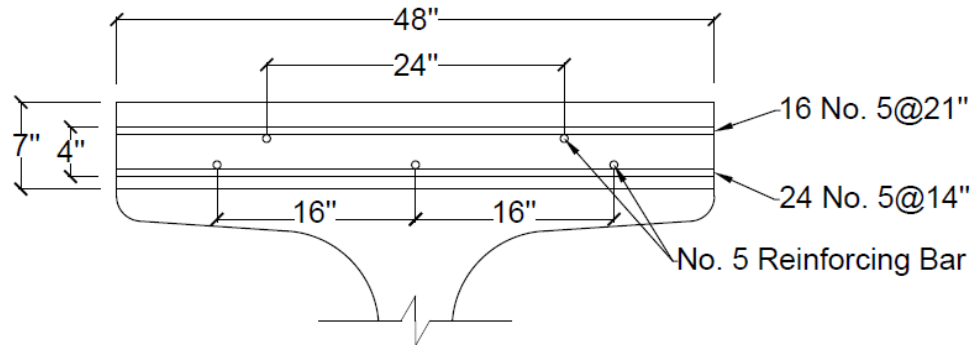


Figure 4.4: Concrete Bridge Deck Reinforcement

4.1.4 Materials

The mixture proportions used for the NU35 girder and bridge deck are shown in Table 4.1. The concrete used to cast the NU35 girder had a specified compressive strength of 8 ksi. The reported compressive strength of the concrete (measured through tests of cylinders) was 7.2 ksi at tendon release (19 hours after casting) and 9.5 ksi on the day the girders were shipped to the laboratory (8 days). The deck was cast using concrete from a local ready-mix company that had a specified compressive strength of 4 ksi. The measured compressive strengths at 28 days and on demolition day were 4.9 and 5.2 ksi respectively based on tests of 4 by 8 in. cylinders. The same mixture was used for the replacement deck cast after demolition of the first deck. The fatigue and monotonic test described in Section 4.4 and 4.5 were done with the replacement deck. The compressive strength of the concrete in the replacement deck was 4.9 ksi at 28 days and 5.4 ksi at the time of both the fatigue and monotonic tests based on tests of 4 by 8 in. cylinders. Details regarding mixture constituents are provided in the footnotes to Table 4.1.

The NU35 girders were constructed with Grade 60 mild steel reinforcement compliant with ASTM A615/A615M-16 and Grade 270 0.6 in. diameter seven-wire low-relaxation prestressing strands compliant with ASTM A416/A416M-16. The transverse reinforcement and interface shear reinforcement was epoxy coated, as typically done in practice. No further information was provided regarding the steel material properties.

The reinforcement used to fabricate the deck was Grade 60 mild steel reinforcement compliant with ASTM A615/A615M-16. A sample plot of stress versus strain is shown in Figure 4.5 and measured average reinforcement properties are listed in Table 4.2.

Table 4.1: Concrete Mixture Proportions per yd³ for NU35 Girder and Bridge Deck (SSD)

Constituent	NU35 Girder	Bridge Deck
Water (lb)	252	274
Cement ^a (lb)	729	583
Fine Aggregate ^b (lb)	1703	1880
Coarse Aggregate ^c (lb)	1140	1230
Air Entraining Admixture ^d (oz)	70	0
High Range Water Reducing Admixture ^e (oz)	35.0-75.0 ^f	17.0
Measured Density (pcf)	NA ^g	145

^a NU35: Type III Portland Cement; Bridge deck: Type I Portland Cement

^b NU35: KSDOT FA-A compliant aggregate; Bridge deck: Kansas River sand

^c NU35: MoDot Grade “E” Rock; Bridge deck: crushed limestone (with maximum aggregate size of 3/4 in.)

^d VR10 (neutralized vinsol-resin), compliant with ASTM C260/C260M-16 and AASHTO M 154M/M154-12

^e NU35: PS 1466; Bridge deck: ADVA 195 (both compliant with ASTM C494/C494M-16)

^f Exact quantity was not provided

^g Not reported

Table 4.2: Measured Reinforcement Properties for Bridge Deck

Material Properties	Grade 60-No.5
f_y ^a (ksi)	66
ϵ_y ^b	0.0024
f_u ^c (ksi)	98
ϵ_u ^d	0.13

^a Yield stress, calculated based on 2% strain offset method

^b Strain at yield stress, calculated as f_y divided by modulus

^c Maximum stress

^d Strain at maximum stress

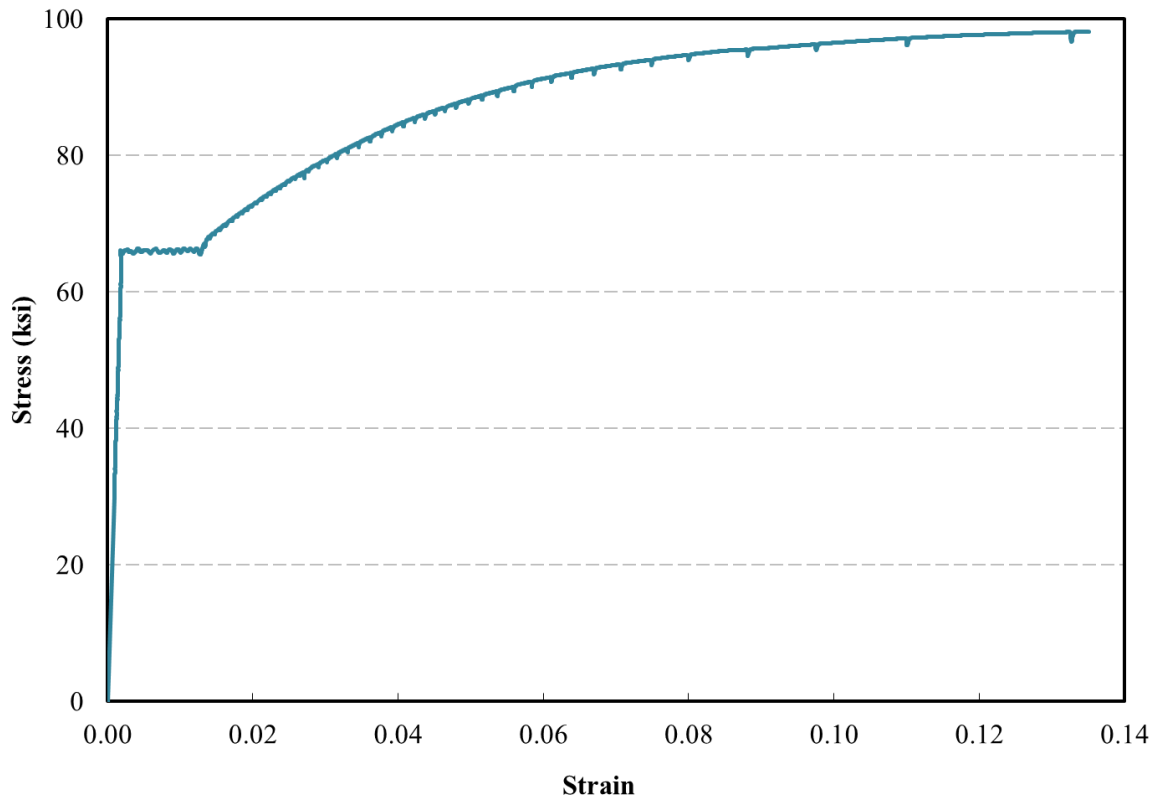


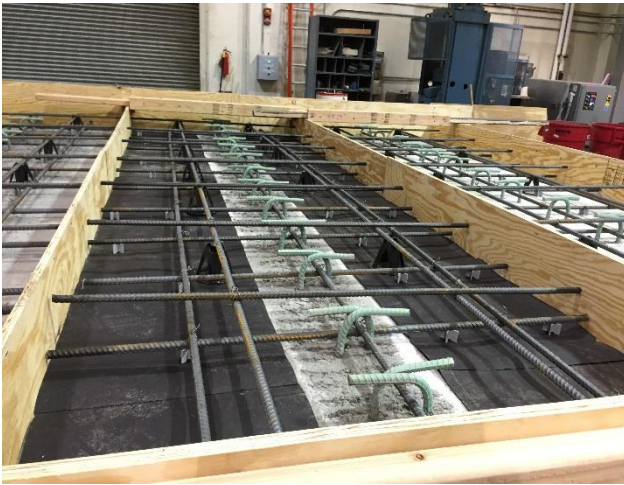
Figure 4.5: Stress versus Strain for No. 5 Bars Used as Deck Reinforcement

4.2 Bridge Deck Construction

Photos of the process of assembling, casting, curing, and demolding the simulated bridge deck are shown in Figure 4.5. To prepare for casting, the three girders were placed side-by-side. The formwork shown in Figure 4.6 was then constructed out of plywood and lumber. Sheets of plywood were placed vertically between the girders so that they extended from the laboratory floor up to 7 in. above the top surface of the top girder flange, side pieces were constructed out of plywood and lumber, and triangular lumber braces were placed along the exterior edges to provide lateral and vertical support.

As shown in Figure 4.6(a), Type I felt was used to cover the troweled edges of the Girder #2 top flange, leaving the 8-in. wide roughened surface exposed. The felt used in this study was a 0.04 in. thick asphalt-saturated organic felt that conformed to ASTM D4869/D4869M-16. For this first deck placement, no roofing felt was used for Girder #1 so that the effort required to remove deck concrete bonded to a troweled concrete surface could be compared to that required to remove

concrete cast over roofing felt. The deck reinforcement was then assembled and supported by rebar chairs as shown in Figure 4.6(a). For casting, concrete from a local ready-mix supplier was delivered with a single truck and placed into the forms for all three girders using a bucket and crane. Concrete vibrators were then used to consolidate the concrete before the top surface of the decks was troweled and finished (Figure 4.6(b)). After casting, damp burlap (Figure 4.6(c)) and plastic sheets were used to cure the concrete for three days. The formwork was removed four to five days after casting. Girders with the demolded decks are shown in Figure 4.6(d).



(a) Deck Reinforcement and Roofing Felt



(b) Concrete Deck after Finishing



(c) Concrete Deck Curing



(d) Demolded Concrete Deck

Figure 4.6: Deck Casting Procedures

4.3 Concrete Deck Removal

The concrete bridge decks were removed from the girders beginning approximately 28 days after casting of the decks to qualitatively evaluate the effort required for, and the damage caused by, bridge deck removal. The purpose was to quantify the extent to which the proposed partially roughened detail (Girder #2 in Figure 4.1) reduced the effort to remove the deck and to document the types and extent of damage caused to the girders by the process.



(a) Walk-Behind Concrete Saw



(b) 65 lb Electric Jackhammer



(c) Variable Impact Demolition Hammer



(d) Hammers and Chisels

Figure 4.7: Primary Tools Used for Deck Removal

The deck removal methods, described in detail below, consisted of saw-cutting, jackhammering, and chipping. In general, the approach was to cut the concrete deck into smaller pieces and then remove/demolish it piece by piece. Note that the scope of this project did not include the simulated removal of bridge decks spanning between girders. The focus of the project was to investigate a time consuming part of the deck removal process: separation of the bridge deck from the supporting girder.

4.3.1 Deck Removal Procedures

The primary tools used for deck removal are shown in Figure 4.7. These included the walk-behind concrete saw shown in Figure 4.7(a), 65 lb electric jackhammer shown in Figure 4.7(b) that was operated with a 1-1/8 in. bit, demolition hammer shown in Figure 4.7(c) that had an adjustable power output from 3.7 to 18.5 foot-pounds of impact energy, and various hammers and chisels shown in Figure 4.7(d). Although the demolition hammer had a weight of 23 lbs, the power output was set to approximately mid-range, or approximately 12 ft-pounds of impact energy, when chipping around the rebar and close to the deck. This was done to simulate the use of a 15 lb demolition hammer, which is typically required for such tasks.

4.3.1.1 Saw-Cutting

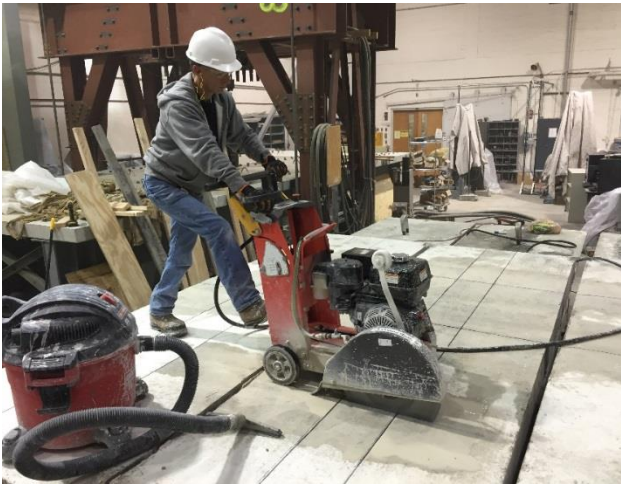
The first step of the demolition process was to saw-cut the concrete deck into 12 sections (Figure 4.8). For each deck, two longitudinal cuts were made 4 in. from the centerline of the girder (near to but not interfering with the horizontal shear transfer reinforcement) and three transverse cuts were made at regular intervals (spaced at 42.5 in.). As shown in Figure 4.8(a), chalk-lines were first set on the top surface of the concrete deck to guide the operator of the saw. The walk-behind saw was then used to make the longitudinal and transverse cuts (as shown in Figures 4.8(b) and 4.8(c)). The depth of cut was set to 6.75 in. to avoid contacting the girder top flange (the deck thickness was 7 in.). The saw-cut decks are shown in Figure 4.8(d).



(a) Chalk Lines Indicating the Location of Saw-Cuts



(b) Longitudinal Saw-Cuts



(c) Transverse Saw-Cuts



(d) Decks after Saw-Cutting

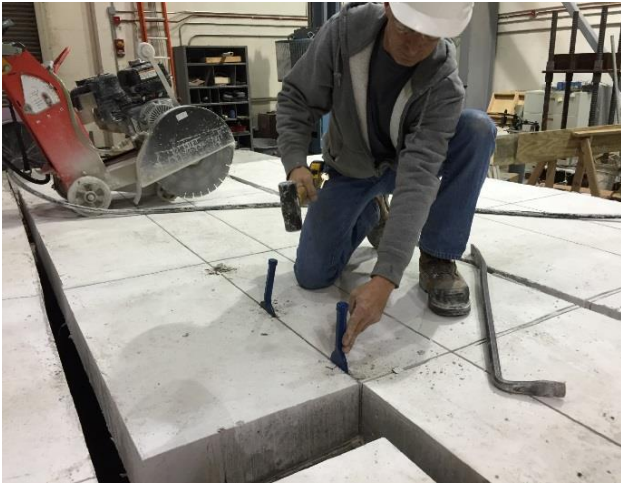
Figure 4.8: Saw-Cutting Procedures

4.3.1.2 Removal of Saw-cut Deck Sections

Removal of the deck sections located above the girder web, which were linked to the girder by bond and reinforcement crossing the interface, required greater effort than removal of the deck sections located along the edges of the flanges that had no interface reinforcement. For

demolishing the edge sections, hammers, chisels, prybars, and demolition hammers were used as shown in Figure 4.9 to break the deck concrete free from the girder top flange and, where necessary, demolish the deck concrete. For Girder #2, which had roofing felt placed over a large portion of the flanges, all eight saw-cut edge sections of the deck were broken free easily by hammering chisels into the gaps created by saw-cutting (Figure 4.9(a)) or using a demolition hammer (required for 50% of the sections) to widen the gap between the deck and girder to break the deck loose (Figure 4.9(b)) before prying them free with a prybar. Once broken free (Figure 4.9(c)), these deck sections could be lifted off the girder and disposed of. For Girder #1, which had a troweled flange and no roofing felt (for this part of the study), it was possible to break six of the eight edge sections free in this same way. For the two remaining edge sections of Girder #1 that could not be debonded, and for seven of the eight edge sections on Girder #3 that had a roughened top flange, it was necessary to use the demolition hammer to demolish the deck directly as shown in Figure 4.9(d). As a result, removal of the deck sections over the troweled and roughened girder flanges took significantly more effort than over the flanges covered with roofing felt.

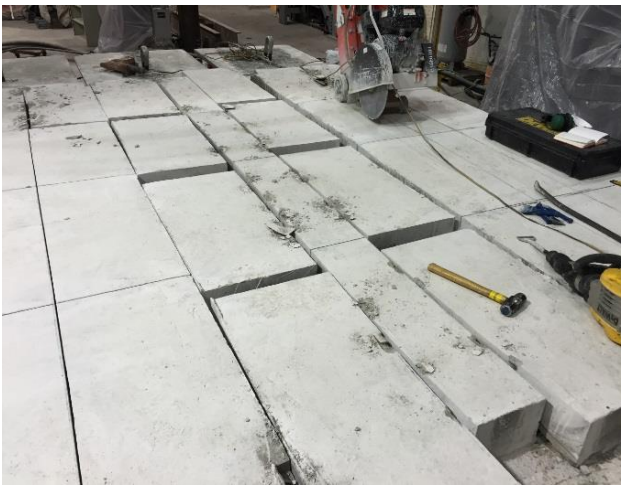
After removal of the edge sections of the deck, the middle portions of the deck located over the beam webs were removed. The steps of the process are shown in Figure 4.10. As shown in Figure 4.10(a), a 65 lb jackhammer was first used to break apart the middle sections down to the level of the interface reinforcement. Although hammers larger than 30 lbs are generally not permitted by Kansas Department of Transportation specifications, the larger hammers were used here on a limited basis with no negative impacts. Use of such large hammers must, however, be well controlled and any contact with or near the girder must be avoided. In practice, it would be prudent to limit hammer sizes to 30 lbs, as currently done in typical KDOT specifications (2015) and recommended by Manning (1991) and the American Concrete Pavement Association (1998). After exposing the interface shear reinforcement, the variable impact demolition hammer, set to a moderate impact energy level consistent with a 15 lb demolition hammer, was used to remove the remaining concrete down to the top of the girder flange as shown in Figures 4.10(c) and 4.10(d).



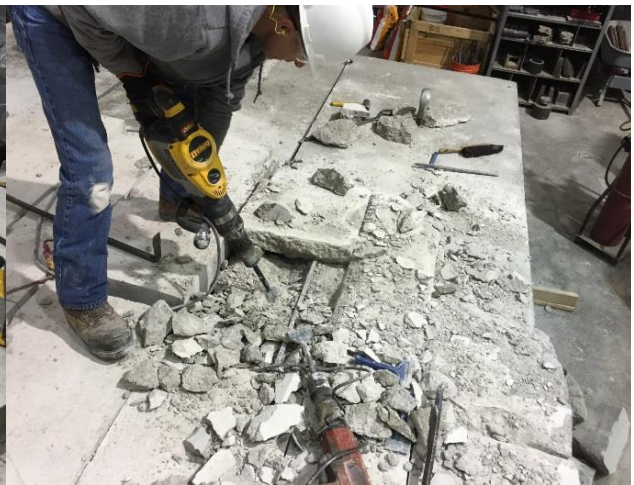
(a) Breaking the Deck Concrete Free with Hammers and Chisels Where Roofing Felt was Placed Prior to Casting



(b) Use of Demolition Hammer at a Low Angle to Break Deck Sections Free

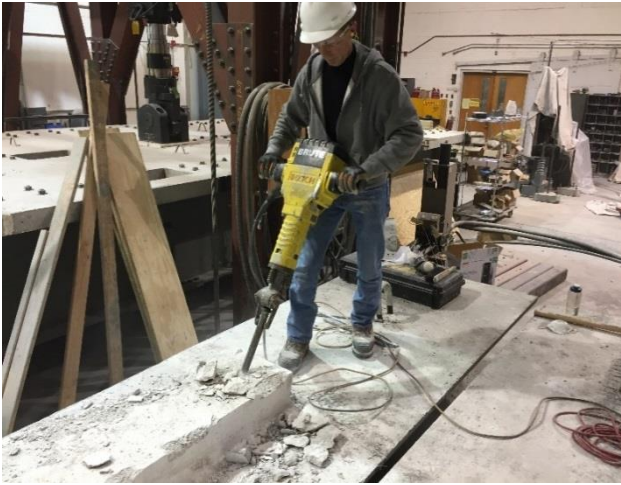


(c) Debonded Edge Pieces on Girder #2 Where Roofing Felt was Used



(d) Demolishing Edge Sections of the Deck Where They were Bonded to the Girder

Figure 4.9: Removal of Bridge Deck Concrete over Girder Edges



(a) Limited use of 65 lb Jackhammer to Remove Concrete above the Interface Shear Reinforcement



(b) Deck Condition After Use of the 65 lb Jackhammer



(c) Prior to use of Variable Impact Demolition Hammer



(d) After Deck Removal

Figure 4.10: Removal of Deck Concrete over Girder Webs

4.3.2 Evaluation of Connection Details

The process of demolishing the bridge decks was carefully documented to allow for a comparison between the three connection details in terms of the effort required for demolition, damage to the girders caused by demolition, and condition of the top girder surface after demolition.

4.3.2.1 Effort Required for Deck Demolition

The effort required for bridge deck demolition was quantified in terms of the person-hours it took to complete the task within the University of Kansas Laboratory (Table 4.3). The number of person-hours reported is not meant to be representative of the productivity of contractors on-site, but this measure allows for relative comparisons of effort among specimens. Bridge deck demolition was performed for the three specimens by the same two workers to reduce variability caused by differences in the pace of work.

Table 4.3: Person-Hours Required for Bridge Deck Demolition

Connection Details	Saw-cutting (person-hrs)	Removal of Edge Sections (person-hrs)	Removal of Middle Sections (person-hrs)	Total Effort (person-hrs)	Total Effort / Total Effort for Girder #3
Girder #1: Fully Troweled	4.5	21	9.5	35	74%
Girder #2: Partially Roughened with Roofing Felt	4.5	3.0	9.5	17	36%
Girder #3: Fully Roughened	4.5	33	9.5	47	100%

The reported person-hours are separated into three parts: saw-cutting, demolishing/removal of edge sections (over the flange tips), and demolishing/removal of the middle portions of the deck over the web. As shown in Table 4.3, the effort spent on saw-cutting and demolishing the middle sections (4.5 and 9.5 hours, respectively) were nominally the same for the three connection details. However, significant differences were documented in the effort required to demolish the edge portions of the decks. For Girder #1, which had a fully troweled surface, 21 person-hours were required to demolish the edge portions down to the level of the girder top flange. Deck removal for Girder #2, which had a roofing felt placed over the top flange prior to casting except for an 8

in. section over the web, complete removal of the edge portions required only 3.0 person-hours. The girder with a mostly roughened surface, Girder #3, required 33 person-hours for complete removal of the edge sections of the bridge deck. In summary, the effort required for bridge deck removal in Girders #1 and #2 was approximately 74% and 36% that of required for Girder #3, respectively. Bridge deck removal for Girder #2 required only 49% of the effort required for the deck over Girder #1.

4.3.2.2 Damage to Bridge Girders Due to Bridge Deck Demolition

Although the girders were generally in good condition after bridge deck demolition, several examples of damage were observed (Figure 4.11). Two examples of damage, shown in Figures 4.11(a) and 4.11(b), resulted from the saw-cutting process. The first, which occurred in Girder #3, was damage to the interface shear reinforcement caused by contact with the saw blade. The second, observed on Girder #2, was damage to the girder top flange caused by contact with the saw blade. Neither damage type is related to the girder surface detail, and contractors risk causing such damage whenever saw-cutting is employed. It should, however, be possible to minimize this damage by a) limiting the number of cuts, b) setting the maximum cut depth to 0.5 in. less than the deck thickness over the flange, and either c) locating the interface shear reinforcement prior to saw-cutting (perhaps through use of GPR-based rebar locators), or d) eliminating transverse cuts through the deck located over the girder web where interface shear reinforcement is located.

The other two types of observed damage are related to the girder-to-deck interface detail. As shown in Figure 4.11(c), a through-thickness wedge-shaped section of the flange tip in Girder #3 (approximately 7 ½ in. long and 2 ½ in. wide) was dislodged due to accidental direct contact between the variable impact demolition hammer and the thin girder top flange. Part of the welded wire reinforcement in the flange was exposed by the damage. This damage would need to be repaired to, at a minimum, protect the exposed reinforcement from moisture and chlorides. Figure 4.11(d) shows another type of observed damage, to the top flange of Girder #1, where a portion of the top flange surface was dislodged along with the deck concrete. The result was an approximately 16 in. long by 10 in. wide by 0.5 in. deep crater in the thin top flange. Although this type of damage is effectively repaired when the replacement bridge deck is cast over the existing girder surface, it

is an indication of the difficulty with which bridge deck concrete is separated from a troweled girder flange. Additional complications may develop if the crater is deep enough to expose reinforcement or, worse, dislodge concrete from the bottom face of the top flange.



(a) Saw-Cut Damage to Rebar (Girder #3)



(b) Saw-Cut Damage to the Girder Top Flange (Girder #2)



(c) Broken Flange Tip (Girder #3)



(d) Crater in Girder Top Flange (Girder #1)

Figure 4.11: Girder Damage Types Due to Deck Removal

4.3.2.3 Condition of Girder Top Flange Surfaces after Bridge Deck Demolition

A motivation for careful bridge deck demolition is to prepare the underlying girders for installation of a new bridge deck. The condition of the top surface of the girders after deck removal was documented and compared to the condition prior to casting of the deck. Although it was observed that deck removal had an influence on the surfaces of the girder top flanges, classification of the surface roughness after deck removal (as troweled, roughened, etc.) was not changed by the process of casting and removal of the bridge deck.

For Girder #3, with an initially roughened top surface, Figure 4.12 shows that the roughness installed at the plant (to a 0.25 in. amplitude using a rake) was not visible after removal of the deck concrete. Instead, a roughened surface with an amplitude of approximately 0.25 in. was observed that resulted from the peaks and valleys caused by the demolition hammer being passed over the concrete surface during the deck removal process and small remnants of deck concrete that remained affixed to the girder surface. Qualitatively, this post-demolition surface appeared to still qualify as roughened according to AASHTO Specification requirements (a clean concrete surface, free of laitance, with surface roughened to an amplitude of 0.25 in.).

For Girder #2, which originally had a roughened strip of concrete over the beam web and roofing felt over the remainder of the flange, the roughened girder surface over the web was similar to the surface of Girder #3 (Figure 4.12). Where roofing felt had been placed, the girder surface was as smooth as it had been prior to casting of the bridge deck (except for the minor saw-cut damage shown in Figure 4.11(b)). The roofing felt effectively prevented the cast-in-place bridge deck from interacting with the girder flange during the casting process and reduced the risk of damage to the girder during deck removal.

The finished surface of Girder #1, which was originally fully troweled, is shown in Figure 4.14. The condition of this surface after deck removal is fairly consistent over the whole surface. Even though the surface was originally troweled smooth, there were small peaks and divots after deck removal where either small remnants of deck concrete remained or where the deck removal process had removed some concrete from the top surface of the girder. It appears that troweled girder surfaces achieve sufficiently high bond between the cast-in-place deck and some parts of the interface to make damage to the girder unavoidable during deck demolition. In general, the



Figure 4.12: Girder #3 Surface after Deck Removal (Originally Fully Roughened)



Figure 4.13: Girder #2 Surface after Deck Removal (Originally Partially Roughened with Roofing Felt over the Flange Tips)

roughness of the Girder #1 surface was between that of the other two girders. For calculation of composite action, it would be prudent to consider the surface of Girder #1 to be troweled.



Figure 4.14: Girder #1 Surface after Deck Removal (Originally Fully Troweled)

4.3.3 Conclusions from Deck Removal

The following conclusions are drawn from the deck removal process:

1. The use of roofing felt over the girder flanges significantly reduced the effort required for bridge deck removal. In this study, the person-hours required for bridge deck demolition over the girder with roofing felt over the flanges was 49% of that for a girder with a fully troweled top flange and 36% of that for a girder with a fully roughened top flange.
2. Use of roofing felt over the girder flanges effectively eliminated damage to the girder caused by hammer impact because it dramatically reduced the need for use of chipping hammers over the flanges. Damage to the girders due to hammer impact included gouging of the top surface

of the girder (Girder #1) and dislodgement of a concrete wedge near the tip of the girder flange (Girder #3).

3. Regardless of connection detail, the girders were vulnerable to damage from saw-cutting. Girder damage due to saw-cutting could be reduced by a) limiting the number of required cuts, b) setting the maximum cut depth to 0.5 in. less than the deck thickness over the flange, and either c) locating the interface shear reinforcement prior to saw-cutting (e.g. based on construction drawings or with GPR-based rebar locators), or d) eliminating transverse cuts through the deck located over the girder web where interface shear reinforcement is located.
4. Casting and removal of a bridge deck does alter the top surface of bridge girders. However, it was possible to return the surfaces of all three girders to a condition similar to their original state with reasonable effort. For instance, although the raking used to roughen parts of the girder flanges was not evident after deck removal, a rough surface consisting of peaks and valleys caused by the chipping process was present. In practice, project specifications should clearly articulate the required roughness of the top flange after deck removal.
5. Roofing felt was easy to install over the flanges immediately prior to placement of the deck reinforcement. No adhesive was used between the roofing felt and top flange because that is where the important debonded plane is located. However, to prevent movement of the roofing felt during construction, it is recommended that contractors use some adhesive to keep the roofing felt in place during construction.
6. Troweled surfaces of the girders exhibited relatively strong bond with the deck concrete that increased the effort required for deck removal and potential for damage to the flanges relative to portions of girders that had roofing felt.
7. Although the use of large jackhammers is not recommended, it may be possible to use jackhammers, like the 65 lb jackhammer used in this study, in very limited field applications. If permitted, use of hammers larger than 30 lbs should be limited to portions of the deck located directly over the girder web and to a depth not greater than the depth of the top deck reinforcement.

Recommendations for deck removal are provided in Section 6.2.

4.4 Fatigue Tests

4.4.1 Construction of Replacement Bridge Deck

Twenty-one days after removal of the bridge decks, replacement bridge decks were cast onto each girder. The dimensions and reinforcement were nominally identical to that described in Section 4.1.3. As described in Section 4.1.4, the concrete mixture proportions and heat of reinforcing steel were the same for both the original and replacement deck. Figure 4.15 shows the surface preparation and deck reinforcement arrangement before casting the replacement decks. For Girder #2 and #3, the surface preparation was the same as for the first deck casting. For Girder #1, roofing felt was applied on the edges of the flanges leaving an 8 in. wide troweled surface exposed over the web (Figure 4.6(a)). The concrete casting and curing procedures were the same as described in Section 4.2.

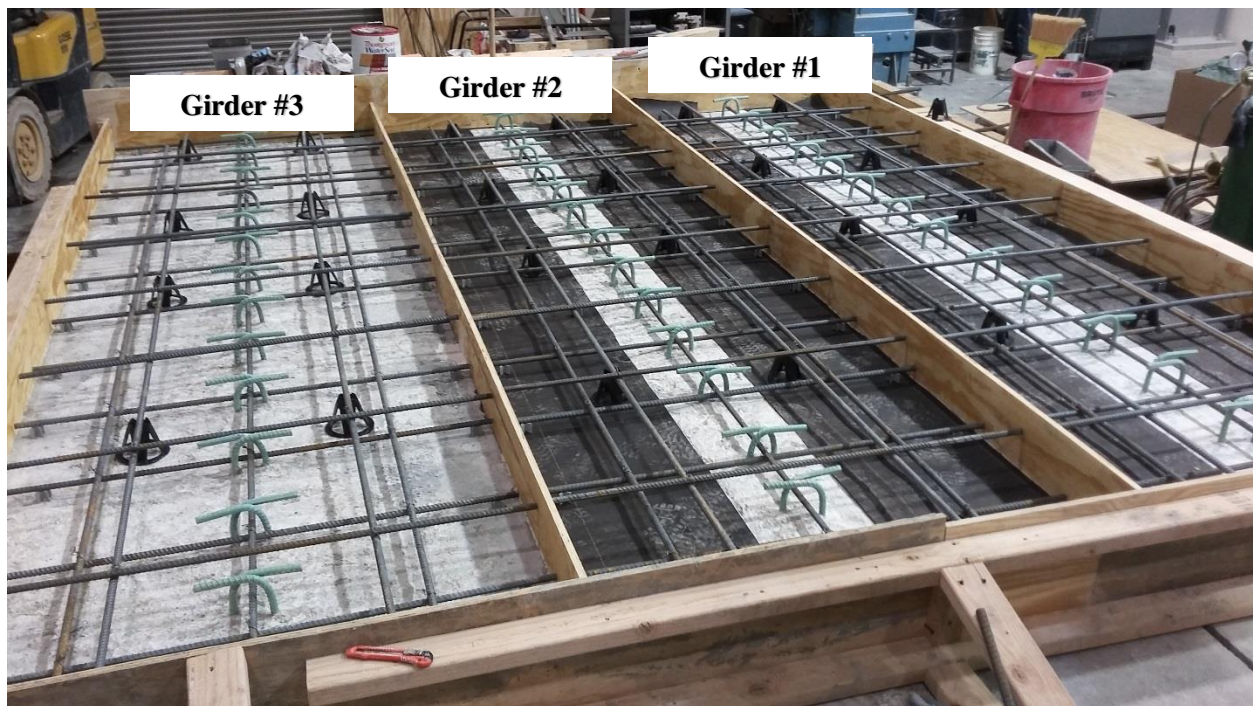


Figure 4.15: Surface Preparation and Deck Reinforcement before Casting

4.4.2 Description of Experimental Program

Beginning 1.5 months after casting the replacement bridge decks, each of the girders was subjected to 2 million cycles of simulated traffic load. Girder #1 was tested first, followed by Girder #2 and then Girder #3.

4.4.2.1 Test Setup and Instrumentation

The test setup and instrumentation used for the fatigue tests are shown in Figure 4.16. Close-up photos of several components of the setup are shown in Figure 4.17 and a photo of the whole setup is shown in Figure 4.18. The composite girder specimens were simply supported, with each support composed of a cylindrical rod placed between two steel plates that rested on a reinforced concrete support block. At one end of the beam, the rod was welded to the bottom plate to serve as a pin (Figure 4.17(a)) while at the other end the rod was free to roll (Figure 4.17(b)). A 110 kip hydraulic actuator was used to apply a cyclic force to simulate traffic loads on the top of the beam at midspan directly over the beam web. A $1 \times 10 \times 20$ in. steel plate (Figure 4.17(c)) was set between the actuator head and concrete deck. The actuator was supported by a steel frame that was bolted to the laboratory strong floor. A bed of gypsum cement was placed wherever steel was to bear directly on a concrete surface.

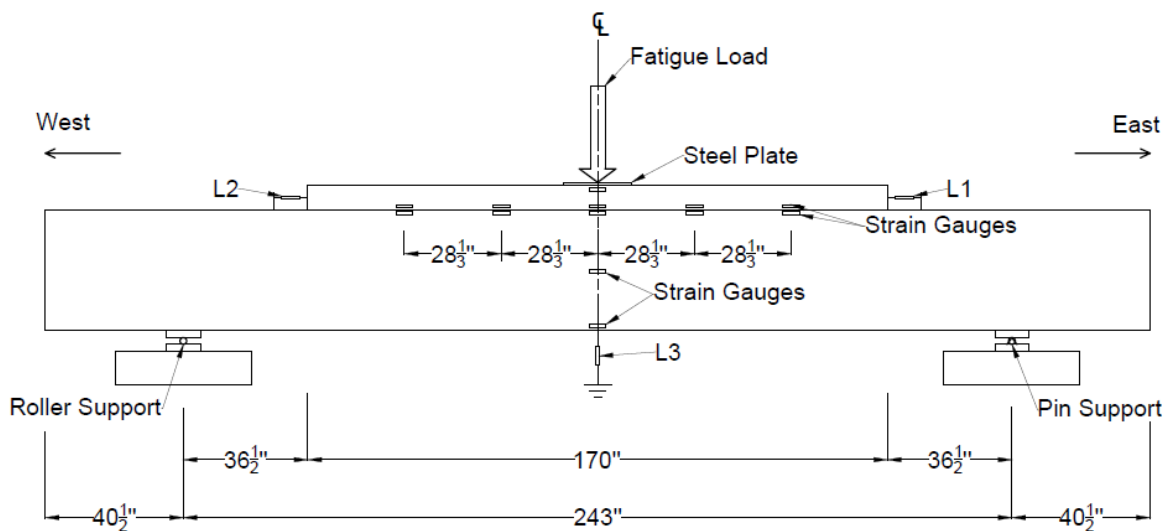


Figure 4.16: Fatigue Test Setup and Instrumentation



(a) Pin Support



(b) Roller Support



(c) Bearing of Actuator on Bridge Deck



(d) LVDT Below Girder at Midspan



(e) LVDT at End of Deck



(f) Strain Gauges

Figure 4.17: Details of Test Setup and Instrumentation

The girder was instrumented with three 0.5-in.-stroke linear variable differential transformers (LVDTs) and 14 foil-type strain gauges. One LVDT (Figure 4.17(d)) was set under the center axis of the girder at midspan to measure deflection. An LVDT (Figure 4.17(e)) was also set at each end of the deck to measure relative slip between the deck and girder. This was of interest because increases in relative slip would be an indication of a change in the horizontal shear transfer mechanism. The strain gauges used for this study were 120-Ohm electrical resistance foil-type gauges with a gauge length of 0.79 in. Six strain gauges were placed along the vertical axis at midspan at depths of 0, 0.5, 6, 8, 21, and 40 in. from the top of the deck concrete and eight strain gauges were located along the deck-girder interface away from midspan to measure girder and deck concrete strains on opposite sides of the interface (1 in. from the interface as shown in Figure 4.17(f)). The strain gauge placed on the top surface of the deck at midspan was 15 in. away from the center axis of the beam, or 9 in. inboard from the side of the deck. The strain gauges were attached directly to the concrete by sanding the concrete smooth, cleaning it thoroughly to remove dust, and then applying an epoxy adhesive.

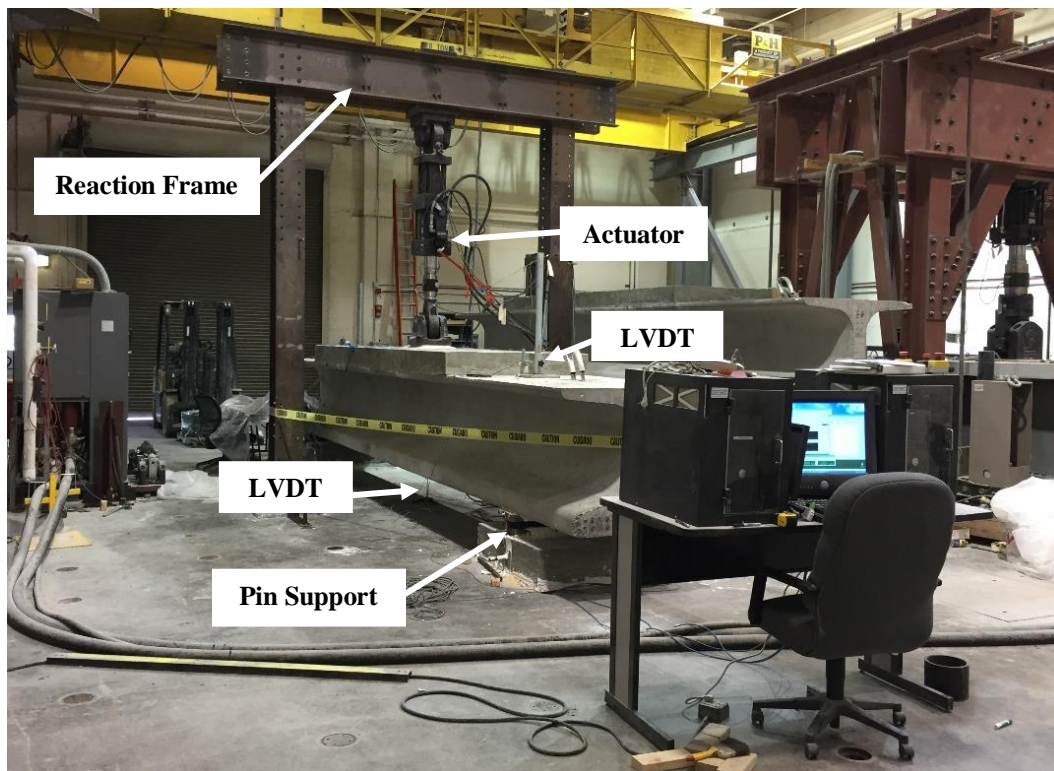


Figure 4.18: Photo of Fatigue Test Setup

4.4.2.2 Loading Protocol

The loading protocol consisted of 2×10^6 cycles of force with an amplitude of 8 to 80 kips. This number of cycles (used by Seamann and Washa, 1964) is expected to allow for a realistic assessment of the long-term performance of bridge girders with details similar to those used in this study. The 8 kip force was used instead of zero force to ensure there would be continuous contact between the actuator and girder throughout the tests. Conveniently, the range of load, 72 kips, is the specified weight of an HS20 truck. The loading does not consider load sharing among girders associated with the axel spacing of a real truck; therefore the simulated loads may be higher than should be expected from a real truck.

Before any cycles were applied, each specimen was first subjected to two cycles of low-frequency (0.02 Hz) ramp-type loading from 8 to 80 kips to allow for collection of LVDT and strain gauge data to provide a baseline measurement (Figure 4.19). The 2×10^6 cycles of force were then applied in 20 loading phases, where each loading phase consisted of 1×10^5 cycles of force applied as a sinusoidal function at a frequency of 2 Hz (Figure 4.20). During the 2 Hz fatigue loading, the number of cycles and actuator force were collected. After each phase of loading, two cycles of low-frequency ramp force were applied following the same protocol as the initial ramp load. Data from all instrumentation was collected during the slower ramp loading.

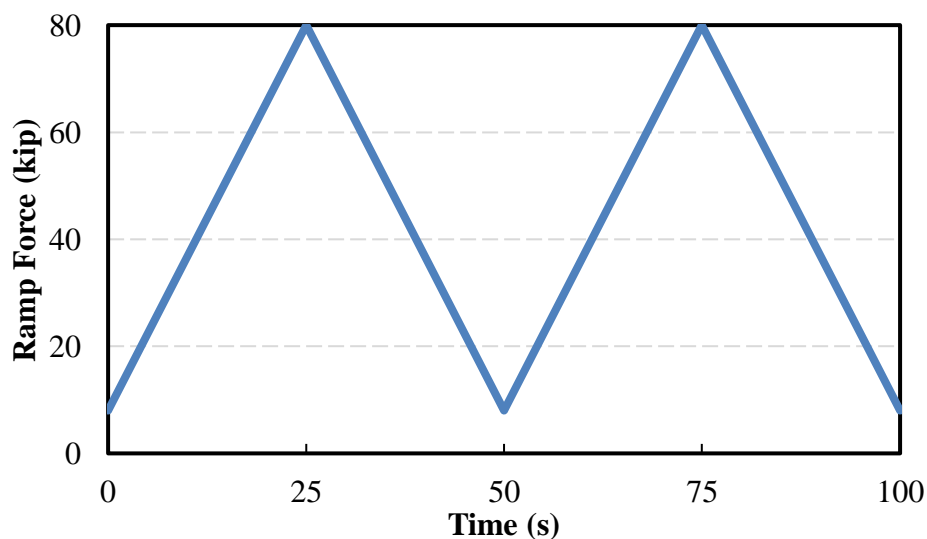


Figure 4.19: Ramp Function used for Data Collection

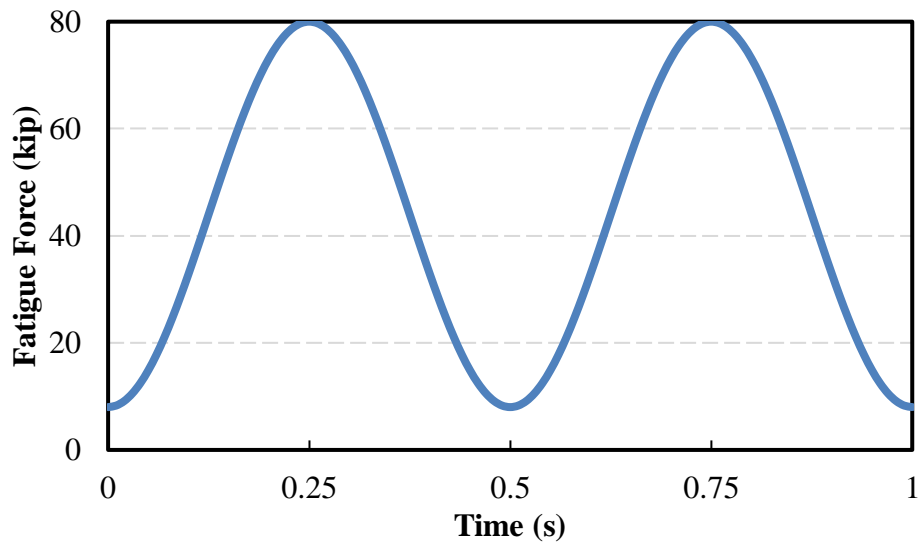


Figure 4.20: Sinusoidal Function used for Application of Cycles of Force

The calculated increment of interface shear stresses, based on a force increment of 72 kips, is shown in Table 4.4 for each specimen. The interface shear stress was calculated assuming that the horizontal shear force transferred across the interface on each half of the girder was equal to the compression force in the deck due to midspan moment (calculated assuming uncracked transformed section properties). This horizontal shear force was then divided by the contact area between the girder and deck, based on a width of 8 in. for Girders #1 and #2 and a 36 in. width for Girder #3. Table 4.4 also shows estimates of cracking stress and peak stress based on the push-off test results as well as calculated peak stress according to the ACI Code and AASHTO Specification. The ratio of interface shear stress at 72 kip to the estimated stress value is also provided in parentheses. Cracking stress was estimated based on results from the fully roughened and troweled-bonded specimens with interface shear reinforcement spaced at 12 in. Peak stress was estimated by summing the estimated cohesion component (460 and 76 psi for roughened and troweled surfaces) with the product of $1.1A_s f_y$ and then dividing by the contact area between the deck and girder top flange. Girders #1 and #2 had the same 8 in. wide contact area, whereas the contact area of Girder #3 was 36 in. wide.

As shown in Table 4.4, the 72 kip load increment imposed a stress increment of approximately 45, 30, and 6.8% of the estimated cracking stresses in Girders #1, #2, and #3. As a

fraction of expected peak stress, the stress increment was 25, 14, and 5.1% for Girders #1, #2, and #3, respectively, based on push-off test results. Compared to the calculated nominal strength of the interface based on provisions of ACI 318-14 and the AASHTO Specifications (Eqs. 2-8 and 2-9, respectively) the stress increments were 55, 33, and 9% of the nominal strengths for Girders #1, #2, and #3 per ACI 318-14 and 42, 19, and 7.7% of the nominal strengths for Girders #1, #2, and #3 per the AASHTO Specification. Although somewhat unclear whether the fatigue loading would cause cracking in Girder #1, failure was not expected in Girders #2 and #3 under fatigue loading for this stress range. To put this in context, Chung and Chung (1976) reported that girders with roughened top flanges have a fatigue strength of at least 55 percent of the static interface shear strength. However, they did not evaluate troweled interfaces.

Table 4.4: Interface Shear Stress at 72 kip Load Increment

Specimen	Interface Shear Stress at 72 kip (psi)	Estimated Stresses Based on Push-off Tests (psi)		Calculated Peak Stress Based on Design Provisions (psi)	
		Cracking Stress	Peak Stress	ACI 318-14 ^b	AASHTO ^c
Girder #1	127	280 (45%) ^a	500 (25%)	230 (55%)	305 (42%)
Girder #2	127	420 (30%)	890 (14%)	390 (33%)	660 (19%)
Girder #3	28	420 (6.8%)	560 (5.1%)	310 (9.0%)	370 (7.7%)

^a The ratio of interface shear stress at 72 kip to estimated value is presented in parentheses

^b See Eq. 2-8

^c See Eq. 2-9

4.4.3 Fatigue Test Results

4.4.3.1 Force-Displacement Relationship

Actuator force was plotted versus midspan displacement (assumed equal to the displacement of the LVDT placed below the beam at midspan) for all 20 loading phases for each specimen. An example of the resulting force versus displacement relationship is shown in Figure 4.21; force and displacement were approximately proportional, as shown, for all loading phases and specimens. The stiffness of each specimen was then estimated for each phase of loading by calculating the slope of a linear best-fit line, as shown in Figure 4.21. Table 4.5 lists the specimen stiffness calculated from measurements prior to loading, after 1×10^6 cycles, and after 2×10^6 cycles.

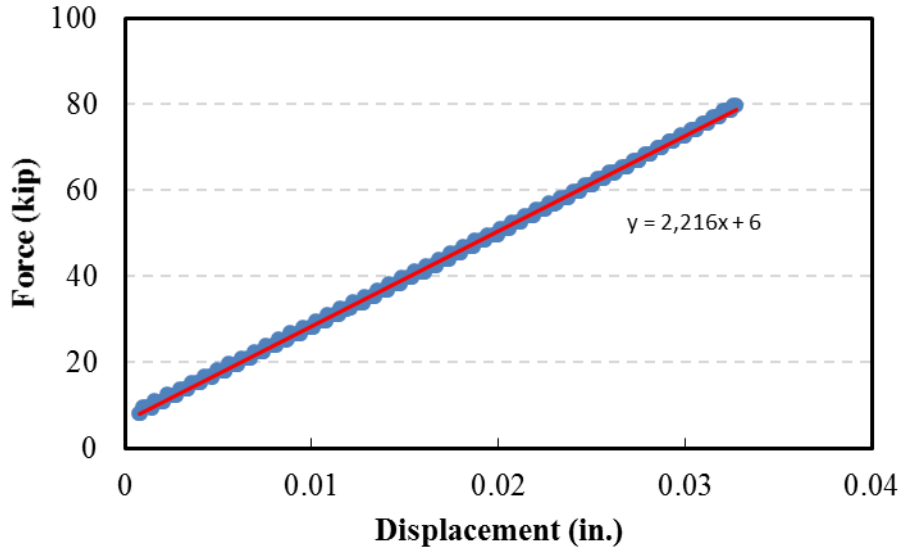


Figure 4.21: Force versus Deflection for Girder #1 Prior to Fatigue Loading

Table 4.5 also shows the estimated specimen stiffness for both perfectly composite and non-composite action including both flexural and shear contributions to deflection. For the perfectly composite case, stiffness was calculated accounting for the deck not extending to the support. For calculating flexural deformations, uncracked transformed section properties were assumed (the gross moment of inertia, I_g , of the girder was 227,000 in.⁴). For calculating shear deformations, only the area of the web was considered active (5.9×35 in. for the non-composite section and 5.9×42 in. for the composite section) according to Iyer (2005). The concrete modulus, E_c , was calculated to be 5,150 ksi using Eq. 4-7 and the shear modulus, G , was assumed equal to $0.4E_c$. Approximately one third of the calculated deflection was attributable to shear deformations.

$$E_c = 33,000K_1w_c^{1.5}\sqrt{f'_c} \quad \text{Eq. 4-7}$$

Where: K_1 is a correction factor for the aggregate source, taken as 1.0, w_c is the concrete density, taken as 0.145 kcf, and f'_c is the specified concrete compressive strength, taken as 8 ksi.

As shown in Table 4.5, the initial stiffness of each specimen was between the stiffnesses estimated assuming either composite or non-composite action, but closer to the value calculated for composite action. The initial stiffnesses of Girders #1 and #2 are similar and slightly less than

the initial stiffness of Girder #3. It is likely that the larger contact area between the deck and girder resulted in a slight increase in composite girder stiffness. More importantly, the changes in specimen stiffness after 1×10^6 and 2×10^6 cycles of load showed that the fatigue loading caused insignificant changes in stiffness for Girders #2 and #3, whereas Girder #1 ended up with an approximately 6.8% reduction in stiffness after both 1×10^6 and 2×10^6 cycles of load.

Table 4.5: Stiffness Summary

Different Cases	Stiffness (kip/in.)		
	Girder #1	Girder #2	Girder #3
Prior to Loading	2220	2170	2330
After 1×10^6 Cycles	2070	2150	2300
After 2×10^6 Cycles	2070	N/A	2300
Estimated Stiffness (composite)	2430		
Estimated Stiffness (non-composite)	1500		

A stiffness ratio was calculated as a measure of how the cyclic loading affected girder stiffness. Stiffness ratio was calculated as the girder stiffness after each loading phase divided by its initial stiffness. The stiffness ratio is plotted versus the number of loading cycles in Figure 4.22 for the three specimens. For Girder #1, a decrease in stiffness ratio of 4.5% is evident after the first phase of loading (10^5 cycles). The stiffness ratio then continued to decrease gradually until it stabilized at approximately 6.8% less than the initial value after 1×10^6 cycles. Girders #2 and #3 exhibited an approximately 1% reduction in stiffness ratio within the first 10^5 cycles of loading that remained stable throughout the remainder of the test.

Results are not plotted for Girder #2 after 13×10^5 cycles in Figure 4.22 and will not be reported herein. This is because approximately 46,000 cycles into the phase 14 loading, the servo-valve of the actuator being used to load the specimen malfunctioned. Repair of the actuator took 5 months, resulting in a 5 month pause in testing that the other specimens were not subjected to. After the actuator was fixed, the specimen was loaded up to the same 2×10^6 cycles imposed on the other specimens to provide parity among specimens before testing them to failure. The long pause, however, allowed for time-dependent effects such as shrinkage and prestress force losses to slightly skew the fatigue test results after the test was resumed.

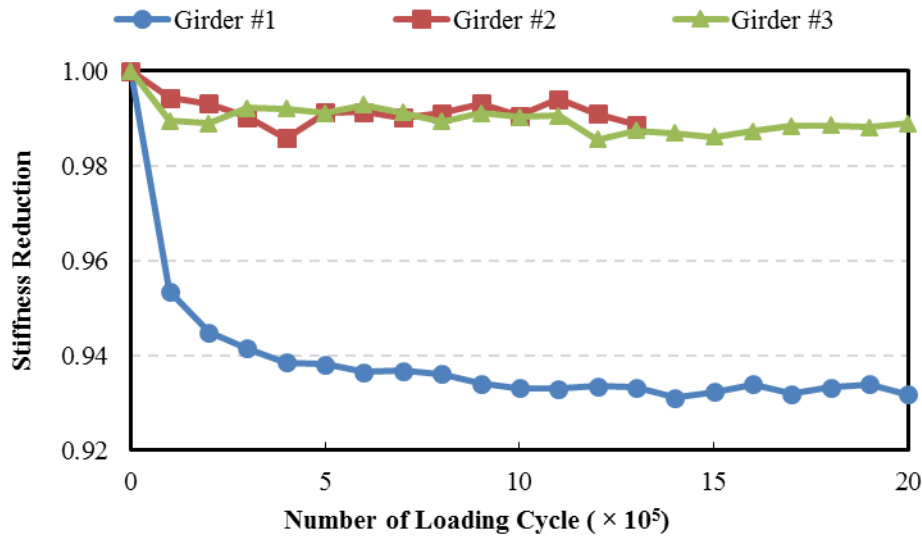


Figure 4.22: Ratio of Girder Stiffness to Initial Girder Stiffness

4.4.3.2 Relative Slip across Interface

Relative slip between the ends of the deck and the girder was calculated based on measurements taken after each phase of loading. Relative slip was calculated as the displacement measured with the LVDTs placed at each end of the deck along the girder centerline (L1 and L2), corrected for shortening of the girder between the end of the deck and the position of the LVDT stand due to flexural stresses (the correction was 0.00065 in. for all specimens based on the strain estimated at the top of the girder from first principals). Instruments L1 and L2 (in Figure 4.16) were set at the east and west ends of the girders, respectively.

The slip measured by each LVDT at 80 kips of force during the slow ramp loading is plotted versus loading cycle number in Figure 4.23 for all three specimens. Measured relative slip was between 0.00072 and 0.0019 in., which is much less than the slip at first cracking for all bonded specimens shown in Table 3.8. As expected, Girder #1 exhibited the largest relative slip and Girder #3 exhibited the smallest relative slip. Given that Girder #3 had 4.5 times more roughened area than Girder #2 (36 in. width compared to 8 in. width), it is notable that Girder #2 exhibited only approximately 50% more slip than Girder #3.

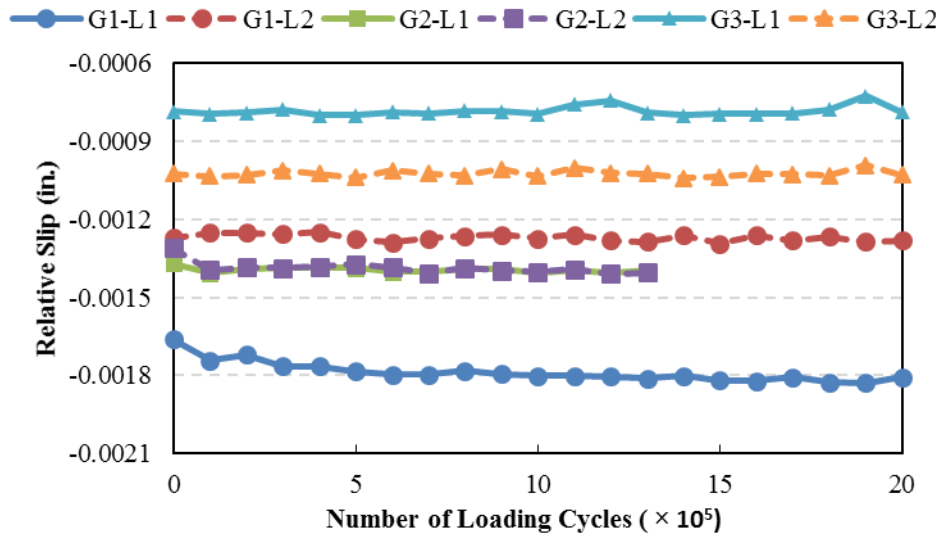


Figure 4.23: Relative Slip at 80 kips throughout Fatigue Tests

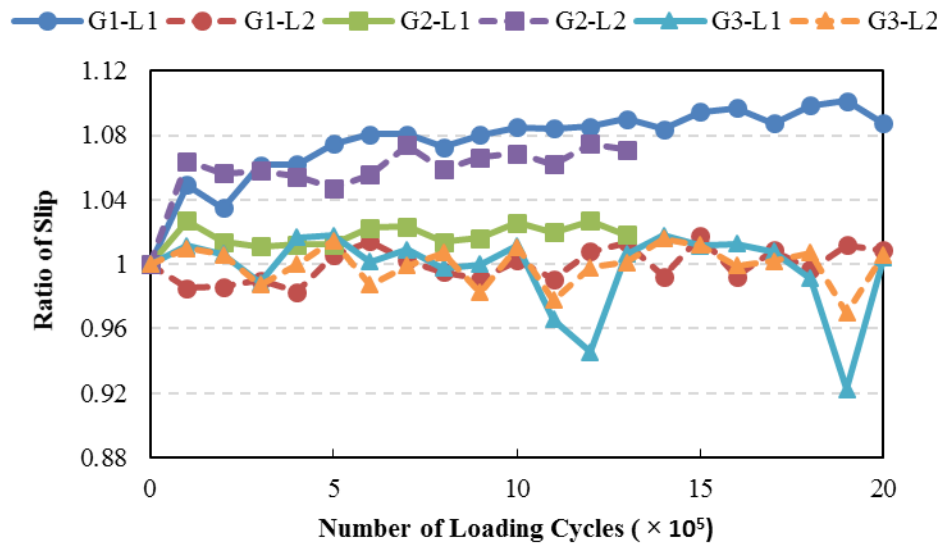


Figure 4.24: Ratio of Deck Slip at 80 kips to the Initial Deck Slip at 80 kips

The ratio of relative slip at a given cycle number to the initially-measured relative slip is plotted as slip ratio versus number of loading cycles in Figure 4.24. Although the slip ratio is very sensitive to measurement noise, a change may also indicate a change in the flexibility of the interface between the girder and deck. For Girder #1, the slip ratio for L1 increased to approximately 1.05 after the first 10^5 cycles of loading and then continued to increase gradually to

approximately 1.09 after 2×10^6 cycles. For Girder #2, the slip ratio for L2 also increased to approximately 1.06 after the first 10^5 cycles of loading, but it then remained stable for the remainder of the test. All other measurements of relative slip were stable throughout the tests.

4.4.3.3 Strain Gauge Results

The strain gauge locations and naming convention are shown in Figure 4.25. Strain gauge results are presented in two different ways to help illustrate the implications of the measurements. First, the distribution of strains measured along the girder depth at midspan at 80 kips of force is plotted for each specimen in Figures 4.26 through 4.28. In these figures, the solid line represents the strain distribution calculated from first principles for fully composite action (assuming the girder and deck concrete strengths were 10 and 5 ksi and using a transformed section based on concrete moduli calculated using Eq. 4-7). The dotted line represents the calculated strain distribution of the girder neglecting the deck. For both the composite and non-composite cases, strains from shrinkage and prestress are neglected. This allows direct comparison with strain gauge data, which are measurements of changes in strain changes due to imposed loads. As shown in Figure 4.25, gauge S11 was on the bottom flange, S12 was near mid-depth of the girder, S5 and S6 were the strain gauges placed right above and below the interface, S13 was close to the top of deck, and S14 was on the top surface of the deck 9 in. from the outside edge. Gauge S5 was not working for Girders #1 and #2.

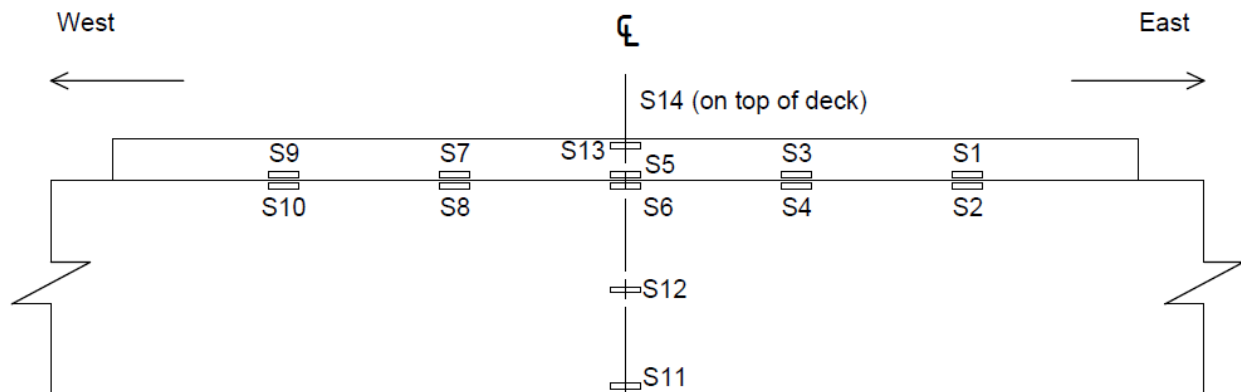


Figure 4.25: Strain Gauge Locations and Naming Convention

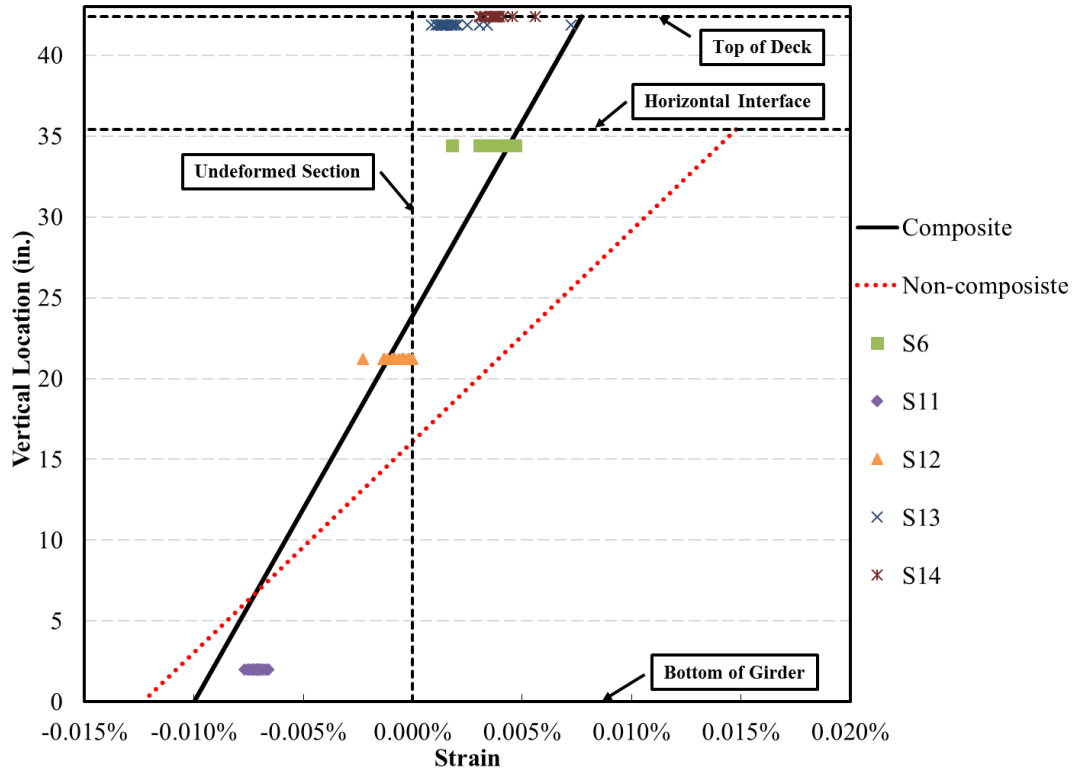


Figure 4.26: Strain Distribution along Girder Depth at Midspan in Girder #1

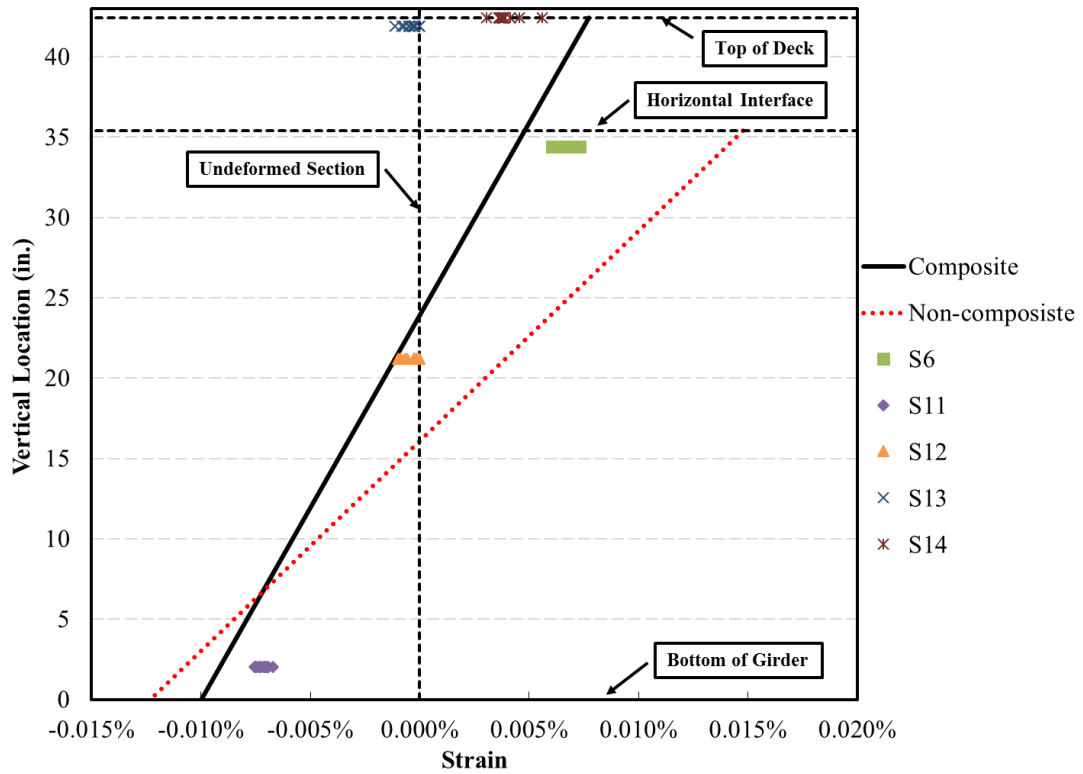


Figure 4.27: Strain Distribution along Girder Depth at Midspan in Girder #2

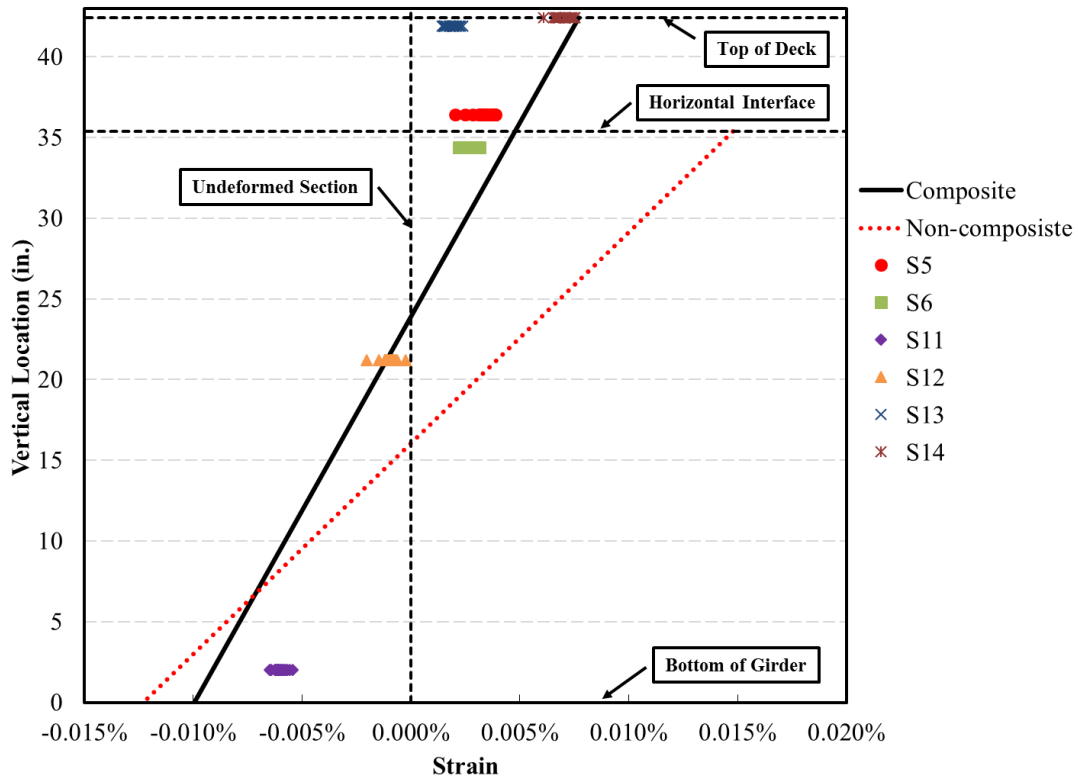


Figure 4.28: Strain Distribution along Girder Depth at Midspan in Girder #3

Although the measured strains varied somewhat among the loading cycles, the measured strains were closer to the solid line than the dotted line in each of the three plots. That strains were generally close to those expected for fully composite action throughout the tests indicates that although there may have been some small increases in flexibility of the horizontal shear connection (indicated by changes in girder stiffness ratio and deck slip ratio), the interface continued to transfer horizontal shear throughout the tests. This is true even late in the test of Girder #1, indicating that despite the 6.8% loss of stiffness the beam was still largely composite near midspan.

Of the measured strains, results from S13 and, to a lesser extent, S14 deviated most from the expected magnitudes. Results from S13 were less than expected for fully-composite action in all three specimens and S14 results were less than expected for Girders #1 and #2. It is believed this is because the deck was more fully engaged over the girder web and less so near the flange tips – especially in specimens with debonded flanges. This would be consistent with S13 recording strains near zero, as observed.

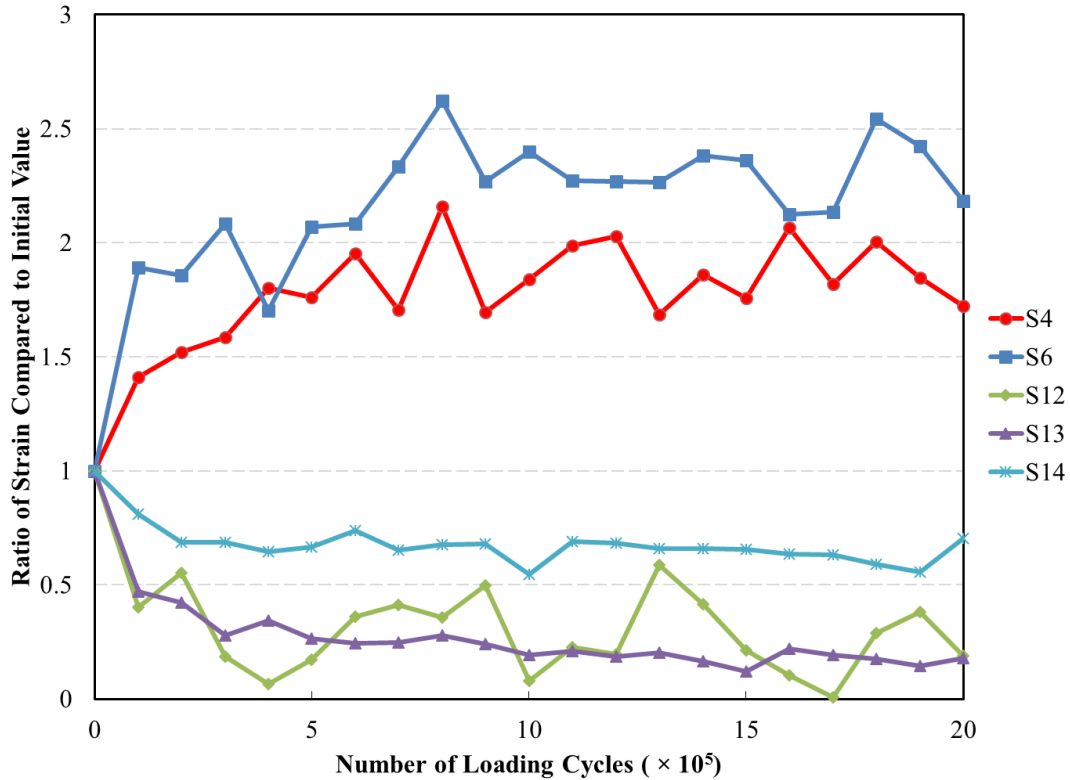


Figure 4.29: Strain Ratio for Girder #1

Strain gauge results are also plotted in Figures 4.29 and 4.30 for selected gauges as a strain ratio: the ratio of strain at 80 kips measured throughout the tests to the initial strain at 80 kips before applying the cyclic forces. The measured strains for Girder #3 and most strains for Girders #1 and Girder #2 were stable throughout the tests, with strain ratios near one. Strain ratios for these stable gauges are not included in the figures. Strain ratios are plotted in Figures 4.29 and 4.30 for gauges on Girder #1 and Girder #2 that had obvious changes during the test. After the first 10^5 cycles force applied to Girder #1, strains measured with S4 and S6 increased about 40 and 80 percent, respectively, compared with initial values. These strains continued to increase until becoming stable at approximately 7×10^5 cycles. This increase in compressive strain in the girder top flange is consistent with a shift away from fully-composite behavior. Unlike S4 and S6, the strains measured with S12, S13 and S14 dropped approximately 60, 50, and 20% respectively. Again, these changes are consistent with a shift away from fully-composite behavior near midspan. For Girder #2, only data from S3 exhibited a measureable change in strain amplitude (Figure 4.30).

Strains measured with S3 dropped 30% after the first 10^5 cycles and continued to drop to approximately 50% of the initial value after 5×10^5 cycles. This isolated change in data measured with S3 in the test of Girder #2 is not clearly consistent with other measurements taken during testing. Rather than indicating a change in shear transfer mechanism, it is likely that the change in strains is instead due to development of a through-thickness shrinkage crack in the deck located approximately 3 in. from S3 that was noted after completion of 2×10^6 cycles.

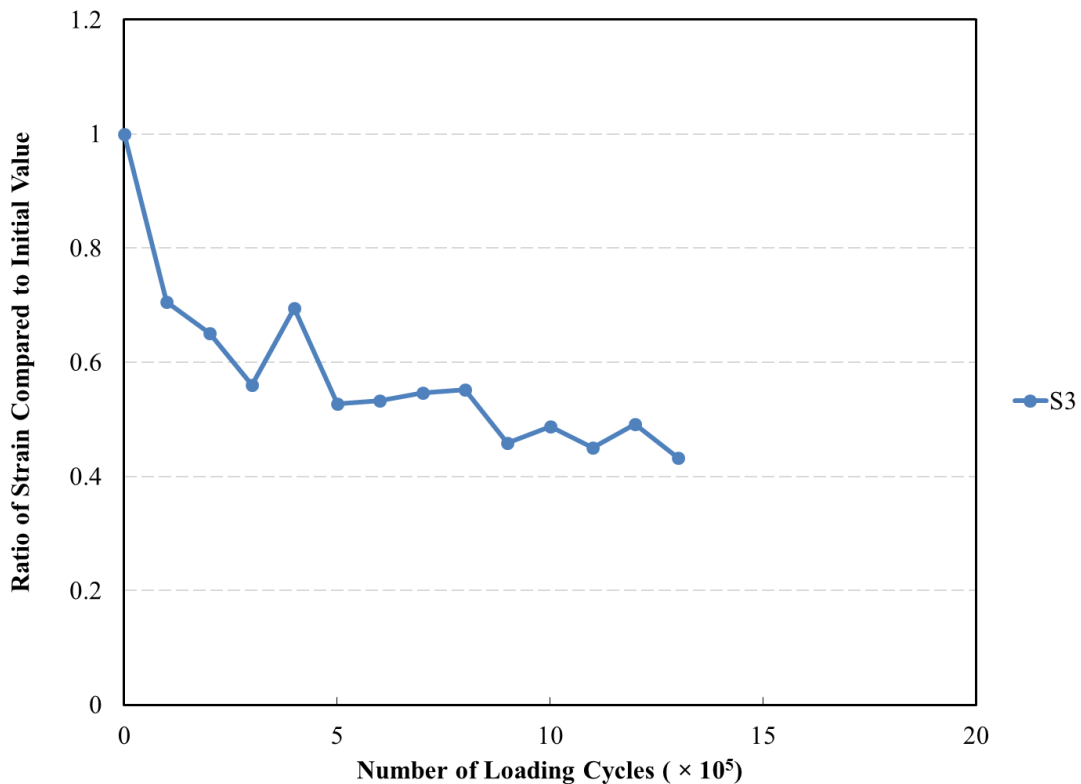


Figure 4.30: Strain Ratio for Girder #2

4.4.4 Conclusions from Fatigue Tests

Girder #1, which had an 8 in. wide troweled interface between girder and deck over the girder web and roofing felt placed over the flanges, exhibited consistent evidence that the stiffness of the girder-deck interface reduced under 2×10^6 cycles of force to 45 and 25% of the estimated cracking and peak stresses. This is indicated by a 6.8% reduction in composite girder stiffness, an approximately 9% increase in relative slip between girder and deck, and changes in recorded

surface strains. Despite the softening of the connection, there is evidence that the girder remained composite throughout the 2×10^6 cycles of force: the specimen had a stiffness after fatigue testing of 2070 kip/in. that was closer to the estimated stiffness for a composite girder than for a non-composite girder, and the strain profile remained close to the profile expected for a composite girder throughout the test. Finally, although micro-cracking may have developed, the recorded relative slip between girder and deck always remained well below the slip associated with macro-cracking (based on push-off test results).

Girder #2, which had an 8 in. wide roughened interface between girder and deck over the girder web and roofing felt placed over the flanges, exhibited evidence that the 2×10^6 cycles of force to 30 and 14% of the estimated cracking and peak stresses did not adversely affect behavior. This is evidenced by the specimen stiffness, which was close to that estimated for a composite girder and changed only 1% under cycling. Measured strains, which were close to those expected for fully composite action, remained stable throughout the test. The only evidence of a change occurring at the interface was the 6% increase in relative slip between the girder and deck at one end of the specimen. Throughout the test however, the measured relative slip remained smaller than the slip associated with cracking (based on push-off test results). Both stiffness and strain measurements indicate the specimen remained composite throughout the fatigue testing.

Girder #3, which had a 36 in. wide roughened interface between girder and deck over the girder web and troweled flange edges, exhibited clear evidence that the 2×10^6 cycles of force to 6.8 and 5.1% of the estimated cracking and peak stresses did not affect behavior. This is based on small to negligible changes in girder stiffness, relative slip between girder and deck, and measured surface strains. As expected, this specimen remained composite throughout the testing and showed no evidence of cracking along the interface.

Based on these results, it is concluded that:

- 1) Composite action can be achieved and maintained through cyclic loads after deck replacement.
- 2) The proposed partially-roughened interface connection detail maintained composite action through 2×10^6 cycles of force to 30% of the expected cracking force.
- 3) The partially troweled/partially debonded interface connection detail maintained composite action through 2×10^6 cycles of force to 45% of the expected cracking force.

4.5 Tests of Girders to Failure

After completing the fatigue tests, and approximately one year after the second bridge deck placement, each of the girders was monotonically loaded at midspan until failure.

4.5.1 Experimental Program

4.5.1.1 Test Setup

The test setup is shown in Figures 4.31 through 4.33. As in the fatigue tests, the girders were placed on simple supports spaced 243 in. apart, or approximately six times the composite girder depth. The girder was monotonically loaded at midspan using the frame shown in Figure 4.32(a). The frame, which was constructed from an HP18×208 cross-beam and built-up channel beams at each end, supported four 150-ton hollow-cylinder hand-operated hydraulic jacks. The force in each jack was transmitted through a hollow-cylinder load cell and into a 1.7 in. diameter high-strength steel threaded rod (through bearing on a nut). The threaded rods passed through the laboratory strong floor and were anchored by spreader beams located below the floor. The threaded rods and load cells were therefore approximately stationary, and extension of the jacks forced the loading frame and girder downward. Bearing of the loading frame onto the top of the girder was through a 10 × 20 in. steel plate set into a bed of gypsum-cement (shown in Figure 4.32 (b)) to distribute the force on the specimen during testing.

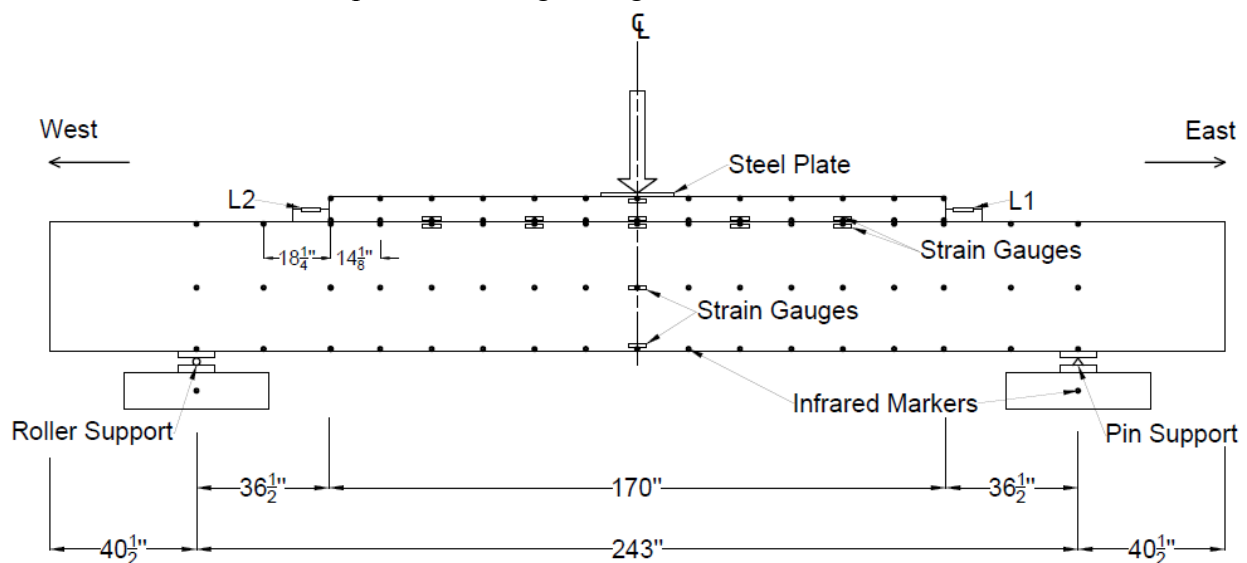
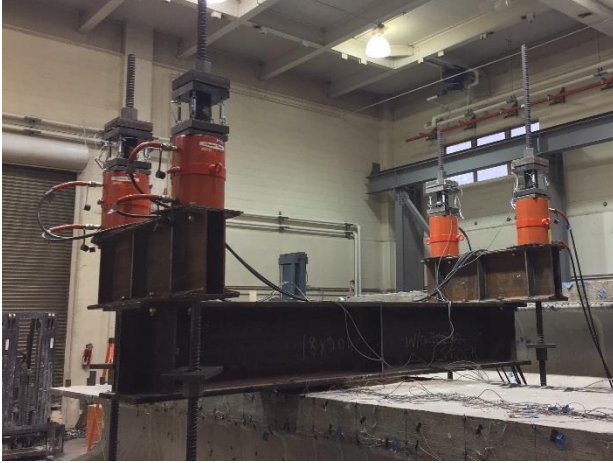


Figure 4.31: Test Setup and Instrumentation



(a) Loading Frame



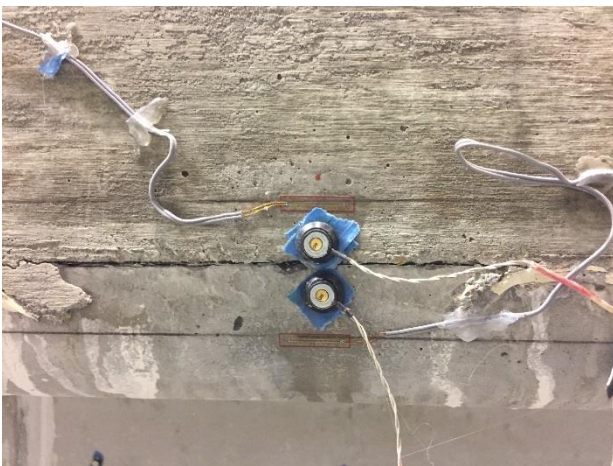
(b) Steel Plate and Gypsum Cement between Loading Frame and Specimen



(c) Load Cell Arrangement



(d) Position Tracking Camera



(e) Infrared Markers for Position Tracking



(f) Pumping Station

Figure 4.32: Test Setup and Instrumentation Details



Figure 4.33: Test Setup

4.5.1.2 Instrumentation

The two LVDTs (L1 and L2) placed at the ends of the deck; the 14 strain gauges used to collect fatigue test data were also used for these tests (Figure 4.31). In addition, an optical position tracking system was used to track the position in 3-dimensional space of 77 high-frequency infrared markers (the dots shown in Figures 4.31, 4.32(e), and 4.33) fixed to the surface of the specimen. Data from this system is useful for calculating strains and relative displacements on the surface of the specimens throughout the tests. Markers were placed along the interface, as shown in Figure 4.32(e), to allow for calculation of the relative slip between the girder and deck. Markers placed along the vertical axis of the girder at midspan and over the supports were used to determine the deflection of the specimens during testing. Force imposed on the specimens was determined using hollow-cylinder load cells placed above each hydraulic jack, as shown in Figure 4.32(c).

4.5.1.3 Testing Procedure

Load was applied with four hand-pumped 150-ton hollow-cylinder hydraulic jacks operated at a consistent speed (the pumping station is shown in Figure 4.32(f)). While the first 400 kip of force was applied, loading was paused at approximately 100 kip increments for specimen observation (to document crack opening, relative slip between the girder and deck, etc.). Cracking was marked by drawing lines alongside each crack and noting the applied force. Slip was documented based on the offset of vertical lines (in Figure 4.34(b)) drawn on the side of the girder prior to testing. After reaching 400 kip, the specimens were loaded directly until failure at the same loading rate but without pausing (except for Girder #1, as described in Section 4.5.2.1). When failure occurred, the specimens were unloaded prior to terminating data collection. After testing, the weight of the test apparatus, 5 kips, was added to the force measured by the load cells so that the reported force includes all forces applied to the top of the girder.

4.5.2 Test Results

4.5.2.1 Observations during Testing

Girder #1 (troweled surface with roofing felt over flanges):

Cracks were first observed during a pause at a force of approximately 200 kips. These cracks were inclined cracks in the girder web on both sides of midspan (Figure 4.34(a)). Further loading caused these cracks to slowly extend towards the bottom and top flanges of the girder. Flexural cracks were first observed in the bottom flange near midspan during a pause at a force of 400 kip. As loading continued, more web shear cracks and flexural cracks were observed and existing cracks propagated and widened. Slip between the deck and the girder top flange was first visible at a force of 450 kip, when approximately 1/8 in. of slip was observed on the east end.

At approximately 460 kips of force, a problem occurred with one of the jacks being used to load the specimen that required the specimen to be unloaded. The problem was addressed and the specimen was reloaded (to approximately 480 kips) to confirm the repair was successful. The specimen was monitored during this second loading procedure, and no new cracking was observed. On the following day, the specimen was loaded until failure.



(a) Web Shear Cracks at 205 kip



(b) Deck Cracking Below the Loading Point after Failure



(c) Specimen after Failure



(d) Girder Top Flange Cracking after Failure



(e) Girder Web after Failure



(f) Permanent Slip between Girder and Deck after Failure

Figure 4.34: Photos of Girder #1 During and After Testing

When loaded beyond 480 kips, existing cracks continued to propagate and widen and the deck on the east half of the girder continued to slide relative to the top girder flange. At large girder deflections, the deck exhibited a wide flexural crack under the loading point (Figure 4.34 (b)) that was not associated with underlying cracks in the girder top flange. This pattern of cracking indicates that the girder and deck were not fully composite late in the test. After reaching a peak strength of 546 kip at a deflection of 1.42 in., a sudden and explosive shear failure occurred on the east end of the girder (Figure 4.34(c)) that caused a total loss of strength at a deflection of 1.93 in. After failure, the inclined cracks extended through the bottom flange to the pin support (Figure 4.34(c)) and through the top flange of the girder (Figure 4.34(d)). Some transverse reinforcement was exposed by the failure, as shown in Figure 4.34(e). Permanent slip (Figure 4.34(f)) was observed between the girder and deck on the east side after unloading.

Girder #2 (roughened middle surface with roofing felt over troweled flanges):

Photos taken during and after the test of Girder #2 are shown in Figure 4.35. The first inclined and flexural cracks were observed when the force was approximately 200 kip and 400 kip respectively (Figure 4.35(a)). Slip between the girder and deck was not observed until the force reached 450 kip, at which time approximately 0.02 in. of relative slip was observed on the west end of the specimen. The specimen reached its peak flexural strength of 577 kips at 3.04 in. of deflection. Loading of the specimen continued until a compression failure (Figure 4.35(b)) occurred in the deck at a deflection of 4 in. (Figure 4.35(c)). As Figure 4.35(b) shows, only one of the four cracks in the deck was connected with a crack from the girder; this shows that the section at midspan was not fully composite at the end of the test. A small amount of permanent slip (Figure 4.35(d)) was observed between girder and deck at both ends after failure.

Girder #3 (roughened surface):

Photos of Girder #3 during and after testing are shown in Figure 4.36. The first inclined and flexural crack were observed during pauses at forces of approximately 300 and 400 kips respectively. The later appearance of inclined cracks is likely attributable to the tighter spacing of transverse reinforcement. The spacing of web shear cracks late in the test of Girder #3 was

measured to be approximately 4.5 in., a closer spacing than observed in the first two specimens (6.5 in. for Girder #1 and 6.0 in. for Girder #2). The peak strength of the specimen, 605 kips, occurred at a deflection of 2.49 in. The specimen then failed by crushing of the compression zone in the deck (Figure 4.36(b)), followed immediately by propagation of a horizontal crack near the bottom of the deck that extended from midspan to the west end of the deck (Figure 4.36(c)). A small residual slip was observed on the west end of the deck after the test as shown in Figure 4.36(d). As Figure 4.36(b) shows, vertical deck cracking near midspan was connected with underlying cracks through the girder top flange, showing that the girder was composite at the end of the test.



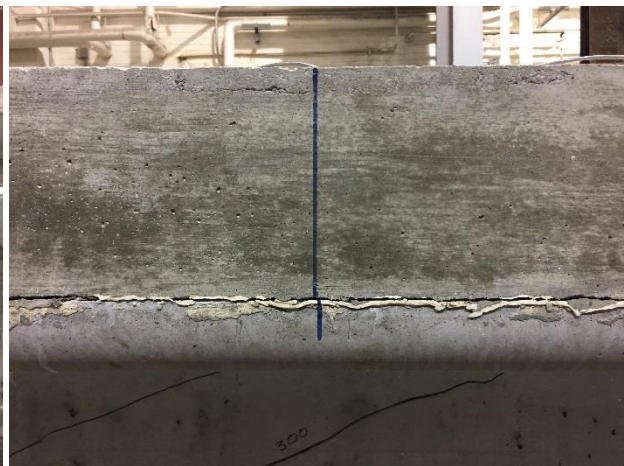
(a) Cracking at 400 kips



(b) Compression Zone Failure



(c) Large Deformation at End of Test



(d) Permanent Slip between Girder and Deck (East Side) after Failure

Figure 4.35: Photos of Girder #2 During and After Testing

As expected, no slip was observed during testing between the bridge deck and girder top flange (except for after failure). Whereas Girders #1 and #2 were designed to ensure that the force required to induce either a flexural or shear failure exceeded that required to cause a horizontal shear failure, the large roughened interface in Girder #3 made that infeasible. The behavior of Girder #3 therefore represents approximately fully composite girder action throughout the test.



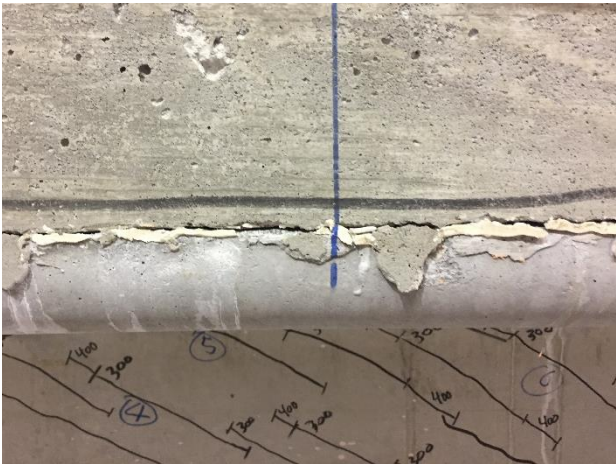
(a) Cracking at 300 kips



(b) Compression Zone Failure



(c) Horizontal Crack Through Deck After Failure (West Side)



(d) Relative Slip of Deck after Failure (West End)

Figure 4.36: Photos of Girder #3 During and After Testing

4.5.2.2 Force versus Displacement

The measured force is plotted versus midspan deflection for each specimen in Figure 4.37 and in Appendix E. Figure 4.38 is the same as Figure 4.37, except the range of deflections is limited to 1.0 in. in Figure 4.38. Force was taken as the sum of forces imposed by the four hydraulic jacks and the weight of the loading frame (5 kips). Midspan deflection was calculated as the average vertical deflection of the markers located along the vertical axis of the girder at midspan minus the average vertical deflection of two markers, each located immediately over one of the supports. Due to issues with the setup, Girder #1 had to be unloaded after reaching approximately 460 kips of force and then subsequently reloaded until failure. The data plotted for Girder #1 in Figure 4.37 are reconstructed from the recorded results using the procedure described in detail in Appendix E.

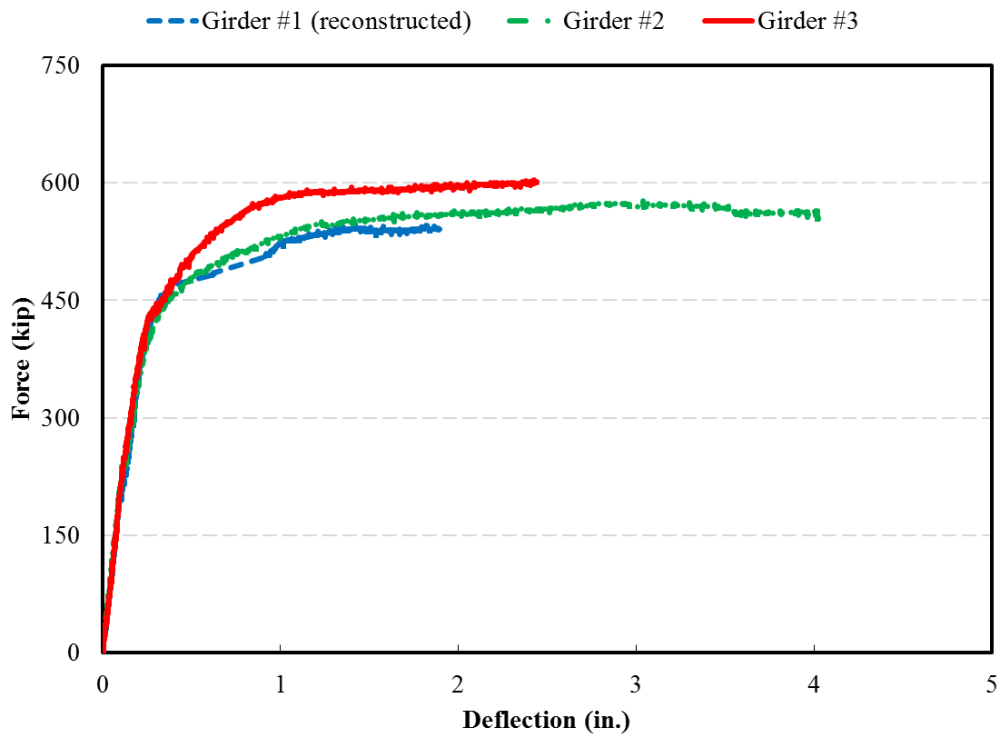


Figure 4.37: Force versus Deflection

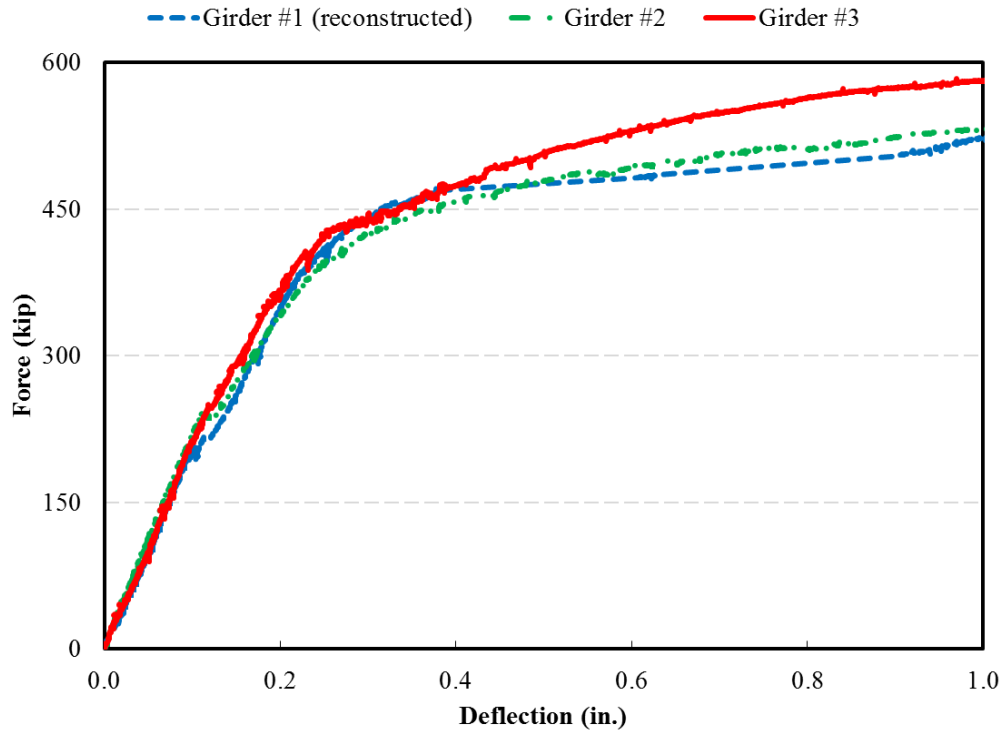


Figure 4.38: Force versus Deflection (different scale)

The shape of the force versus deflection plots is similar among the specimens. Each plot begins with a linear loading branch with approximately the same slope, indicating that the stiffness of the three girders were approximately equal after the fatigue loading described previously. As evident in Figure 4.38, all three specimens had a reduction in stiffness at forces between 200 and 250 kips that coincided with or somewhat preceded the first observed incline cracks in the web of the specimens. The forces at which the slope changed in each specimen and the forces at which inclined cracking was first observed are listed in Table 4.6. The stiffness reduction was significantly less in Girder #3, which should be expected because it had No. 5 transverse bars spaced at 6 in. instead of the 12 in. spacing used in Girders #1 and #2.

After inclined cracking, force and deflection remained approximately proportional until approximately 400 kips of force, which coincides with the first observed flexural cracks in all three specimens. After flexural cracking initiated, the deflection began to increase at a much greater rate than the force. There was little change in the force carried by each specimen at deflections greater than 1 in., indicating that the strands were yielding. As indicated in Table 4.6, Girders #1, #2, and

#3 reached peak forces of 546, 577, and 605 kips at deflections of 1.42, 3.04, and 2.49 in. It is reasonable that Girder #3 had the greatest strength given that it had fully composite action throughout the tests. Girders #1 and #2 both had slightly less strength than Girder #3, perhaps because the deck was only partially composite later in the test. Note that fully composite action until failure need not be the aim in design – in practice stable composite action is only required for the range of expected load demands. The three specimens all exhibited excellent deformation capacity. In terms of maximum deflection, Girder #2 had the largest value of 4.0 in. followed by Girder #3 (2.49 in.) and Girder #1 (1.93 in.).

Table 4.6 Summary of Results

Force of Different Cases	Girder #1	Girder #2	Girder #3
Force at Transition Point (kip)	202	236	246
Force at First Observed Web Shear Crack (kip)	200	250	300
Maximum Force (kip)	546	577	605
Deflection at Maximum Force (in.)	1.42	3.04	2.49

4.5.2.4 Relative Slip across Interface

An elevation view of a girder is shown in Figure 4.39 with twelve stations identified (1-W through 1-E). Relative slip between the girder and deck was calculated at each station throughout the tests based on position data from the 3D position tracking system. Relative slip was calculated as the difference in horizontal position between pairs of markers placed 1 in. above the interface on the deck and 1 in. below the interface on the girder, corrected for girder rotation. Positive slip values on the east side and negative slip values on the west side indicate that the bottom of the deck was compressing less than the top of the girder, i.e. the section was not fully composite. An LVDT was also placed at each end of the deck to provide a redundant measure of relative slip.

The LVDT slip measurements at the ends of the deck closely matched the relative slip calculated at the outermost stations (1-E and 1-W). This is shown in Table 4.7 for each girder at peak force. Although relative slip measured along the length of the deck will be the focus of the following discussions, the parity between slip values recorded with LVDT and infrared-based

instruments means that the relative slip values reported below can be directly compared with the LVDT measurements of slip taken during the fatigue tests.

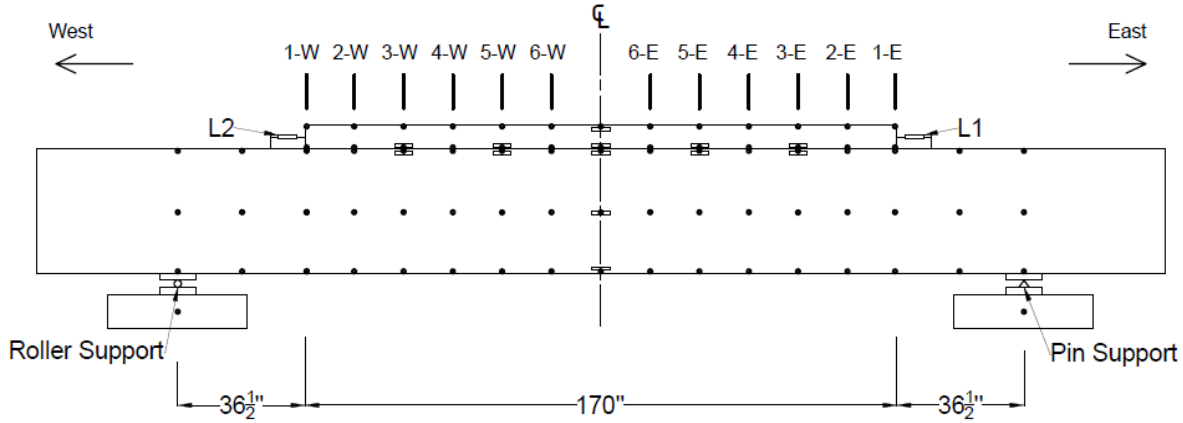


Figure 4.39: Elevation View of Girder with Stations for Relative Slip Calculation

Table 4.7 Slip Measured with LVDT and 3D Position Tracking Systems at Peak Force

Measured Slip Source	Girder #1	Girder #2	Girder #3
	Slip at Peak Force (in.)	Slip at Peak Force (in.)	Slip at Peak Force (in.)
L1 (East)	NA ^a	NA ^a	-0.011
1-E	0.17	0.249	from -0.006 to 0.01 ^b
L2 (West)	0.021	-0.134	-0.006
1-W	0.022	-0.134	from -0.006 to 0.006 ^b

^a LVDT reached stroke limit at end of test

^b Calculated slip values based on 3D position tracking system data were very sensitive to noise when the value was less than 0.01 in. so a range of values is provided here

Girder #1 (troweled surface with roofing felt over flanges):

Slip calculated at each station is plotted versus force in Figure 4.40 for the first test of Girder #1 and Figure 4.41 for the final test. Data from three stations near midspan are omitted due to a localized malfunction of the data acquisition system. Slip was much larger on the east half of the girder than on the west half. On the east half, slip was very small (less than 0.01 in.) during the first test until the force reached approximately 420 kip. As the force increased to 460 kips, the slip on the east half increased to between 0.02 and 0.03 in. Based on the push-off tests reported in

Chapter 3, this amount of slip is consistent with formation of a crack along the troweled interface. In the final test of Girder #1, relative slip up to approximately 450 kips of force was consistently larger than it had been in the first test, which would be expected if a crack had formed along the interface in the first test. Slip continued to increase proportionally with force until approximately 500 kips, at which point slip continued to increase while force remained relatively constant due to flexural yielding. By the end of the test, the east half of the deck had slid more than 0.25 in. relative to the top flange of the girder. Based on the push-off tests, this amount of slip would not be expected to result in fracture of the horizontal shear reinforcement; instead, the horizontal shear strength of the connection would be relatively stable and independent of slip. On the west half of the girder, slip remained small throughout the tests of Girder #1. Slip was between -0.015 in. and 0.010 in. except at station 1-W, where slip increased suddenly to 0.03 in. at peak strength and 0.04 in. at the end of the test.

Slip is also plotted versus position at selected levels of force in Figure 4.42. Slip shown for forces up to 450 kips are from the first test, whereas slip shown for 500 kips and at peak strength are from the final test. This plot shows that slip was near zero up to 450 kips of force and then began to increase quickly on the east half of the girder at forces of 500 kips and greater. The figure also shows that sections closer to the deck ends had larger slip than those closer to midspan.

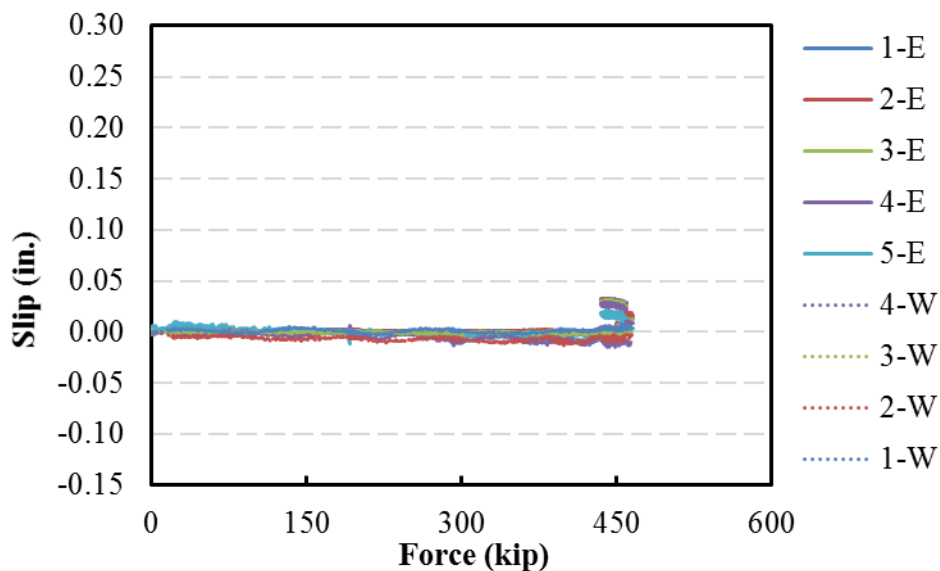


Figure 4.40: Slip versus Force for the First Test of Girder #1

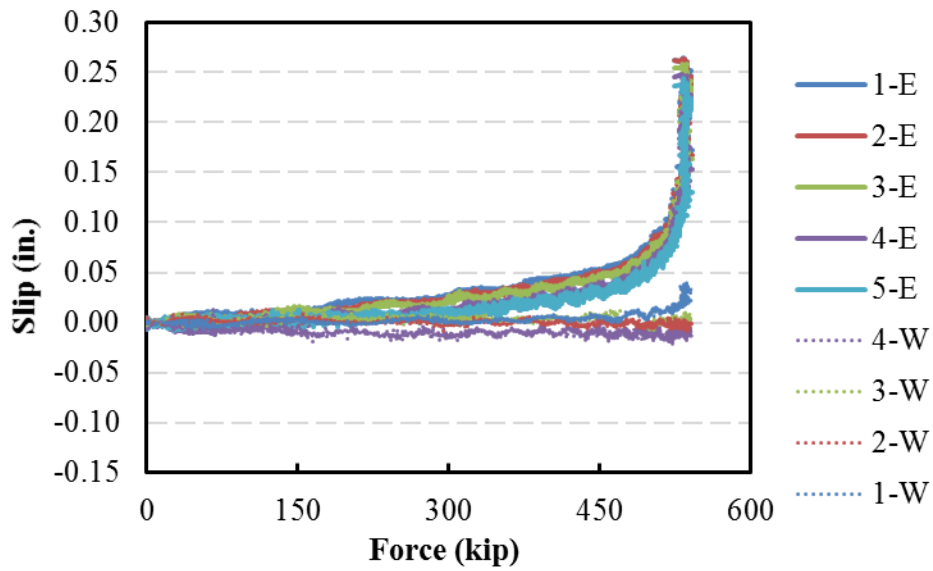


Figure 4.41: Slip versus Force for the Final Test of Girder #1

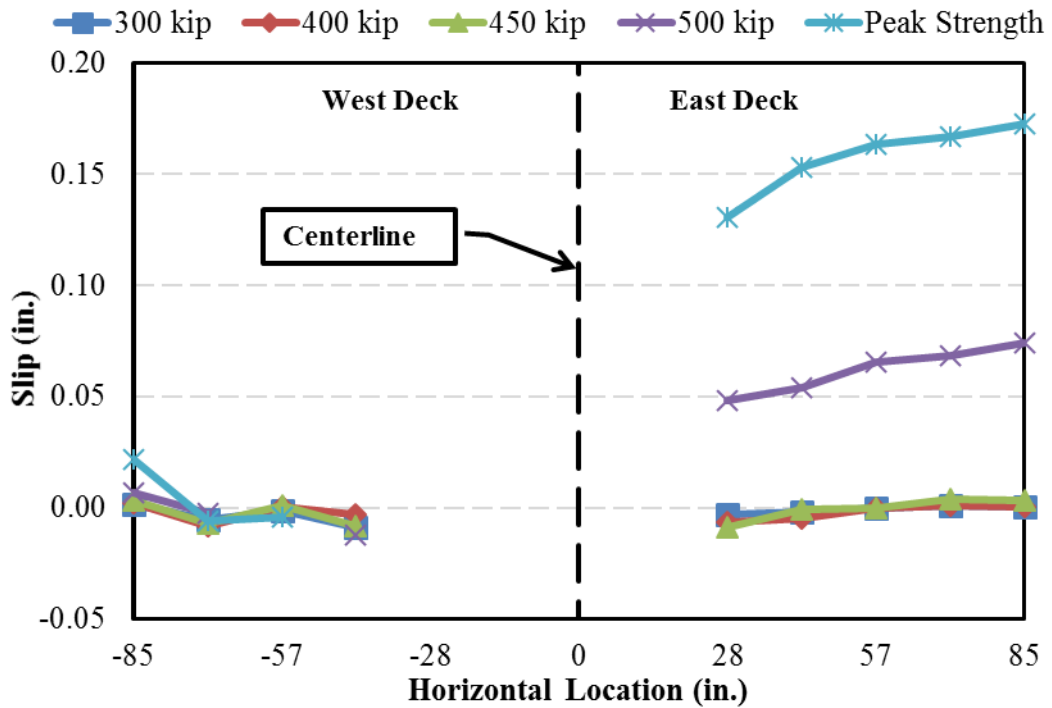


Figure 4.42: Distribution of Slip over Girder Length (Girder #1)

The concentration of slip on one half of the girder is consistent with results from the troweled push-off specimens, which exhibited their peak strength at or close to the first cracking strength. The strength of the cracked portion of the girder was therefore lower than that of the uncracked portion. It is, however, possible that moving loads and repeated (fatigue-type) loads could cause the crack along the interface to propagate through the uncracked portion. This was outside the scope of the study.

Girder #2 (roughened middle surface with roofing felt over troweled flanges):

Slip calculated at each station is plotted versus force in Figure 4.43. Slip was very small (less than 0.01 in.) until the force reached approximately 450 kip, when slip at station 5-W increased to 0.006 in. As force increased to 480 kip, slip along the west half of the girder increased to between 0.01 and 0.03 in. while slip remained near zero along the east half of the girder. Based on the push-off tests reported in Chapter 3, the amount of slip on the west half of the girder was consistent with cracking. This is only slightly larger than the load at which slip was believed to occur in the test of Girder #1 (460 kips), indicating that troweled and roughened interfaces developed cracking at similar loads.

When the force passed 507 kip, slip along the east half of the girder suddenly jumped to between 0.005 and 0.02 in., indicating that cracking may have occurred along parts of the east half of the span. Unlike troweled push-off specimens, the roughened push-off specimens exhibited much higher strength after cracking than at cracking. For this reason, it is not surprising that cracking developed on the east half shortly after it occurred on the west half. Slip continued to increase along both halves of the girder as load increased, with slip increasing more rapidly on the east half than the west half. By the end of the test, slip along the east half exceeded that along the west half (with peak values of 0.25 and 0.14 in. on the east and west halves, respectively).

The distribution of slip along the span at different forces is shown in Figure 4.44. Slip on the west side started first, with slip being greatest at the middle sections (2-W, 3-W, 4-W, 5-W). This was especially true when force was larger than 500 kip. On the east side, slip developed somewhat evenly except that station 3-E had much lower slip than surrounding stations. It is not

clear why the 3-E results were this way. At peak strength, slip was greatest at station 2 on both ends of the girder.

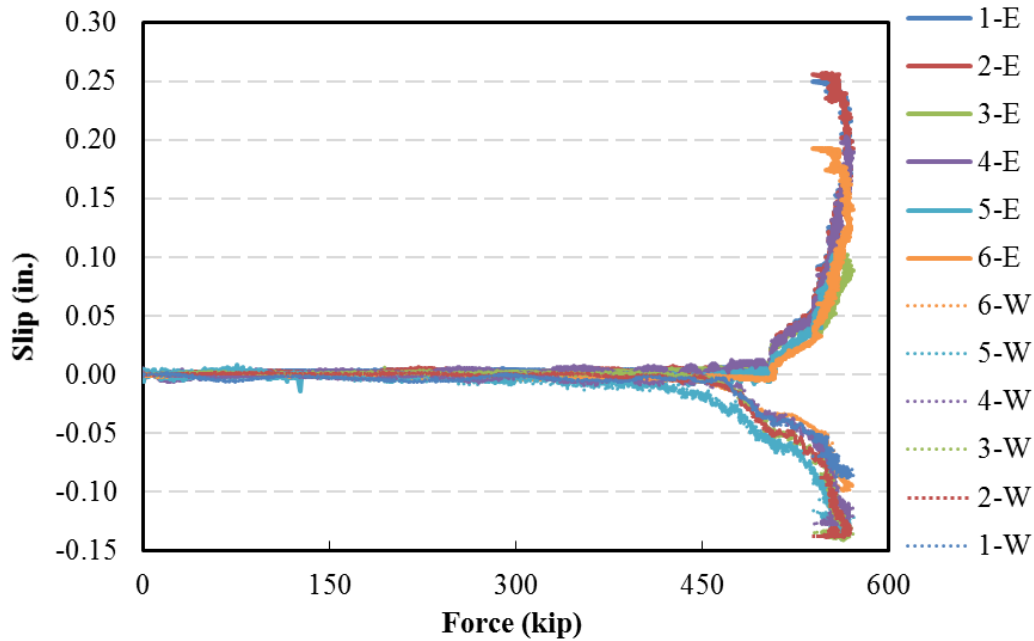


Figure 4.43: Slip versus Force (Girder #2)

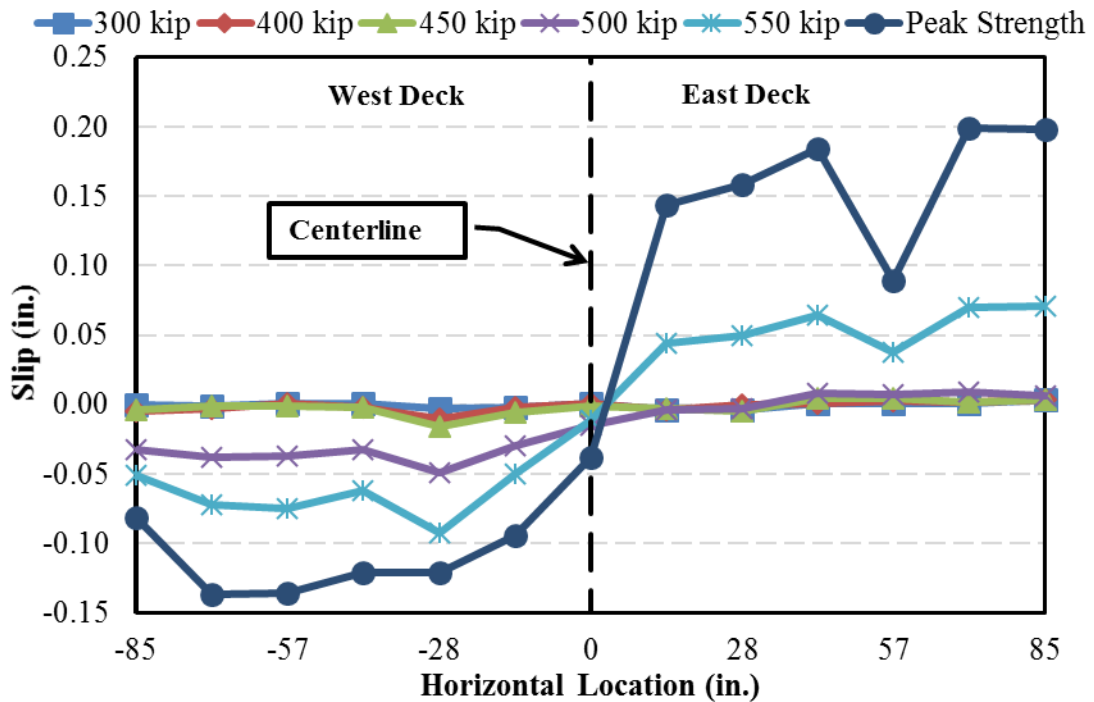


Figure 4.44: Distribution of Slip over Girder Length (Girder #2)

Girder #3 (roughened surface):

Slip at each station is plotted versus force in Figure 4.45 and the distribution of slip along the girder length is plotted in Figure 4.47 at different levels of force. Data for station 6-E is omitted due to localized problems with data acquisition. Except for the slip calculated at Station 6-W, values of slip at all stations were less than approximately 0.02 in. throughout the test of Girder #3. Based on the push-off test results reported in Chapter 3, the maximum slip at first crack is 0.02 in. This is consistent with the lack of cracking observed along the interface during testing of the girder. The only exception is station 6-W, which is plotted versus force in Figure 4.46 separately. Slip at 6-W was constant near zero until the force reached about 450 kip. It became slowly positive and increased to 0.025 in. at the end of the test. However, if there was sliding along the interface, slip calculated at 6-W would have been expected to become negative. Rather than indicating slip along the interface, it is believed the apparent slip may be due to the extension of flexural cracks from the girder and into the deck that interfered with the station 6-W results.

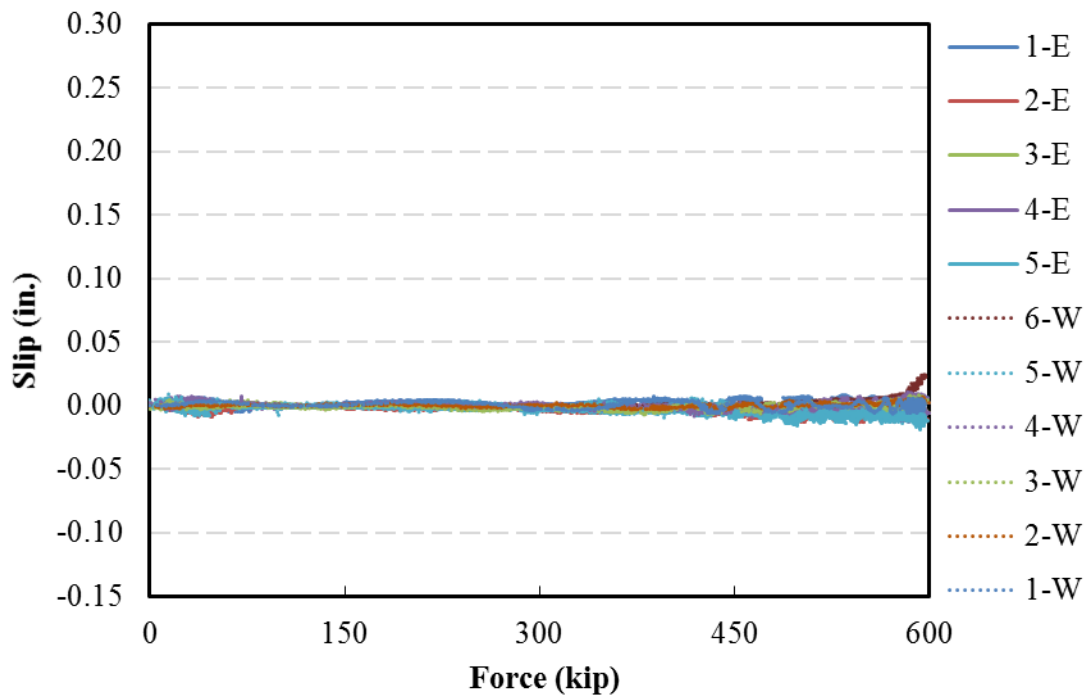


Figure 4.45: Slip versus Force (Girder #3)

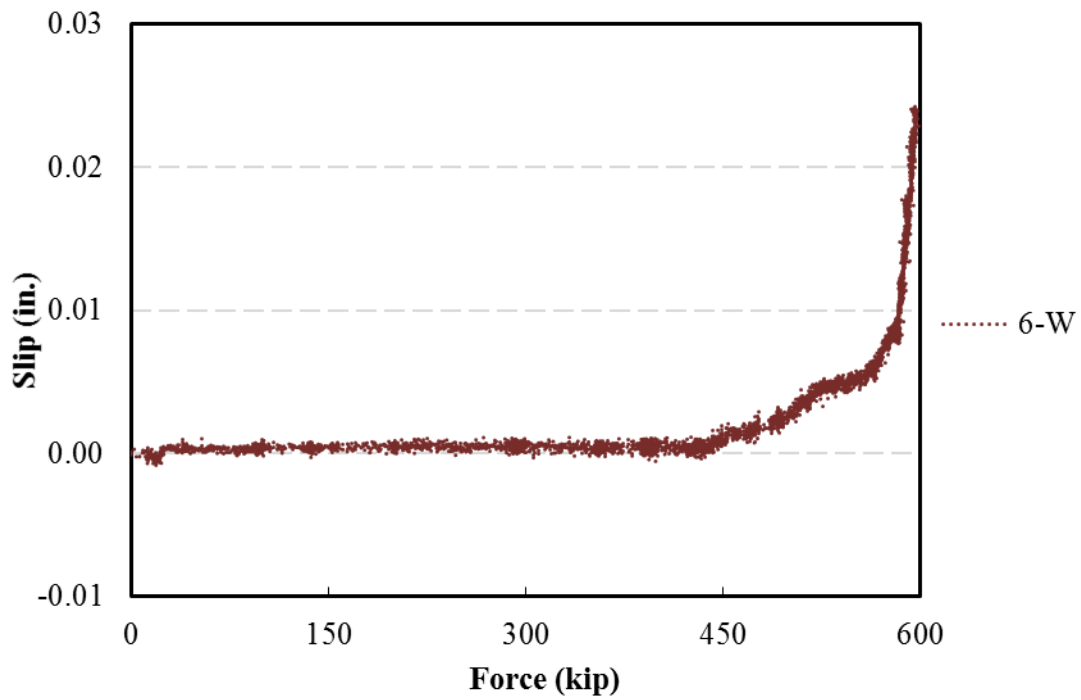


Figure 4.46: Slip versus Force for 6-W (Girder #3)

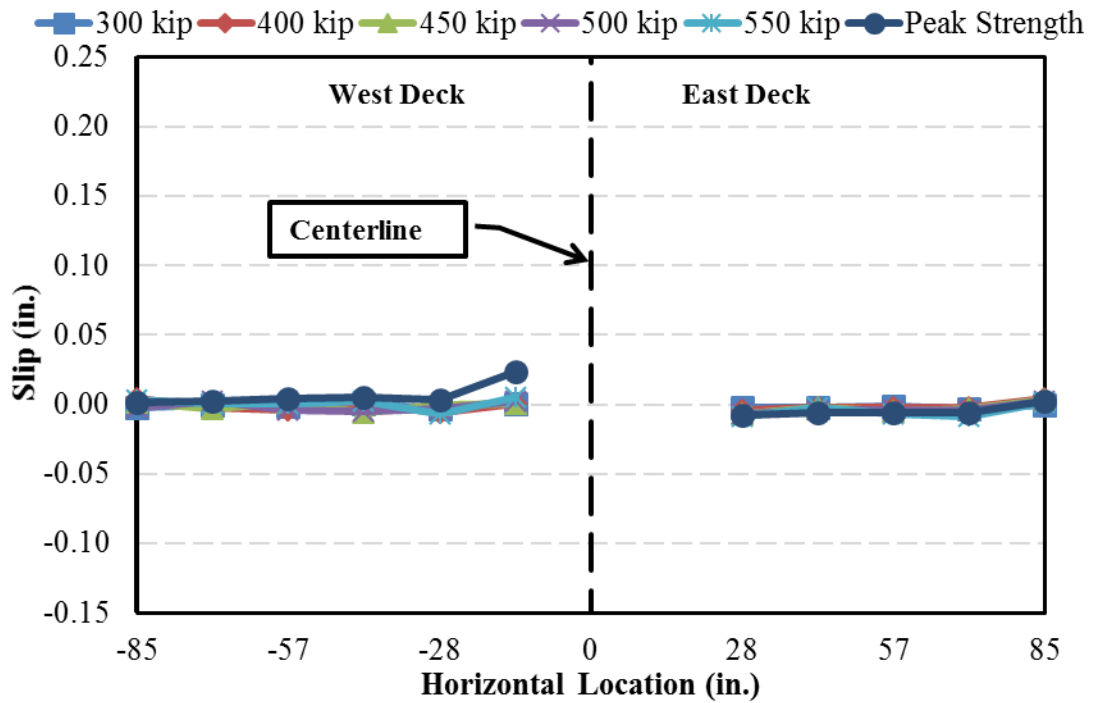


Figure 4.47: Distribution of Slip over Girder Length (Girder #3)

4.5.2.5 Relative Rotation along Girder Span

Relative rotation between nearby stations along the girder span are plotted in Figure 4.48 and 4.49 at various forces for Girders #2 and #3, respectively. Relative rotation was calculated based on the change of angle between consecutive stations calculated with data collected with markers placed vertically on the girder at each station (Figure 4.39). Rotation values that were influenced by instrumentation malfunctions are not presented.

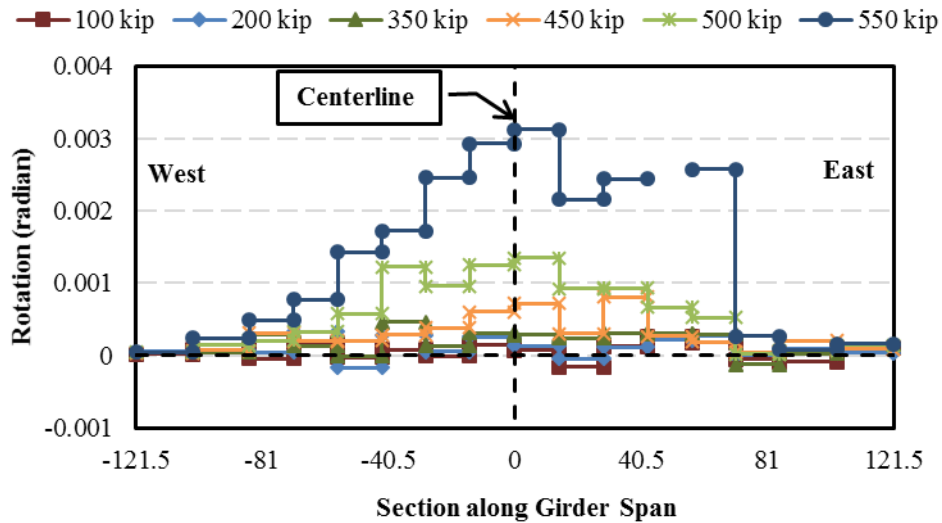


Figure 4.48: Relative Rotation along Girder Span (Girder #2)

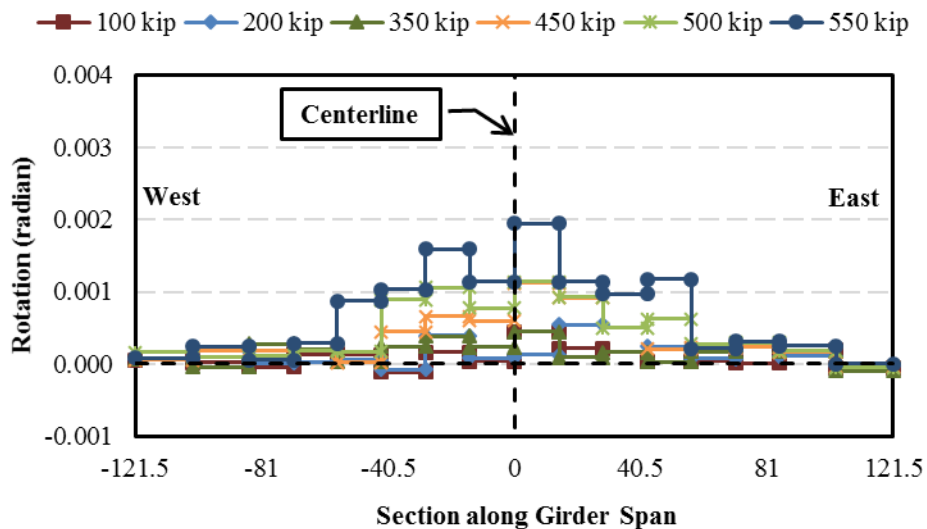


Figure 4.49: Relative Rotation along Girder Span (Girder #3)

Before flexural cracking (force less than 400 kip), relative rotation was small along the length of both girders. The relative rotation started to increase more rapidly as flexural cracks formed near midspan. As force increased, relative rotation near midspan increased much faster than near supports. This was due to the more extensive flexural cracking at midspan. Before 500 kip, the magnitude of relative rotation was similar between the two girders. After that, however, the relative rotation at each station of Girder #2 became much larger than in Girder #3, which is consistent with a gradual loss of composite action.

4.5.3 Interface Shear Stress

Interface shear stress was calculated at first cracking and at peak stress for each of the three girder specimens (Table 4.8). The interface shear stress was calculated assuming the compression zone force, C , due to midspan moment was located within the bridge deck and that the horizontal shear force transferred across the interface on each half of the girder was equal to C . This horizontal shear force was then divided by the interface area between the girder and deck, omitting areas with roofing felt (a width of 8, 8, and 36 in. were used for Girders #1, #2, and #3, respectively). This method was used because the girder exhibited flexural and shear cracking at loads that were less than that required for interface cracking to occur. For Girder #1, cracking occurred when the imposed force was approximately 460 kips, resulting in an interface shear stress at cracking of approximately 1100 psi. Based on the push-off test results, which indicate that first cracking and peak stress are typically close or coincide for troweled interfaces, this was likely the peak interface shear stress for Girder #1. The girder therefore resisted subsequent loads in a partially-composite manner, with some of the compression zone shifting to the top flange of the girder. This is consistent with observation, as no cracking of the top flange was observed until the shear failure occurred. The stress at cracking of the girder interface was significantly greater than expected based on the push-off tests (Table 4.4). It is possible this was due to unintentional roughening of the interface due to deck replacement. For Girder #2, interface shear stress at first cracking was approximately 1140 psi (the imposed force was approximately 480 kip). Slip then began to increase gradually to a force of approximately 500 kip (Figure 4.43), after which slip increased rapidly. Unlike the other two specimens, the maximum interface shear stress imposed during the test of

Girder #3 was at peak force. Due to the large bonded interface area, the maximum interface shear stress in Girder #3 was only 240 psi; much less than the cracking stress for bonded roughened specimens (Table 3.11). This is consistent with the lack of cracking observed during testing.

Table 4.8 Estimate of Cracking and Maximum Interface Shear Stresses

Girder ID	Interface Shear Stress at First Cracking (psi)	Peak Imposed Interface Shear Stress (psi)
Girder #1	1100	– ^a
Girder #2	1140	– ^a
Girder #3	– ^b	240 ^c

^a The point at which peak interface shear stress was reached cannot be identified

^b No cracking occurred

^c The peak interface shear stress is the calculated interface shear stress at peak force

4.5.4 Conclusions from Ultimate Strength Tests

- 1) Test results demonstrated that composite action was developed across troweled and roughened interfaces after deck removal and replacement and 2×10^6 cycles of force. The estimated stress transferred across the interfaces at cracking and peak stress exceeded 1000 psi, approximately double the cracking stress observed in push-off tests (Chapter 3).
- 2) Girders with troweled and roughened interfaces (Girders #1 and #2) exhibited increases in slip consistent with cracking at similar force (460 and 480 kips).
- 3) After cracking, the roughened interface of Girder #2 continued to control slip and transfer increased force across the interface. This is different from the troweled interface, which exhibited significantly increased slip and no evidence of increased force transfer. This is consistent with the troweled interface reverting to dowel action only after cracking.
- 4) At the end of the tests, even specimens with large interface slip (0.25 in.) maintained partially composite action sustained by dowel action across the interface. No evidence of dowel bar fracture was observed during testing.
- 5) As expected, sections furthest from the loading point exhibited the largest slip.

Chapter 5: Modeling of Composite Action

A simplified 3D model was created in SAP2000 to simulate the composite action between precast girders and cast-in-place decks. Because the focus of this analysis was on the behavior under service-level loads, the girder was modeled as an elastic frame element and the deck was modeled with elastic shell elements. The girder and deck were connected with a series of link elements used to simulate the transfer of shear between the precast girder and cast-in-place deck. The approach was validated with comparisons to the girder test results (Chapter 4). A series of prototype composite girders were then modeled with aim of better understanding the distribution of shear stress along the interface. Motivated by prior studies (Seamann and Washa, 1964; Badoux and Hulsbos, 1967), the effects of beam aspect ratio and load position on the distribution of interface shear were both investigated.

5.1 Description of Models

5.1.1 Girder and Deck Elements

The girder was modeled as a simply supported elastic frame element. The element was assigned cross-sectional dimensions patterned after an actual NU35 girder; the moment of inertia of the frame element was only 1.2% less than the nominal value for an NU35 section. The deck was modeled using 7 in. thick shell elements that neglect transverse shear deformations. The deck and girder were assigned material properties representing concretes with specified concrete compressive strengths of 4 and 8 ksi respectively (Table 5.1). Reinforcement was not explicitly modeled for this analysis. The models were designed to remain within the elastic range because service-level loads were of interest in this analysis. Additional details are provided in Appendix F.

Table 5.1: Assigned Material Properties

Concrete Properties	Girder	Deck
Specified Compressive Strength (ksi)	8.0	4.0
Modulus of Elasticity (ksi)	5100	3600
Shear Modulus (ksi)	2100	1500
Poisson's Ratio	0.2	0.2

5.1.2 Link Properties

The interface was modeled with a series of multilinear plastic links spaced at 21.25 in., or one-half the overall depth of the composite section (a sensitivity study, not reported here, indicated that use of half that spacing changed the initial stiffness of the force versus deflection relationship by only 2%). Each link connected a node on the frame element (girder) to a node on the centerline of the mesh of shell elements representing the deck. The link was free to deform in a shearing mode in the vertical plane coincident with the longitudinal axis of the girder and rigid in the other five degrees of freedom. The relationship between force and slip in the free direction was defined based on experimental results reported in Chapters 3 and 4. Additional details are provided in Appendix F.

Four different link elements were created to simulate different interface conditions based on previous test results: Link #1 for a troweled surface based on push-off tests, Link #2 for a rough middle surface based on push-off tests, Link #3 for a roughened surface based on push-off tests, and Link #4 for a rough middle surface with properties inferred from results of the Girder #2 test. Force and slip properties assigned to the links at key points are shown in Table 5.2. For the first three links developed based on results from the push-off tests, force was calculated as the product of the stress attributed to the interface (based on Chapter 3) and the total interface area in the model divided by the number of links. Cracking and peak strengths were calculated based on the average stresses obtained from the tests given in Table 3.11. Slip at key points was estimated for Link #1 based on average values obtained from tests of troweled bonded specimens (Table 3.8). Slip at key points for Links #2 and #3, which were the same, were calculated based on average values obtained from tests of roughened specimens (Table 3.8). Post-peak strength for all links was calculated using Eq. 3-3 with C_2 equal to 1.1 based on Table 3.10. Post-peak strength and slip were taken to be the same for all link elements because the amount of reinforcement was assumed to not change. Force and slip at cracking for Link #4 were selected to so that the model results matched the test result from Girder #2 in terms of force at cracking and initial stiffness (Chapter 4). A plot of force versus slip for the four link elements is shown in Figure 5.1 alongside the push-off test result for RM-12-E-12-NR (Figure 3.7).

Table 5.2: Link Element Properties

Link ID	Key Points					
	Cracking Strength		Peak Strength		Post-peak Strength	
	Force (kip)	Slip (in.)	Force (kip)	Slip (in.)	Force (kip)	Slip (in.)
Link #1: Trowel Surface (Push-off Test) ^a	54	0.010 ^b	92	0.020 ^b	72 ^c	≥ 0.1
Link #2: Rough Middle Surface (Push-off Test) ^a	85	0.012 ^d	120	0.03 ^d	72	≥ 0.1
Link #3: Rough Surface (Push-off Test) ^e	380	0.012 ^d	550	0.03 ^d	72	≥ 0.1
Link #4: Rough Middle Surface (Girder #2) ^a	150 ^f	0.01 ^f	200 ^g	0.03 ^h	72	≥ 0.1

^a Force at cracking and peak strength were calculated based on an 8 in. wide interface

^b Slip was selected based on average slip for troweled bonded specimens in Table 3.8

^c Post-peak force was calculated based on Eq. 3-3 with C_2 equal to 1.1

^d Slip was selected based on average slip for roughened specimens in Table 3.8

^e Force at cracking and peak strength were calculated based on a 36 in. wide interface surface

^f Force and slip values were selected so the model output matched the Girder #2 experimental results

^g Force at peak was calculated based on 500 kip force

^h Slip at peak was assumed to be the same as Links #2 and #3

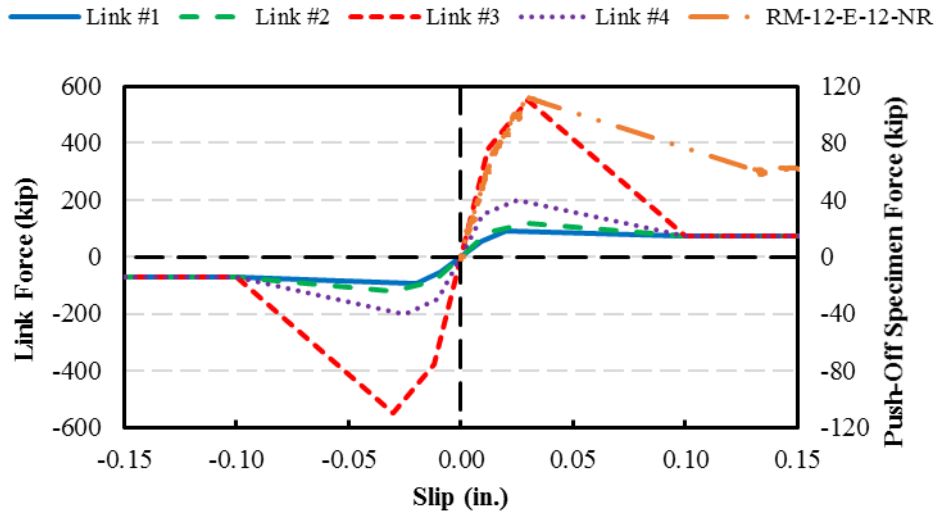


Figure 5.1: Force versus Slip of Link Element

5.2 Model Verification with Experimental Test Results

Five models were created to simulate results from the tests of Girders #1 through #3 described in Chapter 4 (Table 5.3). The five models were the same except that the link element was varied. Models #1 through #4 used the links described in 5.1.2 and Model #5 used a rigid link,

as recommended by Kalny (2016) for modelling fully composite action. As shown in Figure 5.2, each model was simply supported and the deck was not extended to the full girder length (just like in the girder tests). Force was monotonically applied to the deck as a point load at midspan. For simplicity, self-weight was neglected.

Table 5.3: Models of Girder Test Results

Model ID	Simulation Target	Link Property
Model #1	Girder #1	Link #1
Model #2	Girder #2	Link #2
Model #3	Girder #3	Link #3
Model #4	Girder #2	Link #4
Model #5	Girder #3	Rigid Link

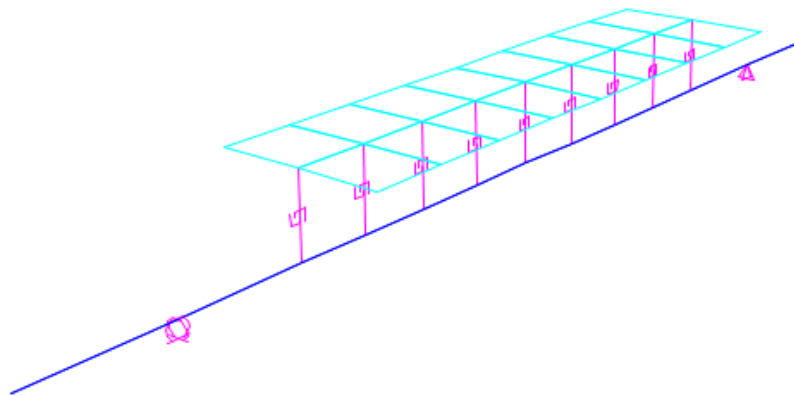


Figure 5.2: Composite Girder Model

5.2.1 Force versus Deflection and Girder Stiffness

Force is plotted versus midspan deflection in Figure 5.3 for each of the five models alongside the test result from Girder #2. All of the model results were linear elastic up to at least 400 kips, whereas the test result was linear elastic up to approximately 250 kips. The deviation from linearity at approximately 250 kips was due to inclined cracking of the girder web that was not simulated in the models (this was considered acceptable because the aim was to model

composite action under service-level loads). Among the first three models, the initial stiffness of Model #3 was largest followed by Model #2 and then Model #1 (as expected). This is mainly due to the different initial stiffnesses of the link elements used for each model. Given how close the initial stiffness of these models was to the respective test result (Table 5.4), it appears that link stiffness can be reasonably estimated based on results from push-off tests. Model #4, which used Link #4 that was designed to provide a close match between model and test result for girder load at initial cracking, had a stiffness that was 5% greater than Model #2. This shows that composite girder stiffness is not very sensitive to link stiffness, given that Link #4 was approximately twice as stiff as Link #2. Nevertheless, use of a link stiffness based on push-off test results led to a better modelling result than use of rigid links: Model #5 overestimated girder stiffness by 3% for Girder #3 and 11% for Girder #1.

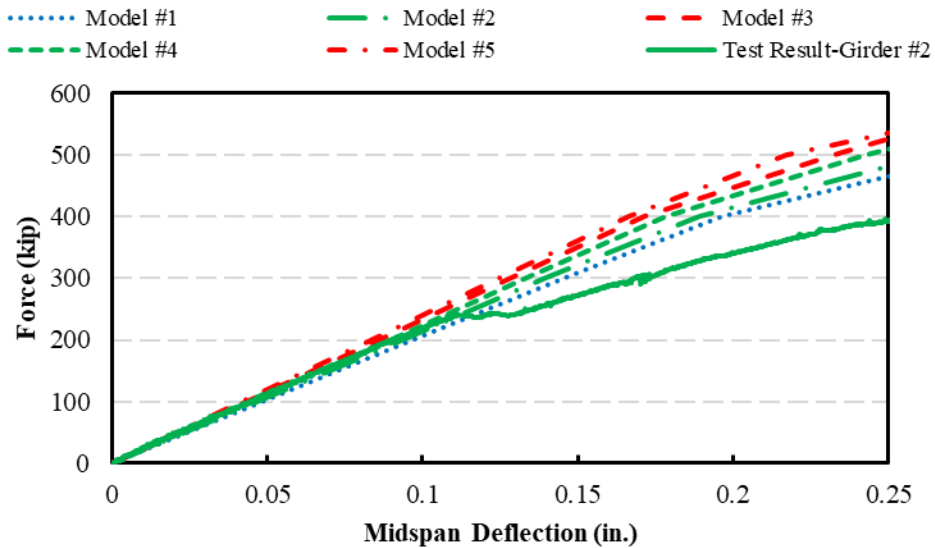


Figure 5.3: Plot of Force versus Midspan Deflection

Table 5.4: Stiffness Summary

Parameter	Model #1	Model #2	Model #3	Model #4	Model #5
Model Stiffness (kip/in.)	2080	2150	2330	2250	2400
Stiffness of Corresponding Girder (kip/in.)	2220	2170	2330	2170	2330
Error (%)	-6%	-1%	0%	3%	3%

5.2.2 Distribution of Link Forces and Interface Cracking

The distribution of link forces along the deck length in Model #4 is shown in Figure 5.4 at varied levels of imposed force. The values of force shown in Figure 5.4 are absolute values (sign does not indicate directionality). The distributions of force and slip were both symmetric about midspan where slip was zero regardless of the amount of imposed force. For most applied forces shown, link forces increased as the distance between link and midspan increased, which agrees well with the measured slip distribution for Girders #1 and #2 in Chapter 4 (Figures 4.42 and 4.44). Also, the difference between the forces in consecutive links increased as force increased. At approximately 480 kips of force on the girder, the force in the links furthest from midspan reached the cracking force (Table 5.2), after which link force increased more gradually. This is evident in Figure 5.4; the difference in force between consecutive links diminished for links with internal forces exceeding the cracking force.

The applied force at first cracking of a link is summarized in Table 5.4. It was reported in Section 4.5.4 that evidence of cracking along the interface was first observed in the tests of Girders #1 and #2 at 460 and 480 kip respectively. For Model #1, which was to simulate Girder #1, a link first reached cracking when the applied force was approximately 220 kip. This is a large difference, but is consistent with observations in Chapter 4 and by others (Hanson, 1960) that indicated the apparent interface shear strength tends to be greater in girders than in push-off tests. The difference between experimental and analysis results may be especially large in this case because the surface was somewhat unintentionally roughened by the process of deck removal and replacement. Both Model #2 and #4 were created to simulate Girder #2; in these models a link first reached the shear force associated with cracking at 320 and 480 kip (67 and 100% of the experimental value), respectively. Again, the model based directly on push-off test results underestimated the cracking force for the girder. As expected, Model #4, which used Link #4 that was calibrated based on the girder test results, provided a more accurate estimate of the interface cracking load. For this reason, Link #4 is used in subsequent models discussed in this chapter.

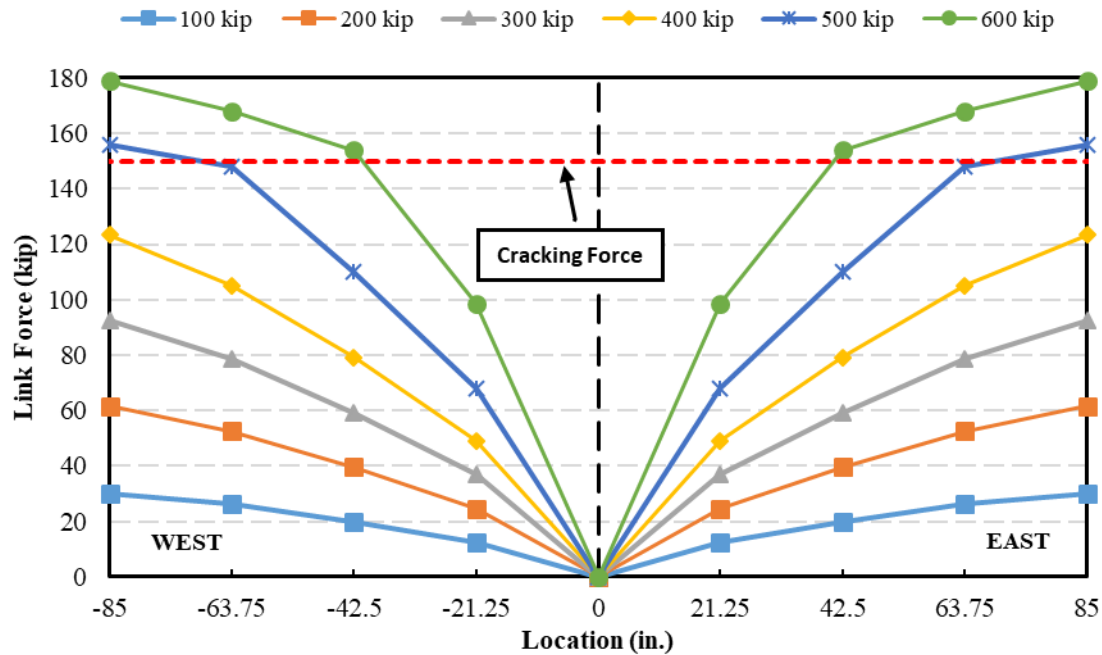


Figure 5.4: Link Force versus Link Location for Model #4 at Varied Imposed Forces

Table 5.5: Cracking Force

	Model #1	Model #2	Model #3	Model #4	Model #5
Cracking Force (kip)	220	320	NA ^a	480	NA ^a

^a Link element did not crack or was rigid

5.3 Effect of Aspect Ratio

Four more models with different span lengths were created to investigate the influence of shear span to effective depth ratio on the distribution and intensity of interface shear force demands between a girder and deck. This investigation is motivated by prior studies (Seamann and Washa, 1964; Badoux and Hulsbos, 1967) that reported that interface shear strength decreased as aspect ratio increased. These studies did not provide an explanation for the phenomenon and it was challenged by Hall and Mast (1964) in a discussion of the paper.

The models are summarized in Table 5.6. The composite girders were modeled as simply supported using the same assumptions described in Section 5.1.1. Link #4 (Table 5.2) was used for all models at the same spacing used for the analysis described in Section 5.2 (21.25 in.). The

deck was extended to the full girder length, as shown in Figure 5.5, to be consistent with construction practice. A static point load of 200 kip was applied at midspan.

Table 5.6: Model Details

Model Name	a (in.) ^a	a/d ^b	Number of Links in Half Span ^c
Model #6	106	2.7	5
Model #7	170	4.4	8
Model #8	255	6.5	12
Model #9	340	8.7	16

^a Shear span length, defined as the distance from the point load to each support

^b Ratio of shear span length to effective depth. The effective depth was 39 in.

^c Not including the link at midspan

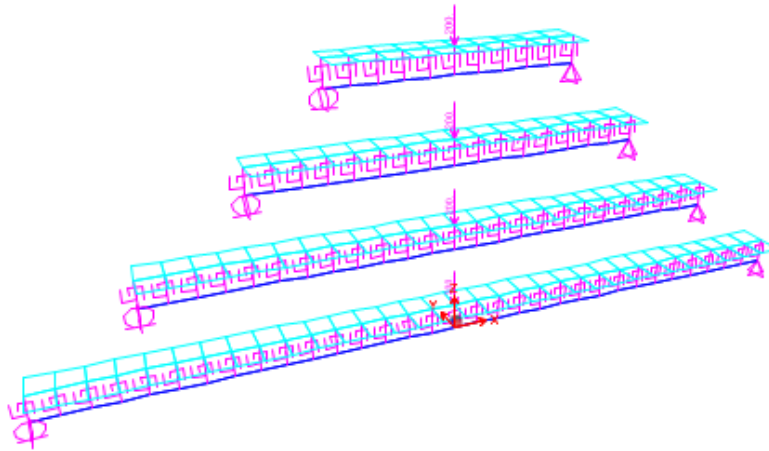


Figure 5.5: Models of Girders with Different Aspect Ratios

Under the forces applied, all link elements exhibited linear elastic behavior (none of the links reached the force associated with cracking). The distribution of link forces along half the beam span at 200 kips is shown in Figure 5.6. The horizontal shear force demand calculated with Eq. 5-1 is also shown in Figure 5.6.

$$V_u = \left(\frac{V_{u1}}{b_{vi}d_v} \right) (b_{vi} \times 21.25 \text{ in.}) \quad \text{Eq. 5-1}$$

Where: V_{u1} is the envelope of transverse shear force demand (calculated here based on the point load alone), b_{vi} is the width of the interface, and d_v is the distance between the centroid of the tension steel and mid-thickness of the deck. The ratio in parenthesis in Eq. 5-1 is the same as Eq. 5.8.4.2-1 in the AASHTO Specification for calculating interface shear stress demand. The second term is added here to convert this stress to the expected force in a given link, where 21.25 in. is the spacing between links.

For each model, link forces tended to increase as distance from midspan increased until reaching a peak and then decreasing at the very end of the girder. The locations at which link forces (and therefore interface slip because the models were within the elastic range of behavior) were greatest are listed in Table 5.7. For values of a/d between 2.7 and 8.7, the maximum force occurred between approximately 1/5 and 1/2 of half the span length from the support (or between 1/10 and 1/4 of the full span length), with the location approaching 1/4 of the full span length as a/d increased. This finding agrees with Hanson's (1960) observation from the girder tests that slip at the contact interface was usually maximum at approximately a quarter of the span from the girder end. Except for near midspan and the end of the girder, the force was, however, fairly consistent throughout much of the span for values of a/d greater than approximately 4.0. The decrease in force near the end of the girder was not due to cracking in this case, as the model components remained elastic. Rather, the decrease in link force is attributable to a decrease in slip near the girder ends.

Among the different models, the maximum link force increased as the beam aspect ratio increased. This observation is similar to the contested assertion by Badoux and Hulsbos (1967) that nominal shear strength decreases as a/d increases. Rather than a reduction in strength, however, the model indicates that peak shear force demand increases as a/d increases. The result is the same: the ratio between shear capacity and shear demand does appear to decrease somewhat as a/d increases. This effect appears to diminish with increases of a/d . In this study, the change in maximum force was minimal for a/d greater than approximately 4.0.

Regardless of a/d , the maximum link force was never greater than approximately 75% of the link force demand calculated with Eq. 5-1.

Table 5.7: Location of Maximum Force/Slip

Model Name	Location of Maximum Slip as a Fraction of Full Span Length	Maximum Link Force (kip)	Link Horizontal Shear Demand (kip) ^a
Model #6	1/10	36	57
Model #7	3/16	41	57
Model #8	5/24	43	57
Model #9	7/32	43	57

^a The link horizontal shear demand was calculated at 200 kip using Eq. 5-1

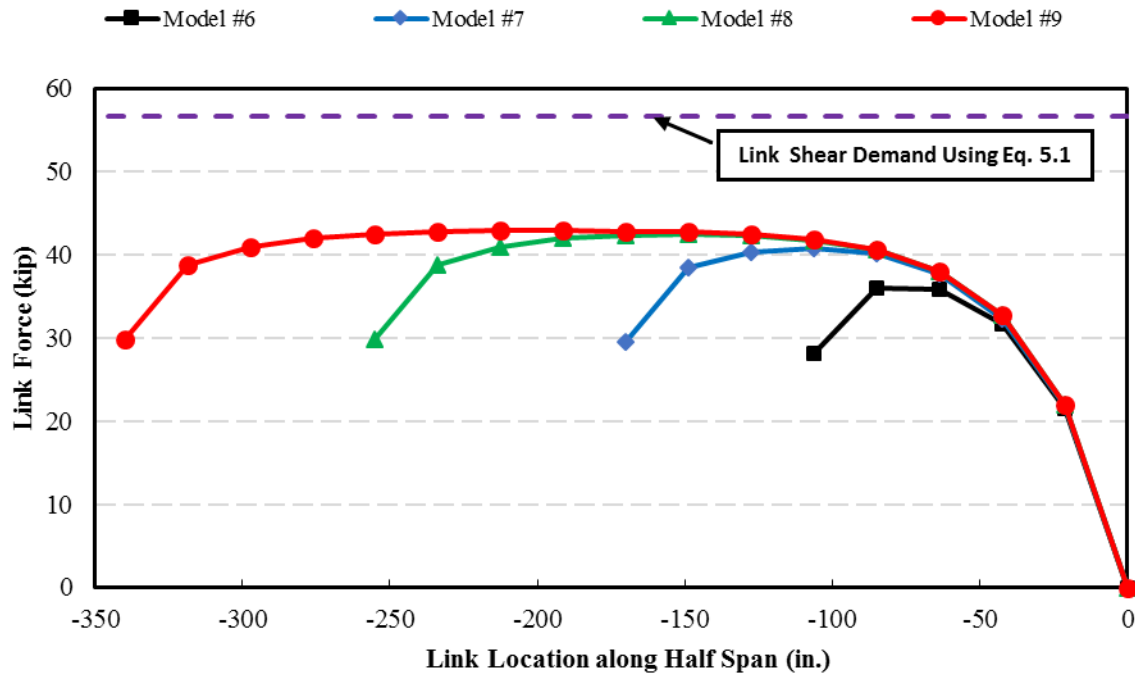


Figure 5.6: Link Shear Force versus Position along Half Span at 200 kips

5.4 Effect of Load Position

Model #8 (Table 5.6) was used as the basis for investigation of the influence of load position on the distribution of interface shear demand between the girder and deck. Five load positions were selected (in terms of total span length, loads were positioned at: $L/12$, $L/8$, $L/6$, $L/4$, $3L/8$, and $L/2$). The distribution of link force along the span length obtained from the model is shown in Figure 5.7 for two load positions, $L/8$ and $3L/8$, along with the link force demand calculated with Eq. 5-1. For both cases, slip at the loading point was not zero. Instead, the zero

force/slip point was located between the load point and midspan. Similar results were observed for other load positions. The slip is only zero under the load point when the load is at midspan. Accordingly, the direction of shearing near the load points is not strictly consistent with the distribution of transverse shear demand.

The maximum link force and its location are shown in Table 5.8 for each case as well as the estimated link force. The estimated link force was calculated based on Eq. 5-1, which relies on two assumptions: 1) all compression forces from bending moment are in the deck at every cross-section, and 2) interface shear is uniformly distributed along the shear span. For all load positions and link locations, the link force estimated with Eq. 5-1 was greater than the link force reported by the models.

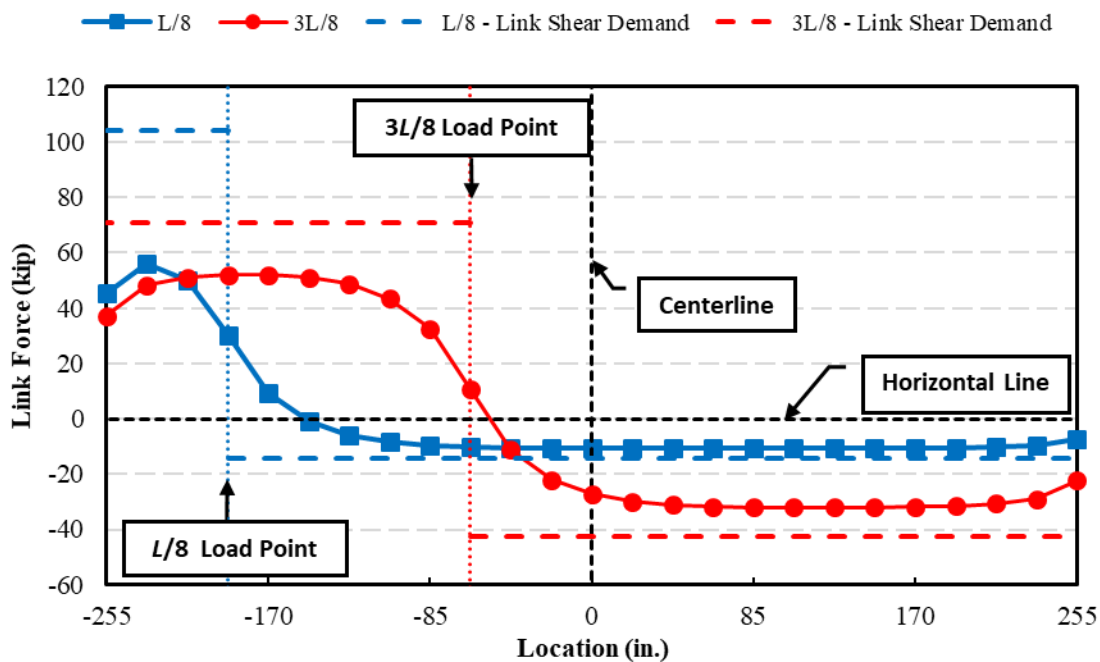


Figure 5.7: Link Shear Force Distribution for a 200 kip Point Load Located at $L/8$ and $3L/8$

As shown in Figure 5.8, the estimated link force (based on Eq. 5-1) is linearly related to load position: as the load position approaches midspan the link force reduces. This exactly follows the shape of the influence line for the reaction at the nearer girder support. This is somewhat different from the link forces obtained from the model, which were a maximum for loads placed

near $L/4$. Overall, the estimated link force was higher than the measured values. This is partially due to the assumption that all of the compression force from bending is located within the deck: the models were developed assuming that the girders remain uncracked, which should be representative of typical in-service conditions. For an uncracked girder, the neutral axis remains within the girder, thereby lowering the interface shear demand. What is also evident in Table 5.8 is that the location of maximum interface force/slip changes as the load position moved from the support to midspan. The maximum slip location is approaching to approximately $1/4$ of full span length to the support, when distance from load position to support increases.

Table 5.8: Summary of Maximum Link Forces and Location

Position of Load Placement ^a	Link Force (kip)		Maximum Slip Location ^b
	Measured Maximum Force	Estimated Link Force	
$L/12$	47	104	$1/24$
$L/8$	56	99	$1/24$
$L/6$	59	94	$1/24$
$L/4$	59	85	$2/24$
$3L/8$	52	71	$4/24$
$L/2$	43	57	$5/24$

^a Load placement is presented in terms of full span length

^b Maximum slip location is presented in terms of full span length

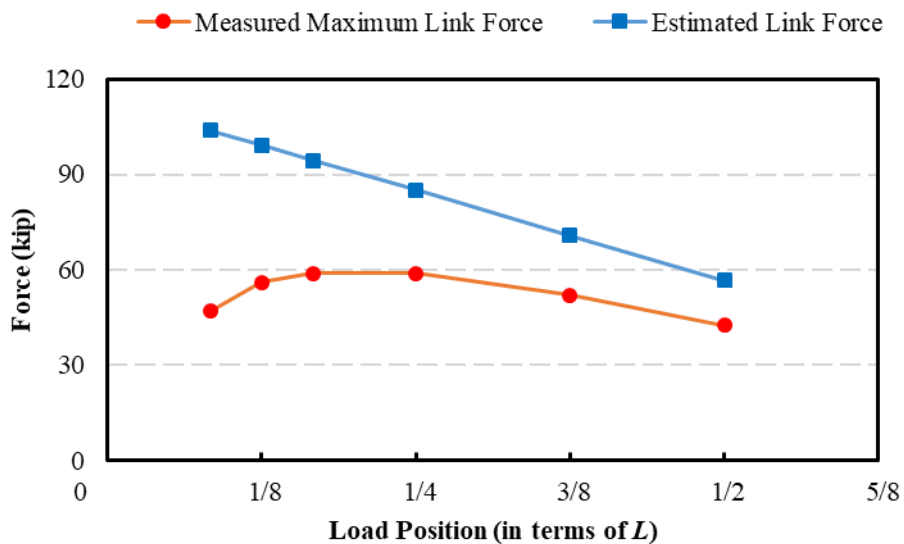


Figure 5.8: Maximum Link Shear Force for Load Positions between $L/12$ and $L/2$ (Maximum Link Force is plotted at the Load Position, Not the Position of Maximum Link Force)

5.5 Conclusions from Modelling of Composite Action

The following conclusions are drawn based on the analysis results:

1. For all aspect ratios and load positions considered in this study, interface shear demand was conservatively estimated with Eq. 5-1 (modified from Eq. 5.8.4.2-1 in the AASHTO specification). This analysis did not consider cracking of the prestressed girders.
2. For models of composite action, the stiffness of the interface can be reasonably estimated based on results from push-off tests. The girder stiffness is not, however, sensitive to changes in link stiffness. Use of a rigid interface, as recommended by Kalny (2016) and others, will somewhat overestimate girder stiffness (by 3 to 11% in this study) and distort the distribution of interface shear forces.
3. As expected based on results reported in Chapters 3 and 4 and Hanson (1960), the girder models with interface properties derived from push-off test results underestimated the force at which the horizontal shear interface cracked. This affirms that design for composite action in girders based on push-off test results will conservatively underestimate strength.
4. Similar to observations by Hanson (1960), it was observed that the maximum interface shear demand (and therefore slip) was located near $L/4$ when a/d exceeded 4.0 and a point load was located at midspan. The interface shear demand was, however, approximately constant throughout most of the span (except near midspan and the ends of the span) when a/d exceeded 4.0. For a/d of 2.7, the maximum interface shear demand occurred closer to the end of the span ($L/10$).
5. For a/d of 2.7 to 8.8, the maximum interface shear demand increased as a/d increased, although the relative increase diminished with a/d and was minimal for a/d greater than 4.0. This indicates that previous studies (Seamann and Washa, 1964; Badoux and Hulsbos, 1967) were incorrect that interface shear strength decreases as a/d increases; they were instead observing an increase in shear demand with a/d . This effect is not, however significant at the large aspect ratios found in practice.

6. For loads not positioned at midspan, zero interface slip/force occurs between the load point and midspan and not under the point load. Accordingly, the direction of shearing near the load points is not strictly consistent with the distribution of transverse shear demand.
7. The maximum interface shear demand occurs when forces are located between approximately $L/8$ and $L/4$. This is contrary to the implication of Eq. 5.8.4.2-1 in the AASHTO specification, which indicates that the maximum interface shear demand occurs when loads are located near the supports.

Chapter 6: Conclusions and Recommendations

6.1 Conclusions

6.1.1 Conclusions from Push-off Tests

1. As expected, surface preparation has a large influence on shear transfer performance up to peak strength. Stiffness (in terms of stress versus slip), stress at cracking, and peak strength are greatest for specimens with a fully roughened surface followed by those with a rough middle surface, troweled specimens, and fully debonded specimens.
2. Use of an interface that is partially roughened and partially troweled (with a bond breaker) is a viable connection detail for horizontal shear transfer. Shear transfer performance should be considered in terms of stress calculated based on roughened area. A conservative estimate of strength can be obtained for partially roughened specimens with a bond breaker by neglecting the debonded area when calculating interface shear strength.
3. The ascending branch of the force versus slip relationship for specimens with at least a partially roughened interface is composed of two distinct branches representing behavior before and after cracking of the interface. Interface cracking occurs, on average, at a stress of 500 psi in specimens with a fully roughened interface. In troweled bonded specimens, cracking (at an average stress of 320 psi) is approximately equal to the peak strength.
4. Cohesion was sensitive to variability of testing results, with calculated averages of 460, 320, 76, and -120 psi for roughened, rough-middle, troweled, and debonded specimens, based on the assumption that shear strength is composed of cohesion and reinforcement terms. The negative cohesion value for debonded specimens indicates that the reinforcement was not fully effective when the entire interface was debonded. These values are approximately double and equal to the values recommended in the AASHTO Specification for roughened and troweled interfaces (240 and 75 psi). The contribution of normal strength (Grade 60) reinforcement to maximum strength was, on average, $1.1A_s f_y$. The coefficient of 1.1 is larger than those recommended by AASHTO Specifications (1.0 and 0.6 for roughened and troweled interfaces).

5. If concrete compressive strength is considered when calculating horizontal shear strength between interfaces with different concrete strengths, as recommended by some researchers, the lower concrete strength should be used.
6. Increasing the amount of interface shear reinforcement increases the initial stiffness of the connection, interface shear strength at cracking, peak strength, and post-peak strength, though not in proportion to the increase in reinforcement area. Use of high-strength steel as interface shear reinforcement has no discernable effect on stiffness or cracking strength, and a less substantial effect on peak strength and post-peak strength than a similar increase in reinforcement area.
7. Use of headed bars as interface shear reinforcement appears viable, as pairs of specimens with either headed or hooked bars exhibited similar behavior.

6.1.2 Conclusions from Deck Removal

1. The use of roofing felt over the girder flanges would significantly reduce the effort required for bridge deck removal. Furthermore, use of roofing felt over the girder flanges could effectively eliminate damage to the girder caused by hammer impact because it dramatically reduces the need for use of chipping hammers over the flanges.
2. Regardless of connection detail, the girders were vulnerable to damage from saw-cutting. Girder damage due to saw-cutting could be reduced by a) limiting the number of required cuts, b) setting the maximum cut depth to 0.5 in. less than the deck thickness over the flange, and either c) locating the interface shear reinforcement prior to saw-cutting (e.g. with GPR-based rebar locators), or d) eliminating transverse cuts through the deck located over the girder web where interface shear reinforcement is located.
3. Casting and removal of a bridge deck does alter the top surface of bridge girders. However, it was possible to return the surfaces of all three girders to a condition qualitatively similar to their original state with reasonable effort. However, it would be prudent to assume troweled-like conditions for design of composite action after deck removal unless measures are taken to ensure an adequately roughened interface is present after deck removal.

4. Roofing felt was easy to install over the flanges immediately prior to placement of the deck reinforcement. No adhesive was used between the roofing felt and top flange because that is where the important debonded plane is located. However, to prevent movement of the roofing felt during construction, it is recommended that contractors use some adhesive to keep the roofing felt in place during construction.
5. Troweled surfaces of the girders exhibited relatively strong bond with the deck concrete that increased the effort required for deck removal and potential for damage to the flanges relative to portions of girders that had roofing felt.
6. Although the use of large jackhammers is not recommended, it may be possible to use jackhammers, like the 65 lb jackhammer used in this study, in very limited field applications. If permitted, use of hammers larger than 30 lbs should be limited to portions of the deck located directly over the girder web and to a depth not greater than the depth of the top slab reinforcement.

6.1.3 Conclusions from Composite Girder Tests

1. Composite action can be developed across partially troweled/partially debonded and partially-roughened/partially debonded interfaces after deck replacement and 2×10^6 cycles of loading to 45 and 30% of the expected cracking loads, respectively. Specimens with either detail maintained full composite action throughout the fatigue tests and far beyond the estimated cracking force when loaded to failure.
2. Specimens with partially troweled and partially roughened interfaces exhibited interface cracking at similar levels of imposed force.
3. After cracking, the roughened interface could continue to control slip and transfer increased force across the interface, while the troweled interface exhibited significantly increased slip and no evidence of increased force transfer.
4. At the end of the tests, even specimens with large interface slip (0.25 in.) maintained partially composite action sustained by dowel action across the interface. No evidence of dowel bar fracture was observed during testing.

6.1.4 Conclusions from Modeling of Composite Action

1. For all aspect ratios and load positions considered in this study, interface shear demand was conservatively estimated with Eq. 5-1 (modified from Eq. 5.8.4.2-1 in the AASHTO specification). This analysis did not consider cracking of the prestressed girders.
2. For models of composite action, the stiffness of the interface can be reasonably estimated based on results from push-off tests. The girder stiffness is not, however, sensitive to changes in link stiffness.
3. As expected based on results reported in Chapters 3 and 4 and Hanson (1960), the girder models with interface properties derived from push-off test results underestimated the force at which the horizontal shear interface cracked. This affirms that design for composite action in girders based on push-off test results will conservatively underestimate strength.
4. Similar to observations by Hanson (1960), it was observed that the maximum interface shear demand (and therefore slip) was located near $L/4$ when a/d exceeded 4.0 and a point load was located at midspan. The interface shear demand was, however, approximately constant throughout most of the span (except near midspan and the ends of the span) when a/d exceeded 4.0. For a/d of 2.7, the maximum interface shear demand occurred closer to the end of the span ($L/10$).
5. For a/d of 2.7 to 8.8, the maximum interface shear demand increased as a/d increased, although the relative increase diminished with a/d and was minimal for a/d greater than 4.0. This indicates that previous studies (Seamann and Washa, 1964; Badoux and Hulsbos, 1967) were incorrect that interface shear strength decreases as a/d increases; they were instead observing an increase in shear demand with a/d .
6. For loads not positioned at midspan, zero interface slip/force occurs between the load point and midspan and not under the point load. Accordingly, the direction of shearing near the load points is not strictly consistent with the distribution of transverse shear demand.
7. The maximum interface shear demand occurs when forces are located between approximately $L/8$ and $L/4$. This is contrary to the implication of Eq. 5.8.4.2-1 in the AASHTO specification, which indicates that the maximum interface shear demand occurs when loads are located near the supports.

6.2 Recommendations for Deck Removal

For removal of deck concrete supported by NU I-Girders, the following deck removal procedures are recommended to limit the potential for damage to the girders.

6.2.1 Procedure A: For girders with a roughened and or troweled top flange

1. Perform a series of saw-cuts between girders transverse to the girder axes to create a series of panels to facilitate lifting and disposal. Through-thickness cuts are appropriate when clear of girders. When near to the girder top flanges, limit the saw-cut depth to 0.5 in. less than the deck thickness.
2. Using a crane or other piece of lifting equipment in tandem with saws, separate the ends of each panel from the deck concrete over the girders and lift clear for disposal.
3. Use 30 lb demolition hammers to remove the concrete over the bridge girders down to the level of the bottom layer of deck reinforcement. The 30 lb demolition hammers should be used at an angle not exceeding 45 degrees from horizontal.
4. Once the bottom layer of deck reinforcement is exposed, 15 lb demolition hammers should be used to remove the remaining concrete and install a roughness in compliance with project specifications. Where the deck concrete immediately over the flange is sound, it may not be necessary to fully remove all deck concrete. In this study it was observed that the deck and girder concrete form a strong bond where the concrete was roughened prior to casting of the deck that makes complete removal of deck concrete difficult. The judgement of the engineer should govern the extent of removal necessary considering the condition of the system and risk of damage to the underlying girders.

6.2.2 Procedure B: For girders with roofing felt placed over the top flange except for directly over the web

1. Locate the centerline of each girder and the extent of horizontal shear reinforcement (the extent of shear reinforcement can be estimated from design documents or determined with GPR-based rebar locating equipment). Clearly mark two longitudinal lines on the deck demarcating

the likely extent of horizontal shear reinforcement. Perform longitudinal saw-cuts (along the longitudinal lines) to a depth of 0.5 in. less than the deck thickness.

- 2a. Perform a series of saw-cuts transverse to the girder axes to create a series of disposable panels. Care should be taken to avoid contact with horizontal shear reinforcement. Through-thickness cuts are appropriate when clear of girders. When near to the girder top flanges, limit the saw-cut depth to 0.5 in. less than the deck thickness.
- 2b. Perform a series of saw-cuts transverse to the girder axes to create a series of disposable panels. The cuts should not penetrate the middle strip of deck located over the web of the girder. Through-thickness cuts are appropriate when clear of girders. When near to the girder top flanges, limit the saw-cut depth to 0.5 in. less than the deck thickness.
3. Using a crane or other piece of lifting equipment in tandem with demolition hammers and prybars, separate the panels from the deck concrete over the girder webs and lift clear for disposal.
4. Use 30 lb demolition hammers to remove the concrete over the bridge girders down to the level of the bottom layer of deck reinforcement. The 30 lb demolition hammers should be used at an angle not exceeding 45 degrees from horizontal.
5. Once the bottom layer of deck reinforcement is exposed, 15 lb demolition hammers should be used to remove the remaining concrete and install a roughness in compliance with project specifications. Where the deck concrete immediately over the web is sound, it may not be necessary to fully remove all deck concrete. In this study it was observed that the deck and girder concrete form a strong bond where the concrete was roughened prior to casting of the deck that makes complete removal of deck concrete difficult. The judgement of the engineer should govern the extent of removal necessary considering the condition of the system and risk of damage to the underlying girders.

6.2.3 Potential modification to either Procedure A or B for use of larger jackhammers

Insert before step 3: Use 65 lb jackhammers directly over the web (within 4 in. of centerline) to expose the top layer of deck reinforcement.

Although this modification was used in this study without detriment, it is noted that the controlled conditions of the laboratory are not easily replicated in the field. It is prudent to avoid use of such powerful equipment.

References

- ACI Committee 318. (2014). *Building Code Requirements for Structural Concrete and Commentary (ACI 318-14)*. Farmington Hills, MI: American Concrete Institute.
- Anderson, A. R. (1960). "Composite Designs in Precast and Cast-In-Place Concrete". *Progressive Architecture*, 41(9), 172-179.
- American Association of State Highway and Transportation Officials. (2012). *AASHTO LRFD Bridge Design Specifications*. Washington, D.C: American Association of State Highway and Transportation Officials.
- American Association of State Highway and Transportation Officials. (1996). *Standard Specifications for Highway Bridges*. Washington, D.C: American Association of State Highway and Transportation Officials.
- American Concrete Pavement Association. (1998). *Guidelines for Partial-Depth Spall Repair*. Skokie, IL: American Concrete Pavement Association.
- Badoux, J. C., & Hulsbos, C. L. (1967). "Horizontal Shear Connection in Composite Concrete Beams under Repeated Loads". *ACI Journal*, 64(12), 811-819.
- Badie, S. S., Tadros, M. K., Kakish, H. F., Kamel, M. R., & Baishya, M. C. (2004). "Rapid Deck Replacement". *Concrete International*, 26(7), 72-79.
- Beacham, M. & Derrick, D. (1999). "Longer Bridge Spans with Nebraska's NU I-Girders". *TRNews Magazine*, 202. Retrieved from <http://onlinepubs.trb.org/onlinepubs/trnews/rpo/rpo.trn202.pdf>
- Birkeland, P. W., & Birkeland, H. W. (1966). "Connections in Precast Concrete Construction". *Journal of American Concrete Institute*, 63(3), 345-367.
- Chung, H. W., & Chung, T. Y. (1976). "Prestressed Concrete Composite Beams under Repeated Loading". *ACI Journal*, 73(5), 291-295.
- Fleck, T. (2015). Personal Communication.
- Hall, J. W & Mast, R. R. (1965). Discussion of paper "Horizontal Shear Connections between Precast Beams and Cast-In-Place" published in *Journal of the American*

- Concrete Institute*, 1964; 61(11), 1383-1410, by Saemann, J. C., & Washa, G. W. *Journal of the American Concrete Institute*, Discussion. 61-69, 1807-1810.
- Hanson, N. W. (1960). *Precast-Prestressed Concrete Bridges: 2. Horizontal Shear Connections*. Portland Cement Association, Research and Development Laboratories.
- Harries, K. A., Zeno, G., & Shahrooz, B. (2012). "Toward An Improved Understanding of Shear-Friction Behavior". *ACI Structural Journal*, 109(6), 835-844.
- Hofbeck, J. A., Ibrahim, I. O., & Mattock, A. H. (1969). "Shear Transfer in Reinforced Concrete". *ACI Journal*, 66(2), 119-128.
- Hsu, T. T., Mau, S. T., & Chen, B. (1987). "Theory on Shear Transfer Strength of Reinforced Concrete". *ACI Structural Journal*, 84(2), 149-160.
- International Federation for Structural Concrete-fib. (2010). *Model Code*. Federal Institute of Technology Lausanne-EPFL, Section Genie Civil, Switzerland.
- Iyer, H. (2005). *The Effect of Shear Deformation in Rectangular and Wide Flange Sections*. Master thesis, Virginia Polytechnic Institute and State University, Blacksburg, United State of America.
- Kahn, L. F., & Mitchell, A. D. (2002). "Shear Friction Tests with High-Strength Concrete". *ACI Structural Journal*, 99(1), 98-103.
- Kahn, L. F., & Slapkus, A. (2004). "Interface Shear in High Strength Composite T-beams". *PCI Journal*, 49(4), 102-111.
- Kalny, O. (2016). *CSI Knowledge Base*. Retrieved from <https://wiki.csiamerica.com/display/tutorials/Composite+section>
- Kamel, M. R. (1996). *Innovative Precast Concrete Composite Bridge Systems*. Doctoral dissertation, University of Nebraska-Lincoln, Lincoln, NB.
- Kansas Department of Transportation. (2015). *Standard Specifications for State Road & Bridge Construction*. Topeka, KS.
- Kovach, J. D., & Naito C. (2008). *Horizontal Shear Capacity of Composite Concrete Beams without Interface Ties (ATLSS Report No. 08-05)*. Bethlehem, PA: National

Center for Engineering Research on Advanced Technology for Large Structural Systems.

- Loov, R. E., & Patnaik, A. K. (1994). "Horizontal Shear Strength of Composite Concrete Beams with A Rough Interface". *PCI Journal*, 39(1), 48-69.
- Loov, R. E. (1978). *Design of Precast Connections*. In a seminar organized by Compa International Pte, Ltd, Singapore.
- Manning, D. G. (1991). *Removing Concrete from Bridges (National Cooperative Highway Research Program Synthesis of Highway Practice 169)*. Washington, DC: Transportation Research Board.
- Mansur, M. A., Vinayagam, T., & Tan, K. H. (2008). "Shear Transfer across a Crack in Reinforced High-Strength Concrete". *Journal of Materials in Civil Engineering*, 20(4), 294-302.
- Mattock, A. H., Johal, L. & Chow, H. C. (1975). "Shear Transfer in Reinforced Concrete with Moment or Tension Acting across the Shear Plane". *PCI Journal*, 20(4), 76-93.
- Mattock, A. H., Li, W. K., & Wang, T. C. (1976). "Shear Transfer in Lightweight Reinforced Concrete". *PCI Journal*, 21(1), 20-39.
- Mattock, A. H. (1976). *Shear Transfer under Monotonic Loading, across an Interface between Concretes Cast at Different Times (Report SM 76-3)*. Washington, DC: National Science Foundation.
- Morcous, G., & Assad, S. (2014). *Evaluating the Impact of Deck Removal Method on the Performance of NU Girders (SPR-PI (12) M325)*. Lincoln, NE: Nebraska Department of Roads Bridge Division.
- Naaman, A. E. (2012). *Prestressed Concrete Analysis and Design*. Ann Arbor, MI: Techno Press 3000.
- Nebraska Department of Roads. (2004). *Bridge Office Policies and Procedure Manual*. Lincoln, NB.
- Patnaik, A. K. (2001). "Behavior of Composite Concrete Beams with Smooth Interface". *Journal of Structural Engineering*, 127(4), 359-366.

- Santos, P. M., & Júlio, E. N. (2012). "A State-of-the-Art Review on Shear-Friction". *Engineering Structures*, 45, 435-448.
- Saemann, J. C., & Washa, G. W. (1964). "Horizontal Shear Connections between Precast Beams and Cast-In-Place". *Journal of the American Concrete Institute*, 61(11), 1383-1410.
- Schwensen, S. & Farlow, C. (2014). Personal Communication.
- Tadros, M. K., & Baishya, M. C. (1998). *Rapid Replacement of Bridge Decks (NCHRP Report 407)*. Washington, DC: American Association of State Highway and Transportation Officials.
- Vorster, M. C., Merrigan, J. P., Lewis, R. W., & Weyers, R. E. (1992). *Techniques for Concrete Removal and Bar Cleaning on Bridge Rehabilitation Projects (No. SHRP-S-336)*. Washington, DC: National Research Council.
- Walraven, J., Frenay, J., & Pruijssers, A. (1987). "Influence of Concrete Strength and Load History on the Shear Friction Capacity of Concrete Members". *PCI Journal*, 32(1), 66-84.
- Zeno, G. A. (2010). *Use of High-Strength Steel Reinforcement in Shear Friction Applications*. Doctoral dissertation, University of Pittsburgh, Pittsburgh, United State of America.
- Zilch, K., & Reinecke, R. (2000). *Capacity of Shear Joints between High-Strength Precast Elements and Normal-Strength Cast-In-Place Decks*. In PCI/FHWA/FIB International Symposium on High Performance Concrete Precast/Prestressed Concrete Institute Federal Highway Administration Federation Internationale du Beton.

Appendix A
Measured Concrete Properties
(Push-off Tests)

Table A.1: Measured Concrete Material Properties

Material Properties		First Series		Second Series	
		Girder Part	Deck Part	Girder Part	Deck Part
Slump (in.)		4.5	3.0	7.0	7.3
Temperature (°F)		71	72	77	75
Air Content (%)		2.0	5.8	1.5	2.4
f_{cm} (ksi)	7-day	6.5	NA	5.2	4.1
	14-day	7.3	NA	6.5	4.9
	28-day	7.7	5.0	6.6	5.6
	Test Day	7.7	5.1	6.6	5.6

Table A.2: Detail of Modulus of Rupture Tests

Push-off Series	Specimen Number	Peak Load (lb)	Average Width (in.)	Average Depth (in.)	Peak Strength (psi)
Series #1-7 ksi	No. 1	6370	6.1	6.0	520
	No. 2	7490	6.1	6.0	593
	No. 3	6710	6.1	6.0	531
Series #1-4 ksi	No. 1	4501	5.9	6.0	376
	No. 2	5090	6.0	6.0	423
	No. 3	5440	5.9	6.0	452
Series #2-7 ksi	No. 1	7580	6.1	6.3	576
	No. 2	7080	6.1	6.1	563
	No. 3	7270	6.1	6.1	575
Series #2-4 ksi	No. 1	5130	6.1	6.0	418
	No. 2	4760	6.1	6.1	385
	No. 3	6420	6.1	6.2	497

Appendix B

Measured Stress versus Strain from Tests of No. 5 Bars (Push-off Tests)

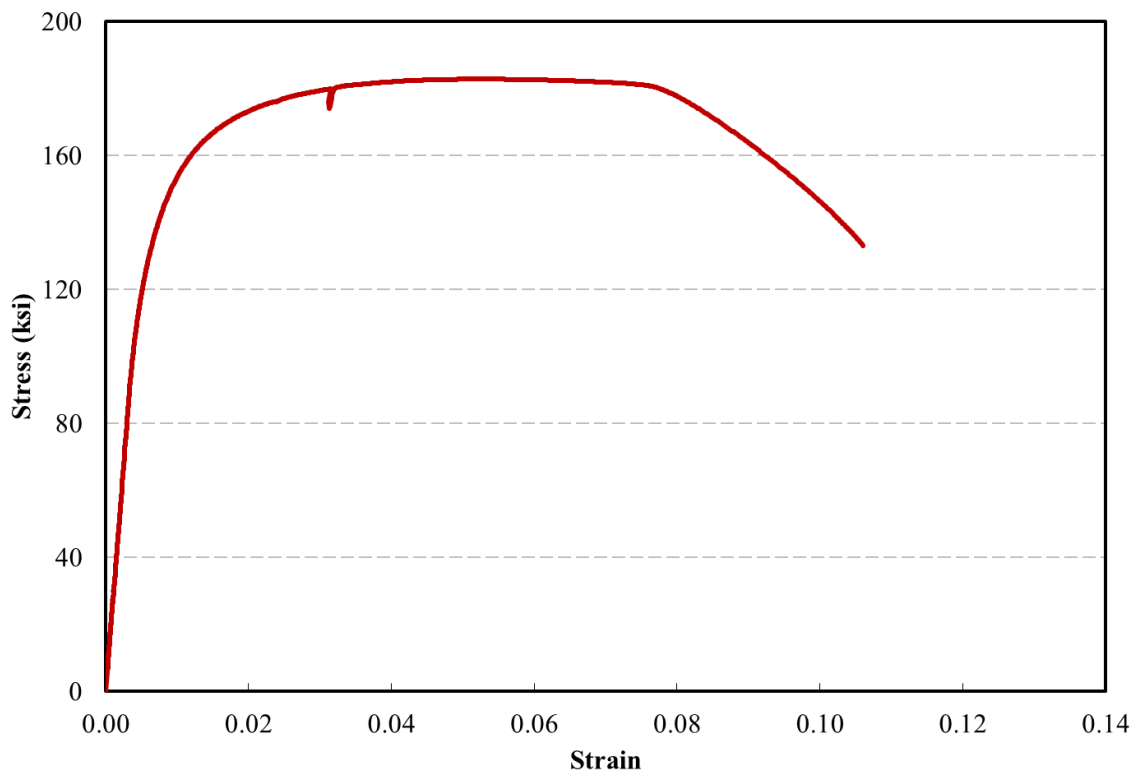


Figure B.1: Stress versus Strain for Grade 120 (Sample 1)

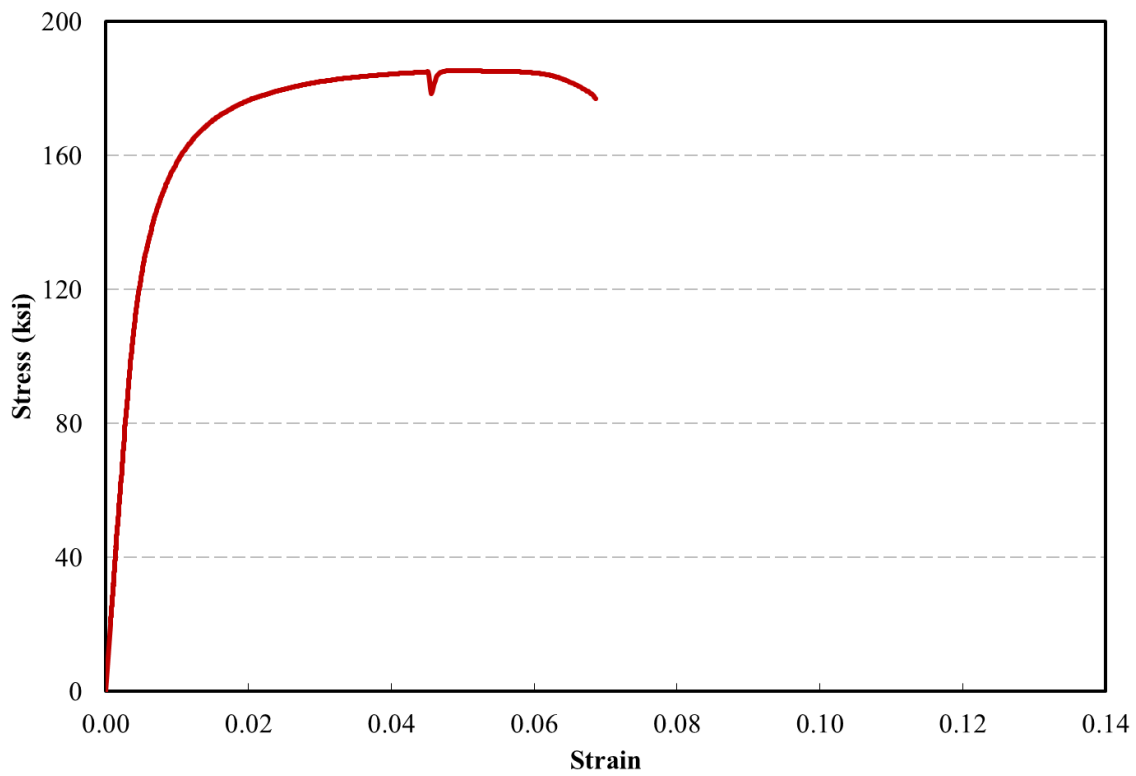


Figure B.2: Stress versus Strain for Grade 120 (Sample 2)

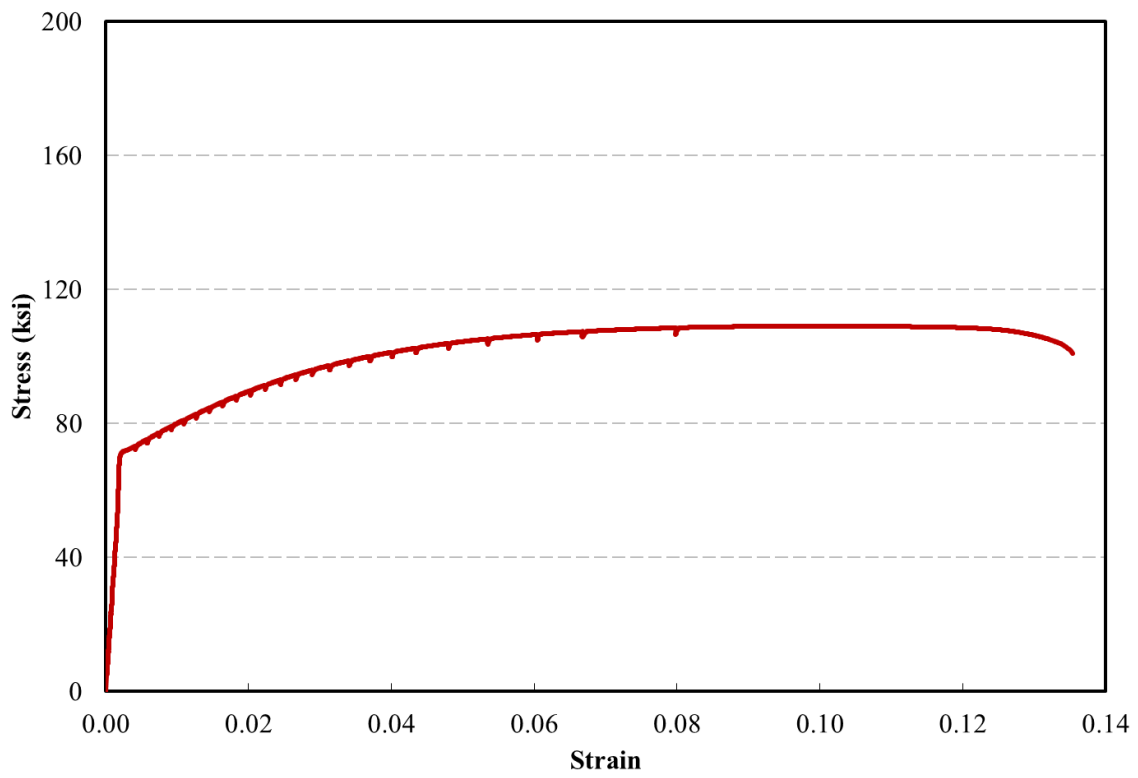


Figure B.3: Stress versus Strain for Grade 60 (Sample 1)

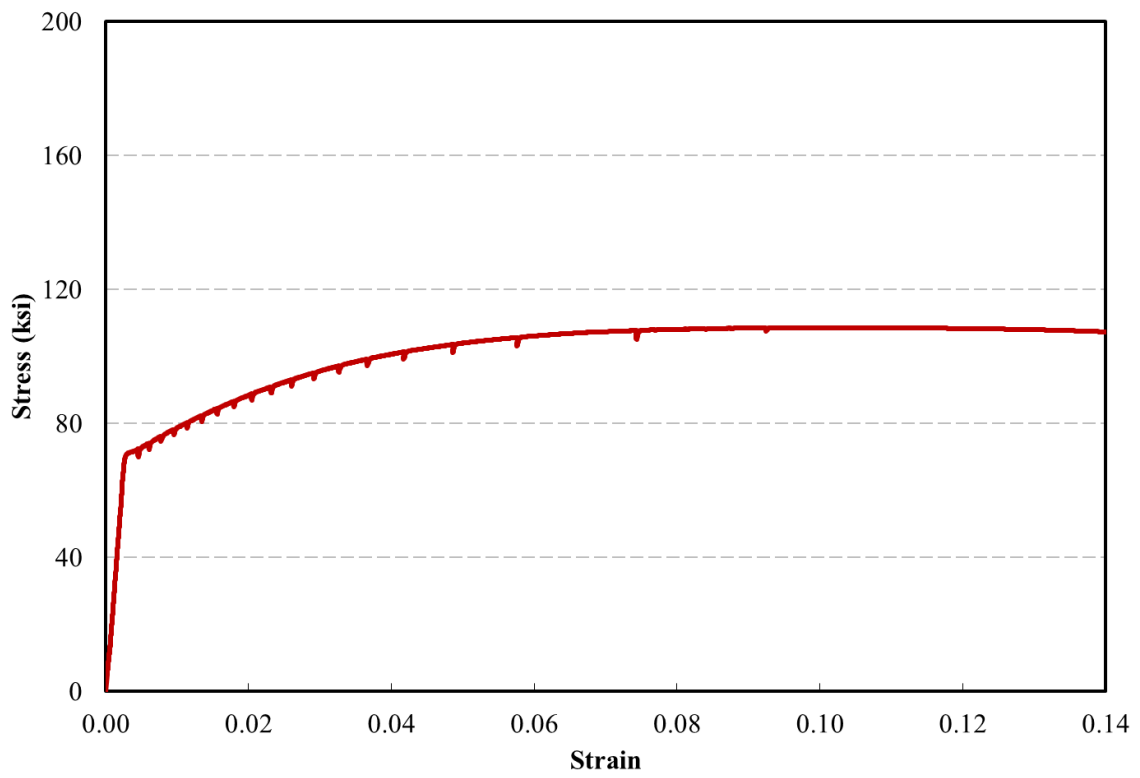


Figure B.4: Stress versus Strain for Grade 60 (Sample 2)

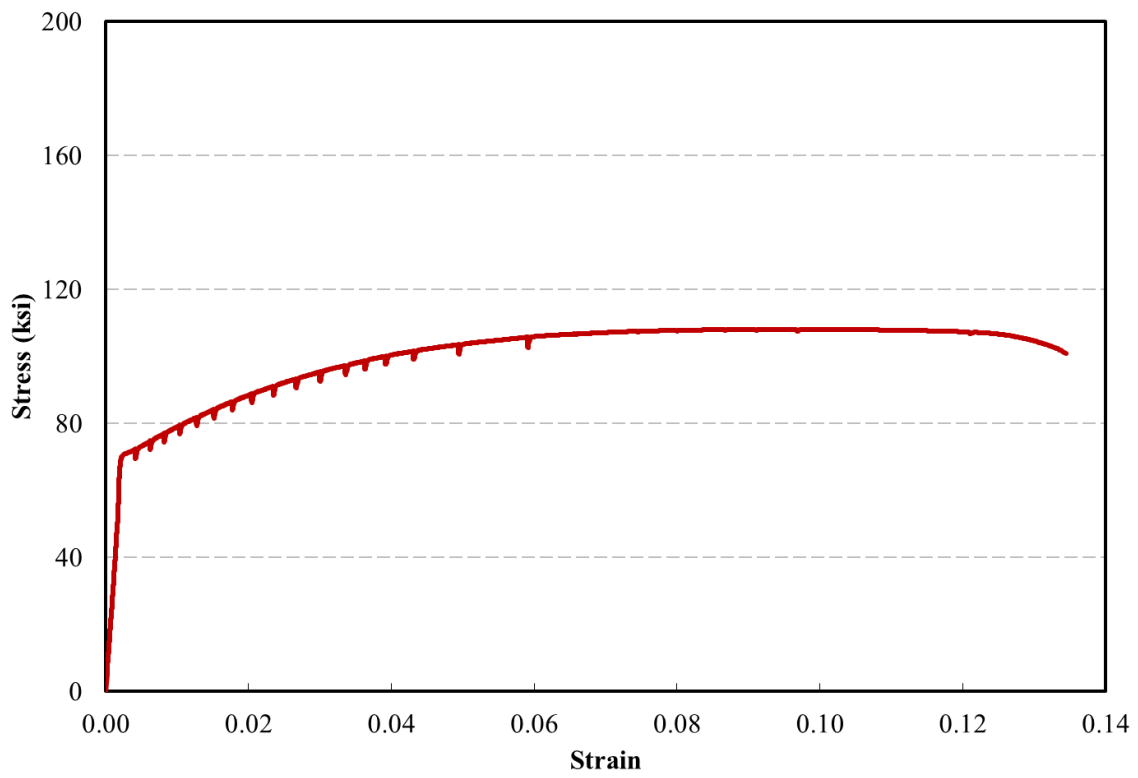


Figure B.5: Stress versus Strain for Grade 60 (Sample 3)

Appendix C

Force versus Slip Relationships in Groups (Push-off Tests)

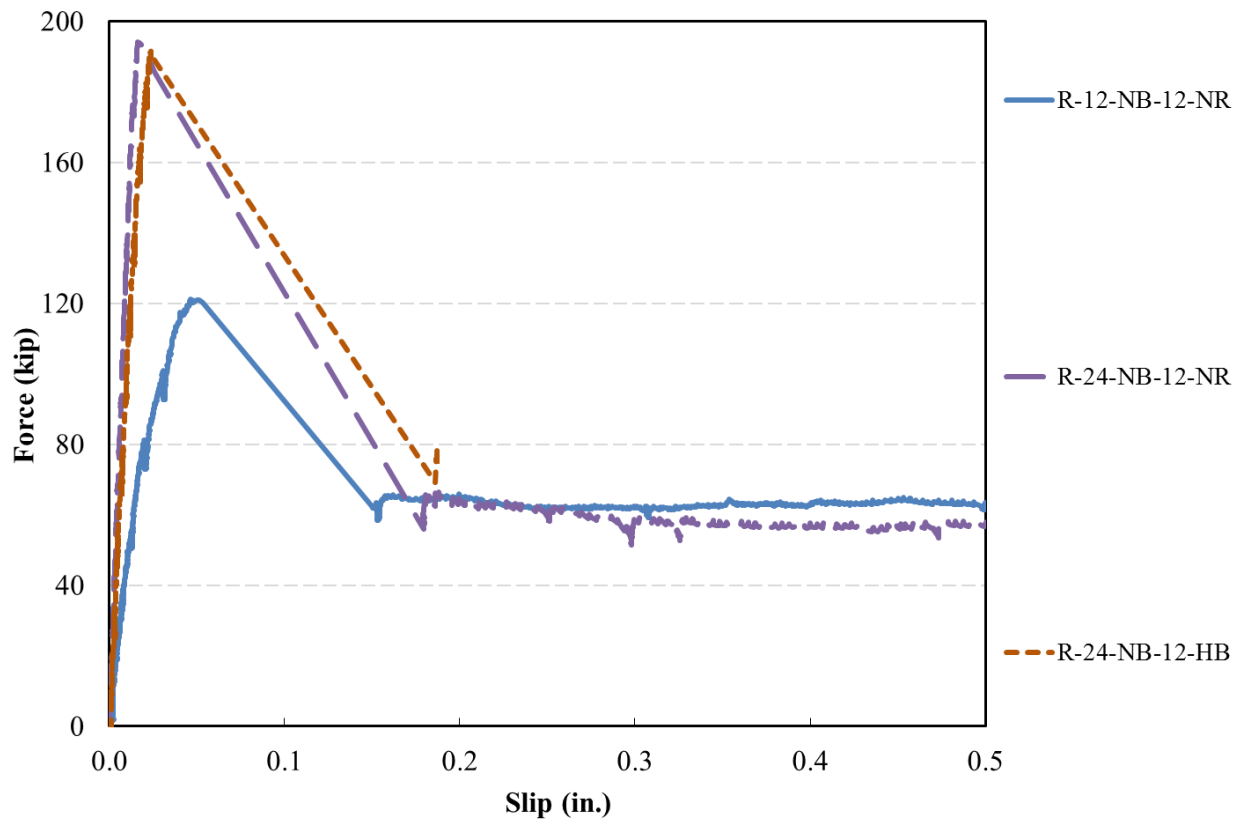


Figure C.1: Force versus Slip for Roughened Specimens with No Bond Breaker

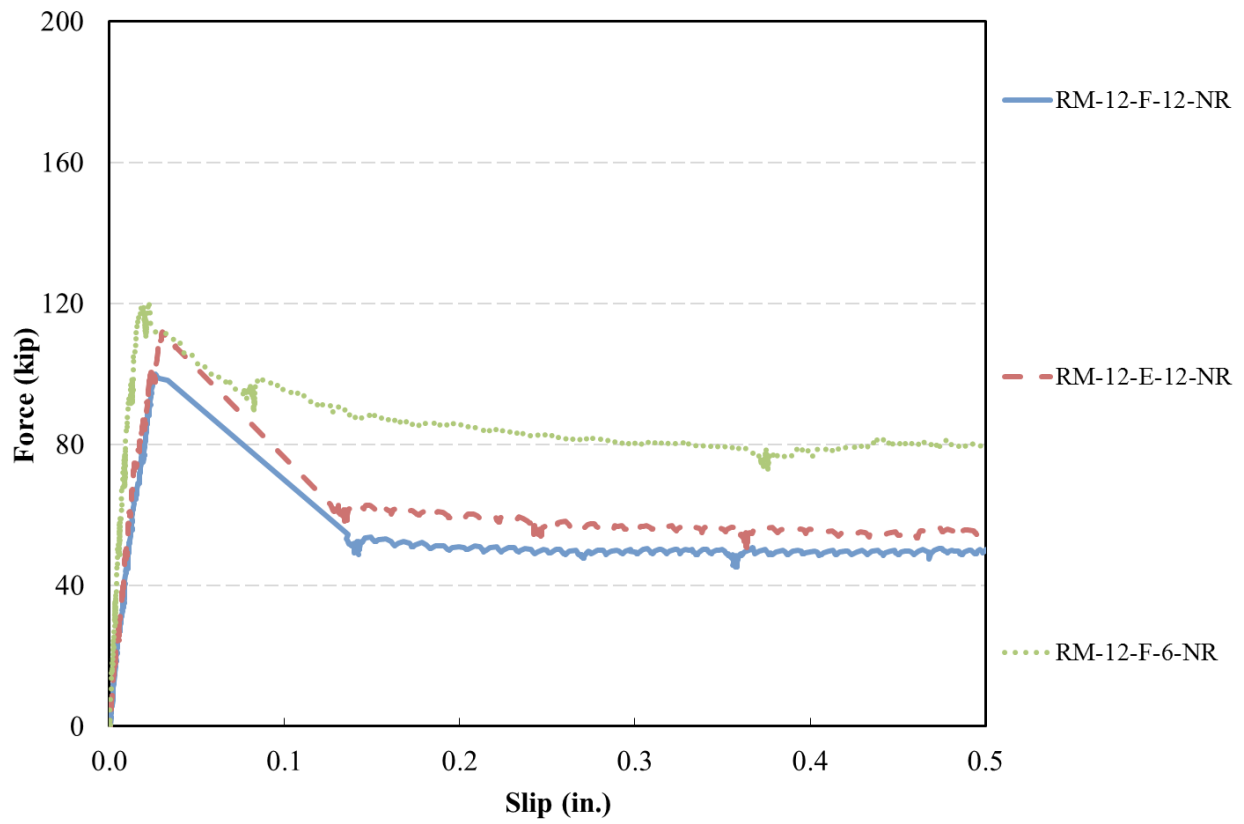


Figure C.2: Force versus Slip for Rough Middle Specimens

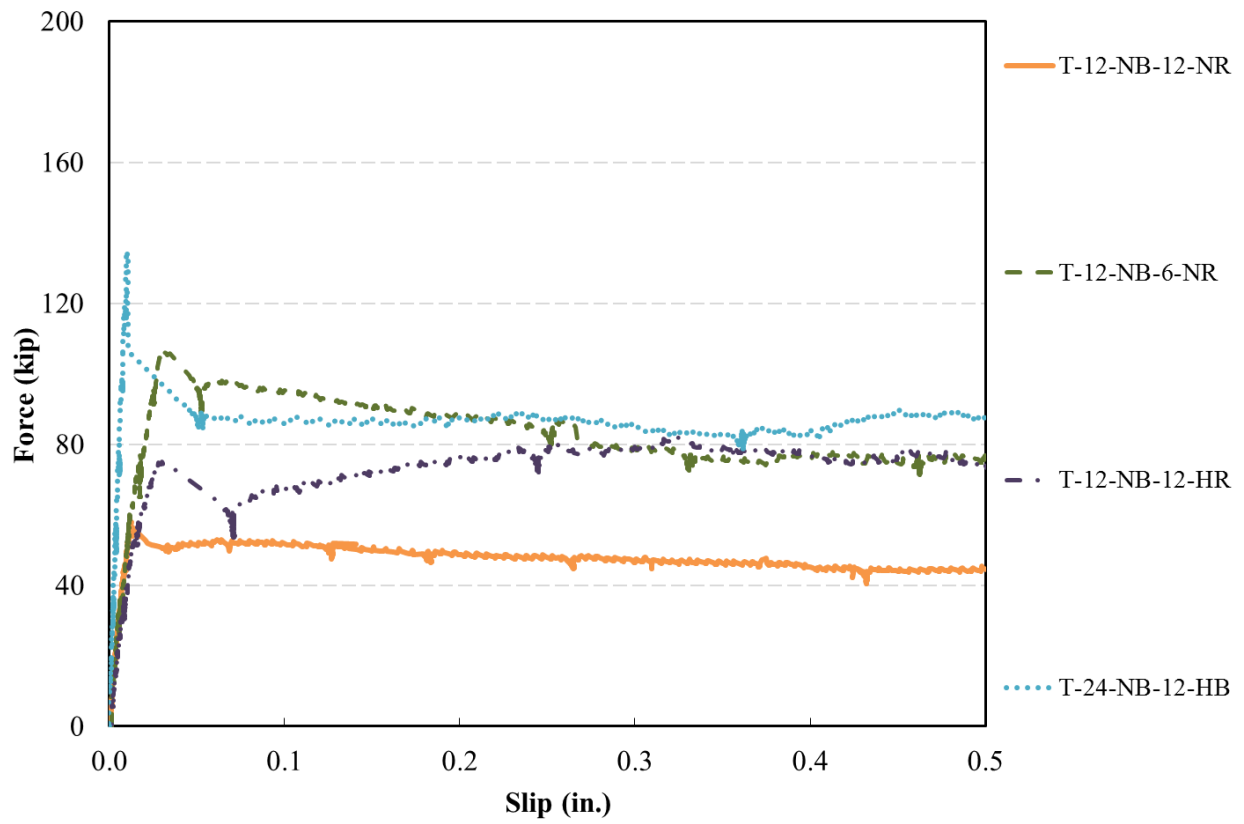


Figure C.3: Force versus Slip for Troweled Specimens with No Bond Breaker

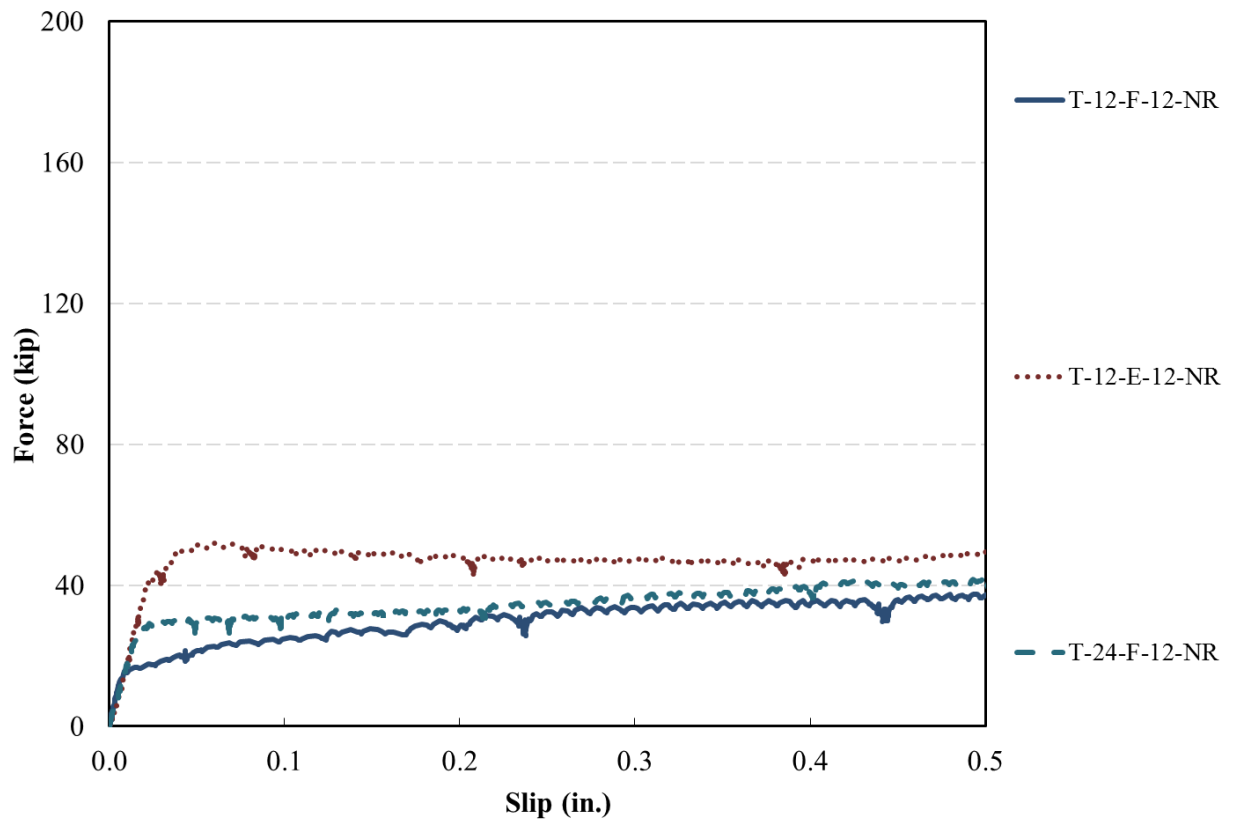


Figure C.4: Force versus Slip for Fully Debonded Specimens

Appendix D
Crack Width versus Slip
(Push-off Tests)

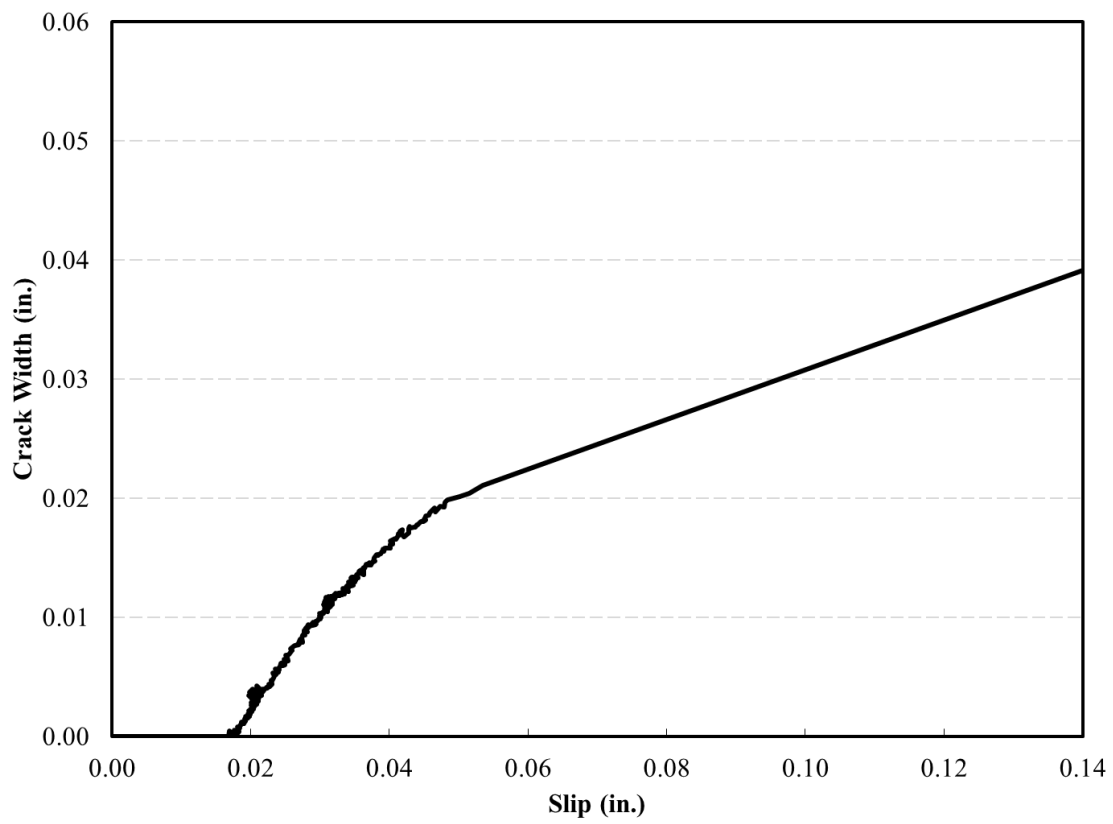


Figure D.1: Crack Width versus Slip for R-12-NB-12-NR

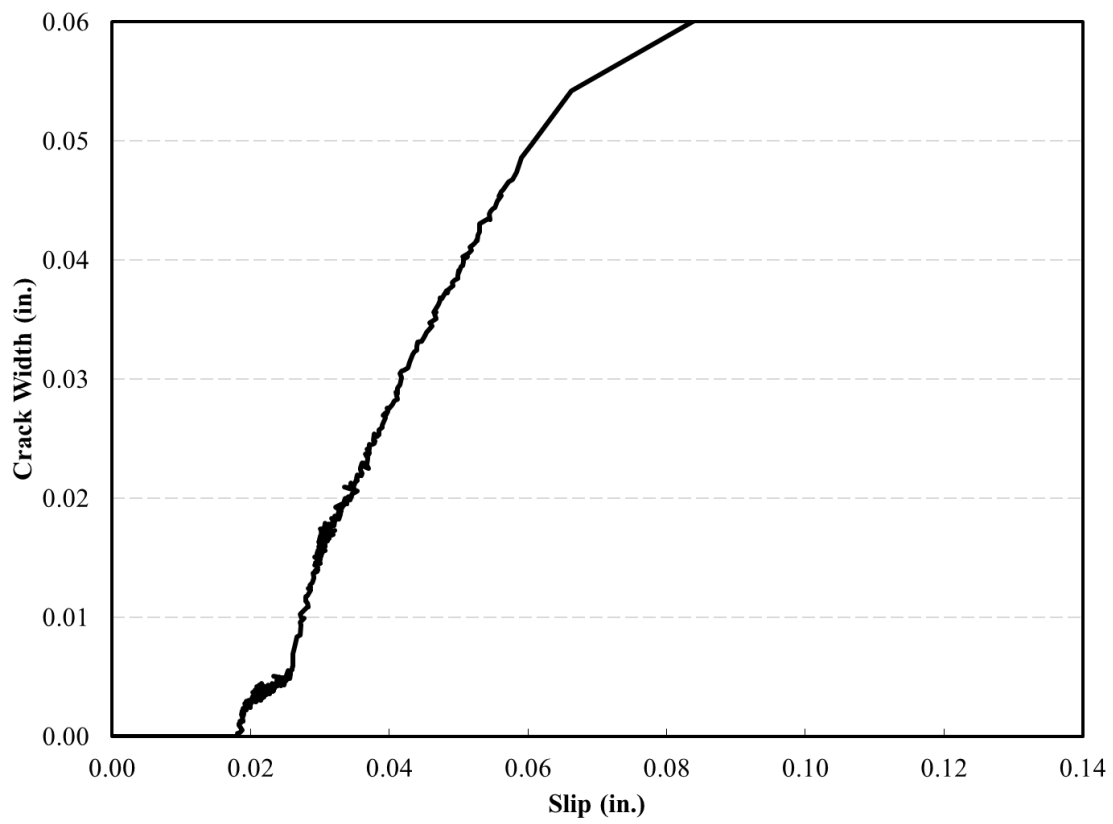


Figure D.2: Crack Width versus Slip for R-12-NB-6-NR

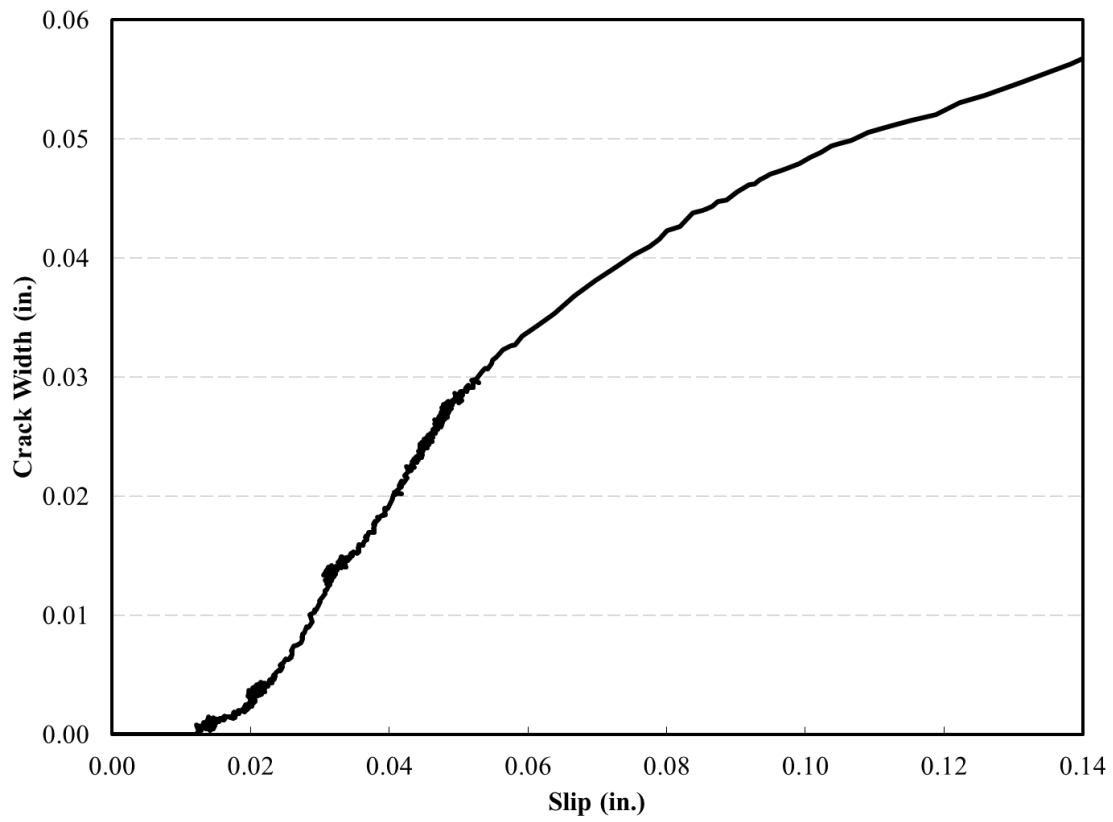


Figure D.3: Crack Width versus Slip for R-12-NB-12-HR

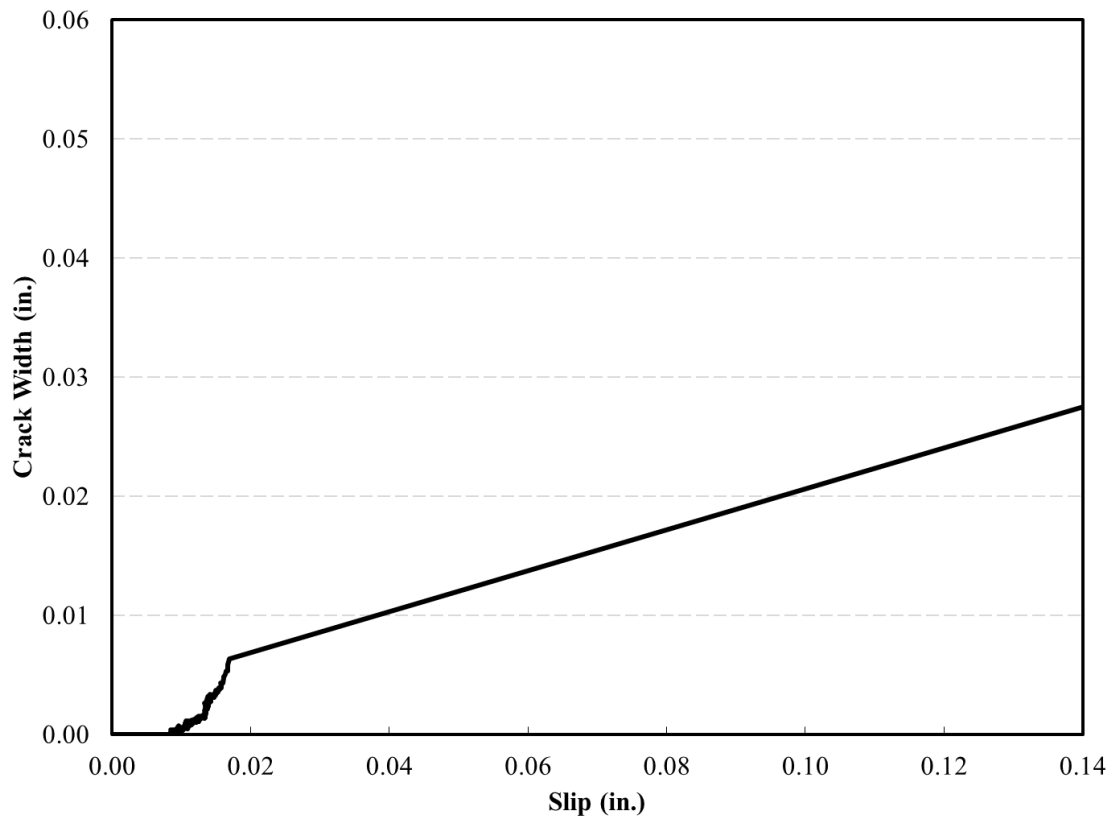


Figure D.4: Crack Width versus Slip for R-24-NB-12-NR

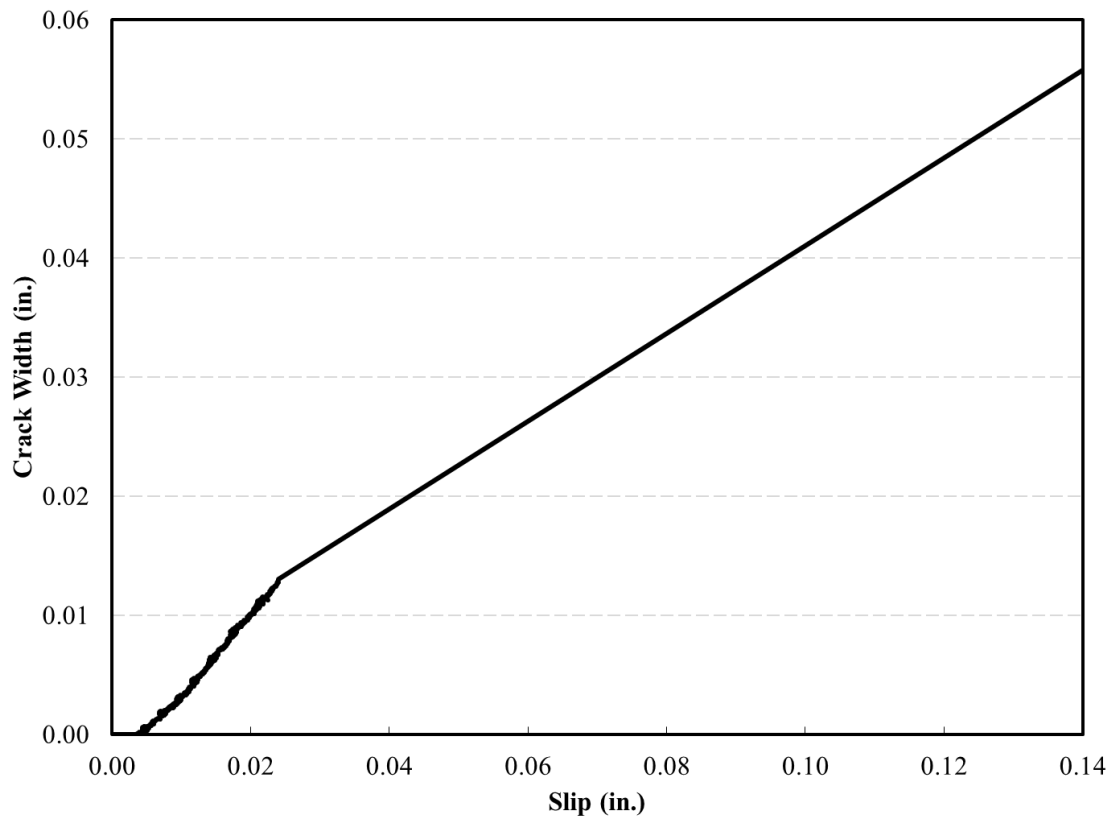


Figure D.5: Crack Width versus Slip for R-24-NB-12-HB

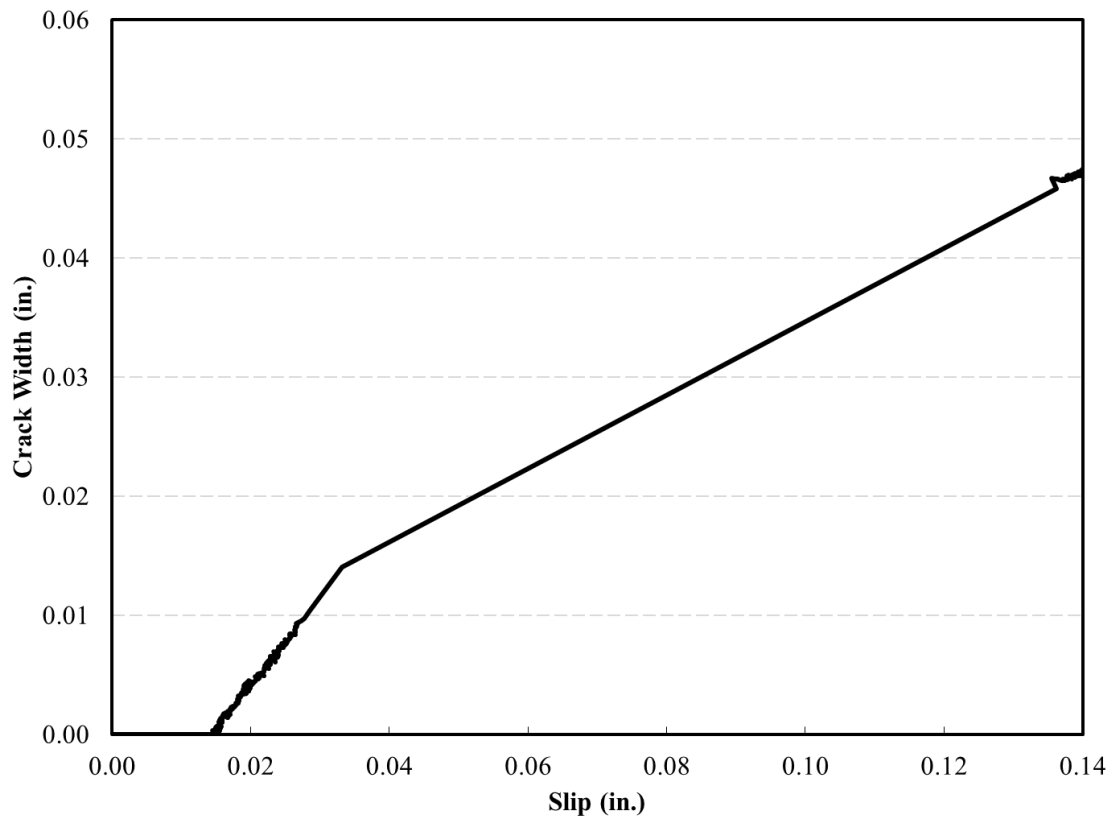


Figure D.6: Crack Width versus Slip for RM-12-F-12-NR

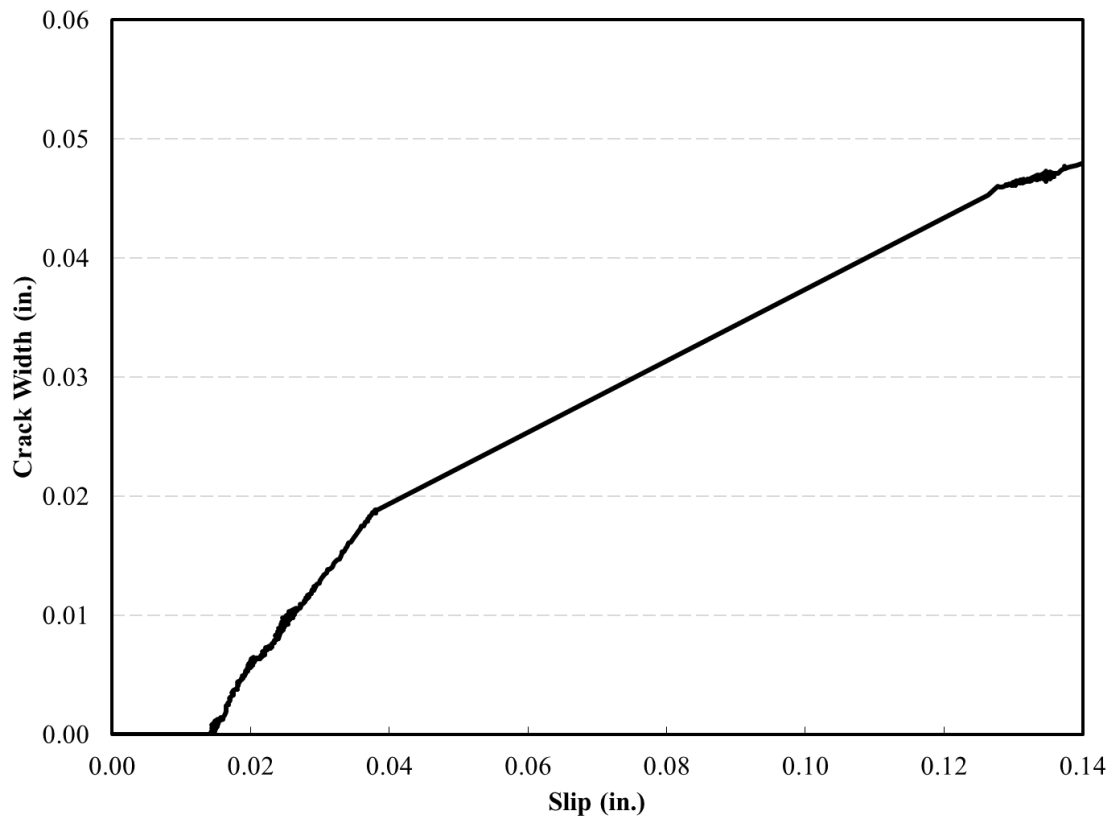


Figure D.7: Crack Width versus Slip for RM-12-E-12-NR

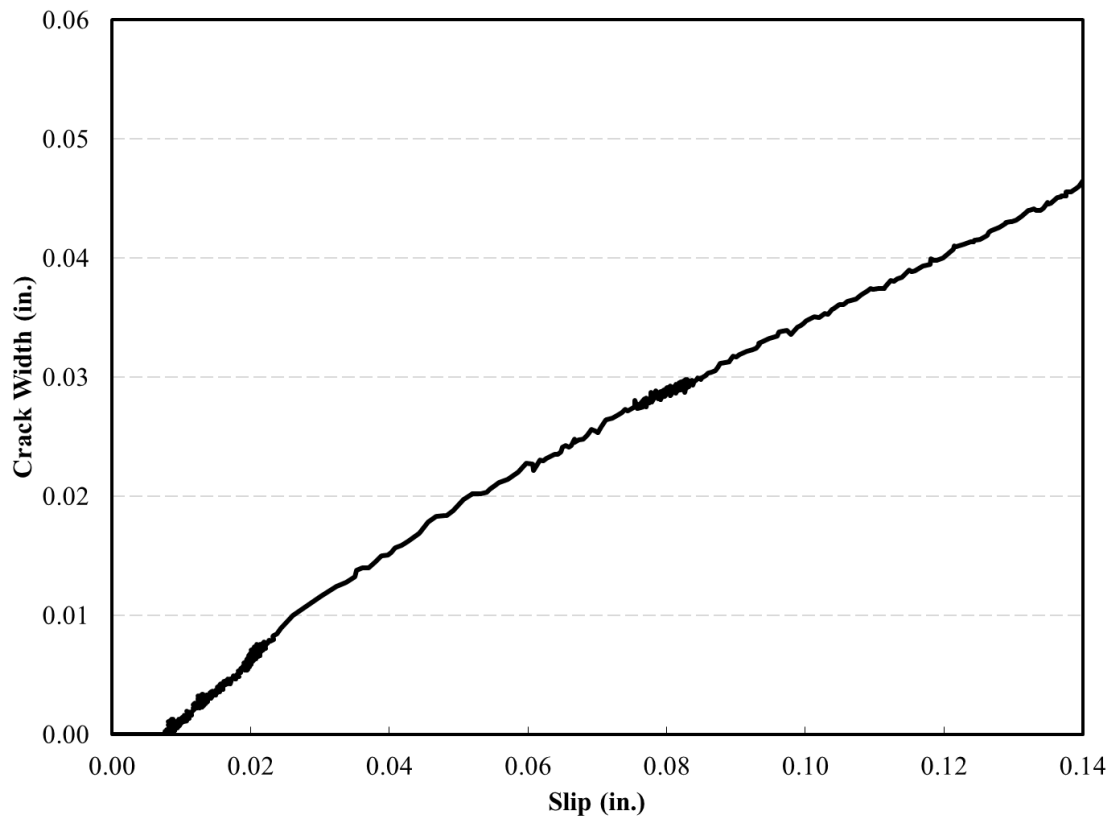


Figure D.8: Crack Width versus Slip for RM-12-F-6-NR

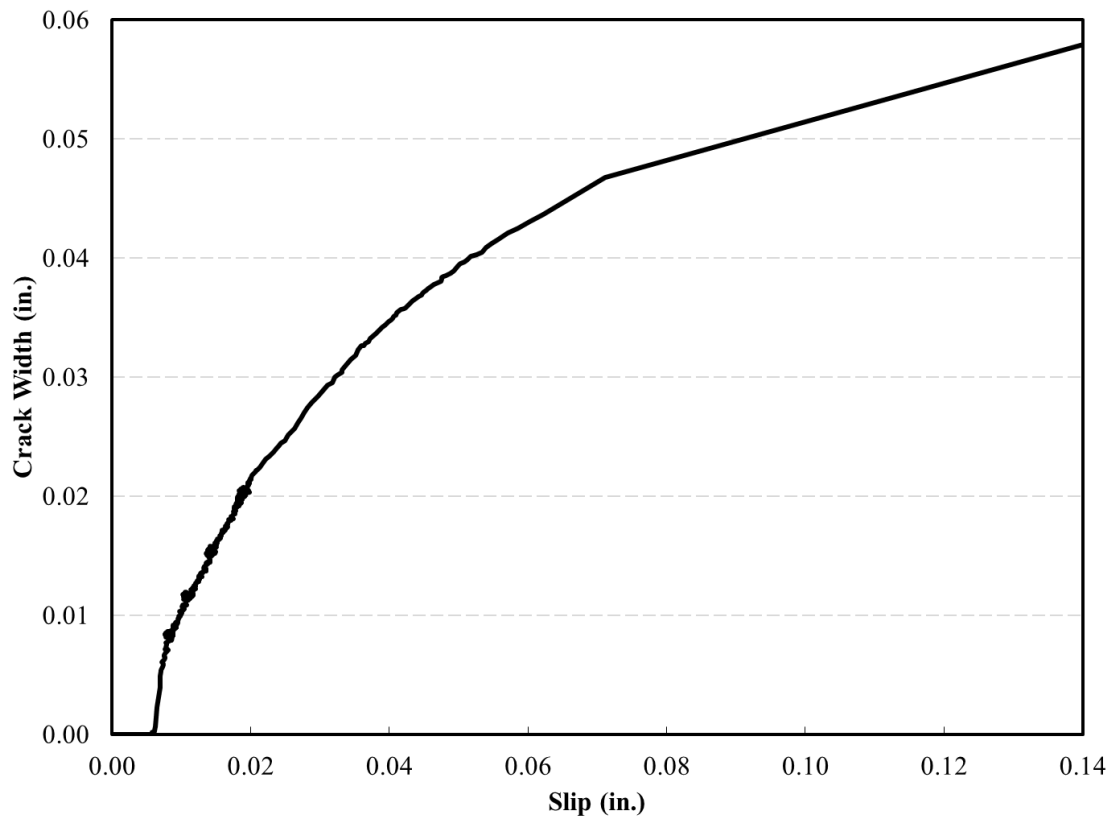


Figure D.9: Crack Width versus Slip for RM-24-F-12-NR

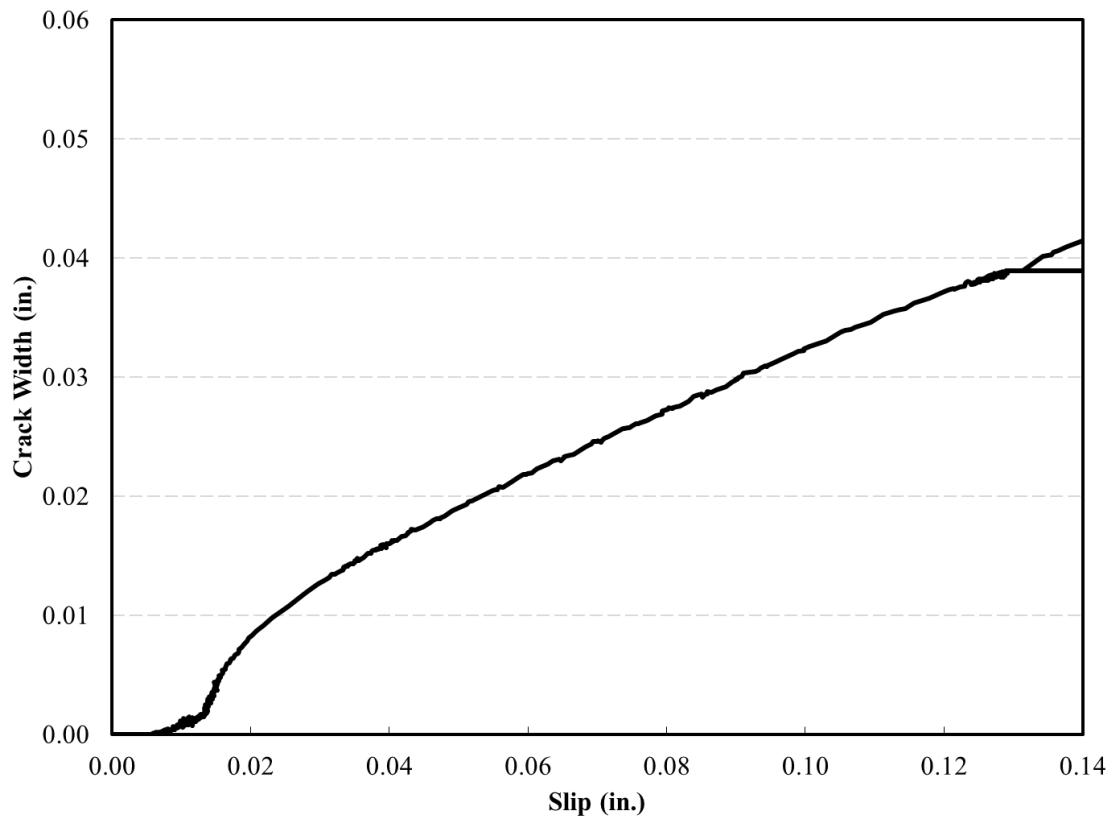


Figure D.10: Crack Width versus Slip for T-12-NB-12-NR

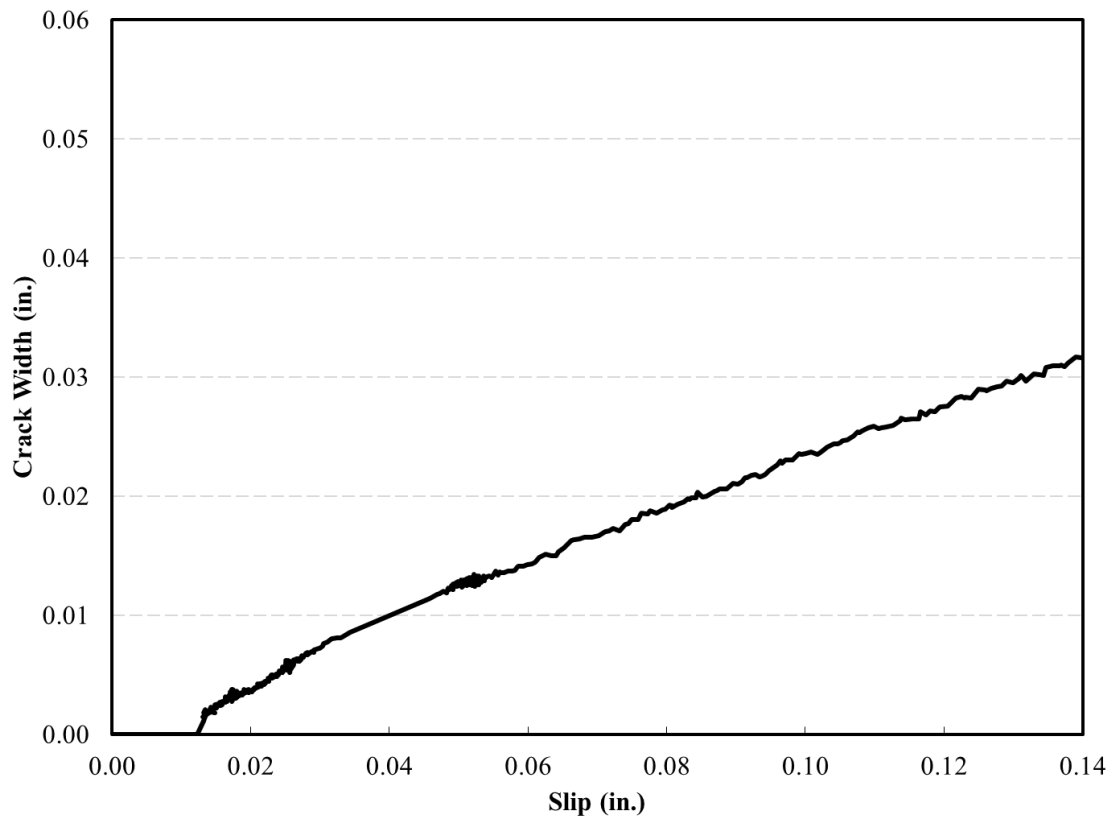


Figure D.11: Crack Width versus Slip for T-12-NB-6-NR

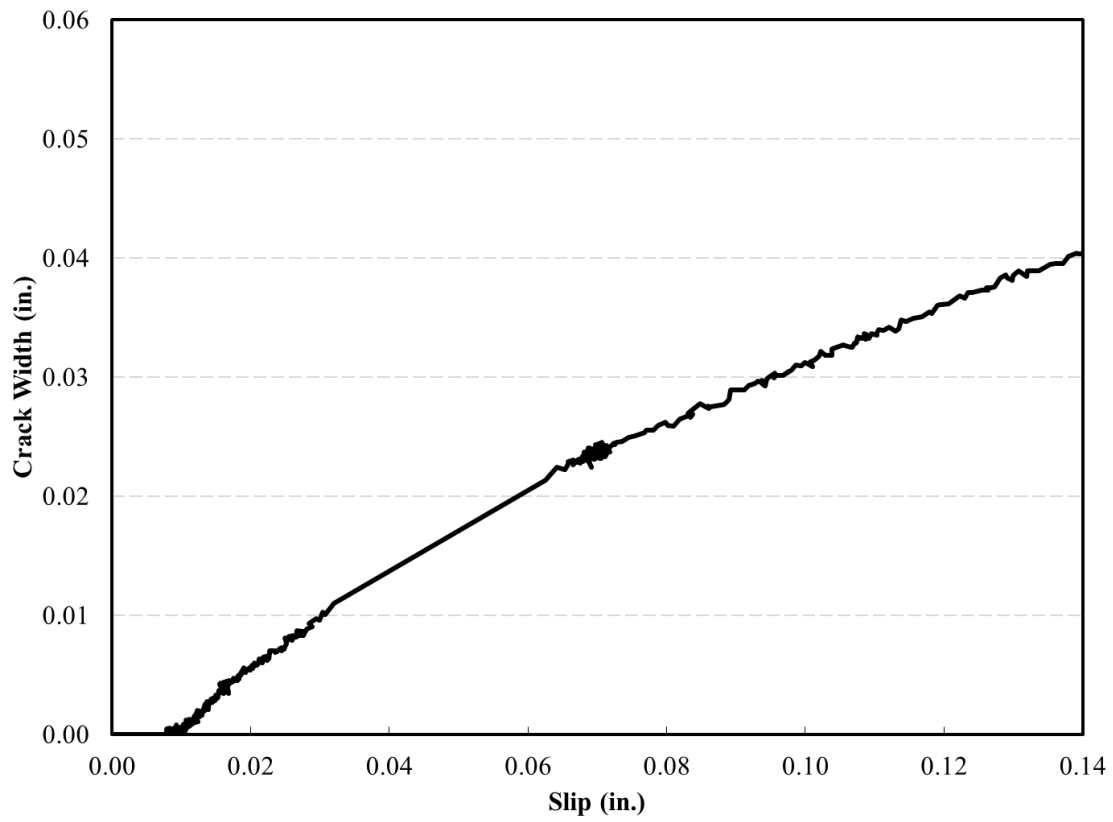


Figure D.12: Crack Width versus Slip for T-12-NB-12-HR

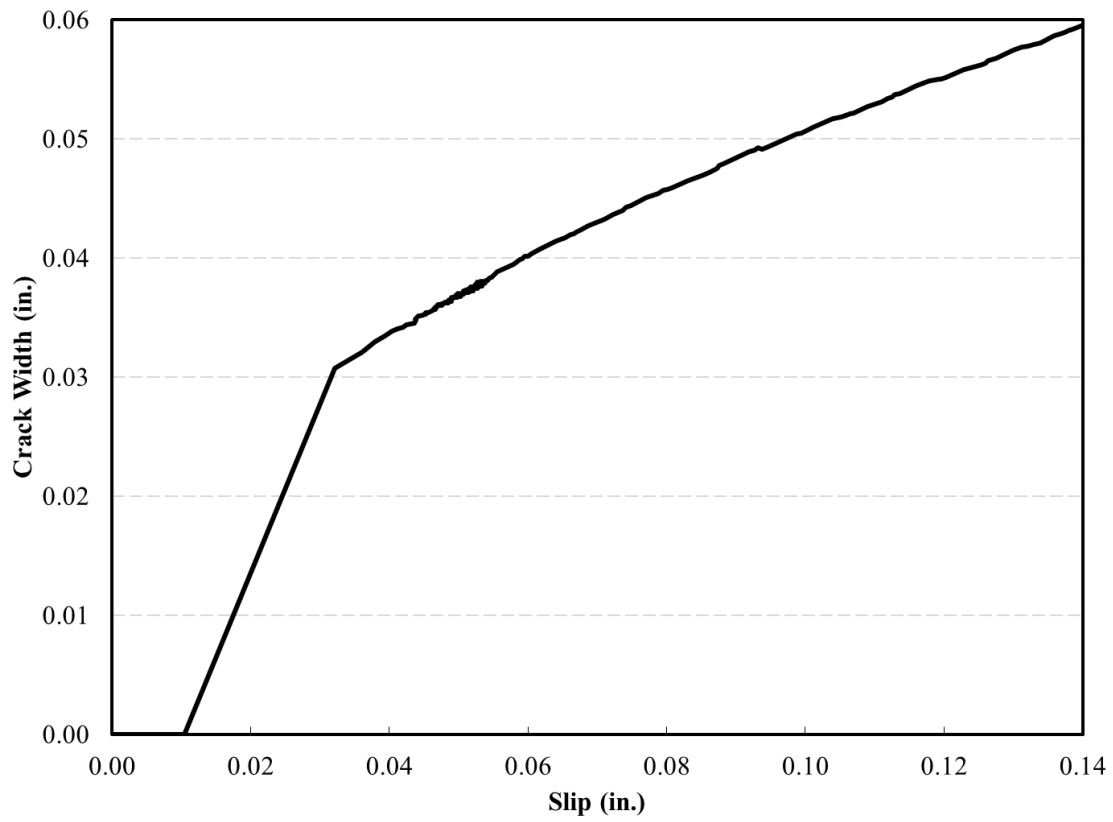


Figure D.13: Crack Width versus Slip for T-24-NB-12-HB

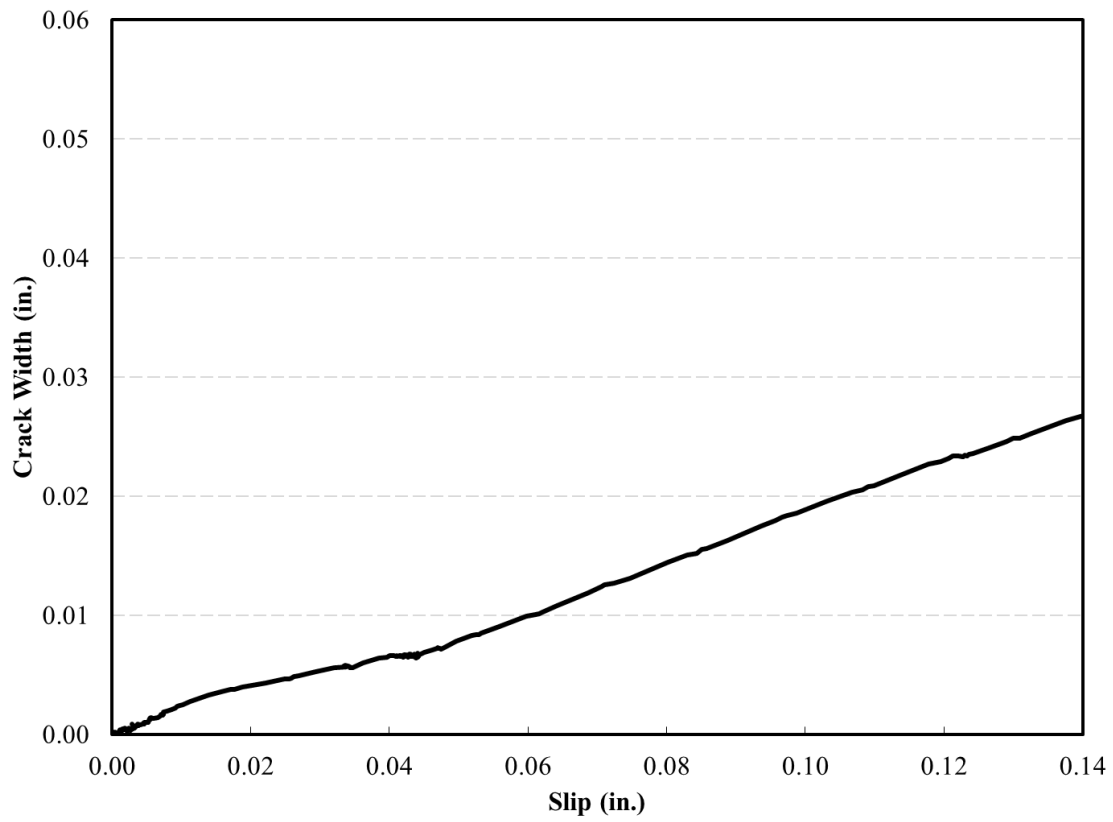


Figure D.14: Crack Width versus Slip for T-12-F-12-NR

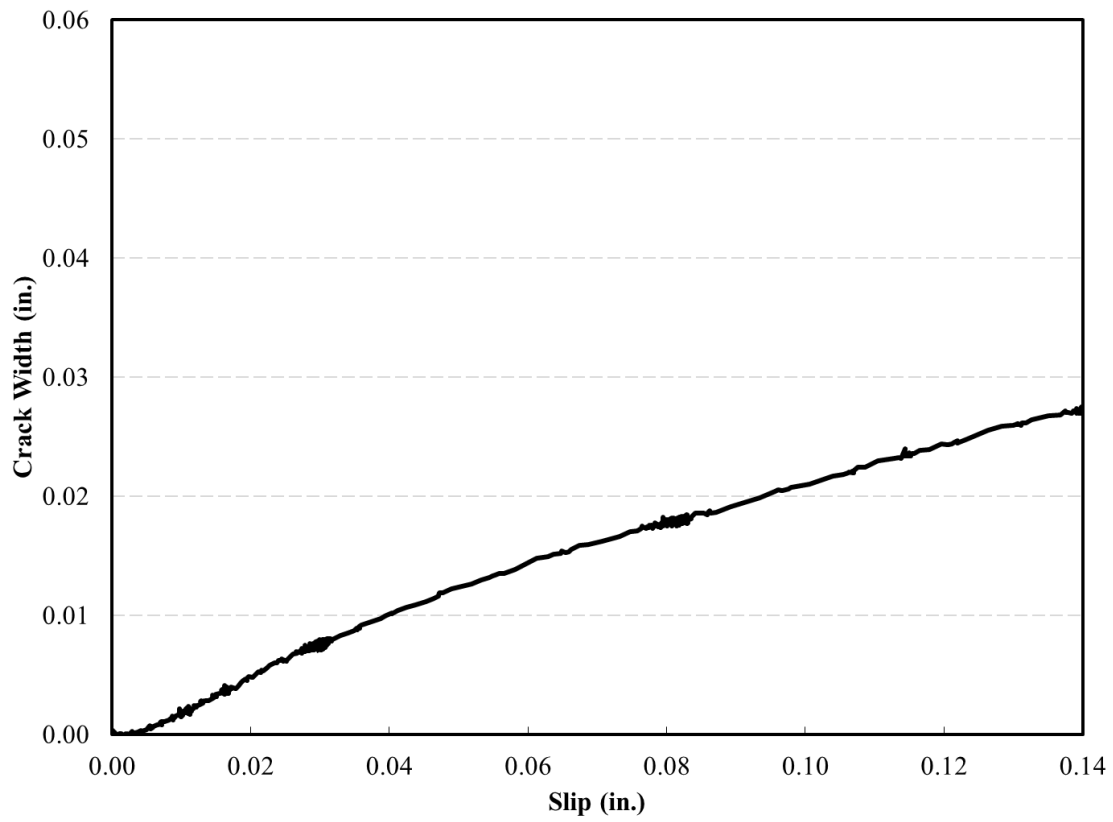


Figure D.15: Crack Width versus Slip for T-12-E-12-NR

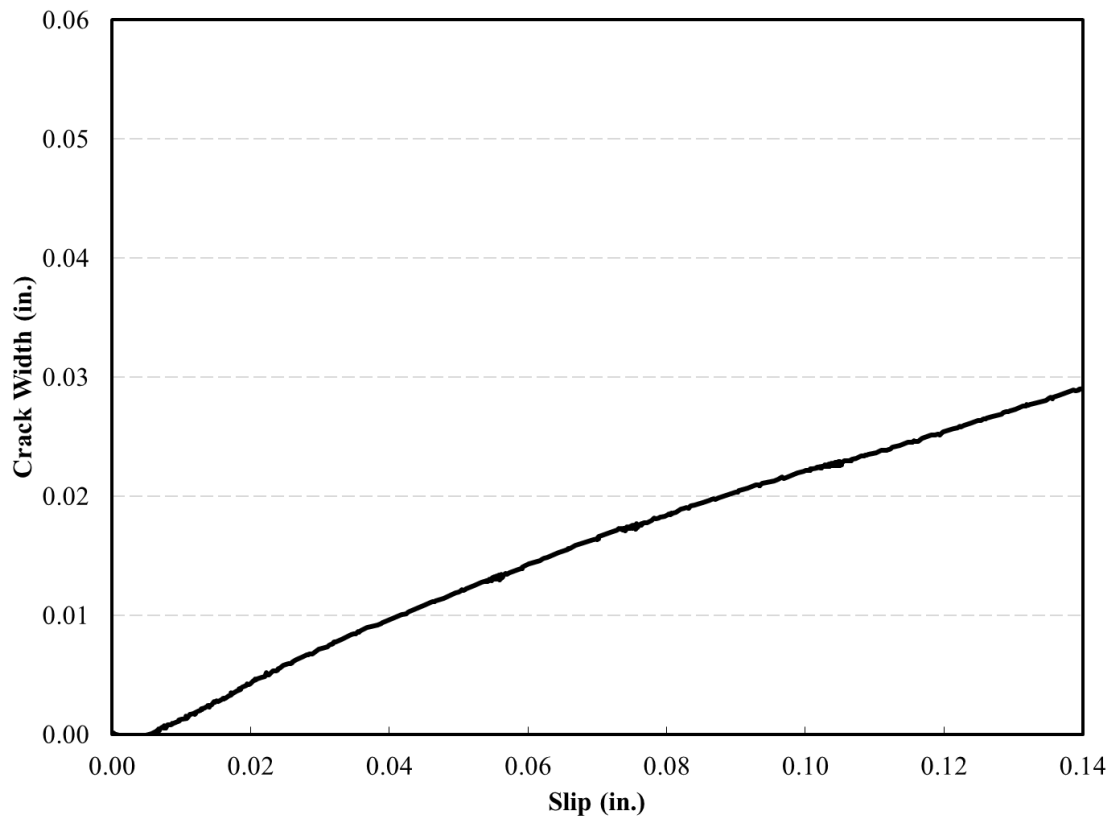


Figure D.16: Crack Width versus Slip for T-24-F-12-NR

Appendix E

Reconstruction of Force versus Deflection Results for Girder #1

As discussed in Chapter 4, Girder #1 was loaded to forces greater than the first cracking force, unloaded due to problems with the test apparatus, reloaded, unloaded again, and loaded a final (third) time until specimen failure occurred. To facilitate comparisons with results from Girders #2 and #3, which were loaded a single time to failure, force versus deflection results for Girder #1 are reported in the report as a reconstructed envelope of the results from all three loading cycles. The process of reconstructing the force versus deflection results for Girder #1 is shown in Figure E.1 and E.2. Force was first plotted versus deflection for all tests in Figure E.1. In Figure E.1 a dashed purple line links the peak of loading cycle #1 and the intercept with the horizontal axis (zero force). The second cycle was assumed to begin at the intersection of the dashed purple line and the horizontal axis. A second dashed purple line is drawn from the peak of cycle #2 at the same slope as the first dashed purple line. The third cycle was assumed to begin at the intersection between the second dashed purple line and the horizontal axis. The reconstructed plot of force versus deflection was then reported as the envelope of the three loading cycles (the red line shown in Figure E.2).

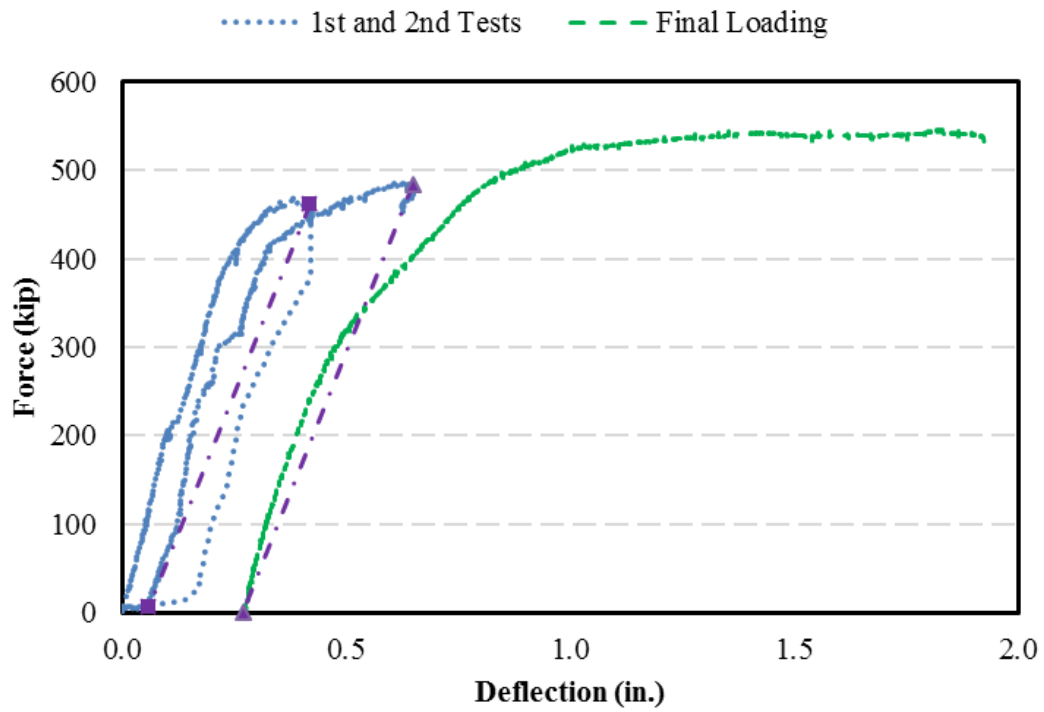


Figure E.1: Plots of Force versus Deflection for All Tests of Girder #1

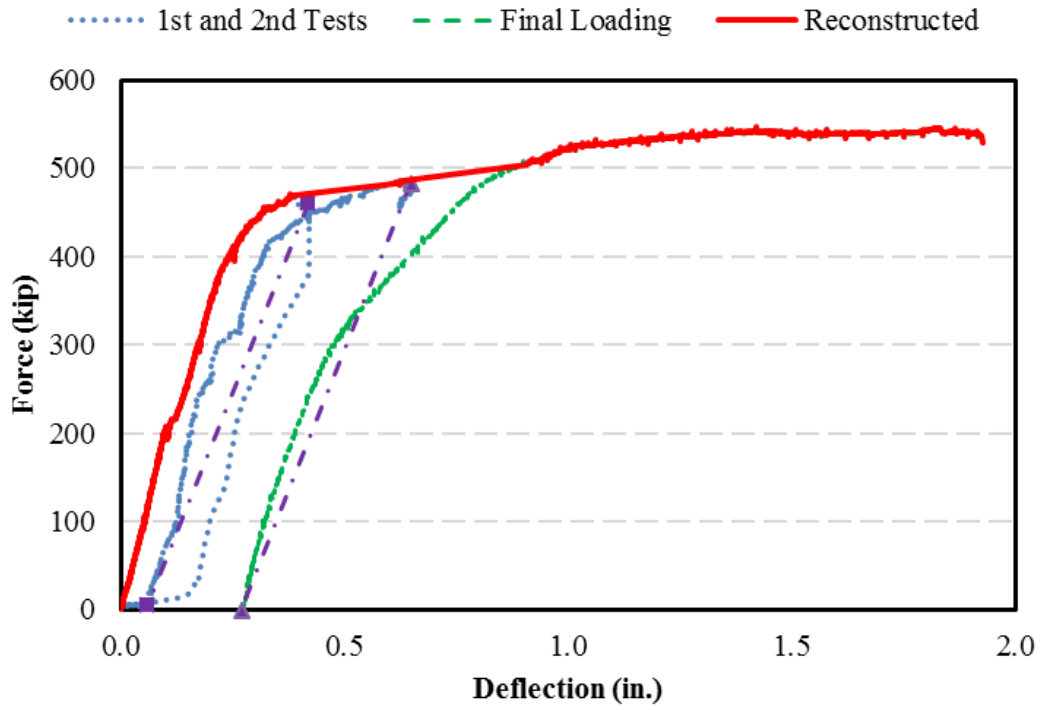


Figure E.2: Reconstructed Plot of Force versus Deflection for Girder #1

Appendix F

Details of the Composite Girder Model in SAP2000

The deck and girder were modeled using shell and frame elements, respectively, that were defined as shown in Figures F.1 and F.2. Properties of the multi-linear plastic links were defined as shown in Figures F.3 and F.4. The steps used to construct the models are follows:

- 1) Create grid lines (Figure F.5)
- 2) Draw girder and deck sections (Figure F.6)
- 3) Insert links (Figure F.7)
- 4) Assign support conditions and apply forces (Figure F.8)

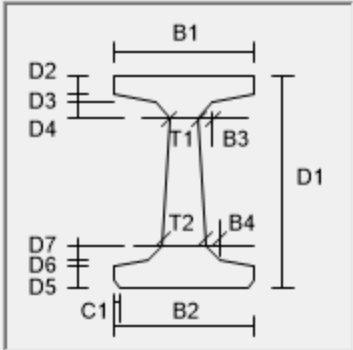
Section Name

Section Notes

Source: User Defined

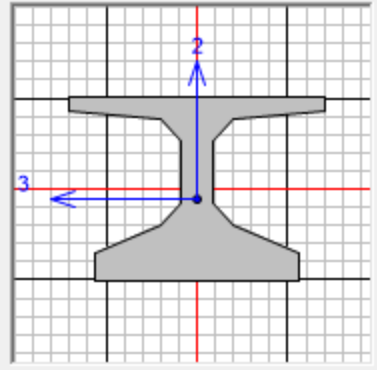
Display Color ■

Section Dimensions



B1	<input type="text" value="1.2243"/>	
B2	<input type="text" value="0.9754"/>	
B3	<input type="text" value="0.1016"/>	
B4	<input type="text" value="0.1016"/>	
D1	<input type="text" value="0.889"/>	
D2	<input type="text" value="0.065"/>	
D3	<input type="text" value="0.0445"/>	
D4	<input type="text" value="0.1016"/>	
D5	<input type="text" value="0.1346"/>	
D6	<input type="text" value="0.1397"/>	
D7	<input type="text" value="0.1016"/>	
T1	<input type="text" value="0.1499"/>	
T2	<input type="text" value="0.1499"/>	
C1	<input type="text" value="0."/>	

Section



Properties

C8

Figure F.1: Girder Section Properties

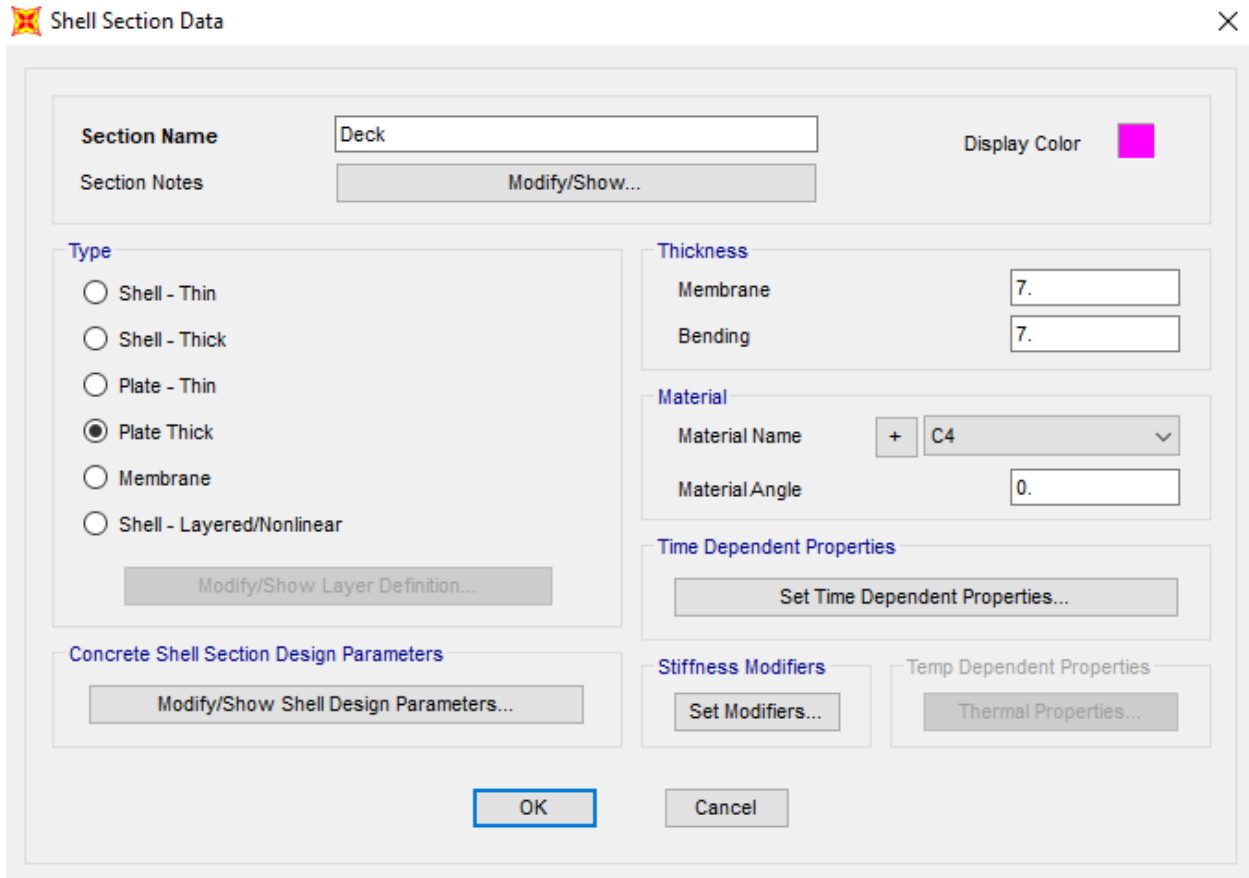


Figure F.2: Deck Section Properties

Link/Support Property Data ×

Link/Support Type: MultiLinear Plastic

Property Name: Nonlinear Set Default Name

Property Notes Modify/Show...

Total Mass and Weight

Mass: 0. Rotational Inertia 1: 0.

Weight: 0. Rotational Inertia 2: 0.

Rotational Inertia 3: 0.

Factors For Line, Area and Solid Springs

Property is Defined for This Length In a Line Spring: 1.

Property is Defined for This Area In Area and Solid Springs: 1.

Directional Properties

Direction	Fixed	NonLinear	Properties
<input checked="" type="checkbox"/> U1	<input checked="" type="checkbox"/>	<input type="checkbox"/>	Modify/Show for U1...
<input checked="" type="checkbox"/> U2	<input type="checkbox"/>	<input checked="" type="checkbox"/>	Modify/Show for U2...
<input checked="" type="checkbox"/> U3	<input type="checkbox"/>	<input type="checkbox"/>	Modify/Show for U3...
<input checked="" type="checkbox"/> R1	<input checked="" type="checkbox"/>	<input type="checkbox"/>	Modify/Show for R1...
<input checked="" type="checkbox"/> R2	<input checked="" type="checkbox"/>	<input type="checkbox"/>	Modify/Show for R2...
<input checked="" type="checkbox"/> R3	<input checked="" type="checkbox"/>	<input type="checkbox"/>	Modify/Show for R3...

P-Delta Parameters

Figure F.3: Multi-Linear Link Properties

Edit

Identification

Property Name:

Direction:

Type:

NonLinear:

Properties Used For Linear Analysis Cases

Effective Stiffness:

Effective Damping:

Shear Deformation Location

Distance from End-J:

Multi-Linear Force-Deformation Definition

	Displ	Force
1	-0.2	-72.
2	-0.1	-72.
3	-0.03	-200.
4	-0.01	-150.

Order Rows Delete Row Add Row 10

Hysteresis Type And Parameters

Hysteresis Type:

No Parameters Are Required For This Hysteresis Type

Hysteresis Definition Sketch

Multilinear Plastic - Kinematic

OK Cancel

Figure F.4: Multi-Link Nonlinear Properties in U2 Direction

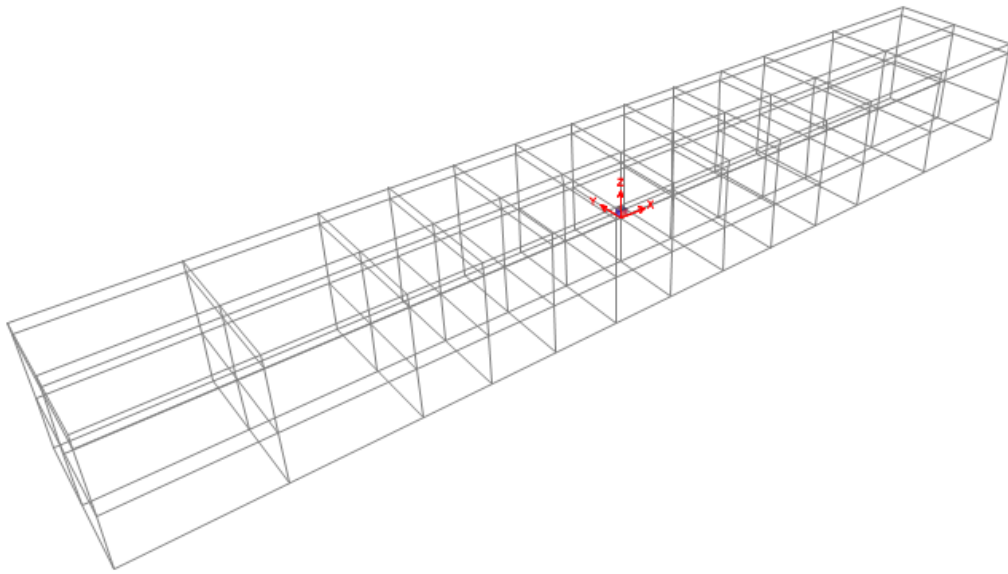


Figure F.5: Grid Lines

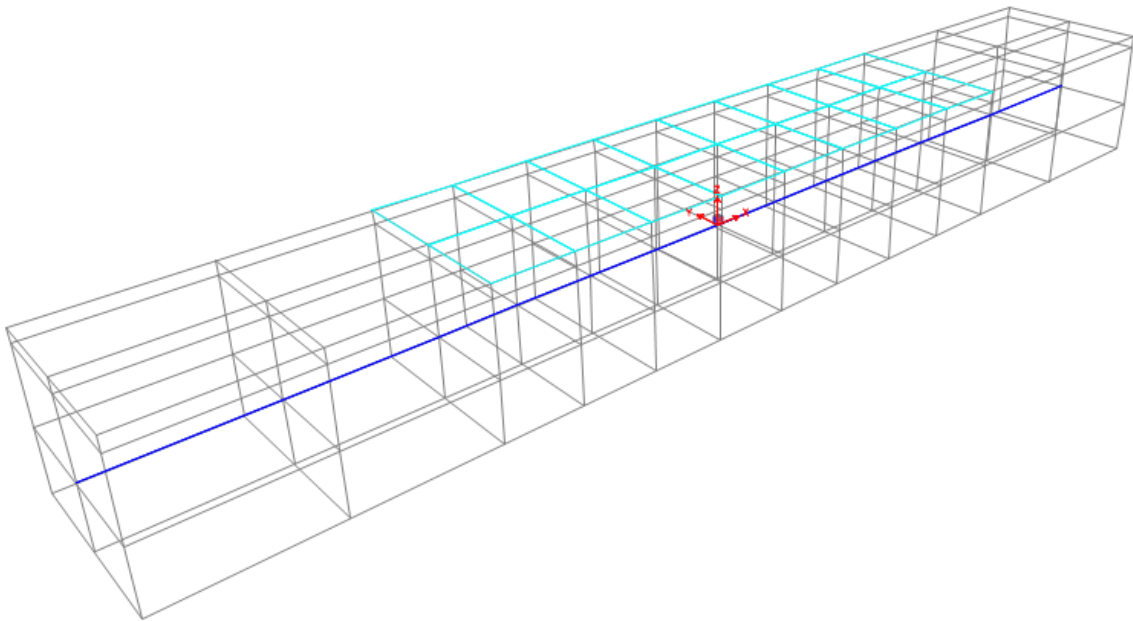


Figure F.6: Insert Girder and Deck Sections

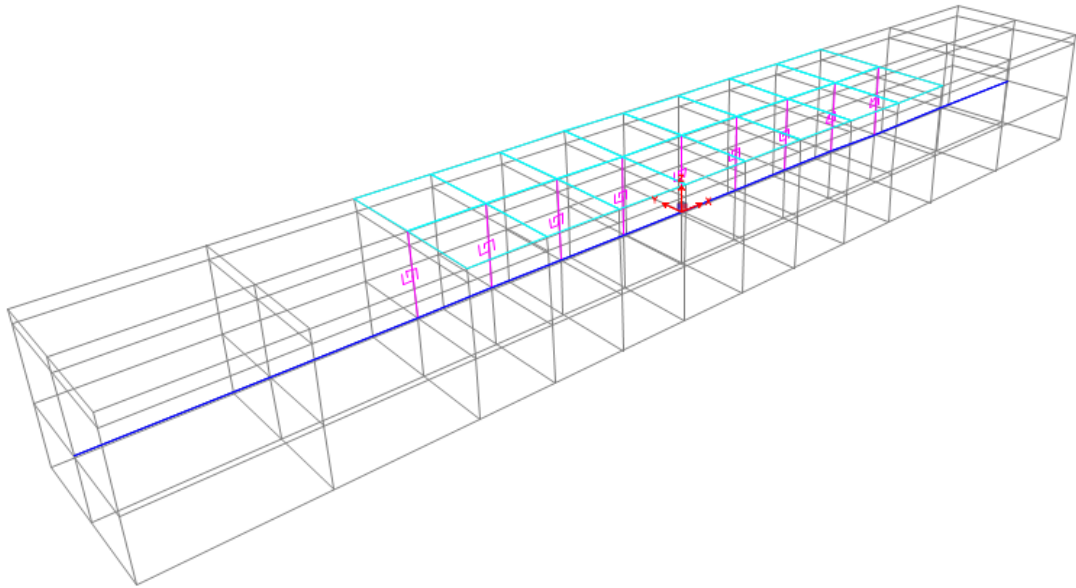


Figure F.7: Inserted Link Elements

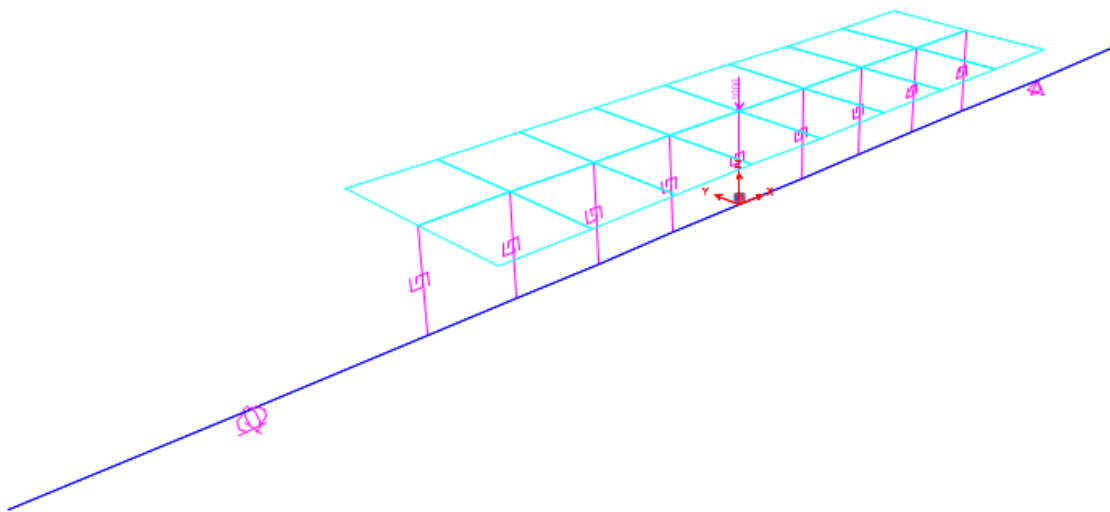


Figure F.8: Support Conditions Assigned and Force Applied